TAXI:
Targeting Antimalarial eX-star drugs for Intracellular delivery

Luísa Aguiar Tavares da Silva
Programa Doutoral em Química Sustentável
Departamento de Química e Bioquímica
2019

Orientadora

Paula Alexandra de Carvalho Gomes,
Professora Associada, Faculdade de Ciências da Universidade do Porto

Coorientadores

Marina Barroso Pereira Pinheiro,
Investigadora, Faculdade de Farmácia da Universidade do Porto

Nuno Filipe de Sousa Vale,
Docente, Instituto de Ciências Biomédicas Abel Salazar da Universidade do Porto

Acknowledgements

Looking back to the past four years, which have been filled with frustrations, with a few victories to celebrate once in a while, I consider myself extremely lucky for all the amazing people I had surrounding me throughout this whole journey, who contributed to my personal growth and without whom the conclusion of this PhD wouldn't have been possible.

First of all, and most importantly, I deeply thank my supervisor - Professor Paula Gomes for all she has taught me for the past 7 years (…!). There's a lot I cannot put into words, but I have to thank you for trusting me and guiding me through this project, for not giving up on me and, most of all, thank you for your friendship. Aside from my scientific development, you have definitely played a major role on my personal growth, by setting an incredible example. It is a privilege to work with you - you are an inspiration!

I would also like to thank my co-supervisors, Professor Nuno Vale and Doctor Marina Pinheiro, for their important contribution to this work and my personal growth. I particularly have to thank Marina for embracing this project midway and having the patience for teaching me; most of all, thank you for your incredible and unconditional support, particularly at (frequent) times when I doubted myself and my work.

To Professor Salette Reis, thank you for allowing me to work in your laboratory and conduct my biophysics experiments there. I also have to thank the MB2 group for making me feel welcome, in particular Ana Rute Neves, for her friendship and for all the help she provided me, as well as Ana Joyce, Isabel Barbosa and João Alburquerque for their companionship!

To Professor Fátima Nogueira, thank you so much for kindly welcoming me in your laboratory and for very patiently and introducing me to the world of biologists. It was a great pleasure working with and learning from you!

To Professor Xavier Fernández-Busquets, thank you for generously accepting me in your laboratory like one of your own and for all your kindness and wisdom. I'm also deeply grateful to the Nanomalaria team, particularly Arnau, Elena, Eli and Lucia: I know that I was a pretty big load on your back and you were invaluably helpful and generous to me! The work I developed at IBEC was vital for this thesis and it wouldn't have been possible without you!

I also have to genuinely thank Professor David Andreu for having me in his laboratory and patiently supporting me and providing me with the means to accomplish my ever changing plans!

A deep ‘Thank you!’ to Javi and Sira: you were super thoughtful and helped me immensely. Sira, thank you so much for helping me with SPR and I’m sorry for constantly putting pressure on you… I’m thankful for all your help, but also to have met you, you’re amazing! To you, Clara, Maria, Mar, Javi, Dani, Sergi – I miss you like hell! I miss the volleyball tournament, my attempts to go to the gym with you, nuestras birras, vuestro Catalán (que no entiendo, pero me encanta…)… You’ve made me feel at home and I’m super lucky I got to meet you all.

I deeply thank Doutora Zélia for her patience, her thoughtfulness and promptness to help me!

To Sara and Marco: there’s so much I’d like to say, but I’m at a loss for words. Meeting you was the best thing that could have happened to me in Barcelona. I miss you every day and I wish we could go back in time just for a week!

To Gabi, mi granadina favorita y mi familia en Barcelona! I was so lucky to have landed in your place :)

To my chemist friends – who are more my ‘beer friends’ these days, for our parties, our nights out, our quiz nights, for Paredes de Coura, for everything! You are amazing :)

To Samuel, thank you for being there from the beginning and for your unconditional love and support!

A major acknowledgement goes to the crew from Laboratory 2.28 (and honorary members), for - regardless where I was, I’d always look forward to come back ‘home’. I’ll always carry in my heart our Christmas videos, our laughters, our Spotify playlists and our lunches/dinners/nights out - your friendship, above all! No matter how bad my work got or how desperate I was sometimes (and insufferable, sorry about that…!), you could always make me laugh and keep me hopeful. So a big ‘Thank you!’ to Cláudia, Ana, Cátia, Mariana, Mafalda, MELANIE (I owe you big time, you are amazing!), Ricardo, Vânia, Filipa, Natália and Rita.

I also have to thank my family: to my brother, to Mafalda – for all the help she has given me, to my grandmother Magui, for her love and interest and (incredibly disproportionate) admiration for my work, to my grandmother Lourdes, for her unconditional love and support (despite having no clue of what on earth I was doing…) and, most of all, to my parents. You are phenomenal people and, with absolutely no doubt, the best parents I could have had. Thank you for all your patience and understanding, particularly during more frustrating times, for all the love you give me every day and for setting a great example for me to follow.

To Laura, Ana and Cátia: you know… <3

Abstract

Malaria is a vector-borne parasitic disease, caused by parasites of the genus *Plasmodium*. It is one of the most severe parasitic infections worldwide: despite the efforts to eradicate it, in 2017, 219 million cases were reported and, ultimately, 435 000 people died from the disease, mostly young children.

While there is a wide arsenal of antimalarial drugs approved for the treatment of malaria, factors such as widespread drug-resistant *Plasmodium* strains, complexity of the parasite's life cycle and lack of affordable and effective new drugs, emphasize the need for novel classes of antimalarials, and/or for new strategies to modify existing ones, to tackle drug-resistant *Plasmodium* strains.

With the advent of cell-penetrating peptides as vehicles for the intracellular delivery of different types of cargos, and considering that some of these peptides have been reported as particularly interesting in the field of antimalarial therapy, this project envisaged the development of drug-peptide conjugates as an opportunity for rescuing classical antimalarial drugs, such as chloroquine, primaquine or mepacrine. Considering that chloroquine is one of the cheapest and safest classical antimalarials ever, eventually losing efficacy due widespread chloroquine-resistant *Plasmodium* strains, rescuing of this antimalarial drug upon conjugation to selected cell penetrating peptides was prioritized.

In connection with the above, a first approach was based on the chemical synthesis of a chloroquine analogue, which incorporated a free primary amine group that was subsequently used for conjugation to the *N*-termini of several peptides through a butanedioyl spacer; this generated a fairly large set of chloroquine-peptide conjugates, which were screened for their *in vitro* activity against blood-stage parasites of a chloroquine-resistant *Plasmodium falciparum* strain. The conjugate with cell penetrating peptide TP10, formerly reported to have intrinsic antimalarial activity, was the one displaying the highest antiplasmodial activity of all conjugates assayed. Still, this conjugate was not as active as the parent antimalarial drug alone.

Having hypothesized that the above result might be due to an unsuitable choice of drug-peptide linker, in a second approach, a new set of chloroquine-TP10 conjugates – differing on the linker between chloroquine and TP10, was prepared. In addition, the influence of the relative position of the drug *versus* peptide*, i.e.,* drug coupled either to the *N*- or *C*-terminus of the peptide, was also evaluated. The new set of conjugates thus produced was next screened *in vitro* for their ability to inhibit the growth of intraerythrocytic parasites of the *P. falciparum* strain 3D7 (chloroquine-sensitive), and also for their hemolytic activity. It was concluded that drug conjugation to the peptide's *N*-terminus results in improved antiplasmodial activity as compared to the parent peptide, regardless of the linker used; in turn, modifying the peptide's *C*-terminal region was damaging for its antimalarial activity. However, while both parent building blocks, peptide and drug, were not hemolytic at the concentrations assayed, conjugates revealed a significantly increased hemolytic character, which was particularly apparent when the drug was conjugated at the peptide's *C*-terminus. Noteworthy, all tested conjugates were visibly more hemolytic for cultures of healthy erythrocytes than for cultures with parasitized erythrocytes.

In the aftermath of the above results, it became important to gain a deeper insight into the different behavior of the conjugates towards membranes of healthy *versus* parasitized red blood cells. Hence, the interactions of two chloroquine-TP10 conjugates, and of their parent building blocks, with lipid model membranes (liposomes) simulating both healthy (zwitterionic DMPC vesicles) and parasitized erythrocytes (anionic DMPG vesicles), were studied. To this end, a toolbox of biophysical techniques, encompassing dynamic light scattering, UV-Vis derivative spectrophotometry, and surface plasmon resonance, was employed. While the partition coefficients of these peptides were fairly similar for both DMPC and DMPG vesicles (UV-Vis derivative spectrophotometry), surface plasmon resonance studies revealed that the conjugates had higher affinity towards anionic DMPG membranes, as expected, but were more disruptive towards zwitterionic DMPC vesicles (results substantiated by dynamic light scattering assays). Relevantly, although model membranes used in this assessment present several limitations as mimics of real erythrocyte membranes, these findings did correlate with results from *in vitro* assays.

The aforementioned constraints of DMPC and DMPG vesicles as mimics of membranes from, respectively, healthy and parasitized erythrocytes, prompted us to engage into further studies using healthy and parasitized erythrocytes. To this end, fluorescently labeled conjugates and parent TP10 were synthesized and their behavior in a parasitized culture (having both healthy and parasitized red blood cells) was monitored through fluorescence microscopy and fluorescence-assisted cell sorting analysis. Observation of the cell cultures revealed an overall lack of selectivity of the test compounds towards healthy *versus* parasitized cells, as internalization was observed in both cases. Moreover, cells which were internalized by the conjugates exhibited extremely thinned membranes, but it remains to be determined if this membrane damage

is a cause for, or a consequence of, conjugate internalization. Fluorescence-assisted cell sorting analysis showed that, both fluorescently labeled TP10 and its chloroquine conjugate internalized parasitized erythrocytes to similar overall levels, but the conjugate internalized a much larger proportion of healthy *versus* parasitized cells. Again, these results support data from *in vitro* hemolysis assays and suggest that, upon conjugation to the drug, TP10 becomes disruptive towards membranes, instead of acting as a cell-penetrating peptide - at least in what concerns human red blood cells.

The global outcome of the above efforts to improve the therapeutic efficacy of a blood-stage antimalarial drug, upon conjugation with cell penetrating peptides, was not as promising as expected. As such, one last approach was tested to investigate whether or not conjugation of cell penetrating peptides would be an interesting tool to rescue classical antimalarials acting on other than blood-stage parasites. To this end, several cell penetrating peptides were coupled to the antimalarial drug primaquine, and the resulting conjugates were screened *in vitro* for their ability to inhibit liver-stage development of *P. berghei* parasites. Similarly to previous observations with chloroquine conjugates, only conjugation to TP10 and its parent peptide, Transportan, resulted in considerable activity *in vitro* against liver-stage parasites. Relevantly, the TP10 conjugate was more active than the parent antimalarial drug alone. Moreover, primaquine-peptide conjugates were generally non-toxic to hepatocytes, the host cells for liver-stage parasites. Hence, primaquine conjugation to cell penetrating peptides, as a tool to enhance antimalarial action on exoerythrocytic stages of infection, seems to deserve further attention in the near future.

Altogether, findings made throughout this work demonstrate that, at least in what concerns antimalarial aminoquinolines, conjugation to any given cell penetrating peptide does not work as a universal tool for improvement of intracellular targeting and therapeutic activity. Our data show that the specific amino acid sequence of the peptide, rather than its size or net charge, determines its activity against both blood- and liver-stage parasites. Hence, a general peptide structure-activity relationship cannot be drawn with data gathered thus far, which makes it difficult to design next generation peptide carriers for this particular application. Also, it is clear that the peculiarities of both intraerythrocytic parasites and their host cells lead to unexpected and undesired effects in the case of blood-stage infection, where a general lack of selectivity was observed. In turn, primaquine conjugates tested on liver-stage infection showed an activity improvement over their parent building blocks, without apparent cytotoxicity, which renders them worthy of further investigation.

Keywords:

Malaria, Cell-penetrating peptides, Antimalarial drug, Peptide-drug conjugates, Model membranes, Dynamic light scattering, Surface plasmon resonance, Fluorescence microscopy, Flow cytometry, *Plasmodium*-infected erythrocytes.

Resumo

A malária, ou paludismo, é uma doença infecciosa transmitida por mosquitos, causada por parasitas do género *Plasmodium*. Apesar de todos os esforços conduzidos para erradicar esta doença, a malária é, ainda hoje, uma das mais graves infeções parasitárias a nível mundial: só em 2017, foram reportados 219 milhões de casos, que levaram à morte cerca de 435 000 pessoas, na sua maioria crianças com menos de cinco anos de idade.

Ainda que exista um grande número de fármacos aprovados para o tratamento da malária, fatores como (i) o rápido aparecimento de estirpes de *Plasmodium* resistentes aos tratamentos existentes, (ii) a complexidade do ciclo de vida do parasita e (iii) a escassez de novas moléculas que conjuguem eficácia contra a malária e baixo custo de produção, evidenciam a necessidade de procurar novas estratégias para combater o parasita.

O desenvolvimento de péptidos penetradores celulares como potenciais veículos para a entrega intracelular de diversos tipos de moléculas, alguns dos quais descritos como tendo particular interesse no âmbito da terapia da malária, está subjacente ao surgimento do presente projeto doutoral, centrado na conjugação desses péptidos a fármacos antimaláricos clássicos, como a cloroquina, a primaquina ou a mepacrina. Desta forma, visou-se testar se a ligação de péptidos penetradores celulares a tais fármacos permitiria melhorar os respetivos índices terapêuticos, eventualmente por aumento da sua biodisponibilidade e/ou por escape a mecanismos de resistência parasitária. A cloroquina, um dos agentes antimaláricos mais baratos e seguros de sempre, deixou de ser um fármaco de primeira linha – especialmente em África – devido ao desenvolvimento de estirpes resistentes de *Plasmodium*. Assim, considerou-se o prioritário o resgate deste fármaco, pelo que a sua conjugação a diferentes péptidos penetradores celulares, e avaliação da atividade dos conjugados obtidos, constituiu o cerne do trabalho aqui descrito.

Uma primeira abordagem consistiu na síntese química de um análogo da cloroquina que possuísse uma amina primária, passível de ser conjugada ao aminoácido *N*-terminal dos diferentes péptidos selecionados, através de um espaçador butanodioílo. Nesta fase, um vasto conjunto de conjugados péptido-cloroquina foram produzidos e, posteriormente, avaliados *in vitro* quanto à sua capacidade de inibição do crescimento, na fase sanguínea, de uma estirpe de *Plasmodium* resistente à cloroquina. Desta

avaliação, constatou-se que a conjugação da cloroquina ao péptido TP10, previamente descrito como tendo atividade antimalárica intrínseca, resultou no conjugado mais ativo. A atividade deste conjugado foi superior à dos péptidos penetradores celulares livres, mas inferior à da cloroquina livre.

Tendo-se avançado a hipótese de ser possível melhorar a atividade antimalárica do conjugado cloroquina-TP10 através da utilização de espaçadores eventualmente mais adequados, uma segunda abordagem consistiu na síntese de novos conjugados cloroquina-TP10 em que este espaçador foi variado. Adicionalmente, avaliou-se a influência da posição de inserção do fármaco relativamente à cadeia peptídica – isto é, de que forma seria afetada a atividade antimalárica conforme o fármaco fosse conjugado na zona *N*- ou *C*-terminal do péptido. Para tal, foram também sintetizados dois conjugados TP10-cloroquina, num deles mantendo o espaçador estável butanodioílo e no outro um espaçador quimio-/bio-reversível persulfureto (ponte dissulfureto). Esta nova família de conjugados fármaco-péptido foi avaliada *in vitro* quanto à sua (i) capacidade de inibir o crescimento de parasitas intraeritrocíticos da estirpe 3D7 (sensível à cloroquina) e (ii) atividade hemolítica. Deste estudo, concluiu-se que a conjugação do fármaco na região *N*-terminal do péptido TP10 resulta invariavelmente numa melhoria de atividade antimalárica em comparação com o péptido livre, independentemente do espaçador utilizado; por outro lado, a modificação do péptido na região *C*-terminal conduz a uma perda de atividade. Contudo, apesar de fármaco e péptido livres não serem hemolíticos às concentrações testadas, os respetivos conjugados apresentaram atividade hemolítica significativa, que se acentuou quando a cloroquina foi inserida na região *C*-terminaldo péptido TP10. É de realçar que todos os conjugados se revelaram significativamente mais hemolíticos em culturas de eritrócitos saudáveis, do que em culturas parasitadas (com eritrócitos saudáveis e parasitados).

Na sequência destes resultados, tornou-se importante tentar perceber o diferente comportamento dos conjugados sintetizados perante eritrócitos saudáveis e parasitados. Assim, decidiu-se estudar as interações de dois dos conjugados cloroquina-TP10, bem como do fármaco e péptido livres, com membranas modelo (lipossomas) – simulando eritrócitos saudáveis (vesículas zwiteriónicas de DMPC) e parasitados (vesículas aniónicas de DMPG). Para o efeito, recorreu-se a um conjunto de técnicas biofísicas, incluindo dispersão dinâmica de luz, espectrofotometria derivativa de ultravioleta-visível e ressonância plasmónica de superfície. Apesar de o coeficiente de partição dos compostos analisados (determinado por espectrofotometria derivativa de ultravioleta-visível) ser bastante semelhante para ambas as membranas modelo, estudos por ressonância plasmónica de superfície revelaram que os péptidos estudados apresentam uma maior afinidade para os modelos aniónicos, como esperado, mas promovem uma maior perturbação dos modelos zwiteriónicos, resultados estes que foram corroborados por dispersão dinâmica de luz. É de salientar que, apesar de os modelos utilizados neste estudo apresentarem diversas limitações como simuladores de membranas eritrocíticas, as observações decorrentes destes estudos apresentaram-se coerentes com os resultados de atividade hemolítica *in vitro*.

Considerando o caráter simplista de vesículas de DMPC e DMPG enquanto modelos de membranas de eritrócitos saudáveis e parasitados, decidiu-se avançar para estudos adicionais, utilizando eritrócitos humanos saudáveis e parasitados. Para isso, sintetizaram-se derivados fluorescentes do péptido TP10 e do seu conjugado mais ativo com cloroquina e monitorizou-se o comportamento destes compostos em culturas parasitadas (contendo células saudáveis e infetadas), aplicando microscopia de fluorescência e citometria de fluxo. A observação das culturas celulares por microscopia de fluorescência revelou uma aparente ausência de seletividade dos compostos testados para eritrócitos saudáveis relativamente a parasitados, na medida em que se detetou internalização em ambos os tipos de células. Adicionalmente, verificou-se que as células internalizadas apresentavam membranas extremamente finas, se bem que não foi possível estabelecer se tal fragilização das membranas será causa, ou consequência, do processo de internalização. A análise das culturas celulares por citometria de fluxo demonstrou que ambos os compostos, péptido livre e seu conjugado com cloroquina, internalizavam as células parasitadas em proporções semelhantes; no entanto, o conjugado internalizava uma porporção muito maior de células saudáveis do que o péptido livre. Estes resultados suportam, novamente, a informação obtida com os ensaios de hemólise *in vitro* e sugerem que, uma vez conjugado à cloroquina, o TP10 parece passar a ter uma ação mais do tipo membranolítico do que penetrador celular.

Em geral, a tentativa de melhorar o índice terapêutico de um fármaco antimalárico dirigido à fase sanguínea, como a cloroquina, por conjugação desta a um péptido penetrador celular, revelou-se infrutífera. Assim, projetou-se uma última abordagem, com o intuito de investigar se a estratégia de conjugação a péptidos penetradores celulares seria interessante para resgatar fármacos antimaláricos clássicos que atuem numa fase que não a sanguínea. Para tal, diversos péptidos penetradores celulares foram acoplados à primaquina, e os conjugados daí resultantes foram avaliados *in vitro* quanto à sua capacidade de inibir o desenvolvimento de formas intra-hepáticas de parasitas *P. berghei*. Tal como observado para os conjugados cloroquina-péptido, apenas a conjugação da primaquina com o péptido TP10 ou com o péptido parental deste, o Transportan, resultou numa melhoria considerável de atividade

in vitro contra parasitas na fase hepática. Foi mesmo possível superar a atividade da própria primaquina, por conjugação desta ao péptido TP10. Para além disso, os conjugados testados revelaram-se inócuos para hepatócitos, as células hospedeiras das formas hepáticas de parasitas *Plasmodium*. Assim, a conjugação de péptidos penetradores celulares à primaquina, como uma estratégia de melhoria da ação antimalárica deste fármaco, parece merecer atenção adicional num futuro próximo.

De um modo geral, os resultados obtidos ao longo deste trabalho evidenciam que, pelo menos no que respeita a aminoquinolinas antimaláricas, a conjugação a péptidos penetradores celulares não é uma estratégia universal para melhoria da entrega intracelular e atividade terapêutica. A informação reunida sugere que a sequência de aminoácidos de um péptido, e não tanto o seu tamanho ou carga global, determina a sua atividade nas fases sanguínea e hepática da infeção; ainda assim, não foi possível elucidar uma relação estrutura-atividade, o que dificulta a conceção e desenvolvimento de uma nova geração de péptidos para este propósito em particular. Para além disso, ficou claro que as peculiaridades do parasita intraeritrocítico e da célula hospedeira conduzem a efeitos inesperados e indesejados no caso de uma infeção na fase sanguínea, onde se observou a ausência de seletividade. Por outro lado, os conjugados primaquina-péptido avaliados na fase hepática demonstraram uma melhor atividade, relativamente ao péptido e fármaco livres, sem aparente toxicidade, o que nos leva a crer que estes compostos são merecedores de estudos adicionais.

Palavras-Chave:

Malária, Péptidos-penetradores celulares, Antimaláricos, Conjugados péptido-fármaco, Membranas modelo, Microscopia de fluorescência, Citometria de fluxo, Biofísica.

Table of Contents

Acknowledgments …… i
Abstract …… v
Resumo …… ix
Table of Contents …… xv
List of Figures …… xxi
List of Schemes …… xxxi
List of Tables …… xxxiii
List of Graphics …… xxxv
Abbreviations …… xxxvi

1. Malaria: a pressing affair …… 1

- 1.1. Malaria …… 3
- 1.2. The Plasmodium parasite …… 4
- 1.3. Clinical features of malaria and current measures for its control …… 6
- 1.4. Antimalarial chemotherapy …… 8
  - 1.4.1. Brief historical overview …… 8
  - 1.4.2. Antimalarial drugs approved for clinical use …… 11
- 1.5. Novel strategies for the battle against malaria …… 14
  - 1.5.1. Malaria vaccines …… 14
  - 1.5.2. Nanovectors for antimalarial drug delivery …… 15
  - 1.5.3. Peptide-based strategies …… 16
    - 1.5.3.1. Antimicrobial peptides …… 16
    - 1.5.3.2. Cell-penetrating peptides …… 17
- 1.6. Bibliography …… 19

2. Rationale …… 29

- 2.1. Working hypothesis …… 31
- 2.2. Choice of the peptide carriers …… 31
- 2.3. Choice of the AM cargoes …… 32
  - 2.3.1. Chloroquine …… 32
  - 2.3.2. Primaquine …… 33
- 2.4. Bibliography …… 35

3. Goals ………………………………………………………………………... 39

4. Synthesis of CQn-C4-CPP conjugates and evaluation of their in vitro activity against blood-stage malaria ……………………………………….. 43

- 4.1. Overview 45
- 4.2. Chemical synthesis 45
  - 4.2.1. Synthesis of 4-(*N*-aminobutyl)amino-7-chloroquinoline (CQn) 46
  - 4.2.2. Synthesis of 4-[*N*-(*N'*-carboxypropanoyl)aminobutyl]amino-7-chloroquinoline (CQn-C4) ……………………………………….. 48
  - 4.2.3. Synthesis of the selected CPP …………………………………. 50
    - 4.2.3.1. The peptide bond ……………………………………… 50
    - 4.2.3.2. Basic principles of solid-phase peptide synthesis (SPPS) …………………………………………………….. 52
    - 4.2.3.3. Peptides' synthesis via SPPS ………………………... 60
  - 4.2.4. Synthesis of the target CQn-C4-CPP conjugates ……………. 61
- 4.3. In vitro assays …………………………………………………………….. 63
- 4.4. Experimental Section …………………………………………………….. 65
  - 4.4.1. Materials, instrumentation and general methods …………….. 65
  - 4.4.2. Synthesis of CQn ……………………………………………….. 66
  - 4.4.3. Derivatization of CQn with succinic anhydride ………………... 66
  - 4.4.4. Solid phase synthesis …………………………….…………….. 67
    - 4.4.4.1. Preparation of the resin ……………………………….. 67
    - 4.4.4.2. Assembly of peptide chains on solid phase ………… 68
  - 4.4.5. On resin coupling of CQn-C4 to the peptides' *N*-termini …….. 68
  - 4.4.6. Cleavage of CPP and respective CQn-C4-CPP conjugates ... 69
  - 4.4.7. *In vitro* assays …………………………………………………. 87
- 4.5. Bibliography ……………………………………………………………….. 88

5. Synthesis and in vitro evaluation of CQn-TP10 conjugates linked through different spacers …………………………………………………….. 93

- 5.1. Overview ………………………………………………………………….. 95
- 5.2. Chemical synthesis ………………………………………………………. 97
  - 5.2.1. CQn-C10-TP10 (15) ……………………………………………... 97

5.2.2. CQn-TR-TP10 (16) ……………………………………………… 99
5.2.2.1. Azide-alkyne coupling: a central piece of the synthetic route ………………………………………… 99
5.2.2.2. Synthesis of CQn-N_3 (23) …………………………….. 102
5.2.2.3. Synthesis of intermediate 42 and of target conjugate CQn-TR-TP10 (16) …………………………………….. 103
5.2.3. CQn-S-S-TP10 (17) ……………………………………………… 105
5.2.3.1. Disulfide bonds and thiol-disulfide exchange reactions ………………………………………………… 107
5.2.3.2. Synthesis of CQn-Cys (34) …………………………… 107
5.2.3.3. Synthesis of Cys(NPys)-TP10 (36) ………………….. 109
5.2.3.4. Synthesis of the target CQn-S-S-TP10 conjugate (17) via a TDER ……………………………………….. 110
5.2.4. TP10-C4-CQn (18) ……………………………………………… 113
5.2.5. TP10-S-S-CQn (19) ……………………………………………… 116
5.2.5.1. Synthesis of CQn-Cys-TP (41) ……………………… 118
5.2.5.2. Synthesis of TP10-Cys (40) and of target conjugate TP10-S-S-CQn (19) …………………………………… 119
5.3. In vitro assays …………………………………………………………….. 121
5.4. Experimental section ……………………………………………………... 124
5.4.1. Materials, instrumentation and general methods …………….. 124
5.4.2. Synthesis of CQn-C10-TP10 (32) ……………………………… 124
5.4.3. Synthesis of CQn-TR-TP10 (16) ………………………………. 125
5.4.4. Synthesis of CQn-S-S-TP10 (17) ………………………………. 126
5.4.5. Synthesis of TP10-C4-CQn (18) ………………………………. 128
5.4.6. Synthesis of TP10-S-S-CQn (19) ………………………………. 129
5.4.7. Growth Inhibition Assays ……………………………………….. 130
5.4.8. Hemolysis assays ………………………………………………... 131
5.5. Bibliography ……………………………………………………………….. 132

6. Study of the interactions between CQn-TP10 conjugates and lipid model membranes …………………………………………………………….. **137**

6.1. Overview …………………………………………………………………... 139
6.2. Concise presentation of relevant phenomena and techniques ……… 139

6.2.1. Modifications on the lipid domain of host RBC's upon Plasmodium invasion ………………………………………………. 139
6.2.2. Membrane model systems ……………………………………… 140
6.2.3. Dynamic light scattering in the study of drug-liposome interactions ……………………………………………………….. 142
6.2.4. UV-Vis derivative spectrophotometry to quantify partition into membranes ……………………………………………………….. 144
6.2.5. Surface plasmon resonance …………………………………… 146
6.3. Results and discussion ………………………………………………... 149
6.3.1. Influence of CQn-TP10 conjugates on lipid model membranes ……………………………………………………….. 149
6.3.2. Compounds partition between aqueous medium and lipid membranes ……………………………………………………….. 151
6.3.3. Binding affinity between TP10 and its conjugates and model membranes ……………………………………………………….. 152
6.4. Experimental procedures ……………………………………………… 156
6.4.1. Preparation of the vesicles ……………………………………… 156
6.4.2. Determination of vesicles size ………………………………….. 157
6.4.3. Determination of phase transition temperature and cooperativity ……………………………………………………… 157
6.4.4. Determination of *K*p by UV-Vis Derivative Spectrophotometry 157
6.4.5. Surface Plasmon Resonance …………………………………... 157
6.5. Bibliography ………………………………………………………………. 159

7. Insights into conjugates and parent peptide interactions with both healthy and parasitized human erythrocytes …………………………….. 163

7.1. Overview ………………………………………………………………... 165
7.2. Synthesis of fluorescently-labelled peptides and their conjugates ….. 165
7.3. Fluorescence-based studies ………………………………………….. 171
7.3.1. Fluorescence microscopy ……………………………………….. 171
7.3.2. Fluorescence-assisted cell sorting analysis (FACS) …………. 175
7.4. Experimental procedures ……………………………………………… 178
7.4.1. Synthesis of TP10-K-CF ………………………………………… 178
7.4.2. Synthesis of CQn-C4-CPP-K-CF ………………………………. 179
7.4.3. Fluorescence microscopy ……………………………………….. 180

7.4.4. FACS analysis ………………………………………………… 180
7.5. Bibliography ……………………………………………………….. 181

8. Application of the cell penetrating peptide conjugation strategy to the liver-stage antimalarial drug primaquine ……………………………... 183

8.1. Overview ………………………………………………………….... 185
8.2. Chemical Synthesis ……………………………………………… 186
8.2.1. PQ-C4-CPP conjugates ………………………………………… 186
8.2.1.1. Synthesis of *N*^{4}-(6-methoxyquinolin-8-yl)pentane-1,4-diamine (PQ-C4) ……………………………..... 187
8.2.1.2. Synthesis of the PQ-C4-CPP conjugates …………… 188
8.2.2. TP10-S-S-PQ conjugate ………………………………………… 190
8.2.2.1. Synthesis of PQ-Cys (69) …………………………….. 191
8.2.2.2. Synthesis of PQ-Cys(TP) (71) ……………………….. 192
8.2.2.3. Synthesis of the target TP10-S-S-PQ conjugate (68) via a TDER …………………………………………... 193
8.3. *In vitro* assays ……………………………………………………….. 195
8.4. Experimental Section …………………………………………….. 198
8.4.1. Materials, instrumentation and general methods …………….. 198
8.4.2. Extraction of Primaquine ………………………………………… 198
8.4.3. Derivatization of PQ with succinic anhydride …………………. 198
8.4.4. Peptides’ synthesis ………………………………………………. 198
8.4.5. Modification of peptides’ *N*-terminus with PQ-C4 …………….. 199
8.4.6. Peptides and PQ-C4-CPP conjugates’ cleavage …………….. 199
8.4.7. Synthesis of TP10-S-S-PQ ……………………………………… 205
8.4.8. *In vitro* assays …………………………………………………… 207
8.5. Bibliography ……………………………………………………….. 208

9. Final remarks and future perspectives …………………………………….. 211

List of Figures

Figure 1.1 – Geographical distribution of Malaria. Countries with 3 consecutive years of zero indigenous cases are considered to have eliminated malaria (represented in green). …………………………………………………………….. 4

Figure 1.2 – Life cycle of the *Plasmodium* parasite. ………………………………. 6

Figure 1.3 – Structure of Quinine. …………………………..……………………. 8

Figure 1.4 – Structures of Pamaquine and Primaquine. …………………………. 9

Figure 1.5 – Structure of Chloroquine. ……………………………………………… 9

Figure 1.6 – Structures of sulfadoxine, pyrimethamine and mefloquine. ………. 10

Figure 1.7 – Chemical structure of artemisinin and three of its derivatives: artesunate, dihydroartemisinin and artemether. …………………………………… 11

Figure 1.8 – Chronology of AM introduction for malaria chemotherapy (in blue) and first report of *Plasmodium* resistance to corresponding AM (in red). ………… 14

Figure 2.1 – Structures of CQ and its analogue, CQn, used henceforward for the synthesis of CQ-CPP conjugates. ……………………………………………… 33

Figure 4.1 – ESI-IT MS spectrum (positive mode) of CQn (**2**). …………………. 46

Figure 4.2 – ESI-IT MS spectrum (positive mode) of CQn-C4. …………………. 46

Figure 4.3 – Chemical structure of HBTU (**10**) and PyBOP (**11**) ……………….. 57

Figure 4.4 – Structure of Fmoc-Rink Amide MBHA Resin (the letter "P" represents the polymer PS-DVB). …………………………..……………………. 61

Figure 4.5 – Experimental setup applicable to manual SPPS. ………………….. 67

Figure 4.6 - Spectrum (ESI-IT MS, positive mode) obtained for crude TP10. … 70

Figure 4.7 – Chromatogram obtained from the analysis of TP10 after purification, with a gradient elution of 0-100% ACN in water (0,05% TFA) in a RP-18E (5 μm), for 30 minutes and a flow of 1 ml/min, with detection at λ = 220 nm. …………………………..…………………………..……………………... 70

Figure 4.8 - Spectrum (ESI-IT MS, positive mode) obtained for crude DPT-sh1 71

Figure 4.9 – Chromatogram obtained from the analysis of DPT-sh1 after purification, with a gradient elution of 0-100% ACN in water (0,05% TFA) in a RP-18E (5 μm), for 30 minutes and a flow of 1 ml/min, with detection at λ = 220 nm. …………………………..…………………………..……………………... 71

Figure 4.10 - Spectrum (ESI-IT MS, positive mode) obtained for crude DPT-sh2 72

Figure 4.11 – Chromatogram obtained from the analysis of DPT-sh2 after purification, with a gradient elution of 0-100% ACN in water (0,05% TFA) in a RP-18E (5 μm), for 30 minutes and a flow of 1 ml/min, with detection at λ = 220 nm. ……………………………………………………………………………………... 72

Figure 4.12 - Spectrum (ESI-IT MS, positive mode) obtained for crude IDR-1018. ………………………………………………………………………………...... 73

Figure 4.13 – Chromatogram obtained from the analysis of IDR-1018 after purification, with a gradient elution of 0-100% ACN in water (0,05% TFA) in a RP-18E (5 μm), for 30 minutes and a flow of 1 ml/min, with detection at λ = 220 nm. ……………………………………………………………………………………...... 73

Figure 4.14 - Spectrum (ESI-IT MS, positive mode) obtained for crude TAT……. 74

Figure 4.15 – Chromatogram obtained from the analysis of TAT after purification, with a gradient elution of 0-100% ACN in water (0,05% TFA) in a RP-18E (5 μm), for 30 minutes and a flow of 1 ml/min, with detection at λ = 220 nm. ……………………………………………………………………………………...... 74

Figure 4.16 - Spectrum (ESI-IT MS, positive mode) obtained for crude PasTAT 75

Figure 4.17 – Chromatogram obtained from the analysis of PasTAT after purification, with a gradient elution of 0-100% ACN in water (0,05% TFA) in a RP-18E (5 μm), for 30 minutes and a flow of 1 ml/min, with detection at λ = 220 nm. ……………………………………………………………………………………...... 75

Figure 4.18 - Spectrum (ESI-IT MS, positive mode) obtained for crude Transportan. ……………………………………………………………………… 76

Figure 4.19 – Chromatogram obtained from the analysis of Transportan after purification, with a gradient elution of 0-100% ACN in water (0,05% TFA) in a RP-18E (5 μm), for 30 minutes and a flow of 1 ml/min, with detection at λ = 220 nm. ……………………………………………………………………………………...... 76

Figure 4.20 - Spectrum (ESI-IT MS, positive mode) obtained for crude Penetratin. ……………………………………………………………………… 77

Figure 4.21 – Chromatogram obtained from the analysis of Penetratin after purification, with a gradient elution of 0-100% ACN in water (0,05% TFA) in a RP-18E (5 μm), for 30 minutes and a flow of 1 ml/min, with detection at λ = 220 nm. ……………………………………………………………………………………...... 77

Figure 4.22 - Spectrum (ESI-IT MS, positive mode) obtained for crude CQn-C4-TP10. ………………………………………………………………………………...... 78

Figure 4.23 – Chromatogram obtained from the analysis of CQn-C4-TP10 after purification, with a gradient elution of 0-100% ACN in water (0,05% TFA) in a RP-18E (5 µm), for 30 minutes and a flow of 1 ml/min, with detection at λ = 220 nm. …………………..…………………..…………………..……………………….. 78

Figure 4.24 - Spectrum (ESI-IT MS, positive mode) obtained for crude CQn-C4-DPT-sh1. …………………..…………………..…………………..…………………… 79

Figure 4.25 – Chromatogram obtained from the analysis of CQn-C4-DPT-sh1 after purification, with a gradient elution of 0-100% ACN in water (0,05% TFA) in a RP-18E (5 µm), for 30 minutes and a flow of 1 ml/min, with detection at λ = 220 nm. …………………..…………………..…………………..…………………….. 79

Figure 4.26 - Spectrum (ESI-IT MS, positive mode) obtained for crude CQn-C4-DPT-sh2. …………………..…………………..…………………......................... 80

Figure 4.27 – Chromatogram obtained from the analysis of CQn-C4-DPT-sh2 after purification, with a gradient elution of 0-100% ACN in water (0,05% TFA) in a RP-18E (5 µm), for 30 minutes and a flow of 1 ml/min, with detection at λ = 220 nm. …………………..…………………..…………………..…………………….. 80

Figure 4.28 - Spectrum (ESI-IT MS, positive mode) obtained for crude CQn-C4-IDR-1018 …………………..…………………..…………………......................... 81

Figure 4.29 – Chromatogram obtained from the analysis of CQn-C4-IDR-1018 after purification, with a gradient elution of 0-100% ACN in water (0,05% TFA) in a RP-18E (5 µm), for 30 minutes and a flow of 1 ml/min, with detection at λ = 220 nm. …………………..…………………..…………………..…………………….. 81

Figure 4.30 - Spectrum (ESI-IT MS, positive mode) obtained for crude CQn-C4-TAT. …………………..…………………..…………………..……………………… 82

Figure 4.31 – Chromatogram obtained from the analysis of CQn-C4-TAT after purification, with a gradient elution of 0-100% ACN in water (0,05% TFA) in a RP-18E (5 µm), for 30 minutes and a flow of 1 ml/min, with detection at λ = 220 nm. …………………..…………………..…………………..…………………........ 82

Figure 4.32 - Spectrum (ESI-IT MS, positive mode) obtained for crude CQn-C4-PasTAT. …………………..…………………..…………………..……………………. 83

Figure 4.33 – Chromatogram obtained from the analysis of CQn-C4-PasTAT after purification, with a gradient elution of 0-66% ACN in water (0,05% TFA) in a RP-18E (5 µm), for 20 minutes and a flow of 1 ml/min, with detection at λ = 220 nm. …………………..…………………..…………………..…………………….. 83

Figure 4.34 - Spectrum (ESI-IT MS, positive mode) obtained for crude CQn-C4-R9. …………………..…………………..…………………..…………………........ 84

Figure 4.35 – Chromatogram obtained from the analysis of CQn-C4-R9 after purification, with a gradient elution of 0-100% ACN in water (0,05% TFA) in a RP-18E (5 µm), for 30 minutes and a flow of 1 ml/min, with detection at λ = 220 nm. …………………..…………………..…………………..……………………....... 84

Figure 4.36 - Spectrum (ESI-IT MS, positive mode) obtained for crude CQn-C4-Transportan. …………………..…………………..…………………..……….......... 85

Figure 4.37 – Chromatogram obtained from the analysis of CQn-C4-Transportan after purification, with a gradient elution of 0-100% ACN in water (0,05% TFA) in a RP-18E (5 µm), for 30 minutes and a flow of 1 ml/min, with detection at λ = 220 nm. …………………..…………………..……………………...... 85

Figure 4.38 - Spectrum (ESI-IT MS, positive mode) obtained for crude CQn-C4-Penetratin. …………………..…………………..…………………..………………… 86

Figure 4.39 – Chromatogram obtained from the analysis of CQn-C4-Penetratin after purification, with a gradient elution of 0-100% ACN in water (0,05% TFA) in a RP-18E (5 µm), for 30 minutes and a flow of 1 ml/min, with detection at λ = 220 nm. …………………..…………………..…………………..…………………….. 86

Figure 5.1 – Structures of CQn-TP10 conjugates **15-19**. ……………………......... 96

Figure 5.2 – Chromatogram obtained from the analysis of CQn-C10-TP10 (**15**) after purification, with a gradient elution of 0-100% ACN in water (0.05% TFA) in a RP-18E (5 µm), for 30 minutes and a flow of 1 ml/min, with detection at λ = 220 nm. …………………..…………………..…………………......................... 98

Figure 5.3 - Spectrum (ESI-IT MS, positive mode) obtained for crude CQn-C10-TP10 (**15**). …………………..…………………..…………………..……………….. 98

Figure 5.4 – Schematic view of a 1,3-dipolar cycloaddition of type 3+2→5. Adapted from [13] …………………..…………………..…………………................ 101

Figure 5.5 - Huisgen's 1,3-dipolar cycloaddition between an alkyne and an organic azide. …………………..…………………..…………………..…………... 101

Figure 5.6 - Spectrum (ESI-IT MS, positive mode) obtained for CQn-N_3 (**23**). 103

Figure 5.7 – Chromatogram obtained from the analysis of CQn-TR-TP10 (**16**) after purification, with a gradient elution of 0-100% ACN in water (0.05% TFA) in a RP-18E (5 µm), for 30 minutes and a flow of 1 ml/min, with detection at λ = 220 nm. …………………..…………………..…………………..…………………….. 104

Figure 5.8 - Spectrum (ESI-IT MS, positive mode) obtained for crude CQn-TR-TP10 (**16**). …………………..…………………..…………………......................... 105

Figure 5.9 - Spectrum (ESI-IT MS, positive mode) obtained for **37**. ……………. 108

Figure 5.10 - Spectrum (ESI-IT MS, positive mode) obtained for **34**. ………….. 109

Figure 5.11 - Spectrum (ESI-IT MS, positive mode) obtained for crude Cys(NPys)-TP10 (**36**). ……………………..……………………..…………………....... 110

Figure 5.12 – Chromatogram obtained from the analysis of CQn-S-S-TP10 (**17**) after purification, with a gradient elution of 0-100% ACN in water (0.05% TFA) in a RP-18E (5 µm), for 30 minutes and a flow of 1 ml/min, with detection at λ = 220 nm. ……………………..……………………..…………………........................... 112

Figure 5.13 - Spectrum (ESI-IT MS, positive mode) obtained for crude CQn-S-S-TP10 (**17**). ……………………..……………………..…………………................... 112

Figure 5.14 - Chromatogram obtained from the analysis of TP10-C4-CQn (**18**) after purification, with a gradient elution of 0-100% ACN in water (0.05% TFA) in a RP-18E (5 µm), for 30 minutes and a flow of 1 ml/min, with detection at λ = 220 nm. ……………………..……………………..……………………..………………….. 115

Figure 5.15 - Spectrum (ESI-IT MS, positive mode) obtained for crude TP10-C4-CQn (**18**). ……………………..……………………..…………………................... 115

Figure 5.16 - Spectrum (ESI-IT MS, positive mode) obtained for CQn-Cys-TP (**41**). ……………………..……………………..……………………..…………………...... 118

Figure 5.17 - Spectrum (ESI-IT MS, positive mode) obtained for TP10-Cys (**40**) 119

Figure 5.18 - Chromatogram obtained from the analysis of TP10-S-S-CQn (**19**) after purification, with a gradient elution of 0-100% ACN in water (0.05% TFA) in a RP-18E (5 µm), for 30 minutes and a flow of 1 ml/min, with detection at λ = 220 nm. ……………………..……………………..…………………........................... 120

Figure 5.19 - Spectrum (ESI-IT MS, positive mode) obtained for TP10-S-S-CQn (**19**). ……………………..……………………..……………………..………………......... 120

Figure 6.1 – Schematic representation of different types of lipid vesicles (liposomes). ……………………..……………………..…………………................... 142

Figure 6.2 – Gel (below *T*m) and fluid (above *T*m) phases of lipid bilayers. ……. 143

Figure 6.3 – Variation of a physical property (e.g. count rate) as a function of *T* 144

Figure 6.4 – Example of corrected absorbance spectra of a compound incubated, at a fixed concentration, with increasing concentrations of lipid vesicles. ……………………..……………………..……………………..…………………… 145

Figure 6.5 – Second derivative spectra of the data presented above (Figure 6.4) 146

Figure 6.6 – Third derivative spectra of the data presented above (Figure 6.4). 146

Figure 6.7 – A typical SPR sensorgram. The sensor chip is equilibrated with running buffer prior to injection; the analyte solution is then injected across the chip at a fixed concentration for the desired association period (in red), which stimulates a response increase owing to analyte binding to the surface-immobilized ligand; the sensor chip is then washed with running buffer and a decrease in response is observed as a result of dissociation of the bimolecular complex (in green); finally, the ligand surface is conveniently regenerated for a new analysis cycle. ………………..………………..……………………......... 148

Figure 6.8 – Schematic view of liposomes immobilized onto the surface of an L1 sensor chip. ………………..………………..………………..………… 148

Figure 6.9 – Hydrodynamic diameter of the lipid vesicles after incubation with increasing concentrations of the compounds (bars) and polydispersion of the liposomes sample (dots)….. 150

Figure 6.10 – Main phase transition temperature (T_m; bars) and cooperativity (B; dots) for DMPC and DMPG alone and in the presence of CQn (20 µM), TP10, CQ-C4-TP10 and CQ-S-S-TP10 (5 µM)... 151

Figure 6.11 - SPR sensorgrams obtained upon injection of 18 µM TP10 (dotted lines) and its CQn conjugates over POPC or POPG bilayers deposited onto a L1 chip surface. Analytes were injected for 180 s and dissociation monitored for 600 s. Peptide-to-lipid ratio (P/L; mol/mol) was calculated by converting SPR response units (*i.e.*, RU) into mass (1RU=1 pg·mm^{-2} of lipid or protein) and into moles. ………………..………………..………………............................. 153

Figure 6.12 - Concentration-response curves determined by calculating P/L at the end of peptide injection (*i.e.,* end of the association phase; t=180 s) for each peptide concentration injected over each lipid bilayer (left); fitted curves using a nonlinear regression equation, dose-response binding with Hill slope (right)……. 154

Figure 6.13 – Sensorgram obtained upon interaction of increasing concentrations of CQn-C4-TP10 with POPC membranes. At 24 and 64 µM, it is possible to observe that this conjugate acts like a "detergent", disrupting membranes and removing them from the sensor chip (negative RU)….………… 154

Figure 6.14 – Sensorgram obtained upon interaction of increasing concentrations of TP10 with POPC membranes. At 64 µM, slight membrane disruption is observed as a decrease in RU during the association phase (< 170 s)..………………..………………..………………..………………......... 155

Figure 7.1 – Chemical structure of 5(6)-carboxyfluorescein ……………….…..... 165

Figure 7.2 – Chromatogram obtained from the analysis of TP10-Lys(CF) (**64**) after purification, with a gradient elution of 0-100% ACN in water (0,05% TFA) in a RP-18E (5 µm), for 30 minutes and a flow of 1 ml/min, with detection at λ = 220 nm. ………………..………………..………………..…………….. 168

Figure 7.3 - Spectrum (ESI-IT MS, positive mode) obtained for crude TP10-Lys(CF) (**64**). …………………..…………………..…………………..……………. 168

Figure 7.4 – Chromatogram obtained from the analysis of CQn-C4-TP10-Lys(CF) (**65**) after purification, with a gradient elution of 0-100% ACN in water (0,05% TFA) in a RP-18E (5 µm), for 30 minutes and a flow of 1 ml/min, with detection at λ = 220 nm. …………………..…………………..…………………..... 169

Figure 7.5 - Spectrum (ESI-IT MS, positive mode) obtained for crude CQn-C4-TP10-Lys(CF) (**65**). …………………..…………………..…………………........... 169

Figure 7.6 – Chromatogram obtained from the analysis of CQn-C4-TAT-Lys(CF) (**66**) after purification, with a gradient elution of 0-100% ACN in water (0,05% TFA) in a RP-18E (5 µm), for 30 minutes and a flow of 1 ml/min, with detection at λ = 220 nm. …………………..…………………..…………………................. 170

Figure 7.7 - Spectrum (ESI-IT MS, positive mode) obtained for crude CQn-C4-TAT-Lys(CF) (**66**). …………………..…………………..…………………............ 170

Figure 7.8 – Interaction of fluorescently labelled TP10 (**64**) with human RBC at 3% parasitemia. TP10 is seen accumulating at the membrane of an erythrocyte that, despite not being parasitized, shows a very thin, almost invisible membrane (“ghost” erythrocyte). …………………..………………….................................. 171

Figure 7.9 – Interaction of fluorescently labelled CQn-C4-TP10 (**65**) with human RBC at 3% parasitemia. **65** is seen accumulating at the membrane of two “ghost” erythrocytes. …………………..…………………..…………………..................... 172

Figure 7.10 – Interaction of fluorescently labelled TP10 (**64**) with human RBC at 3% parasitemia. TP10 (green fluorescence) is seen interacting with a late stage PiRBC (blue staining), which presents a very thin membrane, while ring-stage PiRBC – with apparently healthy membranes, were not internalized by this peptide. …………………..…………………..…………………..………………........ 172

Figure 7.11 – Interaction of fluorescently labelled CQn-C4-TP10 (**65**) with human RBC at 3% parasitemia. Internalization is only visualized (green fluorescence) for one of the two observable PiRBC (blue staining), which is – once again – the one that shows a much thinner membrane. …………………...... 173

Figure 7.12 - Co-localization of a merozoite outside the host cell (blue staining), and fluorescently labelled TP10 (green fluorescence), showing the ability to bind to free parasites. …………………..………………….. 174

Figure 7.13 – Superimposition of green fluorescence from CQn-C4-TP10 (green) with blue fluorescence due to Hoechst-stained DNA from free parasites (burst schizont). …………………..…………………..…………………............... 174

Figure 7.14 – FACS analysis of the interaction of peptide TP10 with hRBC and PiRBC. Upper quadrants (Q1 and Q2) refer to peptide-bound cells (CF fluorescence) and right-hand quadrants (Q2 and Q4) refer to PiRBC (Hoechst fluorescence). Q3 includes hRBC which were not internalized by fluorescently-labelled peptide. …………………..…………………..…………………............... 176

Figure 7.15 - FACS analysis of the interaction of conjugate **64** with hRBC and PiRBC. Upper quadrants (Q1 and Q2) refer to peptide-bound cells (CF fluorescence) and right-hand quadrants (Q2 and Q4) refer to PiRBC (Hoechst fluorescence). Q3 includes hRBC which were not internalized by fluorescently-labelled conjugate. …………………..…………………..…………………............ 176

Figure 7.16 - FACS analysis of the interaction of inactive conjugate **65** with hRBC and PiRBC. Upper quadrants (Q1 and Q2) refer to peptide-bound cells (CF fluorescence) and right-hand quadrants (Q2 and Q4) refer to PiRBC (Hoechst fluorescence). Q3 includes hRBC which were not internalized by fluorescently-labelled conjugate. …………………..…………………................. 177

Figure 8.1 – ESI-IT MS spectrum (positive mode) of PQ-C4 (**67**). ……………... 187

Figure 8.2 – ESI-IT MS spectrum (positive mode) of **70**. ……………………......... 191

Figure 8.3 – ESI-IT MS spectrum (positive mode) of PQ-Cys (**69**). …………… 192

Figure 8.4 – ESI-IT MS spectrum (positive mode) of PQ-Cys(TP) (**71**). ……….. 193

Figure 8.5 - Chromatogram obtained from the analysis of TP10-S-S-PQ (**68**) after purification, with a gradient elution of 0-100% ACN in water (0.05% TFA) in a RP-18E (5 µm), for 30 minutes and a flow of 1 ml/min, with detection at λ = 220 nm. …………………..…………………..…………………..………………….. 194

Figure 8.6 – ESI-IT MS spectrum (positive mode) of TP10-S-S-PQ (**68**). ……... 194

Figure 8.7 - *In vitro* screening of the activity of the selected CPP and their respective PQ-C4-CPP conjugates against liver-stage *P. berghei* parasites, according to a previously reported method[1]. Infection burden (bars) and host cell confluency (dots) are expressed as % of control. The compounds were assayed at 1, 5 and 10 µM, and PQ was included as the reference parent drug, for comparison. …………………..…………………..…………………..................... 197

Figure 8.8 – Chromatogram obtained from the analysis of PQ-C4-TP10 after purification, with a gradient elution of 0-100% ACN in water (0,05% TFA) in a RP-18E (5 µm), for 30 minutes and a flow of 1 ml/min, with detection at λ = 220 nm. …………………..…………………..…………………..……………………...... 200

Figure 8.9 – ESI-IT MS spectrum (positive mode) of PQ-C4-TP10…………….. 200

Figure 8.10 – Chromatogram obtained from the analysis of PQ-C4-IDR-1018 after purification, with a gradient elution of 0-100% ACN in water (0,05% TFA) in a RP-18E (5 µm), for 30 minutes and a flow of 1 ml/min, with detection at λ = 220 nm. …………………………………………………………………………… 201

Figure 8.11 – ESI-IT MS spectrum (positive mode) of PQ-C4-IDR-1018. …….. 201

Figure 8.12 – Chromatogram obtained from the analysis of PQ-C4-TAT after purification, with a gradient elution of 0-100% ACN in water (0,05% TFA) in a RP-18E (5 µm), for 30 minutes and a flow of 1 ml/min, with detection at λ = 220 nm. …………………..…………………..…………………..……………………....... 202

Figure 8.13 – ESI-IT MS spectrum (positive mode) of PQ-C4-TAT. …………… 202

Figure 8.14 – Chromatogram obtained from the analysis of PQ-C4-PasTAT after purification, with a gradient elution of 0-66% ACN in water (0,05% TFA) in a RP-18E (5 µm), for 20 minutes and a flow of 1 ml/min, with detection at λ = 220 nm 203

Figure 8.15 – ESI-IT MS spectrum (positive mode) of PQ-C4-PasTAT. ………. 203

Figure 8.16 – Chromatogram obtained from the analysis of PQ-C4-Transportan after purification, with a gradient elution of 0-66% ACN in water (0,05% TFA) in a RP-18E (5 µm), for 20 minutes and a flow of 1 ml/min, with detection at λ = 220 nm. …………………..…………………..………………….......................... 204

Figure 8.17 – ESI-IT MS spectrum (positive mode) of PQ-C4-Transportan. ……. 204

List of Schemes

Scheme 4.1 – Route for the synthesis of CQn-C4-CPP conjugates. …………… 46

Scheme 4.2 – General mechanism of an S_NAr (Y = nucleophile; X = leaving group; W = electron withdrawing group). …………………..……………………....... 46

Scheme 4.3 –S_NAr of butane-1,4-diamine on 4,7-dichloroquinoline, to deliver CQn. …………………..…………………..…………………..……………………..... 47

Scheme 4.4 – Nucleophilic acyl substitution of a symmetric carboxylic anhydride (**6**). …………………..…………………..…………………..……………………….. 48

Scheme 4.5 – Nucleophile acyl substitution of succinic anhydride by CQn, to produce CQn-C4. …………………..…………………..………………….............. 49

Scheme 4.6 - Formation of a stable salt between an amine and a carboxylic acid and its thermal conversion into an amide. …………………..……………………… 51

Scheme 4.7 – Activation of the carboxylic acid, with the formation of a reactive intermediary; this is then prone to suffer a nucleophilic attack from the amine of AA2, with consequent formation of an amide, after elimination of the activating group. …………………..…………………...…………………..……………………... 51

Scheme 4.8 - General scheme of SPPS. *C*-terminal of the final peptide may be obtained as a carboxamide (Y = NH) or carboxylic acid (Y = O). ……………. 53

Scheme 4.9 - Activation of a carboxyl group by a carbodiimide (**7**) and subsequente reaction of the *O*-acyl-isourea (**8**) with a nucleophilic amine, to generate the desired amide. …………………...…………………..………………….. 55

Scheme 4.10 - Nucleophilic attack by HOBt to an *O*-acyl-isourea and consequent aminolysis of the benzotriazolyl ester formed. ……………………....... 56

Scheme 4.11 - Mechanism of acivation of a carboxyl group via reaction with an uronium salt. …………………..…………………..…………………..……………….. 57

Scheme 4.12 – Reaction of Ninhydrin with the α-NH_2 group of an amino acid…. 58

Scheme 4.13 – Cleavage of the resin-peptide bond. This scheme represents a situation where peptide's *C*-terminal is obtained as a carboxamide, synthetized over na MBHA resin, modified with the Rink spacer. …………………............... 59

Scheme 5.1 –Route employed for the synthesis of CQn-C10-TP10 (**15**). ……... 97

Scheme 5.2 – Route for the synthesis of CQn-TR-TP10 (**16**) …………………... 100

Scheme 5.3 - Proposed mechanism for copper-catalyzed azide-alkyne cycloadditions (CuAAC). …………..…………………..…………………..……….... 102

Scheme 5.4 – Route for the synthesis of CQn-S-S-TP10 (**17**). …………………. 106

Scheme 5.5 –A thiol-disulfide exchange reaction (TDER). ……………………...... 107

Scheme 5.6 – Coupling of CQn to Boc-Cys(Trt)-OH. ………………….............. 108
Scheme 5.7 – Acidolytic deprotection of Boc-Cys(Trt)-CQn (**37**) to produce CQn-Cys (**34**). …………………..…………………..…………………................... 109
Scheme 5.8 – TDER between CQn-Cys (**34**) and Cys(NPys)-TP10 (**36**), yielding conjugate **17**. …………………..…………………..…………………................... 111
Scheme 5.9 – Route devised for the synthesis of TP10-C4-CQn (**18**). ………… 114
Scheme 5.10 – Synthetic route towards conjugate TP10-S-S-CQn (**19**). ……… 117
Scheme 5.11 – Activation of the thiol group present in CQn-Cys with 2,2’-dithiodipyridine. …………………...…………………...…………………................. 118
Scheme 7.1 – Synthetic route towards fluorescently labelled CPP (**64**) and conjugates **65** and **66**. …………………...…………………...……………………....... 166
Scheme 8.1 – Route employed for the chemical synthesis of PQ-C4-CPP conjugates. …………………...…………………...…………………...……………… 186
Scheme 8.2 – route employed for the chemical synthesis of TP10-S-S-PQ (**68**) 190

List of Tables

Table 1.1 - Classification of antimalarial drugs used in the clinics based on their structures. …………………..…………………..…………………........................ 12
Table 1.2 – Adverse effects and contraindications of available AM …………….. 13
Table 2.1 – CPP chosen to act as vehicles for AM. ………………….....…………. 32
Table 4.1 – Peptides conjugated to CQn ………………...……………………...... 45
Table 4.2 – Synthesized CPP and respective analytical data, obtained by HPLC (purity and retention time – RT) and LC-DAD/ESI-IT MS (detected m/z)………… 62
Table 4.3 - Synthesized CQn-C4-CPP and respective analytical data, obtained by HPLC (purity and retention time – RT) and LC-DAD/ESI-IT MS (detected m/z). …………………...………………....………………...…………………...... 63
Table 4.4 – Half-maximal inhibitory concentration for free peptides and CQn-CPP conjugates. …………………...…………………...……………………............... 64
Table 5.1 – Adducts of CQn-C10-TP10 (P) with H$^+$, detected by ESI-IT MS…….. 99
Table 5.2 – Adducts of the peptide CQn-TR-TP10 (P), detected by ESI-IT MS… 105
Table 5.3 – Adducts of the peptide Cys(NPys)-TP10 (P), detected by ESI-IT MS 110
Table 5.4 – Adducts of the peptide CQn-S-S-TP10 (P), detected by ESI-IT MS 113
Table 5.5 – Adducts of the peptide TP10-C4-CQn (P), detected by ESI-IT MS…. 116
Table 5.6 – Adducts of the peptide TP10-Cys (P), detected by ESI-IT MS. ……… 119
Table 5.7 – Adducts of the peptide TP10-S-S-CQn (P), detected by ESI-IT MS 121
Table 5.8 - *In vitro* antiplasmodial (on blood stage Pf 3D7 parasites) and hemolytic (on both hRBC and PiRBC) activity of CQn-TP10 conjugates. ……… 121
Table 6.1- Partition coefficients (Log *D*) of the compounds in DMPC and DMPG vesicles, at 37 ºC. …………………...…………………..……………………………. 152
Table 7.1 - Synthesized fluorescently labelled peptides and respective analytical data, obtained by HPLC (purity and retention time – RT) and LC-DAD/ESI-IT MS (detected m/z). …………………..……………….. 167
Table 8.1 – CPP selected for conjugation to PQ. ……………………................... 188
Table 8.2 – Synthesized PQ-C4-CPP and respective analytical data, obtained by HPLC (purity and retention time – RT) and LC-DAD/ESI-IT MS (detected m/z). …………………...………………....………………...…………………...... 189
Table 8.3 – Adducts of the peptide TP10-S-S-PQ (P), detected by ESI-IT MS. 195

Abbreviations

A

A – Alanine

AA – Amino acids

AAC – Azide-alkyne cycloadditions

Abs – Absorbance

ACN - Acetonitrile

ACT – Artemisinin-based combination therapies

Ahx – 6-aminohexanoyl

AM – antimalarial drugs

AMP – Antimicrobial peptides

a.m.u. – Atomic mass units

B

B – Cooperativity

Boc – *terc*-butyloxycarbonyl

Bzl – Benzyl

C

C - Cysteine

CF – Carboxyfluorscein

CHAPS – 3-[(3-Cholamidopropyl)di-methylammonio]-1-propanesulfonate hydrate

CPP – Cell-penetrating peptides

CQ – Chloroquine

CuAAC - Copper-catalyzed AAC

Cys – Cysteine

C4 – Butanedioyl spacer

D

DCM – Dichloromethane

DIPEA – *N*-ethyl-*N,N*-diisopropylamine

DLS – Dynamic light scattering

DMF – Dimethylformamide

DMPC – 1,2-dimyristoyl-sn-glycero-3-phosphocholine

DMPG – 1,2-dimyristoyl-sn-glycero-3-phosphorylglycerol

DNA – Deoxyribonucleic acid

DV – Digestive Vacuole

E

E – Glutamic acid

eq - equivalents

ESI-IT – Electrospray ionization and ion trap detection

EWG – Electron-withdrawing groups

F

F – Phenylalanine

FACS – Fluorescence-activated cell sorter

FC – Flow Cytometry

FDA – Food and drug administration

Fmoc – 9-fluorenylmethyloxycarbonyl

Fmoc-Rink - *p*-(2',4'-dimethoxyphenyl-Fmoc-aminomethyl)-phenoxyacetic acid

FV – Food Vacuole

G

G – Glycine

GSH – Reduced glutathione

H

HATU – *O*-(7-Azabenzotriazol-1-yl)-*N,N,N′,N′*-tetramethyluronium hexafluorophosphate

HBTU – *O*-benzotriazol-1-yl-*N,N,N′,N′*-tetramethyluronium hexafluorophosphate

HEPES – 4-(2-hydroxyethyl)-1-piperazineethanesulfonic acid

HOBt – 1-hydroxybenzotriazole

hRBC - healthy red blood cells

HSPG – Heparin sulphate proteoglycans

I

I - Isoleucine

IC_{50} – Half-maximal inhibitory concentration

IRS – Indoor residual spraying

ITN – Insecticide-treated bed nets

K

K – Lysine

Kp **–** Partition coefficients

L

L – Leucine

LC-DAD – Liquid chromatography with diode array detection

LUV – Large unilamellar vesicles

M

M – Methionine

MBHA – Methylbenzidrylamine

MeOH – Methanol

MLV – Multilamellar vesicles

MPR – Mepacrine

MS – Mass spectrometry

MTBE – *tert*-butyl methyl ether

Mtt – 4-methyltrityl

N

N – Asparagine

Nle – Norleucine

NPys – 3-Nitro-2-pyridinesulfenyl

P

P – Proline

PBS – Phosphate-buffered saline

PC – Phosphatidylcholine

PE – Phosphatidylethanolamine

Pf – *Plasmodium falciparum*

PfCRT – *Pf* CQ resistance transporter

PG – Protecting group

PI – Phosphatidylinositol

***P*iRBC** – *Plasmodium*-infected red blood cells

POPC – 1-palmitoyl-2-oleoyl-glycero-3-phosphocholine

POPG – 1-Palmitoyl-2-oleoyl-sn-glycero-3-phosphoglycerol

PQ – Primaquine

Pra – Propargylglycine

PS-DVB - Polystyrene crosslinked with divinylbenzene

PS – Phosphatidylserine

PV – Parasitophorous vacuole

Pv – *Plasmodium vivax*

PyBOP – (benzotriazol-1-yl-oxy)tripyrrolidinophosphonium hexafluorophosphate

Q

Q - Glutamine

R

RBC – Red blood cells; Erythrocytes

ROS – Reactive oxygen species

RP-HPLC – Reverse phase high-performance liquid chromatography

RNS – Reactive nitrogen species

R_t – Retention time

RU – Resonance units

S

S - Serine

SG - SYBR green I

SM – Sphingomyelin

S_NAr – Nucleophilic aromatic substitution

SPPS – Solid-phase peptide synthesis

SPR – Surface plasmon resonance

SUV – Small unilamellar vesicles

T

T – Threonine

T - Temperature

^{t}Bu – *terc*-butyl

TD – Targeted delivery

TDER – Thiol-disulfide exchange reaction

TFA – Trifluoroacetic acid

TIS – Triisopropylsilane

TLC – Thin-layer chromatography

T_m – Main phase transition temperature

TP – Thiopyridine

TR – 1,2,3-triazoles

Trt – Trityl

V

V – Valine

W

W – Tryptophan

WHO – World Health Organization

Y

Y – Tyrosine

1

Malaria: a pressing affair

1.1. Malaria

Malaria is a vector-borne parasitic disease, caused by protozoan parasites belonging to the genus *Plasmodium*. This is one of the most severe parasitic diseases worldwide, with a serious impact on both health and economic levels, owing to its prevalence, virulence and emergence of drug resistance[1,2]. Patients typically present nonspecific symptoms, including fever, rigors, and chills, and while the majority will not require hospital admission, severe malaria can develop in a minority of cases. Most of these cases involve young children, who are affected by high fever, impaired consciousness, severe anemia, respiratory distress, convulsions, and hypoglycemia, among other symptoms[3,4].

Malaria can almost be regarded as a pandemic disease, as it is endemic in 91 countries (inhabited by roughly 3 billion people) covering tropical and subtropical regions of the world – sub-Saharan Africa, South and East Asia and South America (Figure 1.1). In 2017, 219 million cases of malaria were reported and, ultimately, 435 000 people died from the disease, mostly young children. About 90% of these cases happened in the sub-Saharan Africa, where *Plasmodium falciparum* – the species responsible for the most severe forms of malaria, is prevalent[1]. While malaria deaths have declined by approximately 30% since 2010, in the past few years its morbidity and mortality rate has stalled, with several factors hindering the efforts to eradicate this disease, such as (i) emergence of parasite resistance to antimalarial drugs (AM), (ii) mosquito resistance to insecticides, (iii) anomalous climate patterns, (iv) risks posed by conflict in malaria endemic zones, and (v) lack of sustainable and predictable international and domestic funding[1].

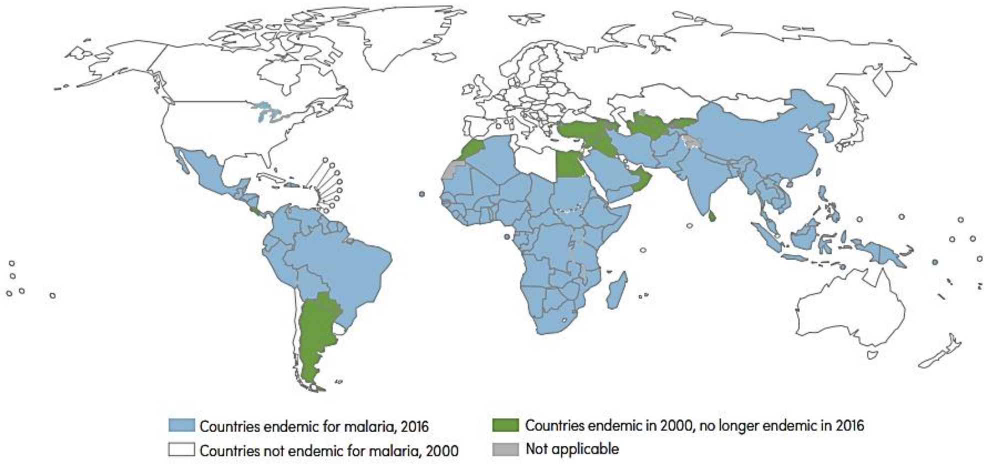
Countries endemic for malaria, 2016
Countries not endemic for malaria, 2000
Countries endemic in 2000, no longer endemic in 2016
Not applicable

Figure 1.1 – Geographical distribution of Malaria. Countries with 3 consecutive years of zero indigenous cases are considered to have erradicated malaria (represented in green). Adapted from [5].

Malaria incidence depends on environmental suitability for local vectors in terms of altitude, climate, flora, and implementation of control measures; hence, it is intimately linked to poverty, natural disasters, and war[6]. Although predictions as to how climate change will affect the global distribution of malaria in the future usually vary, it has been suggested that the population at risk of contracting malaria will increase, particularly in tropical highland areas[6–8].

1.2. The *Plasmodium* parasite

A human malarial infection can be caused by five species of *Plasmodium* parasites: *P. falciparum*, *P. vivax*, *P. malariae*, *P. ovale* and *P. knowlesi*. *P. falciparum* (*Pf*) is found in almost every malaria endemic region of the world; yet, it is predominant in sub-Saharan Africa, where it is responsible for almost every case of malaria reported[1]. This species causes the most aggressive forms of the disease (severe malaria), and is responsible for virtually all deaths related to malaria[9,10]. *P. vivax* (*Pv*), despite rarely producing severe malaria, is the most widely distributed *Plasmodium* species worldwide, as it easily adapts to a variety of climate conditions; it is noticeably "absent" from Africa, due to naturally acquired immunity of most populations in that area[11,12]. Although *Pv* usually produces a milder infection, it is able to generate dormant forms of the parasite in liver cells – hypnozoites; these dormant parasites lead to a high risk of relapse and are responsible for the high morbidity rate associated to vivax malaria[6]. *P. malariae* and

P. ovale are globally distributed but have very low incidence rates; the severity of malaria caused by these species is similar to that of an uncomplicated vivax malaria, although *P. ovale*, similarly to *Pv*, can produce hypnozoites, thus causing relapses[10]. The simian parasite *P. knowlesi* was considered of little importance, as it was thought to only be able to infect monkeys, up until 2004, when it was recognized to cause zoonotic malaria in populations from Malaysia and some other areas in Southeast Asia[13]. Despite its low incidence, *P. knowlesi* can rapidly replicate, leading to high parasitaemias, so the risk of severe malaria is as high as in cases of falciparum malaria[10,14].

One of the factors hampering the eradication of malaria is the complex life cycle of the *Plasmodium* parasite (Figure 1.2), which alternates between female *Anopheles* mosquitoes and the vertebrate human host and goes through several different stages. Malaria infection starts upon the blood meal of a *Plasmodium*-infected female *Anopheles* mosquito, with the injection of about a hundred parasitic sporozoites into the host's subcutaneous tissue; the sporozoites then migrate to the liver, where they invade hepatocytes and start to replicate, producing thousands of merozoites. After this asymptomatic incubation period, which may vary depending on the *Plasmodium* species[15], thousands of merozoites are released into the bloodstream, where each invades an erythrocyte. Intraerythrocytic merozoites then undergo an asexual replication cycle, culminating in the rupture of mature infected erythrocytes (schizonts), with concomitant release of new merozoites, ready to infect healthy red blood cells, starting a new intraerythrocytic replication cycle. In each of these cycles, a small proportion of parasites may differentiate into sexual forms: the male and female gametocytes. These can be ingested by an uninfected mosquito vector upon its blood meal and, in its midgut, gametocytes go through fertilization and maturation, resulting in an infective ookinete form which invades the midgut epithelium wall of the mosquito, where it develops into oocysts. These grow until they suffer a disruption that releases sporozoites, which migrate to the mosquito's salivary glands. There, sporozoites are stored until being inoculated into another human host, upon the next blood meal of the mosquito vector, thus perpetuating the malaria life cycle[16,17].

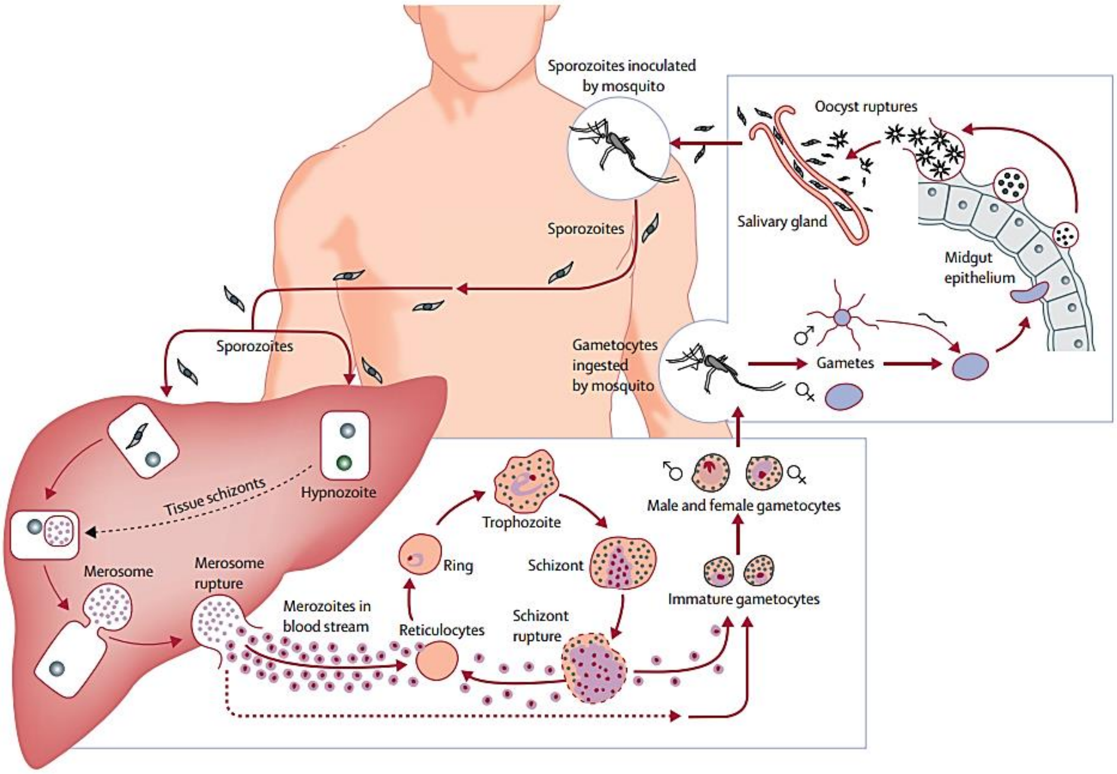
Sporozoites inoculated by mosquito
Oocyst ruptures
Salivary gland
Midgut epithelium
Sporozoites
Sporozoites
Gametocytes ingested by mosquito
♂
Gametes
♀
Tissue schizonts
Hypnozoite
Trophozoite
♂
♀
Male and female gametocytes
Ring
Schizont
Merosome
Merosome rupture
Merozoites in blood stream
Reticulocytes
Schizont rupture
Immature gametocytes

Figure 1.2 – Life cycle of the *Plasmodium* parasite. Adapted from [18].

During the intraerythrocytic stage, the parasite uses host hemoglobin as a food source. Hemoglobin degradation products, including amino acids (AA), are essential for the parasite's own protein biosynthesis and metabolism. Hemoglobin is initially transported to the parasite's acidic food vacuole (FV) where a number of active proteases are expressed and ready to degrade hemoglobin[19]. During this degradation process, free heme groups are released and oxidized from the ferrous (Fe^{+2}) to the ferric (Fe^{+3}) state hematin [20]. Both heme and hematin are potentially toxic to *Plasmodium* [21]; as such, the parasite has developed a detoxification mechanism, that yields an hemozoin pigment, which is an inert crystalline hematin polymer [20,22,23].

1.3. Clinical features of malaria and current measures for its control

The clinical symptoms of malaria occur during the blood stage of the infection, and are related to the rupture of *Plasmodium*-infected erythrocytes (*P*iRBC), adhesion of mature *P*iRBC in the vasculature, release of parasite-related exogenous molecules, and consequent immunological and inflammatory response of the host[24–26]. The first symptoms of malaria often resemble those of common viral infections - fever, headaches, nausea, chills, abdominal pain and mild diarrhea, which may lead to a delay in diagnosis. If not early diagnosed and treated, infections caused by *Pf* may produce more severe symptoms that can ultimately lead to the death of the infected host. Severe malaria symptoms consist of cerebral malaria, pulmonary edema, acute renal failure and severe anemia[26].

Currently, and given that a widely effective antimalarial vaccine remains elusive, the most relevant measures for the control of the disease are (i) use of indoor residual spraying (IRS) to control mosquito populations, (ii) distribution of insecticide-treated bed nets (ITN), (iii) use of insect repellents and (iv) prescription of prophylactic/therapeutic drugs[1,27].

Both IRS and ITN strategies have been progressively adopted across an increasing number of malaria-endemic countries, which has in turn led to a significant reduction in the number of new cases diagnosed. However, vector control strategies are currently threatened by a number of different factors, including sustainability of ITN implementation, as many of the nets delivered during the past few years are due for replacement. Increased resistance to insecticides is also undermining the effectiveness of vector control strategies; current IRS and ITN approaches are mainly reliant on a single class of insecticides, pyrethroids, due to their low toxicity to humans, rapid knockdown effect, low cost and relative long residual activity. New insecticides that retain these benefits are urgently needed as an important tool for malaria control[28].

As mentioned above, there is still no antimalarial vaccine available to provide protection against malaria, which requires for alternative approaches targeted at malaria prevention. Hence, chemoprophylaxis – administration of an AM to prevent the development of malaria in nonimmune individuals – is used on people travelling to endemic countries, in order to protect them from becoming infected. Also, intermittent preventive antimalarial treatments are applied on pregnant women in endemic countries, particularly in sub-Saharan Africa[1], a measure that has been shown to reduce maternal anemia, low birth weight and perinatal mortality often associated with mother-to-child malaria transmission. Prevention of seasonal malaria in children is also an important strategy to fight this disease, as it leads to a significant reduction of clinical cases and of severe malaria and can ultimately lead to the avoidance of millions of infections and thousands of infant deaths[1].

1.4. Antimalarial chemotherapy

1.4.1. Brief historical overview

Antimalarial chemotherapy dates back to at least 350 years, with the use of the bark of the South American cinchona tree for the treatment of intermittent fevers[29]. Its active components are quinine (Figure 1.3), its diastereoisomer quinidine and the corresponding demetoxylated diastereoisomers cinchonidine and cinchonine[30]. Around 1820, quinine became standard therapy for intermittent fever throughout the world. However, during World War II (WWII), a huge shortage of this drug[31] – due to high demand, inaccessibility to cinchona plantations, and an extremely complex and expensive synthetic process, prompted the use of quinacrine, a synthetic blood schizonticide acridine that was one of the two other antimalarials available at the time, to replace quinine[32].

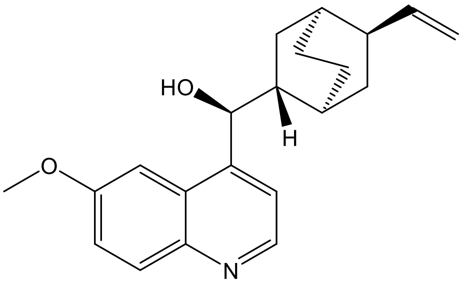

Figure 1.3 – Structure of Quinine.

The other synthetic antimalarial available at the time of quinine shortage during WWII was pamaquine (Figure 1.4), a tissue schizonticide and gametocytocide 8-aminoquinoline that was soon found to be too toxic for clinical use. This drug eventually inspired the subsequent synthesis of primaquine (PQ; Figure 1.4), which remains to date as one of the most important tissue schizonticides and gametocytocides used to fight malaria. By around the same time, the 4-aminoquinoline chloroquine (CQ), emerged as a new AM whose potency, bioavailability, safety and cost outshined those of all antimalarials available by then[33]. Indeed, CQ became the first-line treatment for all malarial infections, and inspired, together with PQ and mepacrine (MPR), several attempts to develop novel AM, based on their respective 4-aminoquinoline, 8-aminoquinoline, and acridine scaffolds[33].

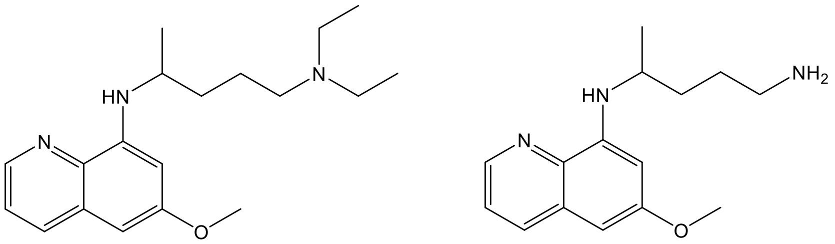

Pamaquine **Primaquine**

Figure 1.4 – Structures of Pamaquine and Primaquine.

CQ was such a brilliant AM that, in 1957, the World Health Organization (WHO) initiated a project aiming at global eradication of the *Plasmodium* parasite, for which massive amounts of that drug were needed. Worldwide parasite populations were therefore subjected to an intense selection pressure for survival in the presence of CQ. Moreover, the safety and low cost of this AM motivated its indiscriminate use in malaria-endemic countries, whenever malaria-like symptoms (*e.g.*, fever and chills) were observed, thus contributing to the emergence and spread of CQ-resistant parasite strains. CQ resistance was first detected in South America in 1959, and independently in Southeast Asia the following year[30].

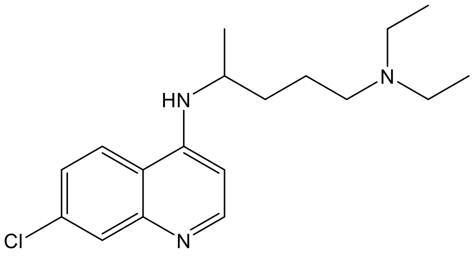

Figure 1.5 – Structure of Chloroquine.

Widespread emergence of CQ-resistant *Pf* casted a shadow in the control of the disease, as little had been done to prepare for its failure[34]. This urged several countries to shift their first-line treatment from CQ to, for example, sulfadoxine-pyrimethamine (Figure 1.6). However, resistance to this treatment developed rapidly, requiring yet again for a change in the treatment protocol in a relatively short period[35]. Succeeding drugs (*e.g.*, mefloquine[36]) soon followed the same trail (Figure 1.6).

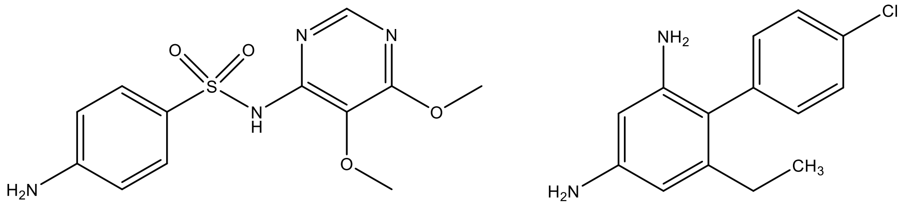

Sulfadoxine **Pyrimethamine**

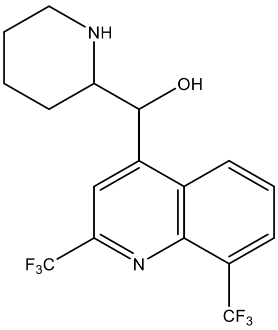

Mefloquine

Figure 1.6 – Structures of sulfadoxine, pyrimethamine and mefloquine.

Nowadays, following the WHO guidelines, areas with endemic malaria are encouraged to resort to artemisinin-based combination therapies (ACT), *i.e.*, co-formulations of an artemisinin derivative and a slow-acting, less potent partner drug (*e.g.* mefloquine, piperaquine or lumefantrine) as first-line treatments for CQ-resistant *Pf*[1]. Artemisinin and its derivatives (artesunate, artemether, dihydroartemisinin; Figure 1.7) are highly potent against nearly all blood stages of *Pf*, including immature gametocytes,[37] and their combination with slow-acting AM is an effort to minimize the risk of the development of resistances[1,38]. ACT include artemether-lumefantrine, artesunate-amodiaquine, artesunate-mefloquine, artesunate-sulphadoxine-pyrimethamine and dihydroartemisinin-piperaquine combinations.

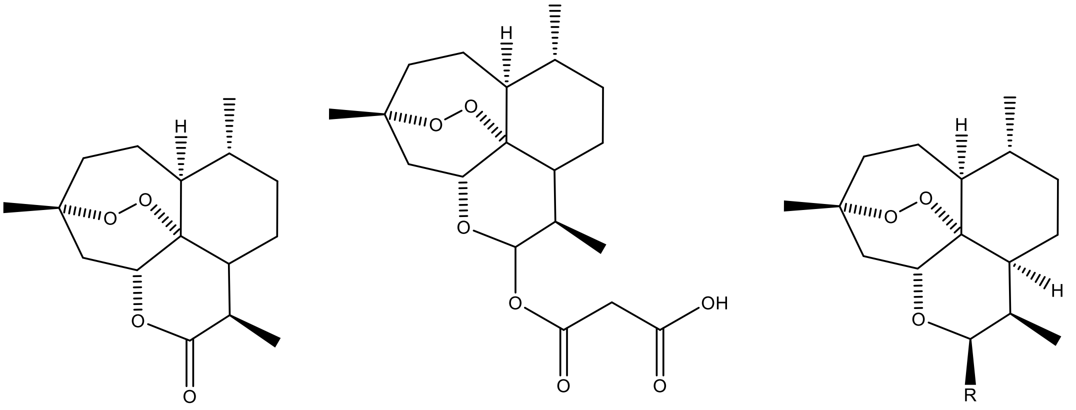

Artemisinin

Artesunate

R = OH: Dihydroartemisinin
R = CH_3: Artemether

Figure 1.7 – Chemical structure of artemisinin and three of its derivatives: artesunate, dihydroartemisinin and artemether.

While the use of artemisinin was previously restricted in order to avoid the emergence of artemisinin-resistant *Plasmodium* strains - and recommended only in cases of complicated cerebral malaria, the increasing ineffectiveness of CQ urged the systematic use of this drug. Without many alternatives in the AM pipeline, the emergence of resistance against ACT - nowadays the frontline treatment of antimalarial chemotherapy, could result in a catastrophe on the battle to eradicate malaria[38,39]. In fact, there have been reported cases of *Pf* resistance to artemisinin in Southeast Asia (the epicenter for AM resistance)[40–44], which is defined as slower parasite clearance rate[44] and reflect the reduced susceptibility of ring-stage parasites to this drug[40].

1.4.2. Antimalarial drugs approved for clinical use

Current antimalarial chemotherapy requires in all cases a blood schizonticide and a gametocytocide, while a tissue schizonticide is essential for *Pv* and *P. ovale* infections[45]. Currently available AM may be categorized according to their biological activity or chemical structure (Table 1.1).

The vast majority of AM are **blood schizonticides**, which act in the erythrocytic stage of the infection and are responsible for eliminating the clinical symptoms of malaria. Among them, we can find 4-aminoquinolines, anti-folates, aryl amino alcohols, antimicrobials and peroxides.

Tissue schizonticides may (i) act on the primary tissue forms of the parasite, to avoid their development inside hepatocytes (8-aminoquinolines, peroxides and anti-folates)[46,47], and/or (ii) eliminate *Pv* and *P. ovale* hypnozoites, thus preventing malarial relapses (PQ and tafenoquine - a PQ's analogue recently approved by the FDA, are the only drugs clinically available that are capable of acting on hypnozoites).

Gametocytocides destroy the sexual forms of the parasite in the blood, thus preventing the transmission of the infection to the mosquito vector. CQ and quinine have gametocytocidal activity against *Pv* and *P. malariae*, but PQ, tafenoquine and artemisinin (and its derivatives) are the only AM available that act against gametocytes of all human malarial parasite species, including *P. falciparum*.

Sporontocides prevent the development of oocysts in the mosquito and thus ablate the formation of sporozoites, blocking transmission to a new human host. PQ and chloroguanidine are known to have activity against this stage[48].

Table 1.1 - Classification of antimalarial drugs used in the clinics based on their structures.

Family	Examples
4-aminoquinolines	Chloroquine, amodiaquine, hydroxychloroquine, piperaquine
8-aminoquinolines	Pamaquine, primaquine, tafenoquine
Peroxides	Artemisinin and derivatives - artemether, arteether, artesunate, dihydroartemisinin
Anti-folates	Sulphones, sulphonamides; proguanil and chloroproguanil; pyrimethamine
Aryl amino alcohols	Quinine, quinidine, mefloquine, halofantrine and lumefantrine
Antimicrobials	Tetracycline, doxycycline, clindamycin, azithromycin and fluoroquinolones

While there's a wide panoply of AM, they are often accompanied by several adverse effects – some of them particularly serious, as well as various contraindications. Detailed information regarding this subject is summarized in Table 1.2.

Table 1.2 – Adverse effects and contraindications of available AM (adapted from [36]).

AM	Contraindications	Adverse effects	Severe adverse effects
Chloroquine	Epilepsy	Gastrointestinal upset, itching, dizziness	Death from overdose
Sulfadoxine-pyrimethamine	Pregnancy, renal disease	-	Stevens–Johnson syndrome
Quinine	G6PD deficiency, pregnancy, optic neuritis, tinnitus, thrombocytepenic purpura, blackwater fever	Tinnitus, vertigo, headache, fever, syncope, delirium, nausea	Hemolytic anemia, coma, respiratory arrest, renal failure
Mefloquine	Depression, schizophrenia, anxiety disorder, any psychosis, irregular heartbeat	Vomiting, headache, insomnia, vivid dreams, anxiety, dizziness	Psychosis
Atovaquone–chloroguanide	Weight of <11 kg in children, pregnancy, breast-feeding, renal impairment	Gastrointestinal upset, headache, stomatitis	-
Artemether-lumefantrine	Pregnancy, severe malaria	Dizziness, palpitations	Impaired hearing
Artesunate–mefloquine	Depression, schizophrenia, anxiety disorder, any psychosis, irregular heartbeat	Vomiting, anorexia, diarrhea	-
Halofantrine	Conduction abnormalities, pregnancy, breast-feeding, infancy, use of mefloquine	Gastrointestinal upset, prolonged QTc	Cardiac arrest
Primaquine	Pregnancy, G6PD deficiency, breast-feeding	Gastrointestinal upset, elevated levels of methemoglobin	Hemolytic anemia

Apart from the toxicity associated with several of these compounds, effective malaria chemotherapy strategies are – as previously stated, constantly hampered by the emergence of parasite resistance to several AM (e.g., chloroquine, mefloquine, sulfadoxine, pyrimethamine and, more recently, artemisinin, Figure 1.8)[33,49,50].

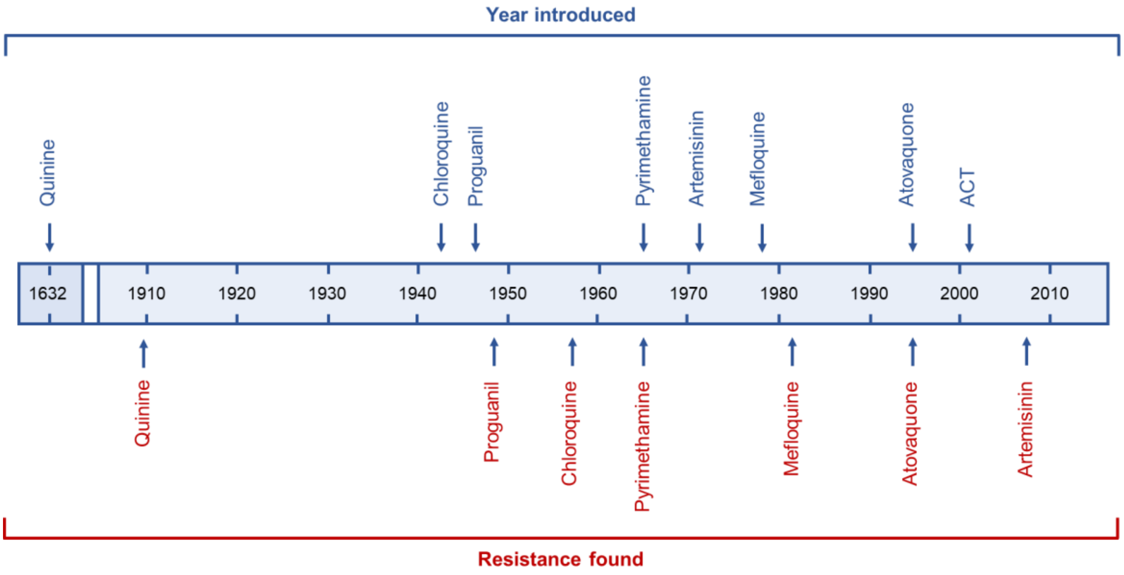

Figure 1.8 – Chronology of AM introduction for malaria chemotherapy (in blue) and first report of *Plasmodium* resistance to corresponding AM (in red). Adapted from [28]

1.5. Novel strategies for the battle against malaria

From the above, it stems that the wide arsenal of AM approved for the treatment of malaria is nevertheless insufficient to tackle this disease, mainly due to widespread drug-resistant *Plasmodium* strains and lack of affordable and effective new drugs[48]. Moreover, the parasite´s surface proteins and metabolic pathways keep changing during the different stages of infection, which help the parasite to evade immune clearance, while also hindering the development of efficient antimalarial drugs and vaccines[51]. These aspects emphasize the necessity for new classes of antimalarial agents, and/or new strategies to modify the existing ones, targeted at alternative mechanisms of action to tackle parasite resistant strains.

1.5.1. Malaria vaccines

While it is crucial to develop new drugs for malaria chemotherapy, eradication is considered to be impossible without an effective vaccine. Numerous developments have been made in this field, extensively reviewed by Draper *et al.*[52] and there are several vaccines currently under preclinical development or clinical trials[53]. In 2015, the European Medicines Agency approved the first pre-erythrocytic malaria vaccine - RTS,S/ASOI (or Mosquitrix®)[54,55], the most advanced vaccine candidate up to date, which comprises a fusion protein of *Pf* and hepatitis B surface antigens combined with a new potent adjuvant. Currently, three countries (Kenya, Ghana and Malawi) are taking part in a pilot program designed to evaluate the protective efficacy of this vaccine against *Pf* infections. While RTS,S partially limits clinical malaria infection in the field, its modest and rapidly fading efficacy highlights the need to develop vaccines with higher and more long-lasting protection[56,57]. Recently, in 2018, Pb(PfCS)@UIS4 (PbVac) – developed by Prudêncio *et al.*, was accepted for phase I and II clinical trials, in the Netherlands. Briefly, this vaccine generates immunity against pre-erythrocytic stages of *Pf* with genetically modified whole-sporozoites of *P. berghei* Rodent malaria parasites[57].

1.5.2. Nanovectors for antimalarial drug delivery

Targeted delivery (TD) applied to AM may be extremely efficient, as it may (i) increase the amount of drug reaching the pathogen, thus minimizing the risk of resistance development, (ii) reduce side effects, so often associated with AM, as they are directed specifically to the site of action, (iii) improve the efficacy of currently used hydrophilic (low membrane permeation capacity) and lipophilic (poor aqueous solubility) AM, and (iv) make use of drugs never assayed for malaria chemotherapy, because of their high and/or wide-spectrum toxicity[58,59].

Several studies have been carried out in this field, particularly with modified lipid- or polymer-based vectors[60]. In recent work, it has been demonstrated that TD of PQ with PEGylated galactosylated nanostructured lipid carriers improved the drug's antimalarial activity *in vitro* against blood-stage *Pf*, while reducing its toxicity towards healthy erythrocytes, as well as *in vivo*[61]. Moreover, incorporation of artemisinin derivatives onto polymers, extensively reviewed by Aderibigbe[62], resulted in enhanced water solubility, improved stability and increased bioavailability by extending the circulation half-life of the drugs; it may also be useful for combination therapy, upon incorporation of other AM[62].

The modification of liposomes with heparin to target *P*iRBC's surface has proven to be a successful strategy in drug delivery as well[63], as the parasite heavily relies on binding to glycosaminoglycans (*e.g.*, heparin) for essential parts of its life cycle[64,65]. In another work, the efficacy of the anti-malarial drug CQ was improved when delivered inside *P*iRBC-specific monoclonal antibody BM1234 functionalized liposomes[66]. This strategy has also been recently employed for the delivery of novel antimalarial compounds, whose potent *in vitro* antimalarial activity severely decreased *in vivo*; encapsulation of these novel compounds into immunoliposomes resulted in a significantly enhanced antimalarial activity[67].

A wide panoply of studies regarding the modification of lipid- or polymer-based vectors for AM have been reported[68–70], and recent work on this topic has been thoroughly reviewed by Thakkar and Brijesh[27].

1.5.3. Peptide-based strategies

Membrane active peptides present several advantages over small molecules, since they may possess higher specificity and affinity towards therapeutic targets, but also over proteins of higher molecular weight, in terms of synthetic viability, derivatization flexibility, low immunogenicity and physico-chemical characteristics compatible with their employment as therapeutic agents[71]. In this class of peptides, one can find (i) cell penetrating peptides (CPP), a class of molecules capable of efficiently translocating different cell membranes, while maintaining the integrity of the cell, and (ii) antimicrobial peptides (AMP), which are able to interact with different pathogens or malignant cells through destabilization of their membranes.

1.5.3.1. Antimicrobial peptides

AMP are often expressed in the organism as the result of an immune response upon invasion by a pathogen, and are considered key elements of the innate immunity of almost all living beings – from prokaryotes to animals and plants - protecting them against diverse microbial pathogens[72,73]. Because of their broad spectrum activity - not only against bacteria, but also against fungi[74], malignant cells[75], viruses[76,77] and parasites[78], AMP have been receiving great attention for their potential application as therapeutic agents. These peptides may be of natural origin or fully synthetic, in the later case often inspired by the properties of natural AMP. Although AMP present a huge diversity in terms of size, charge and three-dimensional structure, their vast majority is positively charged and likely to adopt and amphipathic structure[79,80], as a consequence of their high content in cationic and hydrophobic AA. These characteristics confer AMP the ability to interact with negatively charged membranes – thus sustaining the hypothesis that their primary mode of action derives from their ability to destabilize or destroy the membranes of pathogenic agents[81]. The membrane of *P*iRBC provides a similar anionic target due to the externalization of phospholipids with negatively charged phosphatidylserine headgroups onto the outer membrane surface[82]. Since AMP mainly act on the membrane of pathogenic agents and their activity is independent of specific receptors – unlike conventional drugs, the development of resistance mechanisms is highly unlikely[83], which constitutes a very seductive feature of AMP for antimalarial therapies. This fact, along with the need for innovative strategies to treat malaria, boosted the search for antiplasmodial peptides; in fact, there's a wide plethora of AMP with reported antimalarial activity, against different stages of the infection[78,84]. These can be naturally derived, either from the *Anopheles* mosquito immune responses or other living organisms, or designed *de novo*.

As an example, Gambicin is derived from the mosquito vector and is able to diminish the viability of ookynetes, but the concentration required for this effect is significantly high (50 µM)[85]. Other naturally occurring peptides, such as Drosomicins I and II[86] and Scorpine[87], display activity against different stages of the mosquito infection in the µM range (10-20 µM), while the latter is able to clear erythrocytic *Pf* infection *in vitro*, in a time-dependent manner (with concentrations ranging from 0.1-5 µM)[88]. Human PF4 - expressed upon erythrocyte invasion by *Plasmodium*[90], presents high potency against *Pf* - with an IC_{50} of 4.2 µM, and no significant hemolysis[89].

Additionally, synthetic peptides may be of therapeutic interest against malaria. D-HALO-rev, a histidine-rich peptide, showed a remarkable activity against *Pf* (IC_{50} = 100 nM), while its HC_{50} (peptide dose that causes 50% hemolysis of RBC *in vitro*) was around 700 µM, well above the reported IC_{50} value[91]. IDR-1018, a peptide with wide-range antimicrobial and immunomodulatory action, was found to potentiate the efficacy of pyrimethamine-chloroquine treatment for protection against cerebral malaria. This AMP itself did not affect the levels of parasitemia, which suggests that it does not present antiplasmodial activity *per se*; it probably acts in a host-directed manner[92].

Several other antiplasmodial peptides have been reported, with activities against the different mosquito stages and/or the human erythrocytic cycle. This issue has been extensively reviewed by Vale *et al.*[84] and Bell[72].

1.5.3.2. Cell-penetrating peptides

CPP are cationic amphipathic oligopeptides, with short AA sequences (usually less than 30 residues) that can be (i) derived from naturally existing proteins, (ii) chimeric or (iii) designed *de novo*[93,94]. This class of peptides consists of a system with the intrinsic ability to translocate across biological membranes without specific receptor recognition and with very limited toxicity[95,96]. These properties prompted the exploitation of CPP as a novel approach to promote internalization of exogenous substances into living cells. In fact, CPP have been described as able to transport and deliver inside the cells a wide variety of cargos - covalently linked or not, which include nucleic acids[93,97–99], peptides and proteins[100–103], liposomes[94,104–107], nanoparticles[108–110] and low molecular weight drugs[111–113], among others. Regardless of the rising interest in this class of peptides, focus has been mainly directed towards cancer and gene therapy, namely in the development of peptide-drug conjugates[114,115].

The absence of studies regarding AM conjugation to CPP constitutes a relevant void in the field of malaria chemotherapy, as carefully selected peptides might act as selective shuttles for intracellular delivery of antimalarials into *P*iRBC. This is particularly pertinent, considering that CPP uptake into *P*iRBC might be significantly enhanced, when compared to that of healthy erythrocytes (hRBC). CPP uptake into heparan sulphate proteoglycans (HSPG)-deficient cells, like hRBC, can be low[116]; however, upon infection, RBC undergo significant changes, including acquired adhesion properties via HSPG-like molecules[117]. Therefore, *P*iRBC might be more permeable to cationic amphipathic CPP than hRBC, as HSPG have been widely associated to internalization of such peptides[116].

Some CPP with particular interest for malaria therapy have been identified. For example, TP10 - a synthetic CPP derived from Transportan, was able to almost completely inhibit blood-stage *Pf* growth (~99%), after 24 h incubation *in vitro* at a concentration of 30 µM, without inducing significant hemolysis at this molarity (5%)[118]. Moreover, DPT-sh1 (derived from casein kinase 2α) and DPT-sh2 (designed *de novo*) were described to efficiently and selectively internalize *P*iRBC[119]. In 2016, crotamine - a naturally occurring CPP with anti-tumoral and anti-fungal properties, was also shown to have antiplasmodial properties, with an IC_{50} of 1.87 µM against *Pf* and high selectivity towards *P*iRBC[120].

These CPP present a key opportunity for the rescuing of classical AM, whose therapeutic value has been spoiled by the emergence of resistant *Plasmodium* strains or whose toxicity overshadows its efficacy. TD may increase these drugs' concentration at site of action, reducing side effects associated to high doses. Furthermore, drug masking with a suitable carrier may elude parasite resistance.

1.6. Bibliography

1. *World Malaria Report 2017,* World Health Organization, Geneva, 2017, *ISBN 978–92–4-156552-3.*
2. K. K. Dayananda, R. N. Achur and D. C. Gowda, *J. Vector Borne Dis.*, 2018, **55**, 1–8.
3. I. N. Nkumama, W. P. O’Meara and F. H. A. Osier, *Trends Parasitol.*, 2017, **33**, 128–140.
4. K. Marsh, D. Forster, C. Waruiru, I. Mwangi, M. Winstanley, V. Marsh, C. Newton, P. Winstanley, P. Warn, N. Peshu, G. Pasvol and R. Snow, *N. Engl. J. Med.*, 1995, **332**, 1399–1404.
5. *World Malaria Report 2016*, World Health Organization, Geneva, 2016, *ISBN 978-92-4-15117- 1*.
6. E. A. Ashley, A. Pyae Phyo and C. J. Woodrow, *Lancet*, 2018, **391**, 1608–1621.
7. B. Thomas, M. Fiore, G. C. Daskhan, N. Spinelli and O. Renaudet, *Chem. Commun.*, 2015, **51**, 5436–5439.
8. E. T. Ngarakana-Gwasira, C. P. Bhunu, M. Masocha and E. Mashonjowa, *Malar. Res. Treat.*, 2016, **2016**, 1–7.
9. N. J. White, S. Pukrittayakamee, T. T. Hien, M. A. Faiz, O. A. Mokuolu and A. M. Dondorp, *Lancet*, 2014, **383**, 723–735.
10. N. F. Walker, B. Nadjm and C. J. M. Whitty, *Med. (United Kingdom)*, 2018, **46**, 52–58.
11. J. D. Batchelor, B. M. Malpede, N. S. Omattage, G. T. DeKoster, K. A. Henzler-Wildman and N. H. Tolia, *PLoS Pathog.*, 2014, **10**, 1, e1003869.
12. R. E. Howes, R. C. Reiner, K. E. Battle, J. Longbottom, B. Mappin, D. Ordanovich, A. J. Tatem, C. Drakeley, P. W. Gething, P. A. Zimmerman, D. L. Smith and S. I. Hay, *PLoS Negl. Trop. Dis.*, 2015, **9**, 1–27.
13. B. Singh, L. K. Sung, A. Matusop, A. Radhakrishnan, S. S. G. Shamsul, J. Cox-Singh, A. Thomas and D. J. Conway, *Lancet*, 2016, **363**, 1017–1024.
14. B. E. Barber, M. J. Grigg, T. William, T. W. Yeo and N. M. Anstey, *Trends Parasitol.*, 2017, **33**, 242–253.

15. M. C. Bruce and K. P. Day, *Curr. Opin. Microbiol.*, 2002, **5**, 431–437.
16. M. Prudêncio, A. Rodriguez and M. M. Mota, *Nat. Rev. Microbiol.*, 2006, **4**, 849–856.
17. A. F. Cowman, J. Healer, D. Marapana and K. Marsh, *Cell*, 2016, **167**, 610–624.
18. I. Mueller, M. R. Galinski, J. K. Baird, J. M. Carlton, D. K. Kochar, P. L. Alonso and H. A. del Portillo, *Lancet Infect. Dis.*, 2009, **9**, 555–566.
19. K. Ersmark, B. Samuelsson and A. Hallberg, *Med. Res. Rev.*, 2006, **26**, 626–666.
20. S. E. Francis, D. J. J. Sullivan and D. E. Goldberg, *Annu. Rev. Microbiol.*, 1997, **51**, 97–123.
21. H. Atamna and H. Ginsburg, *Mol. Biochem. Parasitol.*, 1993, **61**, 231–241.
22. S. Pagola, P. Stephens, D. Bohle, A. Kosar and S. Madsen, *Nature*, 2000, **404**, 307–310.
23. C. Teixeira, J. R. B. Gomes and P. Gomes, *Curr. med. chem.*, 2011, **18**, 1555–1572.
24. L. H. Miller, D. I. Baruch, K. Marsh and O. K. Doumbo, *Nature*, 2002, **415**, 673–679.
25. I. A. Clark, A. C. Budd, L. M. Alleva and W. B. Cowden, *Malar. J.*, 2006, **5**, 1–32.
26. A. Trampuz, M. Jereb, I. Muzlovic and R. M. Prabhu, *Crit. Care*, 2003, **7**, 315–323.
27. M. Thakkar and S. Brijesh, *Drug Deliv. Transl. Res.*, 2016, **6**, 414–425.
28. F. Calderón, D. M. Wilson and F. J. Gamo, in *Progress in Medicinal Chemistry*, Elsevier, 2013, vol. 52, pp. 97–151.
29. E. A. Steck, *The chemotherapy of protozoan diseases*, Walter Reed Army Institute of Research, Washington, 1972.
30. A. F. G. Slater, *Pharmacol. Ther.*, 1993, **57**, 203–2355.
31. T. Cassauwers, Medium.com, medium.com/@tcassauwers/the-global-history-of-the-world-s-first-anti-malaria-drug-d1e11f0ba729.
32. G. R. Coatney, *Am. J. Trop. Med. Hyg.*, 1963, **12**, 121–128.
33. C. Teixeira, N. Vale, B. Pérez, A. Gomes, J. R. B. Gomes and P. Gomes, *Chem. Rev.*, 2014, **114**, 11164–11220.
34. B. M. Greenwood, K. Bojang, C. J. M. Whitty and G. A. T. Targett, *Lancet*, 2014, **365**, 1487–98.

35. U. D'Alessandro, *Expert Opin. Pharmacother.*, 2009, **10**, 1291–1306.
36. J. K. Baird, *N. Engl. J. Med.*, 2005, **352**, 1565–1577.
37. R. M. Fairhurst and A. M. Dondorp, *PLoS Pathog.*, 2016, **11**, 1–14.
38. S. Tripathy and S. Roy, *Asian Pac. J. Trop. Med.*, 2014, **7**, 673–679.
39. N. J. White, *Trends Parasitol.*, 2004, **113**, 1084–1092.
40. H. Noedl, Y. Se, K. Schaecher, B. L. Smith, D. Socheat and M. M. Fukuda, *N. Engl. J. Med.*, 2008, **359**, 2619–2620.
41. C. Amaratunga, S. Sreng, S. Suon, E. S. Phelps, K. Stepniewska, P. Lim, C. Zhou, S. Mao, J. M. Anderson, N. Lindegardh, H. Jiang, J. Song, X. zhuan Su, N. J. White, A. M. Dondorp, T. J. C. Anderson, M. P. Fay, J. Mu, S. Duong and R. M. Fairhurst, *Lancet Infect. Dis.*, 2012, **12**, 851–858.
42. A. C. Uhlemann and D. A. Fidock, *Lancet*, 2012, **379**, 1928–1930.
43. M. P. Kyaw, M. H. Nyunt, K. Chit, M. M. Aye, K. H. Aye, M. M. Aye, N. Lindegardh, J. Tarning, M. Imwong, C. G. Jacob, C. Rasmussen, J. Perin, P. Ringwald and M. M. Nyunt, *PLoS One*, 2003, **8**, 3, e57689.
44. A. M. Dondorp, F. Nosten, P. Yi, D. Das, A. P. Phyo, J. Tarning, K. M. Lwin, F. Ariey, W. Hanpithakpong, S. J. Lee, P. Ringwald, K. Silamut, M. Imwong, K. Chotivanich, P. Lim, T. Herdman, S. S. An, S. Yeung, P. Singhasivanon, N. P. J. Day, N. Lindegardh, D. Socheat and N. J. White, *N. Engl. J. Med.*, 2009, **361**, 455–467.
45. Malaria Site, www.malariasite.com/malaria-drugs/.
46. E. R. Derbyshire, M. M. Mota and J. Clardy, *PLoS Pathog.*, 2011, **7**, 9, e1002178.
47. M. Delves, D. Plouffe, C. Scheurer, S. Meister, S. Wittlin, E. A. Winzeler, R. E. Sinden and D. Leroy, *PLoS Med.*, 2012, **9**, 2, e1001169.
48. S. Vangapandu, M. Jain, K. Kaur, P. Patil, S. R. Patel and R. Jain, *Med. Res. Rev.*, 2007, **27**, 65–107.
49. J. N. Burrows, K. Chibale and T. N. C. Wells, *Curr. Top. Med. Chem.*, 2011, **11**, 1226–1254.
50. S. Singh, A. Singh, M. Singh, D. Sood, B. Rathi, V. Tomar and R. Chandra, *Indian J. Heterocycl. Chem.*, 2018, **28**, 185–193.

51. L. Florens, M. P. Washburn, J. D. Raine, R. M. Anthony, M. Grainger, J. D. Haynes, J. K. Moch, N. Muster, J. B. Sacci, D. L. Tabb, A. A. Witney, D. Wolters, Y. Wu, M. J. Gardner, A. A. Holder, R. E. Sinden, J. R. Yates and D. J. Carucci, *Nature*, 2002, **419**, 520–526.

52. S. J. Draper, B. K. Sack, C. R. King, C. M. Nielsen, J. C. Rayner, M. K. Higgins, C. A. Long and R. A. Seder, *Cell Host Microbe*, 2018, **24**, 43–56.

53. C. H. Coelho, J. Y. A. Doritchamou, I. Zaidi and P. E. Duffy, *npj Vaccines*, 2017, **34**, 1–5.

54. Walsh, F. (24 July 2015). "Malaria vaccine gets 'green light'". *BBC*. Retrieved 25 July 2015

55. S. Casares, T. D. Brumeanu and T. L. Richie, *Vaccine*, 2010, **28**, 4880–4894.

56. R. Gosling and L. von Seidlein, *PLoS Med.*, 2016, **13**, 1–6.

57. A. M. Mendes, M. Machado, N. Gonçalves-Rosa, I. J. Reuling, L. Foquet, C. Marques, A. M. Salman, A. S. P. Yang, K. A. Moser, A. Dwivedi, C. C. Hermsen, B. Jiménez-Díaz, S. Viera, J. M. Santos, I. Albuquerque, S. N. Bhatia, J. Bial, I. Angulo-Barturen, J. C. Silva, G. Leroux-Roels, C. J. Janse, S. M. Khan, M. M. Mota, R. W. Sauerwein and M. Prudêncio, *npj Vaccines*, 2018, **3**, 33.

58. X. Fernàndez-Busquets, *Expert Opin. Drug Deliv.*, 2016, **13**, 919–922.

59. J. Marques, J. J. Valle-Delgado, P. Urbán, E. Baró, R. Prohens, A. Mayor, P. Cisteró, M. Delves, R. E. Sinden, C. Grandfils, J. L. de Paz, J. A. García-Salcedo and X. Fernàndez-Busquets, *Nanomed-Nanotechnol*, 2017, **13**, 515–525.

60. C. Umeyor, F. Kenechukwu, E. Uronnachi, S. Chime, J. Reginald-Opara and A. Attama, *Int. J. Drug Deliv.*, 2013, **5**, 1–14.

61. U. K. Baruah, K. Gowthamarajan, V. Ravisankar, V. V. S. R. Karri, P. K. Simhadri, V. Singh and P. P. Babu, *Artif Cells Nanomed Nanotechnol*, 2017, **46**, 1–21.

62. B. A. Aderibigbe, *Molecules*, 2017, **22**, 1–21.

63. J. Marques, E. Moles, P. Urbán, R. Prohens, M. A. Busquets, C. Sevrin, C. Grandfils and X. Fernàndez-Busquets, *Nanomed-Nanotechnol*, 2014, **10**, 1719–1728.

64. L. N. Borgheti-Cardoso and X. Fernàndez-Busquets, *Future Med. Chem.*, 2018, **10**, 2245–2248.

65. X. Fernàndez-Busquets, *Future Med. Chem.*, 2013, **5**, 737–739.

66. P. Urbán, J. Estelrich, A. Cortés and X. Fernàndez-Busquets, *J. Control. Release*, 2011, **151**, 202–211.

67. E. Moles, S. Galiano, A. Gomes, M. Quiliano, C. Teixeira, I. Aldana, P. Gomes and X. Fernàndez-Busquets, *Biomaterials*, 2017, **145**, 178–191.

68. S. M. Haynes, K. J. Longmuir, R. T. Robertson, J. L. Baratta and A. J. Waring, *Drug Deliv.*, 2008, **15**, 207–217.

69. S. Tripathy, S. Das, S. P. Chakraborty, S. K. Sahu, P. Pramanik and S. Roy, *Int. J. Pharm.*, 2012, **434**, 292–305.

70. S. A. Jain, H. Basu, P. S. Prabhu, U. Soni, M. D. Joshi, D. Mathur, V. B. Patravale, S. Pathak and S. Sharma, *Biomaterials*, 2014, **35**, 6636–6645.

71. R. Tréhin and H. P. Merkle, *Eur. J. Pharm. Biopharm.*, 2004, **58**, 209–223.

72. A. Bell, *Curr. Pharm. Des.*, 2011, **17**, 2719–2731.

73. P. Bulet, C. Hetru, J. L. Dimarcq and D. Hoffmann, *Dev. Comp. Immunol.*, 1999, **23**, 329–344.

74. M. Rautenbach, A. M. Troskie and J. A. Vosloo, *Biochimie*, 2016, **130**, 132–145.

75. M. R. Felício, O. N. Silva, S. Gonçalves, N. C. Santos and O. L. Franco, *Front. Chem.*, 2017, **5**, 1–9.

76. W. E. Robinson, B. McDougall, D. Tran and M. E. Selsted, *J. Leukoc. Biol.*, 1998, **63**, 94–100.

77. H. Tamamura, M. Waki, M. Imai, A. Otaka, T. Ibuka, K. Waki, K. Miyamoto, A. Matsumoto, T. Murakami, H. Nakashima, N. Yamamoto and N. Fujii, *Bioorganic Med. Chem.*, 1998, **6**, 473–479.

78. A. F. Lacerda, P. B. Pelegrini, D. M. De Oliveira, É. A. R. Vasconcelos and M. F. Grossi-de-Sá, *Front. Microbiol.*, 2016, **7**, 1–11.

79. K. V. R. Reddy, R. D. Yedery and C. Aranha, *Int. J. Antimicrob. Agents*, 2004, **24**, 536–547.

80. M. Pushpanathan, P. Gunasekaran and J. Rajendhran, *Int. J. Pept.*, 2013, DOI: 10.1155/2013/675391.

81. W. van't Hof, E. C. Veerman, E. J. Helmerhorst and A. V. Amerongen, *Biol. Chem.*, 2001, **382**, 597–619.

82. N. Lawrence, A. S. M. Dennis, A. M. Lehane, A. Ehmann, P. J. Harvey, A. H. Benfield, O. Cheneval, S. T. Henriques, D. J. Craik and B. J. McMorran, *Cell Chem. Biol.*, 2018, 1–11.

83. R. Feder, R. Nehushtai and A. Mor, *Peptides*, 2001, **22**, 1683–1690.

84. N. Vale, L. Aguiar and P. Gomes, *Front. Pharmacol.*, 2014, **5**, 275.

85. J. Vizioli, P. Bulet, J. A. Hoffmann, F. C. Kafatos, H.-M. Muller and G. Dimopoulos, *Proc. Natl. Acad. Sci.*, 2001, **98**, 12630–12635.

86. C. Tian, B. Gao, M. del C. Rodriguez, H. Lanz-Mendoza, B. Ma and S. Zhu, *Mol. Immunol.*, 2008, **45**, 3909–3916.

87. R. Conde, F. Zamudio, M. Rodríguez and L. Possani, *FEBS Lett.*, 2000, **471**, 165–168.

88. R. Carballar-Lejarazú, M. Rodríguez, F. de la Cruz Hernández-Hernández, J. Ramos-Castañeda, L. Possani, M. Zurita-Ortega, E. Reynaud-Garza, R. Hernández-Rivas, T. Loukeris, G. Lycett and H. Lanz-Mendoza, *Cell. Mol. Life Sci.*, 2008, **65**, 3081–3092.

89. M. S. Love, M. G. Millholland, S. Mishra, S. Kulkarni, K. B. Freeman, W. Pan, R. W. Kavash, M. J. Costanzo, H. Jo, T. M. Daly, D. R. Williams, M. A. Kowalska, L. W. Bergman, M. Poncz, W. F. DeGrado, P. Sinnis, R. W. Scott and D. C. Greenbaum, *Cell Host Microbe*, 2012, **12**, 815–823.

90. K. Srivastava, I. A. Cockburn, A. Swaim, L. E. Thompson, A. Tripathi, C. A. Fletcher, E. M. Shirk, H. Sun, M. A. Kowalska, K. Fox-Talbot, D. Sullivan, F. Zavala and C. N. Morrell, *Cell Host Microbe*, 2008, **4**, 179–187.

91. A. J. Mason, W. Moussaoui, T. Abdelrahman, A. Boukhari, P. Bertani, A. Marquette, P. Shooshtarizaheh, G. Moulay, N. Boehm, B. Guerold, R. J. H. Sawers, A. Kichler, M.-H. Metz-Boutigue, E. Candolfi, G. PreVost and B. Bechinger, *J. Biol. Chem.*, 2009, **284**, 119–133.

92. A. H. Achtman, S. Pilat, C. W. Law, D. J. Lynn, L. Janot, M. L. Mayer, S. Ma, J. Kindrachuk, B. B. Finlay, F. S. L. Brinkman, G. K. Smyth, R. E. W. Hancock and L. Schofield, *Sci. Transl. Med.*, 2012, **4**, 135ra64.

93. G. Rádis-Baptista, I. S. Campelo, J.-É. R. L. Morlighem, L. M. Melo and V. J. F. Freitas, *J. Biotechnol.*, 2017, **252**, 15–26.

94. D. Zhang, J. Wang and D. Xu, *J. Control. Release*, 2016, **229**, 130–139.

95. C. Bechara and S. Sagan, *FEBS Lett.*, 2013, **587**, 1693–1702.

96. N. B. Last, D. E. Schlamadinger and A. D. Miranker, *Protein Sci.*, 2013, **22**, 870–882.

97. S. Trabulo, A. L. Cardoso, A. M. S. Cardoso, C. M. Morais, A. S. Jurado and M. C. de Lima, *Curr. Pharm. Des.*, 2013, **19**, 2895–923.

98. I. R. De Figueiredo, J. M. Freire, L. Flores, A. S. Veiga and M. A. R. B. Castanho, *IUBMB Life*, 2014, **66**, 182–194.

99. C. M. Morais, A. M. Cardoso, P. P. Cunha, L. Aguiar, N. Vale, E. Lage, M. Pinheiro, C. Nunes, P. Gomes, S. Reis, M. M. C. A. Castro, M. C. Pedroso de Lima and A. S. Jurado, *Biochim. Biophys. Acta - Biomembr.*, 2018, **1860**, 2619–2634.

100. M. Kristensen, D. Birch and H. M. Nielsen, *Int. J. Mol. Sci.*, 2016, **17**, E185.

101. A. Dinca, W.-M. Chien and M. T. Chin, *Int. J. Mol. Sci.*, 2016, **17**, 263.

102. A. Bolhassani, B. S. Jafarzade and G. Mardani, *Peptides*, 2017, **87**, 50–63.

103. Z. Li, X. Wang, D. Teng, R. Mao, Y. Hao, N. Yang, H. Chen, X. Wang and J. Wang, *Eur. J. Med. Chem.*, 2018, **145**, 263–272.

104. S. S. Kwon, S. Y. Kim, B. J. Kong, K. J. Kim, G. Y. Noh, N. R. Im, J. W. Lim, J. H. Ha, J. Kim and S. N. Park, *Int. J. Pharm.*, 2015, **483**, 26–37.

105. Y. Wang, W. Sub, Q. Li, C. Li, H. Wang, Y. Li, Y. Cao, J. Chang and L. Zhang, *Int. J. Pharm.*, 2013, **441**, 748–756.

106. M. H. Kang, M. J. Park, H. J. Yoo, K. Y. Hyuk, S. G. Lee, S. R. Kim, D. W. Yeom, M. J. Kang and Y. W. Choi, *Eur. J. Pharm. Biopharm.*, 2014, **87**, 489–499.

107. H. Gao, Q. Zhang, Z. Yu and Q. He, *Curr. Pharm. Biotechnol.*, 2014, **15**, 210–219.

108. S. M. Farkhani, A. Valizadeh, H. Karami, S. Mohammadi, N. Sohrabi and F. Badrzadeh, *Peptides*, 2014, **57**, 78–94.

109. B. K. Gan, C. Y. Yong, K. L. Ho, A. R. Omar, N. B. Alitheen and W. S. Tan, *Sci. Rep.*, 2018, **8**, 8499.

110. G. Salzano and V. P. Torchilin, in *Methods in Molecular Biology*, ed. Ü. Langel, Humana Press, New York, NY, 2015.

111. S. Dissanayake, W. A. Denny, S. Gamage and V. Sarojini, *J. Control. Release*, 2017, **250**, 62–76.

112. D. Raucher and J. S. Ryu, *Trends Mol. Med.*, 2015, **21**, 560–570.

113. N. Vale, A. Ferreira, I. Fernandes, C. Alves, M. J. Araújo, N. Mateus and P. Gomes, *Bioorganic Med. Chem. Lett.*, 2017, **27**, 2898–2901.

114. S. Majumdar and T. J. Siahann, *Med. Res. Rev.*, 2012, **32**, 637–658.

115. E. I. Vrettos, G. Mező and A. G. Tzakos, *Beilstein J. Org. Chem.*, 2018, **14**, 930–954.

116. H. L. Åmand, H. A. Rydberg, L. H. Fornander, P. Lincoln, B. Nordén and E. K. Esbjörner, *Biochim. Biophys. Acta - Biomembr.*, 2012, **1818**, 2669–2678.

117. A. M. Vogt, G. Winter, M. Wahlgren and D. Spillmann, *Biochem. J.*, 2004, **381**, 593–7.

118. R. B. G. Arrighi, C. Ebikeme, Y. Jiang, L. Ranford-Cartwright, M. P. Barrett, Ü. Langel and I. Faye, *Antimicrob. Agents Chemother.*, 2008, **52**, 3414–3417.

119. J. Guergnon, F. Dessauge, V. Dominguez, J. Viallet, S. Bonnefoy, V. J. Yuste, O. Mercereau-Puijalon, X. Cayla, A. Rebollo, S. A. Susin, P. Bost and A. Garcia, *Mol. Pharmacol.*, 2006, **69**, 1115–24.

120. S. El Chamy Maluf, C. Dal Mas, E. B. Oliveira, P. M. Melo, A. K. Carmona, M. L. Gazarini and M. A. F. Hayashi, *Peptides*, 2016, **78**, 11–16.

2

Rationale

2.1. Working hypothesis

Considering the potential value of the previously reported antimalarial peptides and the relevance of rescuing formerly approved drugs to tackle both the lack of truly new chemotypes in the antimalarial drug pipeline, and the emergence of parasite strains resistant to virtually all AM available in the clinics, the working hypothesis of this project settled on exploration of CPP as carriers for known AM: by producing covalent CPP-AM conjugates, it is expected that they will be able to display an improved intracellular delivery and antimalarial action, as compared to the parent drugs.

2.2. Choice of the peptide carriers

A few CPP were carefully chosen as building blocks for the target CPP-AM conjugates (Table 2.1): TP10 was selected given its intrinsic antiplasmodial activity[1], DPT-sh1 and DPT–sh2 were chosen, considering their reported ability to specifically accumulate in *P*iRBC[2], and IDR-1018 was also included in the set, as it might be able to potentiate the antimalarial effect of the conjugated AM. Additionally, classical CPP were also considered, such as (i) Tat[3] - derived from the HIV-1 Tat protein, (ii) PasTat[4] - a chimeric peptide, which results from the modification of Tat with a penetration accelerating sequence, (iii) R9[5] – one of the polyarginine peptides that have been early identified as valuable carriers for intracellular cargo delivery, (iv) Penetratin[6] – a widely studied CPP early identified in the *Antennapedia* homeodomain, and (v) Transportan[7] - a chimeric CPP resulting from a combination of the neuropeptide galanin and the wasp venom peptide toxin mastoparan, and from which TP10 is derived.

Table 2.1 – CPP chosen to act as vehicles for AM.

CPP	Amino Acid Sequence	Molecular Weight [a]	Net Charge [a]
TP10	AGYLLGKINLKALAALAKKIL	2182	+5
DPT-sh1	VKKKKIKREIKI	1510	+7
DPT-sh2	RQKRLIRQKRLIRQKRLI	2402	+10
IDR-1018	VRLIVAVRIWRR	1535	+5
Tat	GRKKRRQRRRPPQ	1718	+9
PasTat	FFLIPKGGRKKRRQRRRPPQ	2521	+10
R9	RRRRRRRRR	1423	+10
Transportan	GWTLNSAGYLLGKINLKALAALAKKIL	2840	+5
Penetratin	RQIKIWFQNRRMKWKK	2246	+8

[a] Values obtained from Bachem's Peptide Calculator

2.3. Choice of the AM cargoes

2.3.1. Chloroquine

CQ is a weak base which permeates into the acidic FV of the *Plasmodium* parasite; once inside this compartment, the molecule becomes protonated and consequently trapped, as membranes are not permeable to the charged forms of the drug[8]. Inside the FV, CQ is believed to block heme polymerization and disrupt heme conjugation with glutathione, which are the major heme-detoxification pathways used by the parasite; ultimately, the CQ-induced heme accumulation in cytosol and membranes of the parasite leads to its death[9].

Although parasite resistance to CQ is a multifactorial phenomenon that continues to be an active area of investigation, it is firmly established that the *PfCRT* (*Pf* CQ resistance transporter), which results from a mutation in a transmembrane protein of the FV, plays a central role in the widespread therapeutic failure of CQ. The *PfCRT* transporter is believed to act as an efflux pump for CQ, not allowing for its accumulation inside the FV in sufficient amount to achieve therapeutic concentrations[10–12].

From the above, CQ emerged as an obvious choice to serve as proof of concept on the doctoral project's working hypothesis. In other words, this once brilliant AM – for its efficacy, safety, good pharmacokinetics and low cost – might recover its spark upon conjugation to a CPP, with an expectedly higher internalization efficiency and, possibly, the ability of the conjugate to elude the *PfCRT* "efflux pump" in CQ-resistant *Pf* strains. Moreover, the use of CPP with reported ability to act on *P*iRBC, such as TP10, DPT-sh1 and DPT-sh2, made this approach particularly suited for combating blood-stage infection, on which CQ acts.

It was considered that CPP conjugation should be made at the CQ's aliphatic chain, due both to the long-track record of the research group on modifying antimalarial aminoquinolines and acridines in such a way[13,14], and – more importantly – to the fact that chemical modifications on the quinoline core of CQ have been shown to produce a significantly negative impact on the drug's biological activity[15,16]. As the tertiary aliphatic amine of CQ is unsuitable for covalent conjugation to the CPP carrier *via* a peptide bond, it was decided to use a CQ analogue - 4-(*N*-aminobutyl)amino-7-chloroquinoline (CQn, Figure 2.1), which had been previously synthetized in our research group for the development of novel compounds that displayed remarkable antiplasmodial activity[14].

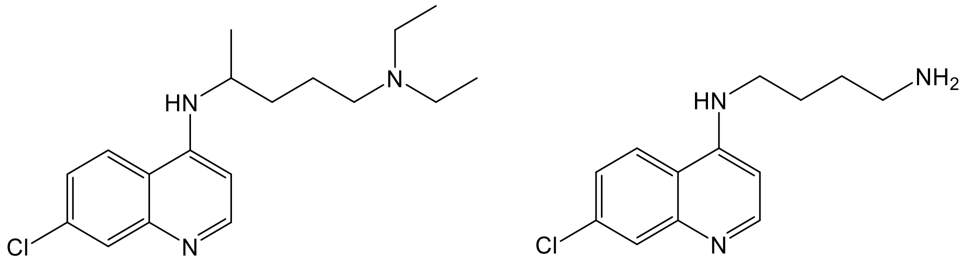

CQ **CQn**

Figure 2.1 – Structures of CQ and its analogue, CQn, used henceforward for the synthesis of CQ-CPP conjugates.

2.3.2. Primaquine

As mentioned in the previous chapter, PQ was until very recently[17] unique in its broad spectrum activity,[18] particularly against liver stage infections, asexual forms of blood stage *Pv* and gametocytes of all species of *Plasmodium.* Thus, it is useful as a primary prophylaxis agent against all species that cause human malaria and for the radical cure of *Pv* or *P. ovale* infections[19]; moreover, in endemic regions, PQ is used as a gametocytocide to prevent transmission of the infection from the human host to the mosquito vector, thus blocking the spread of the disease[20,21]. As for other antimalarial 8-aminoquinolines, the mechanism of action of PQ is not clear, although it has been postulated that it relates to the inhibition of the electron transport respiratory chain[22].

Nonetheless, PQ is not devoid of serious drawbacks. One of the most relevant adverse effects of PQ (and of several of its metabolites), just like of other 8-aminoquinolines, is methemoglobinemia - a pathological condition arising from abnormal accumulation of methemoglobin, the auto-oxidation product of the hemoglobin iron core[21]. Hemolytic anemia is another complication that arises from PQ's metabolism; this is severely aggravated for people deficient in 6-glucose phosphate dehydrogenase, a common genetic trait in areas where malaria is endemic[21,23,24]. On top of this, the low plasma half-life of PQ, which is rapidly and extensively metabolized to carboxyprimaquine (lacking of significant antimalarial activity), increases the doses and frequency of their administration[21], which further amplifies the adverse effects[25].

The above limitations of PQ-based therapies restricted their wider use, and has driven the search for other agents that could replicate its therapeutic value, without the severe adverse effects. In fact, PQ conjugation to amino acids, oligopeptides and peptidomimetics has been reported to delay or even block oxidative deamination into carboxyprimaquine, which in turn would allow the use of lower drug doses[4,26–29]. Hence, PQ was also considered as an appropriate AM for conjugation to CPP, as this might increase its concentration at the site of action as well as limit its metabolic inactivation, thus contributing to decrease its adverse effects.

2.4. Bibliography

1. R. B. G. Arrighi, C. Ebikeme, Y. Jiang, L. Ranford-Cartwright, M. P. Barrett, Ü. Langel and I. Faye, *Antimicrob. Agents Chemother.*, 2008, **52**, 3414–3417.
2. J. Guergnon, F. Dessauge, V. Dominguez, J. Viallet, S. Bonnefoy, V. J. Yuste, O. Mercereau-Puijalon, X. Cayla, A. Rebollo, S. A. Susin, P. Bost and A. Garcia, *Mol. Pharmacol.*, 2006, **69**, 1115–24.
3. E. Vives, P. Brodin and B. Lebleu, *J. Biol. Chem.*, 1997, **272**, 16010–16017.
4. K. Takayama, I. Nakase, H. Michiue, T. Takeuchi, K. Tomizawa, H. Matsui and S. Futaki, *J. Control. Release*, 2009, **138**, 128–133.
5. Z. Li, H. Ding and Y. Ma, *Soft Matter*, 2013, **9**, 1281–1286.
6. B. Christiaens, J. Grooten, M. Reusens, A. Joliot, M. Goethals, J. Vandekerckhove, A. Prochiantz and M. Rosseneu, *Eur. J. Biochem.*, 2004, **271**, 1187–1197.
7. M. Pooga, M. Hällbrink, M. Zorko and Ü. Langel, *FASEB J.*, 1998, **12**, 67–77.
8. R. Thomé, S. C. P. Lopes, F. T. M. Costa and L. Verinaud, *Immunol. Lett.*, 2013, **153**, 50–57.
9. E. Davioud-Charvet, S. Delarue, C. Biot, B. Schwöbel, C. C. Boehme, A. Müssigbrodt, L. Maes, C. Sergheraert, P. Grellier, R. H. Schirmer and K. Becker, *J. Med. Chem.*, 2001, **44**, 4268–4276.
10. J. Papakrivos, J. Sá and T. Wellems, *PLoS One*, 2012, **7**, e39569.
11. F. Calderón, D. M. Wilson and F. J. Gamo, in *Progress in Medicinal Chemistry*, Elsevier, 2013, vol. 52, pp. 97–151.
12. D. Krogstad, I. Gluzman, D. Kyle, A. Oduola, S. Martin, W. Milhous and P. Schlesinger, *Science*, 1987, **238**, 1283–1285.
13. A. Gomes, M. Machado, L. Lobo, F. Nogueira, M. Prudêncio, C. Teixeira and P. Gomes, *ChemMedChem*, 2015, **10**, 1344–1349.
14. B. Pérez, C. Teixeira, J. Gut, P. Rosenthal, J. Gomes and P. Gomes, *ChemMedChem*, 2012, **7**, 1537–1540.
15. A. F. G. Slater, *Pharmacol. Ther.*, 1993, **57**, 203–2355.

16. P. E. Thompson and L. M. Werbel, *Antimalarial Agents: Chemistry and Pharmacology*, Academic Press, 1972.
17. J. E. Frampton, *Drugs*, 2018, **78**, 1517–1523.
18. J. K. Baird, *N. Engl. J. Med.*, 2005, **352**, 1565–1577.
19. D. R. Hill, J. K. Baird, M. E. Parise, L. S. Lewis, E. T. Ryan and A. J. Magill, *Am. J. Trop. Med. Hyg*, 2006, **75**, 402–415.
20. J. K. Baird, *Expert Opin Emerg Drugs*, 2012, **17**, 439–444.
21. N. Vale, R. Moreira and P. Gomes, *Eur. J. Med. Chem.*, 2009, **44**, 937–953.
22. D. Fernando, C. Rodrigo and S. Rajapakse, *Malar. J.*, 2011, **10**, 351.
23. M. D. Cappellini and G. Fiorelli, *Lancet*, 2008, **371**, 64–74.
24. E. Bleuter, *Blood*, 1994, **84**, 3613–3636.
25. G. Mata, V. E. Do Rosário, J. Iley, L. Constantino and R. Moreira, *Bioorg. Med. Chem.*, 2012, **20**, 886–892.
26. L. Constantino, P. Paixão, R. Moreira, M. J. Portela, V. E. Do Rosario and J. Iley, *Exp. Toxicol. Pathol.*, 1999, **51**, 299–303.
27. D. M. Copolovici, K. Langel, E. Eriste and Ü. Langel, *ACS Nano*, 2014, **8**, 1972–1994.
28. N. Vale, J. Matos, J. Gut, F. Nogueira, V. do Rosário, P. J. Rosenthal, R. Moreira and P. Gomes, *Bioorg. Med. Chem. Lett.*, 2008, **18**, 4150–4153.
29. H. Brooks, B. Lebleu and E. Vive, *Adv. Drug Deliv. Rev.*, 2005, **57**, 559–577.

3

Goals

The global aim of this project was the development of novel peptide-drug conjugates where CPP, selected to be used as potential shuttles to promote intracellular delivery of classical antimalarial drugs, were covalently linked to the latter. As mentioned in the previous chapter (*cf.* Chapter 2), a subset of the selected CPP had intrinsic antimalarial activity against the blood stage infection; hence, conjugation to CQn was primarily addressed. With this in mind, the following tasks were planned:

(i) chemical synthesis of CQn-CPP conjugates – this task comprised the synthesis of both the selected CPP (*cf.* Chapter 2) and the chloroquine analogue CQn, followed by conjugation of these two building blocks *via* a succinyl spacer;
(ii) *in vitro* screening of the conjugates' inhibitory activity against blood stage *Plasmodium* parasites;
(iii) exploration of different spacers/conjugation approaches to link CQn to the CPP having shown best antiplasmodial activity in (ii);
(iv) *in vitro* evaluation of the antiplasmodial activity of the novel conjugates synthesized in (iii);
(v) profiling of the interactions between selected conjugates and model membranes (mimicking healthy and parasitized cells), and of the conjugates uptake into hRBC and PiRBC;
(vi) *in vivo* evaluation of conjugates showing potent antimalarial action along with low cytotoxicity.

Complementary to the study above described, the development of similar PQ-CPP conjugates was also planned, to judge on whether the same approach might be useful to address liver stage infections. This additional study encompassed the following tasks:

(vii) chemical synthesis of PQ-CPP conjugates, as done in task (i) for CQn, *i.e.*, starting with the synthesis of selected CPP that were subsequently coupled to PQ *via* a succinyl spacer;
(viii) *In vitro* evaluation of the activity the PQ-CPP conjugates against liver stage infections;
(ix) profiling the conjugates' uptake into healthy and infected hepatocytes.

4

Synthesis of CQn-C4-CPP conjugates and evaluation of their *in vitro* activity against blood-stage malaria

4.1. Overview

This chapter reports the chemical synthesis (**4.2**) and *in vitro* evaluation (**4.3**) of CQn-C4-CPP conjugates against blood-stage *Plasmodium* parasites. It includes (**4.2.1**) the synthesis of CQn, (**4.2.2**) CQn functionalization with a succinyl spacer, to produce CQn-C4, (**4.2.3**) solid-phase synthesis (SPPS) of the selected CPP, (**4.2.4**) on-resin conjugation of CQn-C4 to CPP, and (**4.3**) evaluation of their *in vitro* activity of the against blood-stage *Pf* parasites.

4.2. Chemical synthesis

The synthesis of CQn-C4-CPP conjugates was performed according to the synthetic route presented in Scheme 4.1. Briefly, 4,7-dichloroquinoline (**1**) was initially converted into 4-(*N*-aminobutyl)amino-7-chloroquinoline (CQn, **2**), *via* a nucleophilic aromatic substitution with butane-1,4-diamine (**3**). Then, in order to insert a carboxyl moiety in this molecule – for posterior condensation with the CPP's *N*-terminus, the primary amine of CQn was reacted with succinic anhydride (**4**), *via* an addition-elimination mechanism, to produce 4-[{4-(7-chloroquinolin-4-yl)aminobutyl}amino]-4-oxobutanoic acid (CQn-C4, **5**). The latter was then coupled to the terminal amine of the peptide (anchored to a solid support, in the form of peptidyl-resin), in the presence of appropriate coupling agents, to generate the final CQn-C4-conjugate anchored to the solid support. This procedure was repeated for all CPP indicated in Table 4.1. CQn-C4-CPP synthesis was completed upon their cleavage, i.e., detachment from the solid support (*aka* resin).

Table 4.1 – Peptides conjugated to CQn

CPP	Amino Acid Sequence	Molecular Weight	Net Charge
TP10	AGYLLGKINLKALAALAKKIL	2181.40	+5
DPT-sh1	VKKKKIKREIKI	1510.04	+7
DPT-sh2	RQKRLIRQKRLIRQKRLI	2401.58	+10
IDR-1018	VRLIVAVRIWRR	1535.99	+5
Tat	GRKKRRQRRRPPQ	1718.05	+9
PasTat	FFLIPKGGRKKRRQRRRPPQ	2520.53	+10
R9	RRRRRRRRR	1422.92	+10
Transportan	GWTLNSAGYLLGKINLKALAALAKKIL	2839.71	+5
Penetratin	RQIKIWFQNRRMKWKK	2245.29	+5

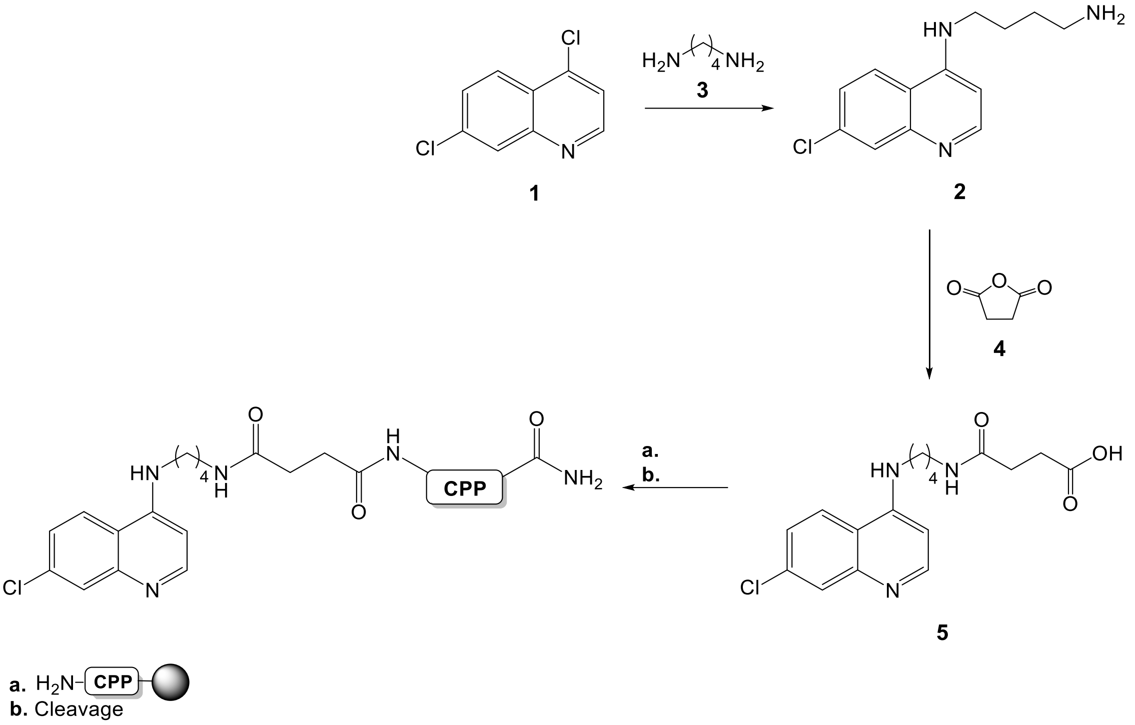
Cl
Cl
N
1
H_2N
4
NH_2
3
HN
NH_2
Cl
N
2
O
O
O
4
HN
4
N
H
O
OH
O
Cl
N
5
a.
b.
HN
4
N
H
O
H
N
O
CPP
O
NH_2
Cl
N
a. H_2N–CPP
b. Cleavage

Scheme 4.1 – Route for the synthesis of CQn-C4-CPP conjugates.

4.2.1. Synthesis of 4-(*N*-aminobutyl)amino-7-chloroquinoline (CQn)

In this work, synthesis of CQn was achieved by a nucleophilic aromatic substitution (S_NAr). Nucleophilic substitutions in aromatic systems usually occur through an addition-elimination mechanism, in which the nucleophile interacts with one of the vacant π orbitals from the aromatic system – addition step. If this attack occurs at a position occupied by a leaving group (**X**), substitution occurs upon a second step, where the leaving group is expelled – elimination step (Scheme 4.2)[1,2].

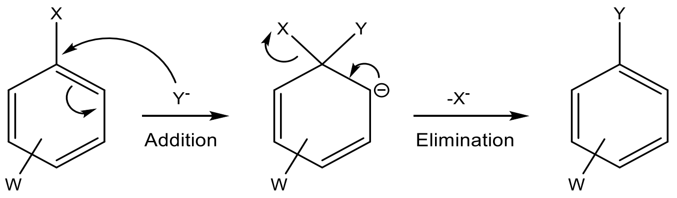
X
W
Y^-
Addition
X
Y
W
-X^-
Elimination
Y
W

Scheme 4.2 – General mechanism of an S_NAr (Y = nucleophile; X = leaving group; W = electron withdrawing group).

Generally, S$_{N}$Ar are energetically demanding reactions, as they generate a temporary disruption of the extremely stable aromatic π system. Yet, the aromatic ring may be activated by the presence of electron-withdrawing groups (EWG), such as nitro, cyano or carbonyl groups. 4-halopyridines and other related heterocyclic compounds are also good substrates for S$_{N}$Ar[1,3]; this includes 4,7-dichloroquinoline, the starting material used in this work to react with butane-1,4-diamine to produce the target CQn *via* the S$_{N}$Ar depicted in Scheme 4.3. In this case, the nucleophilic attack occurs preferentially at carbon 4 of the quinoline ring: it is the most electrophilic carbon in this heterocycle, since it is simultaneously linked to a chlorine atom (in this case, the leaving group) and in *para* position relatively to the pyridinic nitrogen.

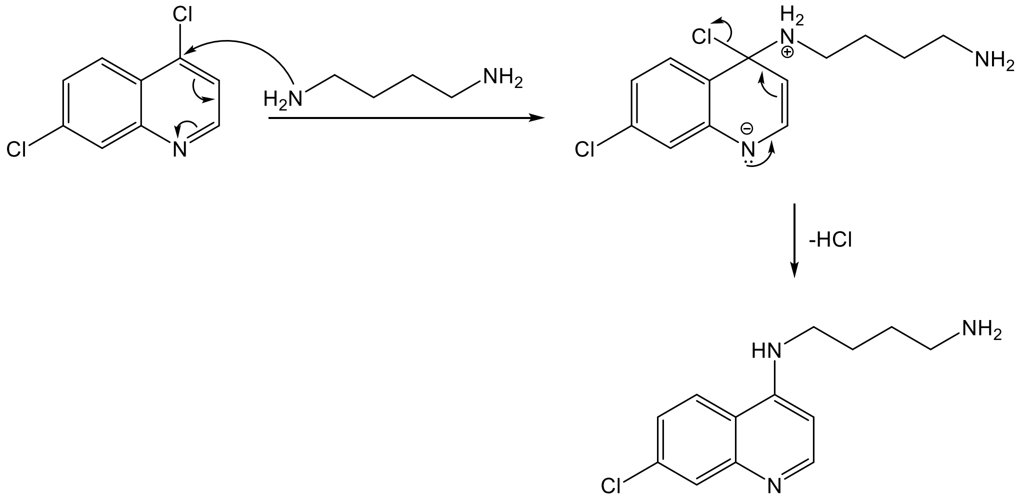

CQn (2)

Scheme 4.3 –S$_{N}$Ar of butane-1,4-diamine on 4,7-dichloroquinoline, to deliver CQn.

Experimentally, the synthesis of CQn was achieved by employing an in-house method, previously reported by Pérez *et al.*[4]. Briefly, 4,7-dichloroquinoline was dissolved in an excess of butane-1,4-diamine, and the reaction allowed to proceed for 3 hours, under reflux (100 ^{o}C). The target product was isolated in high yields (~ 80%), confirming the good nucleophilic character of the diamine and the sufficient activation of the heteroaromatic system to undergo an S$_{N}$Ar. The product obtained (CQn) presented analytical data in agreement with those previously reported[4], and was used with no further purification in the subsequent reaction steps. Figure 4.1 depicts the obtained mass spectrum (ESI-IT MS), which presents a peak at $^{m}/_{z}$ = 250.33, compatible with the quasi-molecular ion (MH^+) of CQn, whose exact mass is 249.10 atomic mass units (a.m.u.).

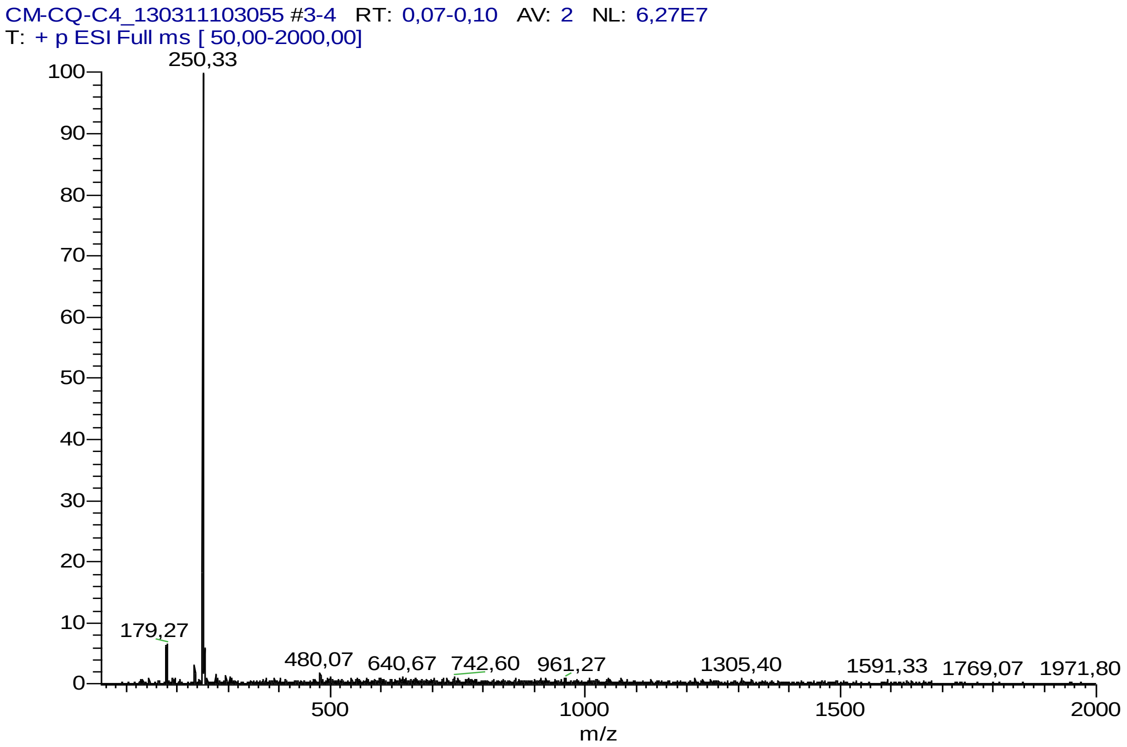

Figure 4.1 – ESI-IT MS spectrum (positive mode) of CQn (**2**).

4.2.2. Synthesis of 4-[*N*-(*N*'-carboxypropanoyl)aminobutyl]amino-7-chloroquinoline (CQn-C4)

CQn was further reacted with a carboxylic anhydride, in order to insert a free carboxyl group for subsequent "on-resin" coupling to the *N*-terminus of the selected CPP. Carboxylic anhydrides (**6**, Scheme 4.4) are susceptible to nucleophilic acyl substitutions, also known as nucleophilic addition-elimination reactions, in agreement with the two-step process that occurs. This reaction starts with a nucleophilic attack on one of the carbonylic carbons of the anhydride, with the formation of a tetrahedral intermediate - addition step. This next leads to the displacement of the leaving carboxylate group – the elimination step.

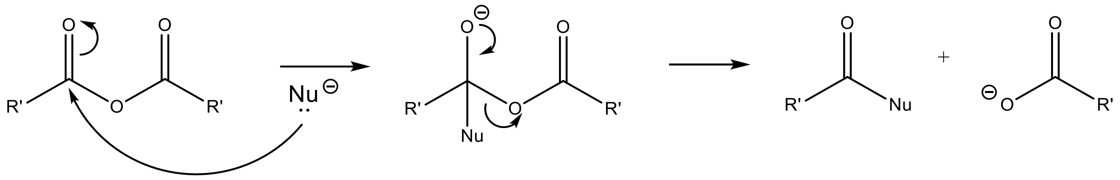

6

Scheme 4.4 – Nucleophilic acyl substitution of a symmetric carboxylic anhydride (**6**).

Carboxylic anhydrides are quite reactive species, for more than one reason. First of all, the carbon of carbonyl group is extremely susceptible to nucleophilic attacks, due to the polarization of the C=O bond - which results in a partially positive carbon and a partially negative oxygen. Besides, the planar configuration in the vicinity of the carbonyl group facilitates the nucleophilic attack. Finally, the reactivity of anhydrides is also justified by the stability of the carboxylate leaving group[5].

In this work, a cyclic symmetric anhydride (succinic anhydride) was used, so that upon nucleophilic attack by the primary amine from CQn, an amide bond between both building blocks is formed, with concomitant opening of the ring and release of the free carboxylate (Scheme 4.5) required for the subsequent conjugation to the CPP.

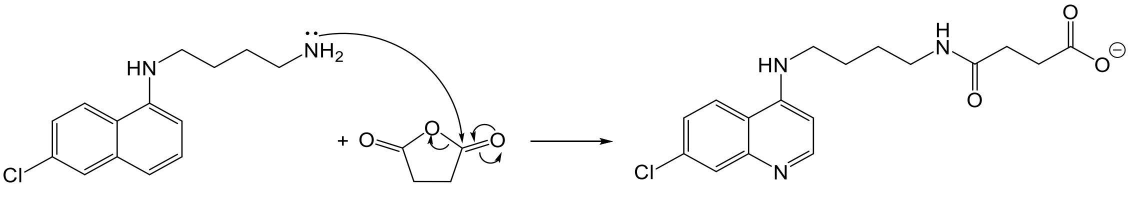

CQn (2) **CQn-C4 (5)**

Scheme 4.5 – Nucleophile acyl substitution of succinic anhydride by CQn, to produce CQn-C4.

The reaction took place at room temperature, for 3 hours, using *N*-ethyl-*N,N*-diisopropylamine (DIPEA) as base and dimethylformamide (DMF) as solvent. Formation of CQn-C4 was followed by thin-layer chromatography (TLC), and observed to be a clean and apparently quantitative process; yet, as traces of succinic anhydride would interfere with the following conjugation step, it was decided to isolate CQn-C4 by liquid chromatography on silica gel, which provided the pure product in high yield (~ 85%).

Structural characterization of the final product by ESI-IT MS confirmed it to be the target molecule; the obtained spectrum (Figure 4.2) presents a peak at $^{m}/_{z}$ = 350.67, which is compatible with the quasi-molecular ion (MH^+) of CQn-C4, whose exact mass is 349.12 a.m.u..

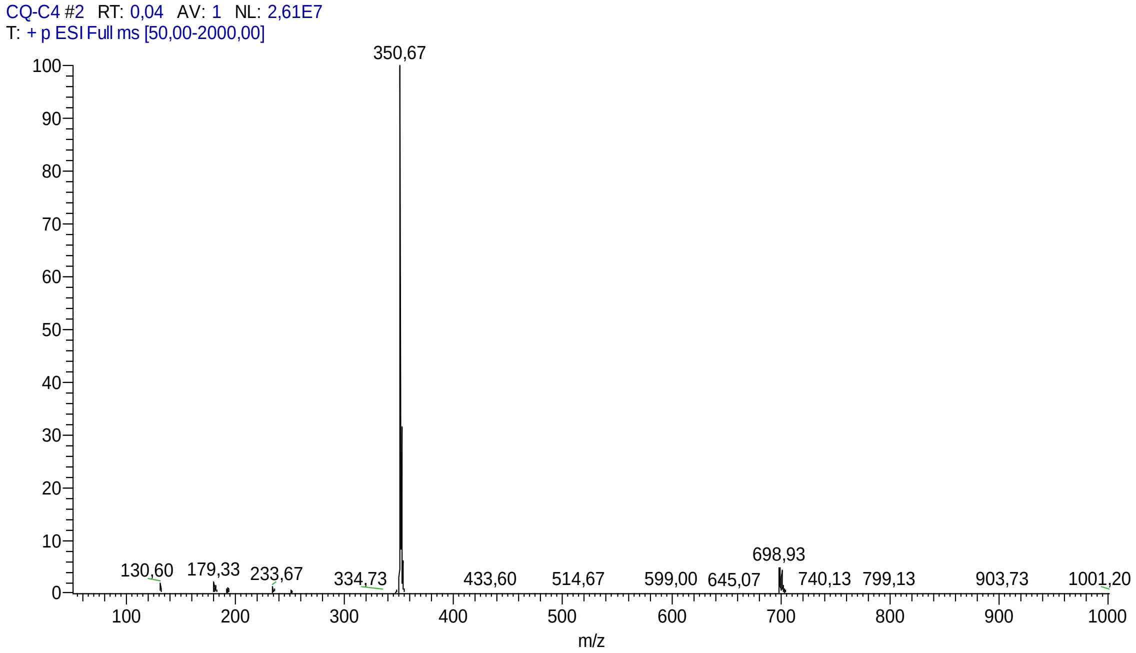

Figure 4.2 – ESI-IT MS spectrum (positive mode) of CQn-C4.

4.2.3. Synthesis of the selected CPP

4.2.3.1. The peptide bond

Peptide synthesis is based on the sequential connection of α-AA through an amide (or peptide) bond, by means of a nucleophilic addition-elimination (condensation) reaction between the α-amino group of the first AA to the carboxylic group of the second AA.

Peptide bonds play a crucial role in biological systems, as they are extremely stable and capable of establishing hydrogen bonds with other atoms due to their high polarity, acting either as donors or acceptors in these interactions[6].

While the reaction between an amine and a carboxylic acid is thermodynamically viable, it is not kinetically favored; thus, at room temperature (or below), without the appropriate activation of the carboxyl moiety, the combination of these groups will result in an acid-base equilibrium, with the formation of a stable salt (Scheme 4.6). The amide bond formation requires significantly higher temperatures (160-180 °C), usually incompatible with peptide synthesis[7,8].

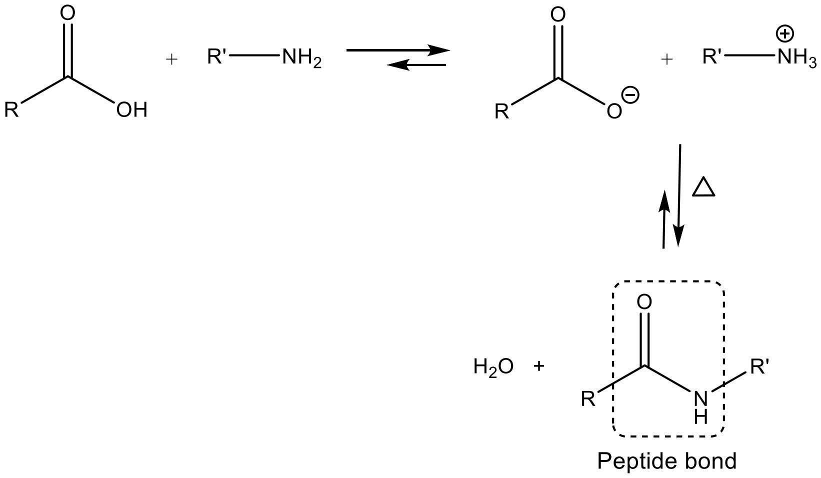

Scheme 4.6 - Formation of a stable salt between an amine and a carboxylic acid and its thermal conversion into an amide.

Alternatively, to avoid resorting to such high temperatures, the carboxylic acid can be activated (converted in a more reactive derivative), so that it promptly reacts with the nucleophile amine, through a condensation reaction (Scheme 4.7). In order to achieve a peptide condensation with soft conditions, two steps are required: (i) activation of the carboxyl moiety of AA1, generally through the so called coupling (activating; condensation) agents, which promote the substitution of the hydroxyl group of the carboxylic acid with a better leaving group (At) and (ii) the nucleophilic attack from the amino group of AA2 to the activated carboxyl group, to generate the desired amide.

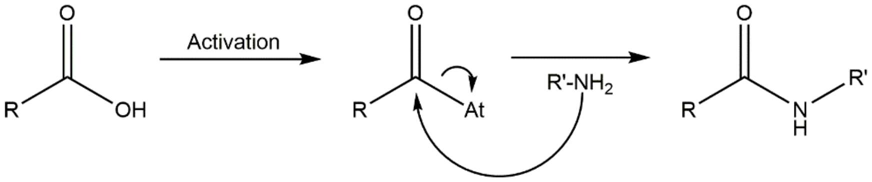

Scheme 4.7 – Activation of the carboxylic acid, with the formation of a reactive intermediary; this is then prone to suffer a nucleophilic attack from the amine of AA2, with consequent formation of an amide, after elimination of the activating group.

4.2.3.2. Basic principles of solid-phase peptide synthesis (SPPS)

Considering peptides’ biological importance, it became imperative to facilitate the access to these molecules in the amounts necessary and with a high purity degree for their biological application.

In 1963 emerged what was considered the greatest revolution in the field of peptide synthesis: the invention of solid-phase peptide synthesis, by Robert Bruce Merrifield, which earned him a Nobel prize in chemistry, in 1984[9,10]. This strategy allows for peptide production in much larger scales than non-synthetic strategies and it affords much higher yields of pure peptides. Moreover, it enables the incorporation of unnatural AA or the introduction of other chemical modifications that aim to improve the therapeutic value of the peptide.

The basic principle of this strategy consists in the anchorage of the first (*C*-terminal) α-amino protected AA to a solid support (resin; Scheme 4.8 – Step 1): this bond must be able to withstand all of the reactions employed during the elongation of the peptide chain, which occurs in $C_t \rightarrow N_t$ direction, and the resin itself must be insoluble and stable to the different physical and chemical conditions employed throughout the elongation of the peptide, as well as easily cleavable upon completion of the AA sequence. Hence, the resin acts both as insoluble support (over which the peptide chain is built) and carboxyl protecting group of the *C*-terminal AA; all AA are sequentially added and any unreacted compounds or byproducts are easily washed away by filtration of the insoluble peptidyl-resin. The following step comprises the deprotection on the α-amino group of the AA incorporated onto the resin, rendering it available to react with the following AA, through a coupling reaction. The peptide chain is elongated through repetitive cycles of (i) incorporation of protected AA and (ii) consequent removal of the α-amino protecting group (PG) – designated temporary PG (Scheme 4.8 – Step 2). All of the coupling and deprotection steps are performed with a large excess of soluble reagents – to enforce the occurrence of quantitative reactions, followed by the washing of the peptidyl-resin with appropriate solvents, such as dichloromethane (DCM) and *N*,*N*-dimethylformamide, for the removal of surplus reagents and byproducts.

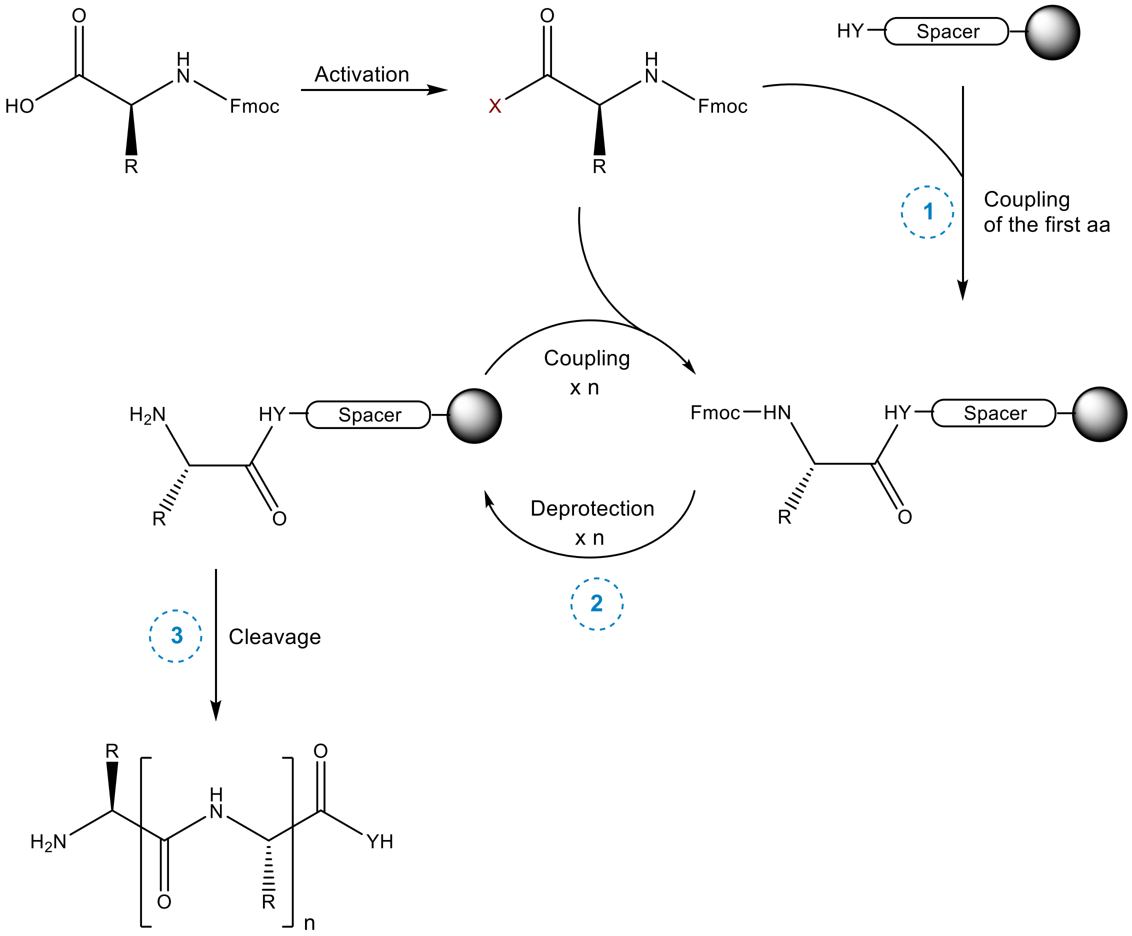

Scheme 4.8 - General scheme of SPPS. *C*-terminal of the final peptide may be obtained as a carboxamide (Y = NH) or carboxylic acid (Y = O).

Considering the diversity of functional groups present in the different AA, the suppression of reactivity of other groups an appropriate combination of protecting groups (protection schemes) is vital for a regioselective reaction. These are intended to prevent the oligomerization between the molecules of the AA that is being incorporated in the peptide chain (temporary N^{α}-PG, removed after a complete coupling reaction) or between functional groups from the AA's side-chains, either among themselves or the activated AA that is being incorporated (permanent PG, only removed upon peptide release from the resin), thus guaranteeing a successful synthesis. In SPPS, two protection schemes are used: (i) Boc/Bzl and (ii) Fmoc/^{t}Bu; these designations arise from the groups used for temporary and permanent protection, respectively. Thus, in the Boc/Bzl protection scheme, *terc*-butyloxycarbonyl (Boc), is used as N^{α}-PG, labile towards acids such as trifluoroacetic acid (TFA) at concentrations higher than 30%; this requires that this PG is combined with permanent PG that can withstand this conditions, such as benzyl (Bzl), among others. This was the first reported protection scheme, used by Merrifield upon the introduction of SPPS[10]. The Fmoc/^{t}Bu orthogonal protection scheme uses 9-fluorenylmethyloxycarbonyl (Fmoc) as the N^{α}-PG, stable in acidic conditions and labile towards bases, particularly secondary amines; this allows for the use of permanent protecting groups that are labile in acidic conditions, including TFA, such as *terc*-butyl (^{t}Bu)[11]. In this protection scheme, Fmoc removal is generally performed with a solution of 20% piperidine in DMF; these smooth conditions don't lead to premature cleavage and are completely compatible with the permanent PG, such as ^{t}Bu, labile in acidic conditions, but stable in a basic medium. Cleavage and concomitant removal of the permanent PG of a peptide that is built using this strategy, is generally performed by acidolysis with TFA. This orthogonal protection scheme leads to much higher yields and purity of the crude peptide. Moreover, its minor chemical aggressiveness makes it compatible with a substantially larger variety of PG and chemical modifications, as well as automated systems for peptide synthesis. This has rendered Fmoc/^{t}Bu the preferential protection scheme for SPPS.

As mentioned above, the reaction between an amine and a carboxylic acid requires prior activation of the latter, attained by coupling agents, which promote *in situ* activation of the carboxyl moiety (Scheme 4.7). This activation is based on the formation of an intermediary active ester - a generally fast reaction, even for sterically hindered AA. There are numerous classes of coupling agents, such as carbodiimides and phosphonium or uronium salts; the latter are usually more efficient, allowing for reduced reaction times and the improvement of the synthetic global yield.

Carbodiimides (**7**) were the first class of *in situ* condensation agent to be developed, in the mid-20th century. When reacting with a carboxylic acid, carbodiimides generate a labile *O*-acyl-isourea (**8**), prone to undergo a nucleophilic attack (Scheme 4.9). Thus, if this isourea is generated in the presence of an amine, these will promptly react to produce the desired amide.

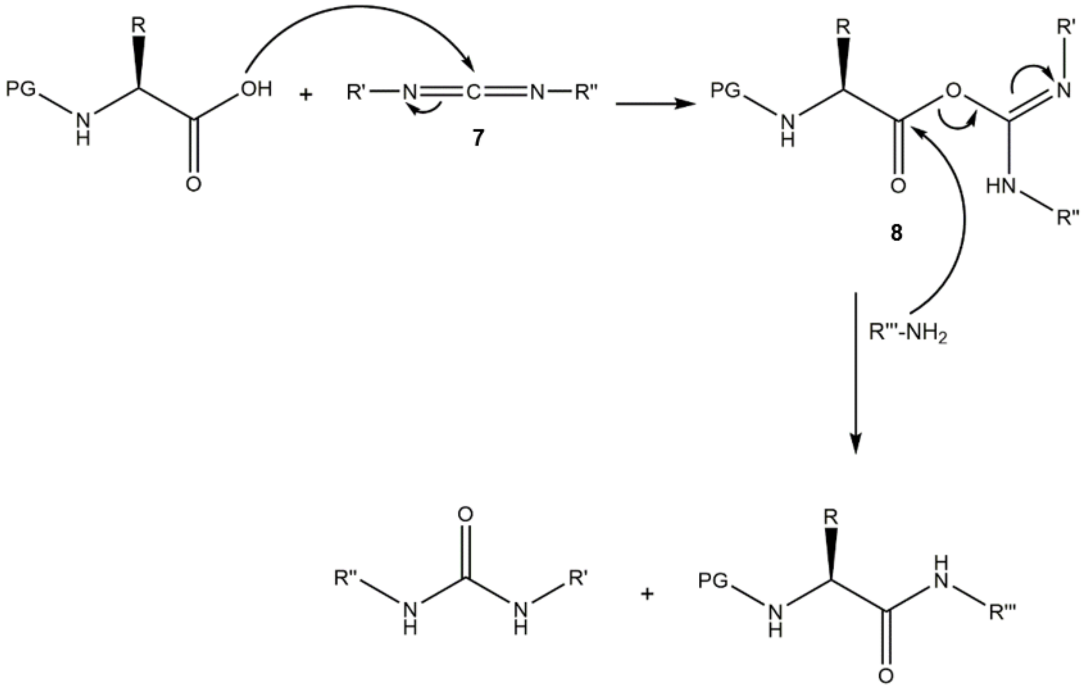

Scheme 4.9 - Activation of a carboxyl group by a carbodiimide (**7**) and subsequente reaction of the *O*-acyl-isourea (**8**) with a nucleophilic amine, to generate the desired amide.

However, the high reactivity of the *O*-acyl-isourea is often associated to side-reactions[12,13]. Soon after, auxiliary nucleophiles, such as 1-hydroxybenzotriazole (HOBt; **9**)[14], were introduced; these nucleophile species were used alongside carbodiimides to promptly react with the *O*-acyl-isourea (**7**) and prevent said side reactions (Scheme 4.10)[15,16].

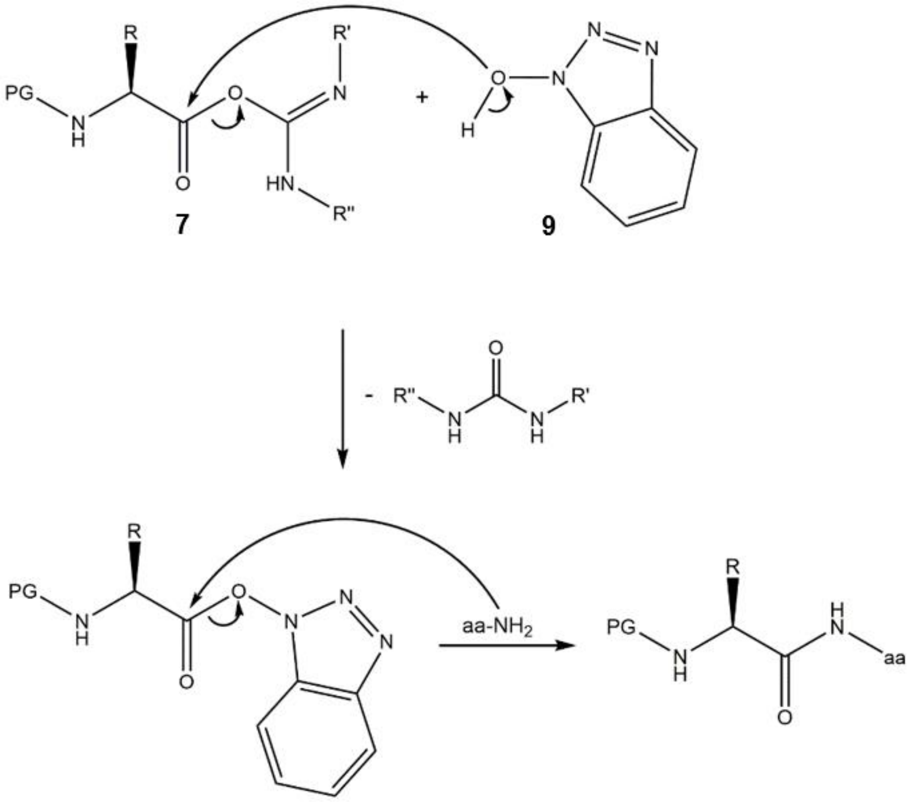

Scheme 4.10 - Nucleophilic attack by HOBt to an *O*-acyl-isourea and consequent aminolysis of the benzotriazolyl ester formed.

The successful combination of HOBt with carbodiimides lead to the synthesis of several new *in situ* coupling agents, capable of producing results comparable to those obtained from this combination. Thus appeared the so called uronium and phosphonium salts, such as *O*-benzotriazol-1-yl-*N,N,N',N'*-tetramethyluronium hexafluorophosphate (HBTU; **10**) or (benzotriazol-1-yl-oxy)tripyrrolidinophosphonium hexafluorophosphate (PyBOP; **11**) – among many others (Figure 4.3). HBTU was introduced as a coupling agent in 1978[17,18] and is, presently, the most widely used for SPPS[19–21].

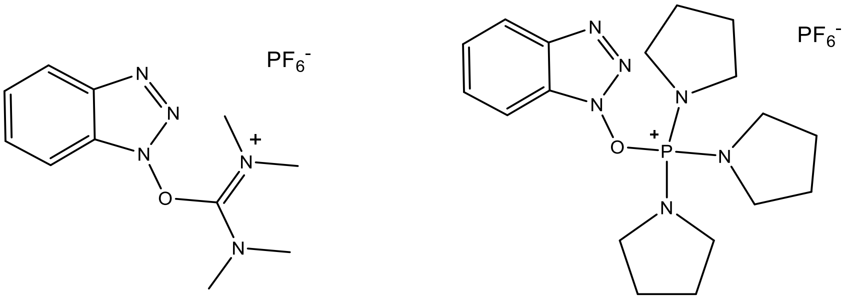
PF$_6^-$
N
N
N
O
N
N
+
PF$_6^-$
N
N
N
O
P
+
N
N
N

10 **11**

Figure 4.3 – Chemical structure of HBTU (**10**) and PyBOP (**11**)

These uronium and phosphonium salts are used in the presence of tertiary amines, such as DIPEA, whose role is to deprotonate the N^{α}-protected amino acid. The latter, now a carboxylate, promptly reacts with the phosphonium or uronium salt, producing a reactive benzotriazolyl ester. Scheme 4.11 depicts the mechanism of reaction between an AA and HBTU (**10**), to generate a reactive benzotriazolyl ester (**12**), prone to suffer a nucleophilic attack from an amine.

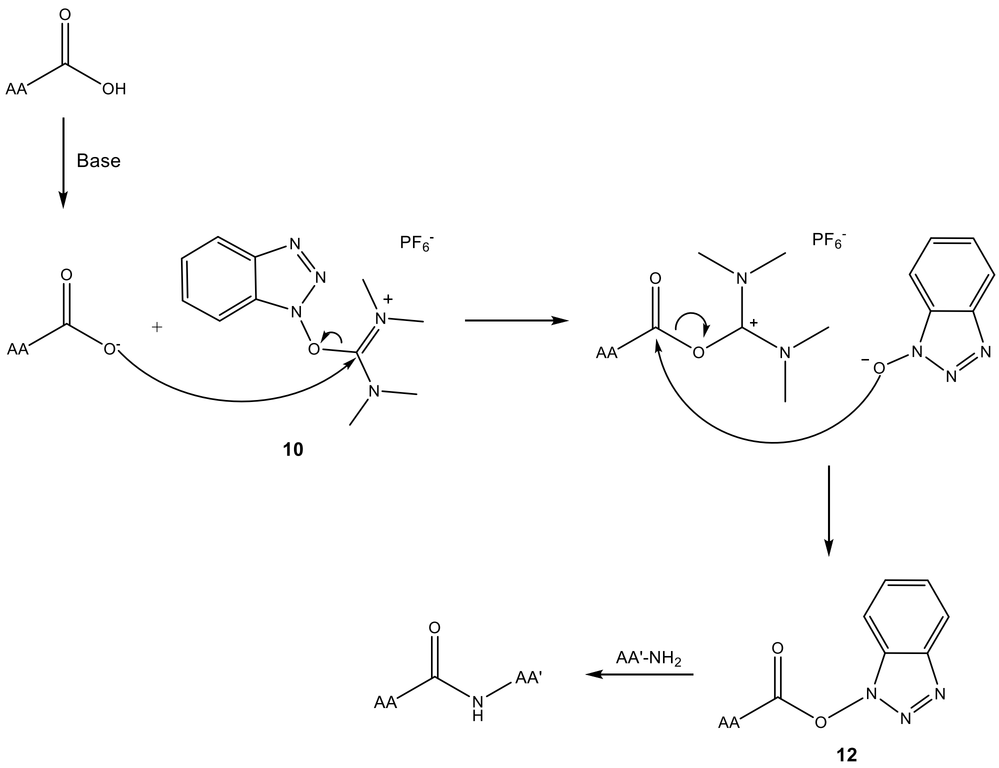
O
AA
OH
Base
O
AA
O-
+
N
N
N
O
N
+
N
PF$_6^-$
10
O
AA
O
N
+
N
PF$_6^-$
-O
N
N
N
O
AA
N
H
AA'
AA'-NH$_2$
O
AA
O
N
N
N
12

Scheme 4.11 - Mechanism of acivation of a carboxyl group via reaction with an uronium salt.

The elongation of the peptide chain is performed, as previously described, through repetitive deprotection/coupling cycles. Notwithstanding the use of appropriate coupling agents or deprotection solutions and favorable experimental conditions, it is possible that (i) an amino acid doesn't react completely with all the free amine groups from the peptidyl-resin or (ii) the removal of the α-amino PG isn't complete. Hence, it is advised to monitor all the coupling/deprotection reactions, in order to avoid the synthesis of deletion sequences. One way of rapidly monitoring the efficiency of each step consists on performing a ninhydrin test, a precise colorimetric test, capable of detecting primary amine groups, even in small amounts. Ninhydrin (**13**, pale yellow) reacts with the α-amino group of an AA at high temperatures, generating a compound intensely purple (**14**, Ruhemann's purple), which accuses the presence of primary amine groups in the sample (Scheme 4.12)[22].

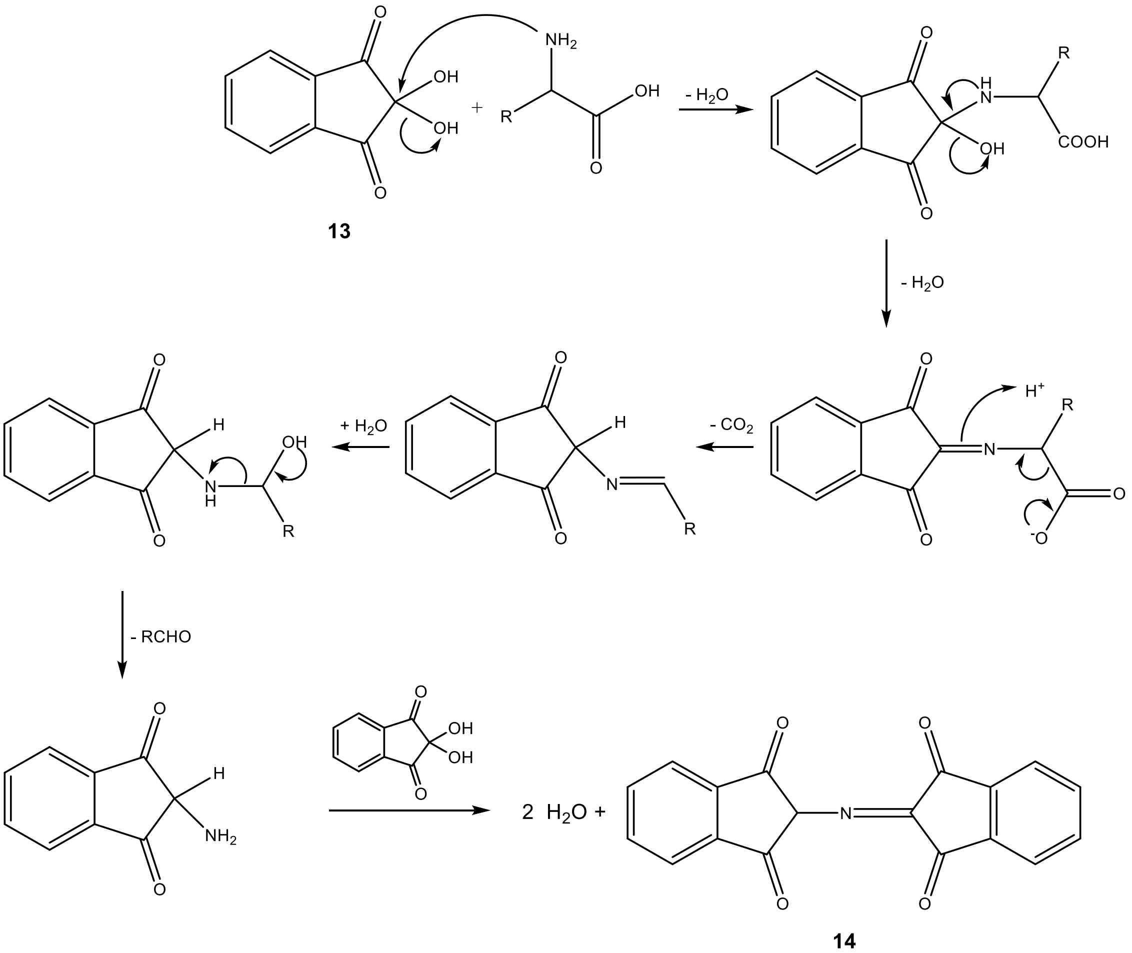

Scheme 4.12 – Reaction of Ninhydrin with the α-NH_2 group of an amino acid.

Once the elongation of the peptide sequence is concluded, the cleavage of the peptide usually takes place, with the goal of separating it from the resin and removing the PG from the AA's side chains. As mentioned above, when the peptide is assembled using a Fmoc/^{t}Bu protection scheme, the cleavage of the peptide-resin bond is usually performed through acidolysis with TFA (Scheme 4.13).

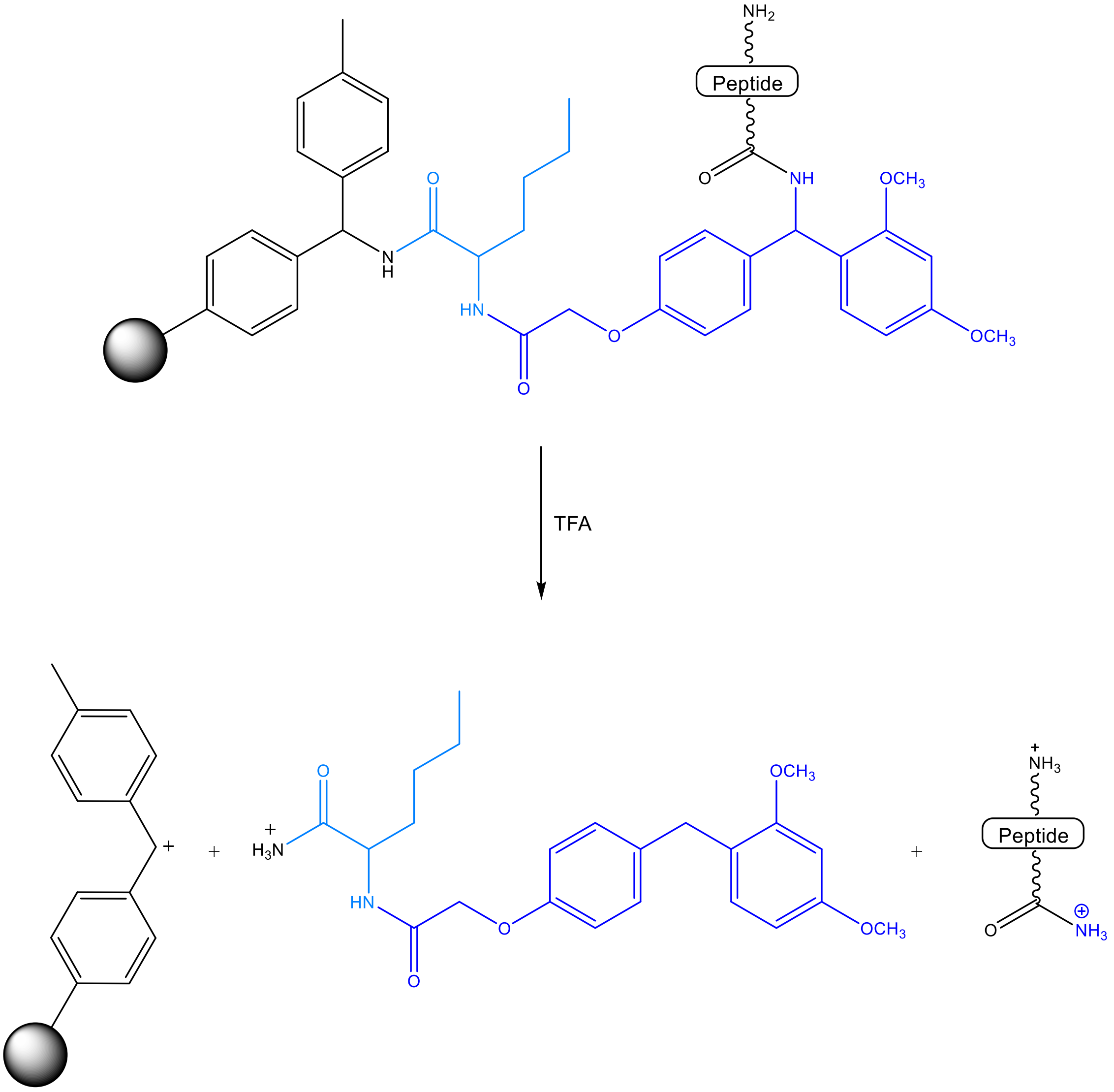

Scheme 4.13 – Cleavage of the resin-peptide bond. This scheme represents a situation where peptide's *C*-terminal is obtained as a carboxamide, synthesized over an MBHA resin, modified with the Rink spacer.

Side chain protecting groups, also removed during the acidolytic cleavage (reaction that usually follows an S_N1 mechanism) originate relatively stable carbocations, either tertiary or stabilized by resonance. These carbocations, however, are still very reactive electrophile species, capable of reacting with some nucleophile side chains, irreversibly modifying the peptide chain. Therefore, it is important to add scavengers – very reactive nucleophile species, capable of quickly neutralizing the electrophiles generated during the acidolysis process, to the TFA solution[23,24]. Thus, cleavage is performed using the so called cleavage cocktail, which consists in a TFA solution (90-95%) with the appropriate scavangers (water, trialkyl silanes, thiols), according to the synthetized amino acid sequence. One of the most popular cleavage cocktails – for being generically efficient and odorless, is composed by TFA (95%), water (2.5%) and triisopropylsilane (TIS; 2.5%). These two scavengers are capable of rapidly capturing carbocations such as *terc*-butyl, trityl, trimethoxybenzyl and arylsulfonyl, generated during the acidolysis[23].

The major advantage of SPPS when compared to peptide synthesis in solution, is its greater simplicity, quickness and efficiency of the synthetic procedure. In solution-phase synthesis, each synthetic intermediary must be isolated and purified after each reactional step, which renders this process a very expensive and prolonged one. Moreover, the use of excess reagents is not convenient, as such would significantly difficult the subsequent purification steps. Following a SPPS strategy, a substantial amount of time can be saved, as there is no need for the isolation nor purification of synthetic intermediaries, and the global yield is considerably improved, since the whole process is conducted in the same reaction vessel and the use of excess reagents is encouraged – these are posteriorly removed by washing and filtrating the peptidyl-resin contained in the reaction vessel.

4.2.3.3. Peptides' synthesis **via** *SPPS*

Peptides were synthetized through SPPS methodologies, using an orthogonal Fmoc/^{t}Bu protection scheme. Fmoc-Rink Amide MBHA resin (with a functionalization of 0,52 mmol/g) was used as a solid support; this consists on a PS-DVB base polymer, modified with methylbenzidrylamine groups (MBHA), which are, in turn, conjugated to *p*-(2',4'-dimethoxyphenyl-Fmoc-aminomethyl)-phenoxyacetic acid (Fmoc-Rink) through a norleucine (Nle) residue (Figure 4.4).

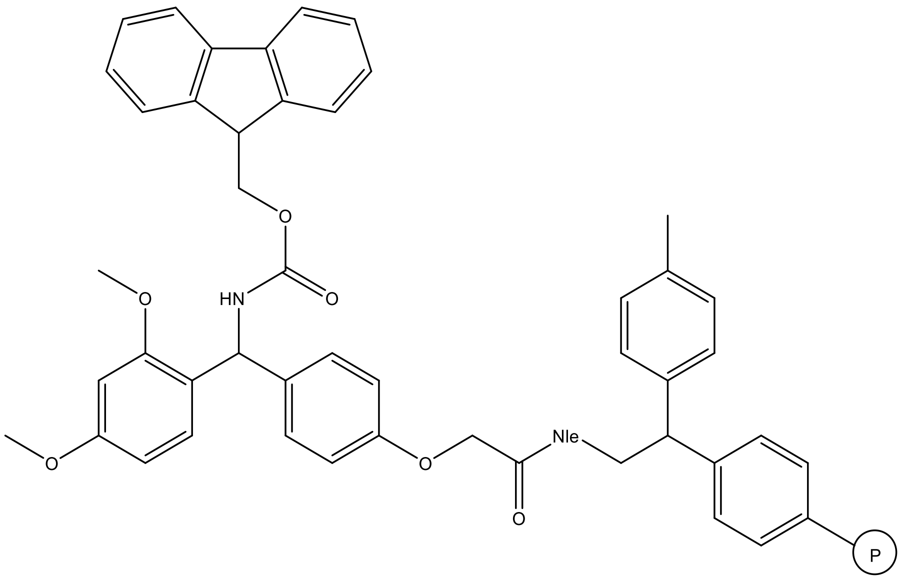

Figure 4.4 – Structure of Fmoc-Rink Amide MBHA Resin (the letter “P” represents the polymer PS-DVB).

The Fmoc group was initially removed from the resin with a solution of piperidine (20%) in DMF, followed by resin-washing steps, with DMF and DCM, with the goal of removing excess reagent and products of the deprotection reaction. The first N^{α}-Fmoc-protected amino acid (Fmoc-AA-OH) was then coupled to the spacer’s free amine, using HBTU as coupling agent, in the presence of DIPEA. Peptide chain elongation was performed through repetitive deprotection and coupling reactions - intercalated by resin washing with DMF and DCM, which were monitored by the Kaiser test. If, at any time, this test revealed the reaction had been incomplete, the latter was repeated. When a Fmoc-AA-OH coupling reaction had to be repeated, the coupling agent HBTU was substituted by *O*-(7-Azabenzotriazol-1-yl)-*N,N,N',N'*-tetramethyluronium hexafluoro-phosphate (HATU), generally more efficient. For the repetition of deprotection reactions, a solution of 50% piperidine in DMF was used.

4.2.4. Synthesis of the target CQn-C4-CPP conjugates

Once the AA sequences of the target CPP were fully assembled on-resin, the peptidyl-resins were divided in two portions; one portion was reserved for subsequent cleavage to produce the free CPP, whereas the other half was further reacted with CQn-C4 through a standard condensation reaction; to this end, the carboxyl group in CQn-C4 was pre-activated with PyBOP, in the presence of DIPEA, for 30 minutes, and the mixture was then added to the peptidyl-resin and left stirring overnight, after which the resin was dried by suction filtration and thoroughly washed with DMF and DCM.

All the peptidyl resins (CPP only and CQn-C4-CPP resins) were cleaved by a two hour acidolysis, generally using a cleavage cocktail constituted by TFA (95%), TIS (2.5%) and water (2.5%). For the cleavage of CPP bearing more than two arginine residues, and also of their CQn-C4 conjugates, a cleavage cocktail containing TFA (90%), thioanisole (5%), 1,2-etanedithiol (3%) and anisole (2%) was used instead. After cleavage, liquid chromatography with diode array detection (LC-DAD) coupled to mass spectrometry using electrospray ionization and ion trap detection (ESI-IT MS), was used to confirm the presence of the target structures in the crude synthetic products; the target structures were then isolated by reverse phase high-performance liquid chromatography (RP-HPLC) at a preparative scale, and finally analyzed by ESI-IT MS and analytical HPLC, to confirm their structure and determine their purity degree. The results obtained are depicted in Table 4.2 and 4.3.

Table 4.2 – Synthesized CPP and respective analytical data, obtained by HPLC (purity and retention time – R_t) and LC-DAD/ESI-IT MS (detected m/z).

CPP	Molecular Weight	Purity / %	R_t / minutes *	Detected $^m/_z$
TP10	2181.40	99	15.6	1091.60 ($[M+2H^+]^{2+}$); 728.13 ($[M+3H^+]^{3+}$); 546.33 ($[M+4H^+]^{4+}$)
DPT-sh1	1510.04	97	9.7	755.54 ($[M+2H^+]^{2+}$); 504.03 ($[M+3H^+]^{3+}$); 378.27 ($[M+4H^+]^{4+}$); 302.82 ($[M+5H^+]^{5+}$)
DPT-sh2	2401.58	91	9.5	801.54 ($[M+2H^+]^{2+}$); 601.41 ($[M+3H^+]^{3+}$); 481.33 ($[M+4H^+]^{4+}$); 401.27 ($[M+5H^+]^{5+}$)
IDR-1018	1535.99	97	11.6	1535.73 ($[M+H^+]^{+}$); 768.60 ($[M+2H^+]^{2+}$); 512.87 ($[M+3H^+]^{3+}$); 385.13 ($[M+4H^+]^{4+}$)
Tat	1718.05	96	7.4	859.54 ($[M+2H^+]^{2+}$); 573.36 ($[M+3H^+]^{3+}$); 430.28 ($[M+4H^+]^{4+}$); 344.42 ($[M+5H^+]^{5+}$)
PasTat	2520.53	92	10.4	631.14 ($[M+4H^+]^{4+}$); 505.12 ($[M+5H^+]^{5+}$); 421.10 ($[M+6H^+]]^{6+}$); 361.09 ($[M+7H^+]]^{7+}$)
R9	1422.92	93	7.5	712.00 ($[M+2H^+]^{2+}$); 475.20 ($[M+3H^+]^{3+}$); 356.73 ($[M+4H^+]^{4+}$)
Transportan	2839.71	89	16.2	1420.67 ($[M+2H^+]^{2+}$); 947.60 ($[M+3H^+]^{3+}$); 711.20 ($[M+4H^+]^{4+}$); 569.27 ($[M+5H^+]^{5+}$)
Penetratin	2245.29	98	10.8	1123.66 ($[M+2H^+]^{2+}$); 749.44 ($[M+3H^+]^{3+}$); 562.33 ($[M+4H^+]^{4+}$); 450.07 ($[M+5H^+]^{5+}$)

* Value determined by HPLC, with a gradient elution of 1-100% ACN in water (0.05% TFA), for 30 minutes, at a flow rate of 1 mL/min.

Table 4.3 - Synthesized CQn-C4-CPP and respective analytical data, obtained by HPLC (purity and retention time – R_t) and LC-DAD/ESI-IT MS (detected m/z).

CPP	Molecular Weight	Purity / %	R_t / minutes	Detected $^m/_z$
CQn-C4-TP10	2512.51	97	15.6	1257.80 ($[M+2H^+]^{2+}$); 839.07 ($[M+3H^+]^{3+}$); 629.47 ($[M+4H^+]^{4+}$)
CQn-C4-DPT-sh1	1841.15	99	10.0	921.59 ($[M+2H^+]^{2+}$); 614.73 ($[M+3H^+]^{3+}$); 431.30 ($[M+4H^+]^{4+}$); 369.24 ($[M+5H^+]^{5+}$)
CQn-C4-DPT-sh2	2732.68	99	10.0	912.27 ($[M+3H^+]^{3+}$); 684.47 ($[M+4H^+]^{4+}$); 547.80 ($[M+5H^+]^{5+}$); 456.93 ($[M+6H^+]]^{6+}$)
CQn-C4-IDR-1018	1867.10	90	13.3	467.79 ($[M+4H^+]^{4+}$); 374.43 ($[M+5H^+]^{5+}$); 313.14 ($[M+6H^+]]^{6+}$)
CQn-C4-Tat	2049.16	87	8.0	684.13 ($[M+3H^+]^{3+}$); 513.47 ($[M+4H^+]^{4+}$); 411.33 ($[M+5H^+]^{5+}$); 342.93 ($[M+6H^+]]^{6+}$)
CQn-C4-PasTat	2851.64	98	12.3	951.89 ($[M+3H^+]^{3+}$); 714.17 ($[M+4H^+]^{4+}$); 571.54 ($[M+5H^+]^{5+}$); 476.45 ($[M+6H^+]]^{6+}$)
CQn-C4-R9	1753.11	94	9.3	585.36 ($[M+3H^+]^{3+}$); 439.27 ($[M+4H^+]^{4+}$); 351.62 ($[M+5H^+]^{5+}$); 293.18 ($[M+6H^+]]^{6+}$)
CQn-C4-Transportan	3170.11	96	17.1	1058.29 ($[M+3H^+]^{3+}$); 793.97 ($[M+4H^+]^{4+}$); 635.38 ($[M+5H^+]^{5+}$)
CQn-C4-Penetratin	2576.40	95	12.7	860.15 ($[M+3H^+]^{3+}$); 645.36 ($[M+4H^+]^{4+}$); 430.58 ($[M+5H^+]^{5+}$); 369.21 ($[M+6H^+]^{6+}$)

* Value determined by HPLC, with a gradient elution of 1-100% ACN in water (0.05% TFA), for 30 minutes, at a flow rate of 1 mL/min.

4.3. *In vitro* assays

The synthetic CQn-C4-CPP conjugates prepared, and their corresponding parent CPP were screened *in vitro* for their ability to inhibit development of blood-stage forms of a CQ-resistant strain (W2) of *Pf*. These assays were carried out at the Prof. Philip J. Rosenthal's lab, in the University of California at San Francisco, United States of America. Briefly, synchronized ring stage W2 *Pf* parasites were cultured with test compounds for 48 h; after this period, parasitemia was estimated *via* a fluorescence-activated cell sorter (FACS)-based analysis[25]. IC_{50} values thus obtained are reported in Table 4.4.

Table 4.4 – Half-maximal inhibitory concentration for free peptides and CQn-CPP conjugates.

CPP	IC_{50} / nM	CQn-C4-CPP	IC_{50} / nM
TP10	5531	CQn-C4-TP10	1521
DPT-sh1	*	CQn-C4-DPT-sh1	*
DPT-sh2	*	CQn-C4-DPT-sh2	*
IDR-1018	*	CQn-C4-IDR-1018	*
Tat	*	CQn-C4-Tat	*
PasTat	*	CQn-C4-PasTat	8502
R9	*	CQn-C4-R9	*
Transportan	3048	CQn-C4-Transportan	5195
Penetratin	*	CQn-C4-Penetratin	*

* These compounds presented an IC_{50} higher than 10 μM.

Unconjugated CPP did not display intrinsic antiplasmodial activity, with the exception of TP10 and Transportan that exhibited, as expected, slight inhibitory activity[26].

Coupling CQn-C4 to the CPP did not contribute to any improvement of antiplasmodial activity, except for TP10, whose intrinsic activity was substantially enhanced upon conjugation. Remarkably, conjugation to Transportan had the opposite effect, even though this peptide and TP10 are closely related, as TP10 derives from Transportan's structure[27]. Another surprising observation was the lack of antimalarial activity for CQn-C4-DPT-sh1 and –sh2 conjugates, as these CPP had been chosen on the basis of their alleged ability to selectively internalize *P*iRBC [28]. This observation, along with the fact that most of the conjugates did not display antiplasmodial activity *in vitro*, was hypothesized to be due to the inability of the antimalarial cargo to exert its action while attached to the CPP carrier through a highly stable amide link, rather than to an inability of the conjugate to get inside the target cells. Actually, according to seminal works on antimalarial aminoquinolines, including CQ and related compounds, the aliphatic basic amine plays a crucial role for activity[29–31]; hence, it may be argued that acylation of this amine for subsequent coupling to the CPP might underlie the overall modest results herein reported. However, such an argument does not explain why the CQn-C4-TP10 conjugate is more active than its parent peptide. Moreover, our group has previously demonstrated that it is possible to produce *N*-acylated derivatives of antimalarial 4-aminoquinolines like CQ[32], 8-aminoquinolines like PQ[33,34], and acridines like MPR[35], with remarkably improved antimalarial activities, as compared to their parent drugs.

In view of the above, it was decided to investigate how a variation of the spacer and conjugation chemistry might affect the *in vitro* antimalarial activity of CQn-CPP conjugates. To this end, CQn and TP10 were invariably used as the AM and CPP building blocks, as described on the next chapter.

4.4. Experimental Section

4.4.1. Materials, instrumentation and general methods

Except where otherwise stated, chemicals used for this work were purchased from Sigma-Aldrich. Rink-amide MBHA resin (0.52 mmol/g), N^{α}-Fmoc-protected amino acids, and HBTU were from NovaBiochem. HPLC gradient or LC-MS grade solvents were from Merck.

Aluminum foils coated with silica-gel 60 F254 from Merck were used for TLC analysis, and TLC chromatograms obtained were revealed under ultra-violet light (254 nm), using a Viber Lourmat lamp, model CN-6.

For purification of CQn-C4, normal phase liquid chromatography was used, utilizing silica gel 60, from Sigma-Aldrich, as stationary phase. A mixture of DCM and methanol (MeOH; 1:1) was used as the mobile phase (eluent).

ESI-IT MS analysis (direct injection mode) were performed with solutions of the pure products in MeOH (LC-MS grade), using a Finnigan Surveyor LCQ DECA XP MAX spectrometer, at the Department of Chemistry and Biochemistry of the Faculty of Sciences of the University of Porto.

LC-DAD/ESI-IT MS analysis of crude synthetic peptides and conjugates was performed on a Finnigan Surveyor LCQ DECA XP MAX spectrometer coupled to a Finnigan Surveyor HPLC, equipped with a photodiode array (PDA) Plus Detector, an Autosampler Plus and an LC Pump Plus, from Thermo Electron Corporation. To this end, samples were prepared by dissolution of crude products in aqueous acetic acid (10% v/v).

Purification of CPP and CQn-C4-conjugates was carried out by preparative HPLC, to a purity of at least 90%. To this end, samples were injected in a LaPrep Sigma VWR preparative HPLC system equipped with an UV detector LP 3104 and an LP 1200 pump; a reverse-phase C18 column (250 × 25 mm ID and 5 µm pore size) from Merck was used, and a gradient elution using a varying relative proportion of 0.05% aqueous

TFA (eluent A) and acetonitrile (eluent B) was carried out for 60 minutes at a flow rate of 15 mL/min.

Peptide analysis by analytical HPLC was done using a Hitachi-Merck Elite LaChrom system equipped with an L-2130 quaternary pump, an L-2200 thermostatted (Peltier effect) automated sampler, and an L-2455 diode-array detector (DAD). Samples were prepared by dissolution of crude products in aqueous acetic acid (10% v/v) and injected in a reverse phase C18 column Purospher star RP-C18 of 125 × 4.0 mm and 5 µm pore size was used. A gradient elution of varying proportions of eluents A and B was carried out for 30 minutes, at a flow rate of 1 mL/min and detection was set at 220 nm. Pure peptide fractions were pooled and freeze-dried, using a VirTis freeze drier, model BenchTop Pro 9L with Omnitronics, from SP Scientific.

4.4.2. Synthesis of CQn

1.0 molar equivalents (eq) of 4,7-dichloroquinoline and 10.0 eq of butane-1,4-diamine were mixed in a round bottom flask, and the resulting solution was heated to 100 ^{o}C and left under reflux for 3 hours. Then, the mixture was allowed to cool down to room temperature, diluted with 25 mL of DCM and washed with an aqueous solution of Na_2CO_3 (three times). The organic phase was then dried with anhydrous Na_2SO_4 and, after filtration, DCM was evaporated under reduced pressure. The resulting white solid was chromatographically homogeneous (TLC), and its structure confirmed by ESI-IT MS.

Experimental data for CQn (**2**)

R_f (DCM/MeOH 1:1 (v/v)): 0.0

$^{m}/_{z}$ ($C_{13}H_{16}ClN_3$, 249.10 a.m.u.): 250.33 ($[M+H^+]^+$).

4.4.3. Derivatization of CQn with succinic anhydride

CQn (**2**, 1.2 eq), succinic anhydride (1.0 eq), and DIPEA (1.2 eq) were dissolved in the minimum amount possible of DMF, and the mixture was stirred for 2 hours, at room temperature. Then, the mixture was diluted with an equivolumetric mixture of DCM and MeOH, and purified by liquid chromatography on a silica gel column, using the same DCM/MeOH mixture as eluent. CQn-C4 (**5**) was obtained as a chromatographically homogeneous white solid, whose molecular weight was confirmed by ESI-IT MS.

Experimental data for CQn-C4 (**5**)

R_f (DCM/MeOH 1:1 (v/v)): 0.27

$^m/_z$ ($C_{17}H_{20}ClN_3O_3$; 349.12 a.m.u.): 350.67 ($[M+H^+]^+$).

4.4.4. Solid phase synthesis

4.4.4.1. Preparation of the resin

After preparing the experimental setup for manual SPPS (Figure 4.5), the dry resin (Fmoc-Rink Amide MBHA) was placed in the syringe, suspended in excess DMF, and stirred for 20 minutes, for convenient swelling; after removal of DMF by suction filtration, the resin was re-suspended in DCM and the same procedure for resin swelling was applied. After 20 minutes, the liquid phase was again removed by suction filtration.

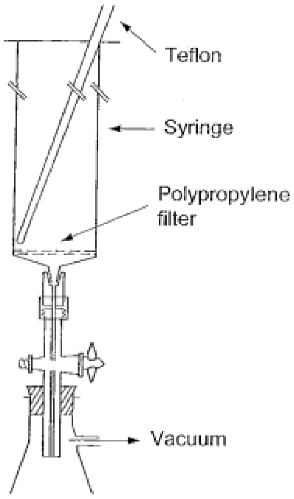

Figure 4.5 – Experimental setup applicable to manual SPPS.

Once conveniently swelled, the resin was treated with a solution of 20% piperidine in DMF (3 mL, 1 × 1’ + 1 × 20’) for removal of the Fmoc protecting group. To this end, the piperidine solution was added to the resin and the suspension was continuously stirred. The resin was then thoroughly washed with DMF (3 mL, 3 × 1’) and DCM (3 mL, 3 × 1’) and a few resin beads were collected to perform the Kaiser test. After a positive result was observed (dark purple solution, presence of free amine groups), the assembly of the peptide chain began.

4.4.4.2. Assembly of peptide chains on solid phase

A mixture of the *C*-terminal Fmoc-AA-OH (5.0 eq.), HBTU (5.0 eq), and DIPEA (10.0 eq) in DMF (3 mL) was added to the deprotected resin, and the resulting slurry was left under stirring for 1 hour. After this time, the resin was filtered and washed with DMF (3 mL, 3 × 1') and DCM (3 mL, 3 × 1'). A few beads of the resin were collected to perform the Kaiser test and, upon a negative result (pale-yellow solution, absence of free amine groups), deprotection of the N^{α}-amino group was carried out with a solution of 20% piperidine in DMF (3 mL, 1 × 1' + 1 × 20'). Then, the resin was once again dried by suction filtration and washed with DMF (3 mL, 3 × 1') and DCM (3 mL, 3 × 1'), and a few beads removed to carry out the Kaiser test. Upon a positive result, the coupling of the following Fmoc-AA-OH was performed, in the conditions described above. Assembly of the full amino acid sequences was thus accomplished through consecutive cycles of deprotection and coupling steps.

Whenever the Kaiser test denounced an incomplete reaction, either deprotection or coupling, the reaction was repeated in different conditions: respectively, Fmoc removal was carried out by a 15-min treatment with a solution of 50% piperidine in DMF, whereas coupling was promoted by use of HATU, in replacement of HBTU.

4.4.5. On resin coupling of CQn-C4 to the peptides' *N*-termini

After completion of the peptide chain – up until the deprotection of the *N*-terminal amino acid, the resin was divided in two parts, for (i) direct cleavage, to obtain the free peptide, and (ii) further *N*-terminal modification by on-resin coupling of CQn-C4. The latter was accomplished by adding a mixture of CQn-C4 (5.0 eq), PyBOP (5.0 eq), and DIPEA (10.0 eq) in DMF to the resin, and allowing the resulting slurry to be stirred overnight. The resin was then filtered and washed with DMF (3 mL, 3 × 1') and DCM (3 mL, 3 × 1'). The success of the coupling was confirmed by a negative Kaiser test (pale-yellow solution, absence of free amine groups). Both unconjugated and conjugated peptidyl-resins were then submitted to acidolytic cleavage, to respectively release the parent CPP and CQn-C4-CPP conjugates, as next described.

4.4.6. Cleavage of CPP and respective CQn-C4-CPP conjugates

TFA-based cleavage cocktails were prepared with compositions that varied according to the specific peptide sequence (95% TFA, 2.5% TIS and 2.5% H_2O for most cases; 90% TFA, 5% thioanisole, 3% 1,2-ethanedithiol and 2% anisole, for peptides with over two arginine residues). Dried peptidyl-resins were placed in 45 mL Falcon tubes and cocktail cleavage was added (in a proportion of 1 mL per 100 mg of dry resin); the mixture was left in continuous stirring for 2 hours, at room temperature. After this time, the resin was filtered under reduced pressure, using a D4 sintered Buchner funnel, and the filtrate containing the peptide, was split onto 2 mL portions to 15 mL Falcon tubes. Each tube was then filled with anhydrous *tert*-butyl methyl ether (MTBE), in order to precipitate the peptide, and the suspension stored at -20 ºC for 15 minutes. The slurry was then centrifuged at 0ºC and 3500 rpm for 10 minutes, and the supernatant decanted to an Erlenmeyer flask that was stoppered and stored in the hood, until further use. The cycle of addition of MTBE, refrigeration, centrifugation and decantation was repeated three more times, then the tubes containing the peptide pellets were placed in a desiccator. Once the supernatant was confirmed to not contain substantial amounts of the synthesized peptides, the supernatants pooled in the flask were discarded.

Once dry, the peptide pellet was dissolved in 10% aqueous acetic acid, and analyzed by HPLC and LC-DAD/ESI-IT MS. Peptides and their conjugates were purified by preparative HPLC and, after purification, fractions containing the isolated product were pooled, frozen, and freeze-dried. An aliquot was set aside for confirmation of the target molecular weight by ESI-IT MS, and determination of the final purity degree (analytical HPLC). Spectra and chromatograms thus obtained are presented below.

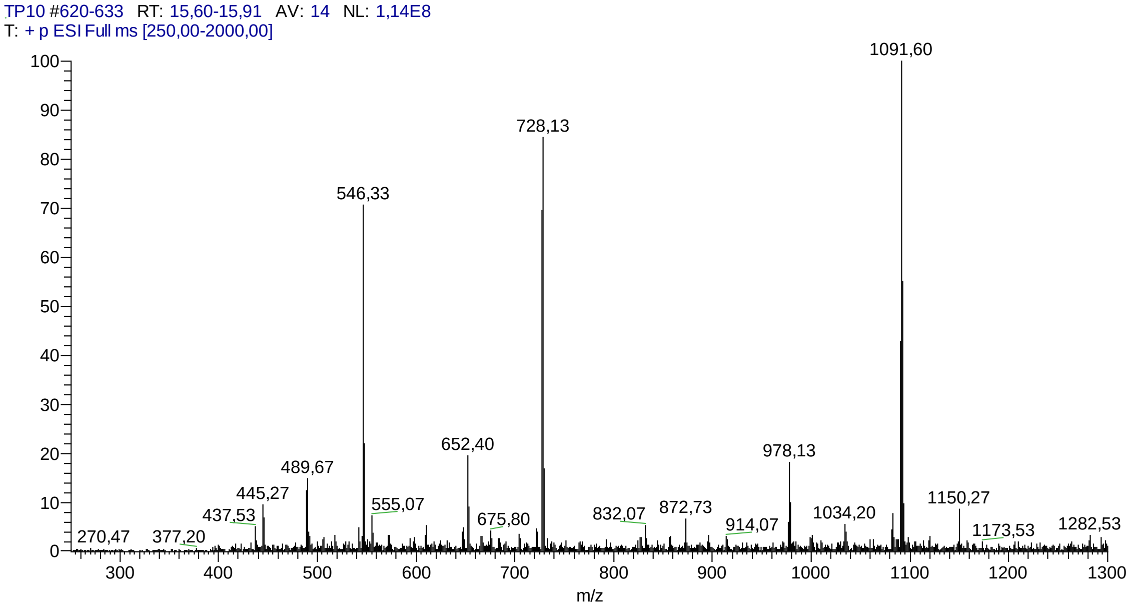

Figure 4.6 - Spectrum (ESI-IT MS, positive mode) obtained for crude TP10.

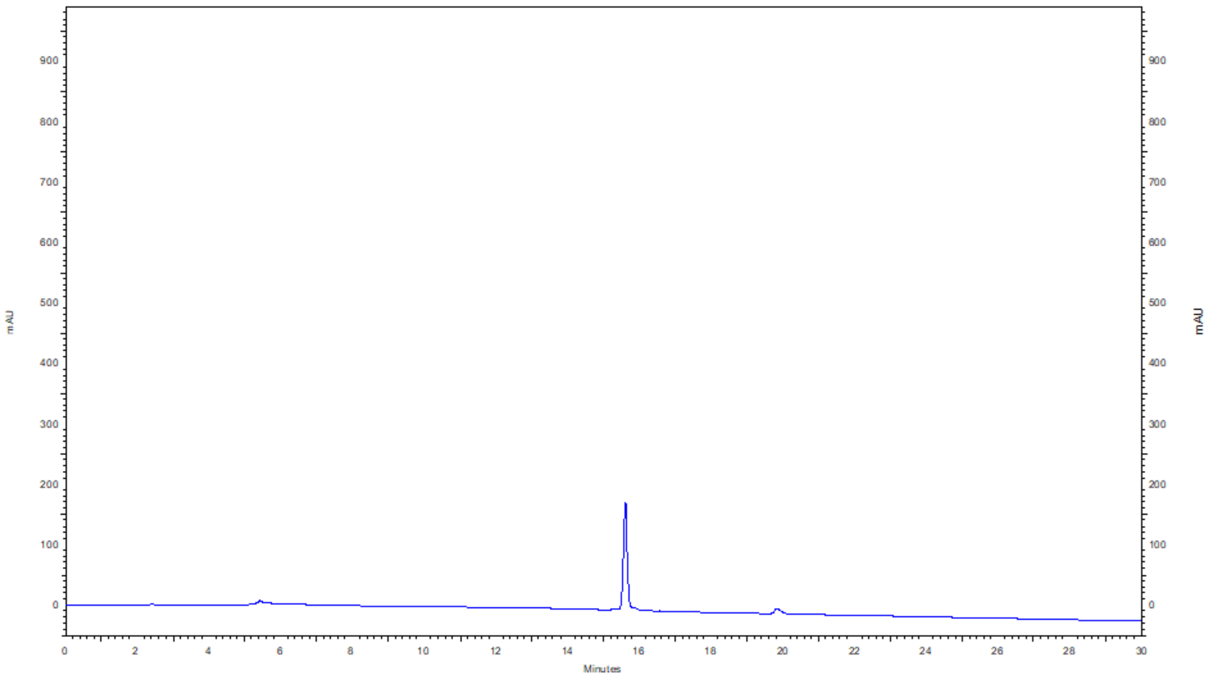

Figure 4.7 – Chromatogram obtained from the analysis of TP10 after purification, with a gradient elution of 0-100% ACN in water (0,05% TFA) in a RP-18E (5 µm), for 30 minutes and a flow of 1 ml/min, with detection at λ = 220 nm.

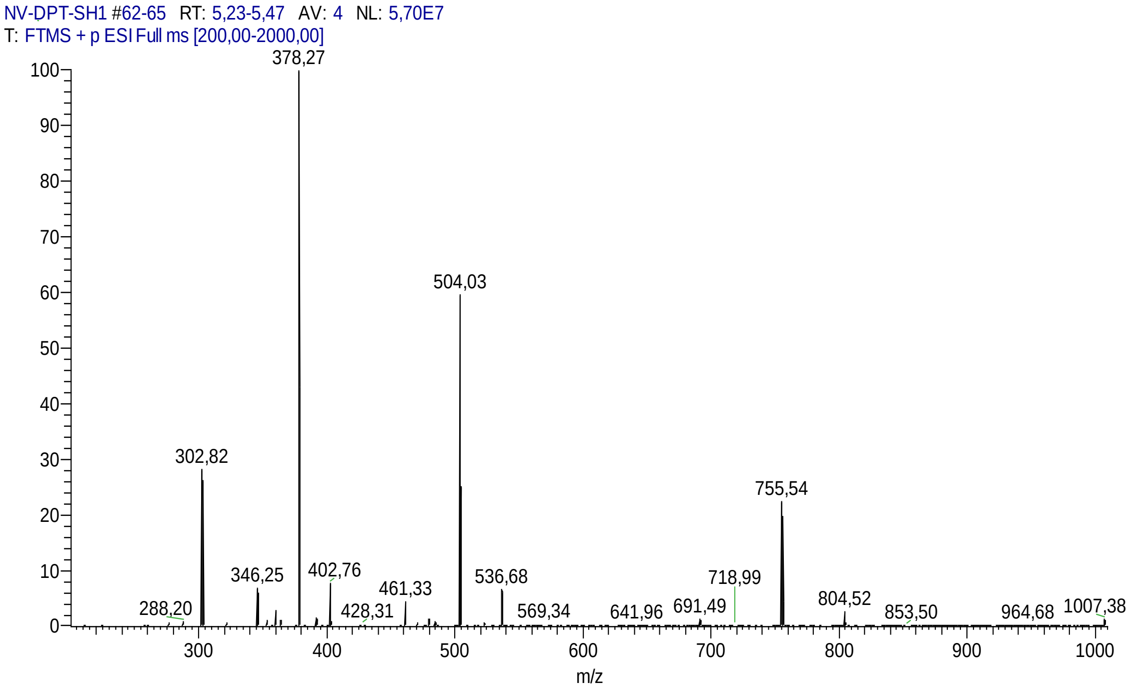

Figure 4.8 - Spectrum (ESI-IT MS, positive mode) obtained for crude DPT-sh1.

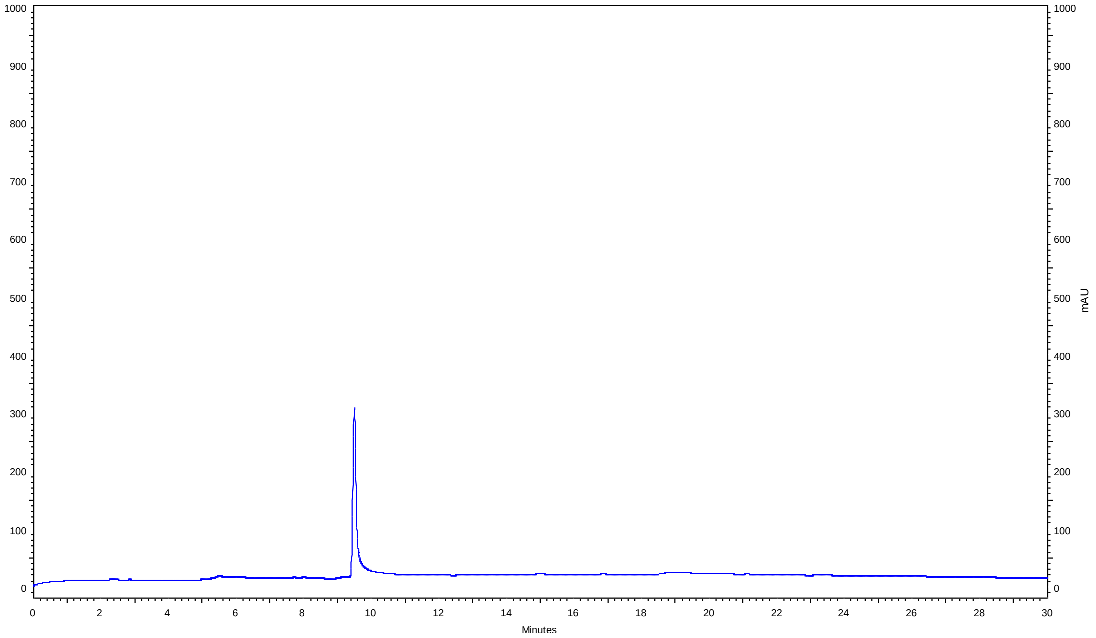

Figure 4.9 – Chromatogram obtained from the analysis of DPT-sh1 after purification, with a gradient elution of 0-100% ACN in water (0,05% TFA) in a RP-18E (5 μm), for 30 minutes and a flow of 1 ml/min, with detection at λ = 220 nm.

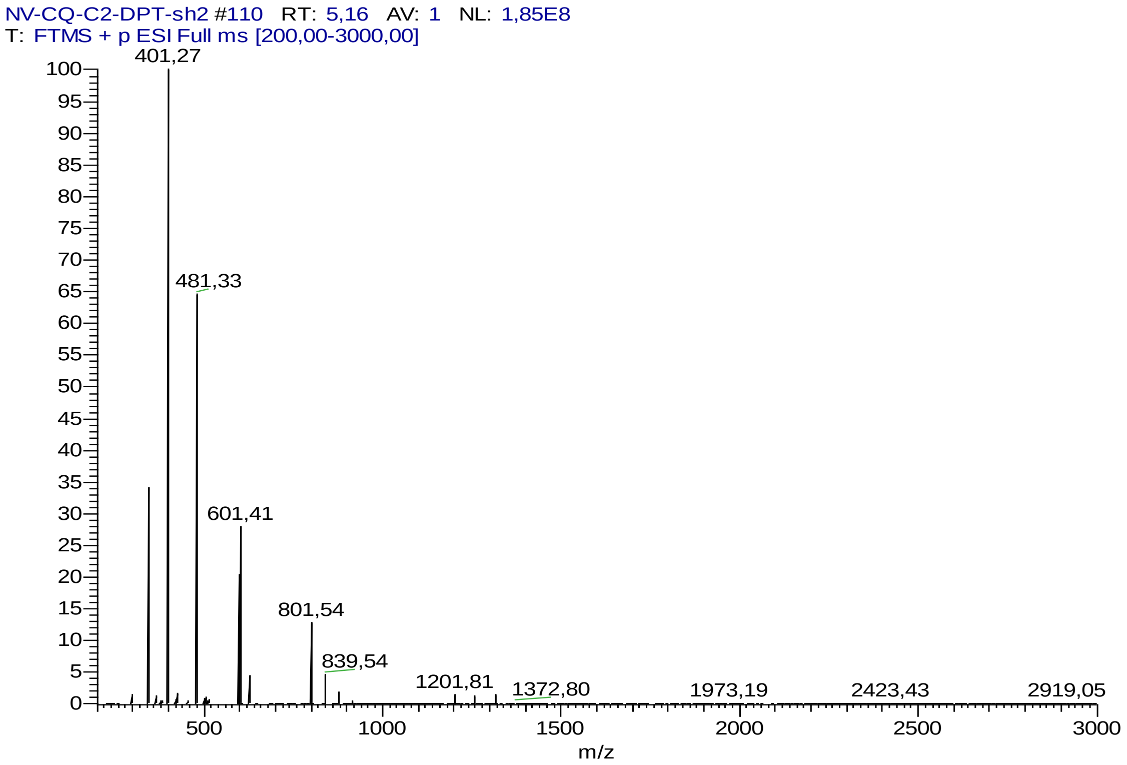

Figure 4.10 - Spectrum (ESI-IT MS, positive mode) obtained for crude DPT-sh2.

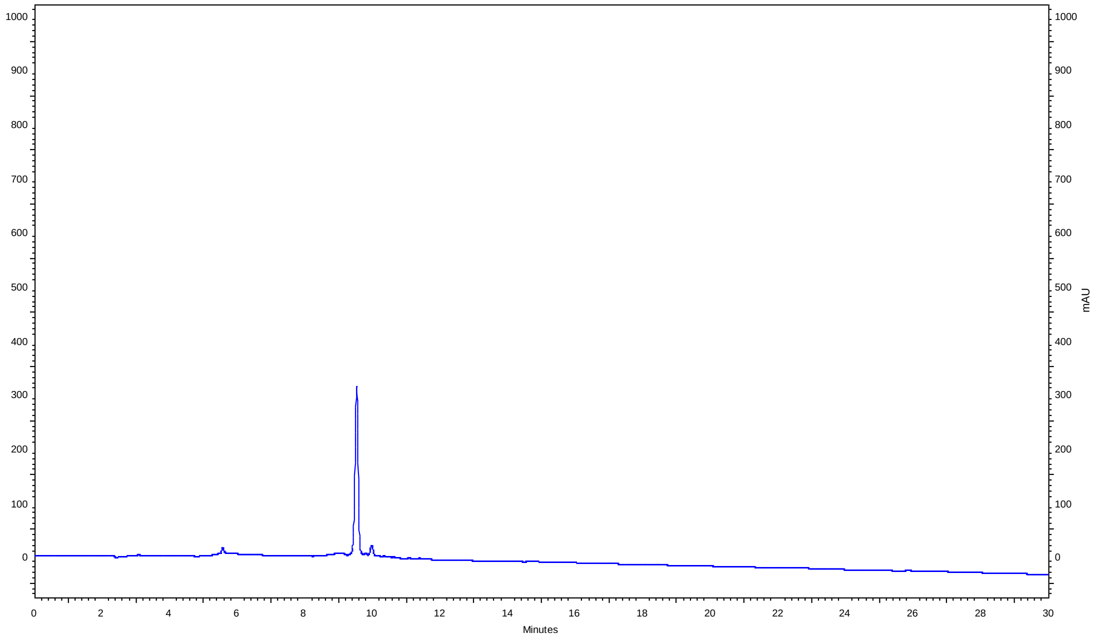

Figure 4.11 – Chromatogram obtained from the analysis of DPT-sh2 after purification, with a gradient elution of 0-100% ACN in water (0,05% TFA) in a RP-18E (5 µm), for 30 minutes and a flow of 1 ml/min, with detection at λ = 220 nm.

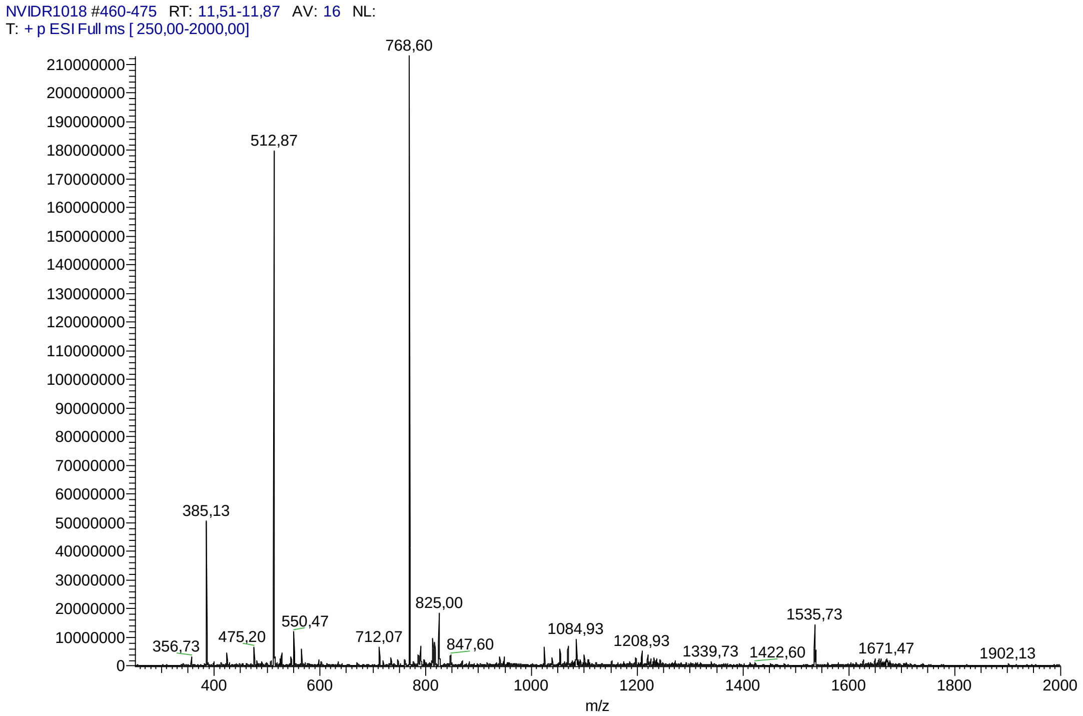

Figure 4.12 - Spectrum (ESI-IT MS, positive mode) obtained for crude IDR-1018.

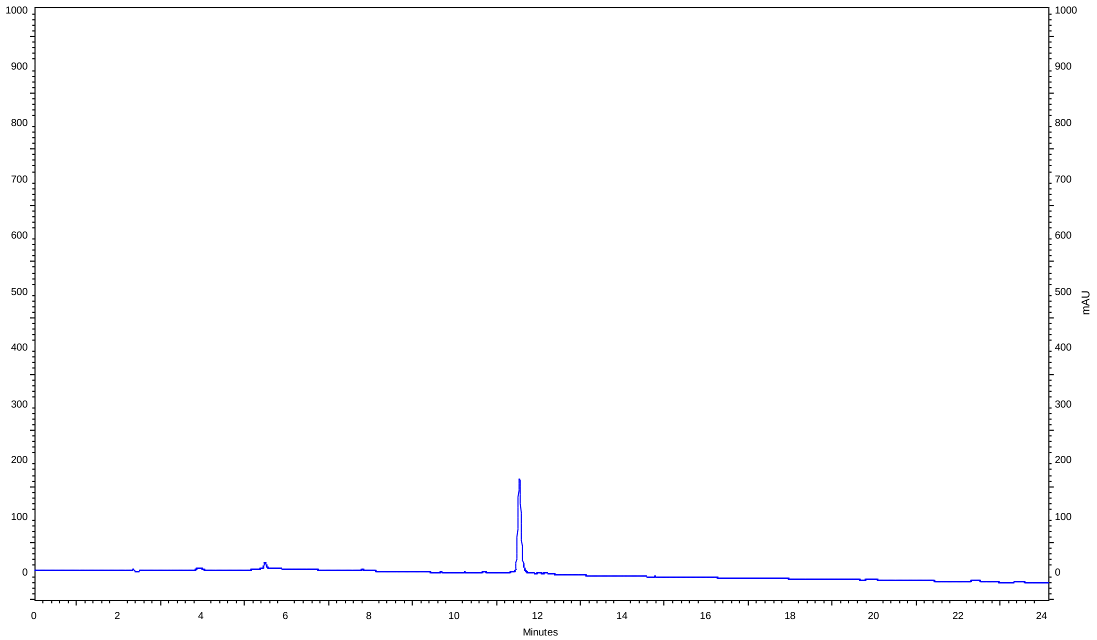

Figure 4.13 – Chromatogram obtained from the analysis of IDR-1018 after purification, with a gradient elution of 0-100% ACN in water (0,05% TFA) in a RP-18E (5 µm), for 30 minutes and a flow of 1 ml/min, with detection at λ = 220 nm.

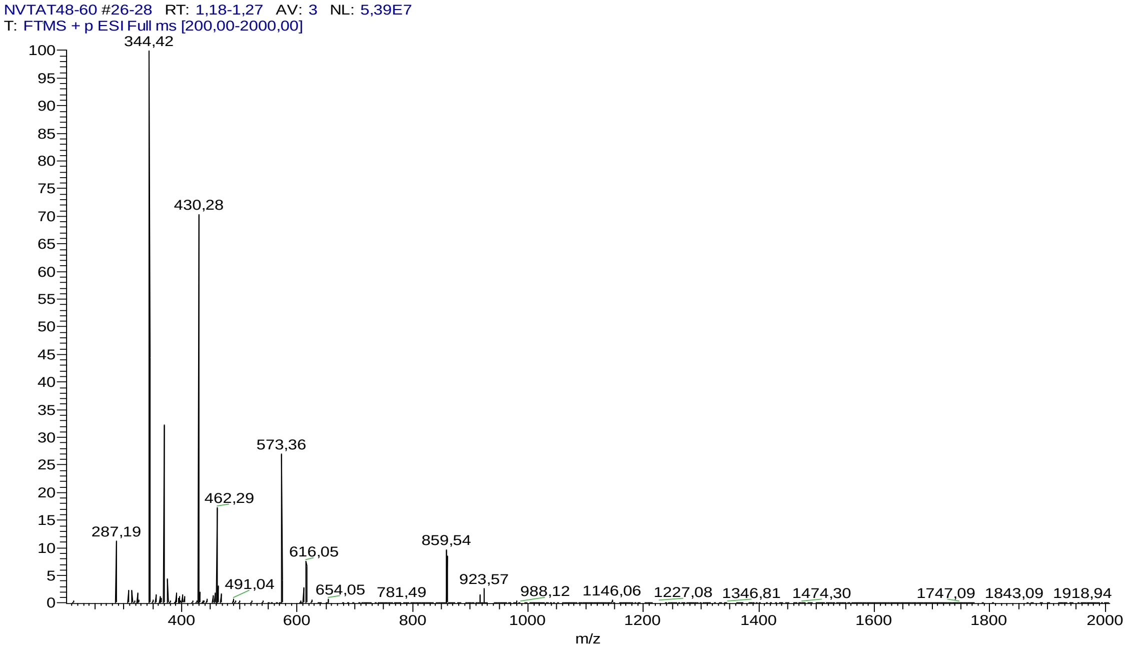

Figure 4.14 - Spectrum (ESI-IT MS, positive mode) obtained for crude TAT.

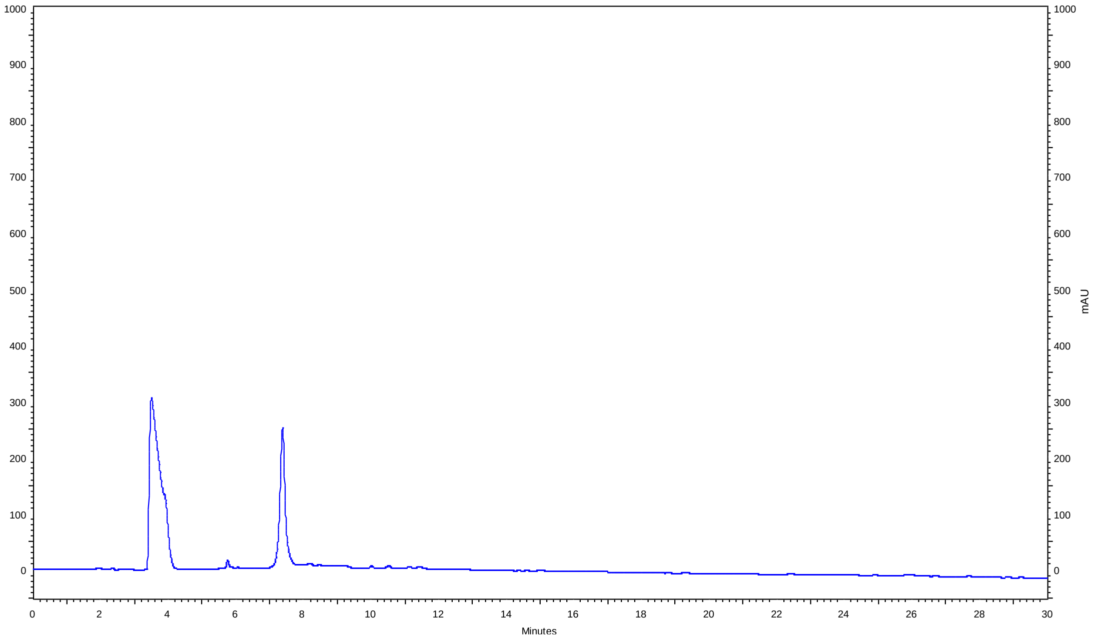

Figure 4.15 – Chromatogram obtained from the analysis of TAT after purification, with a gradient elution of 0-100% ACN in water (0,05% TFA) in a RP-18E (5 μm), for 30 minutes and a flow of 1 ml/min, with detection at λ = 220 nm.

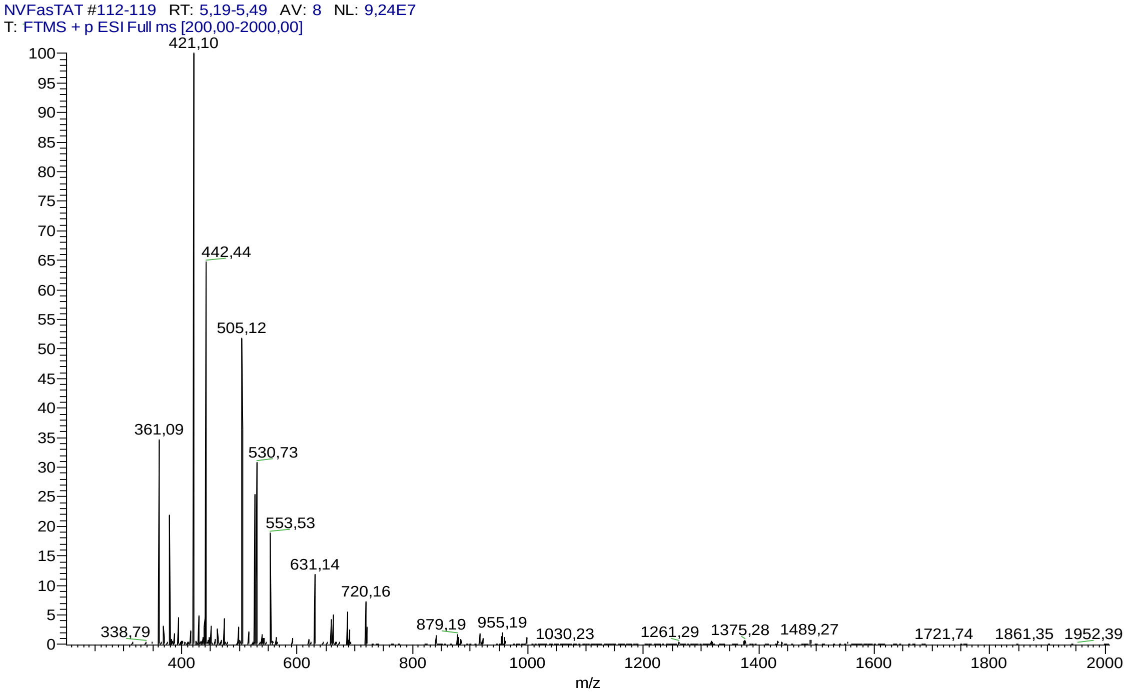

Figure 4.16 - Spectrum (ESI-IT MS, positive mode) obtained for crude PasTAT.

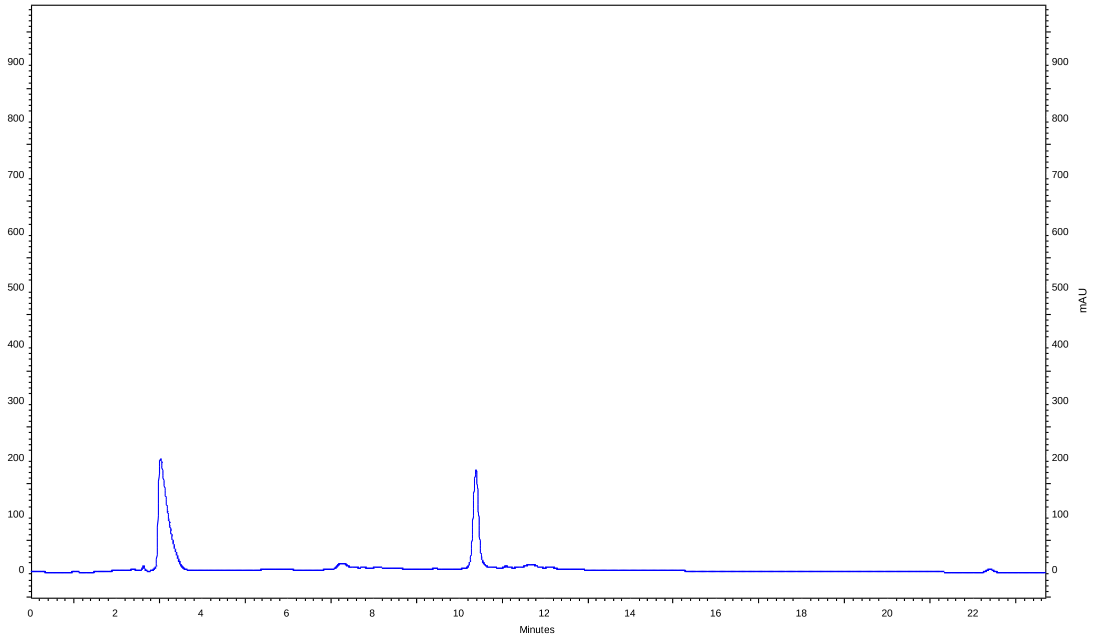

Figure 4.17 – Chromatogram obtained from the analysis of PasTAT after purification, with a gradient elution of 0-100% ACN in water (0,05% TFA) in a RP-18E (5 µm), for 30 minutes and a flow of 1 ml/min, with detection at λ = 220 nm.

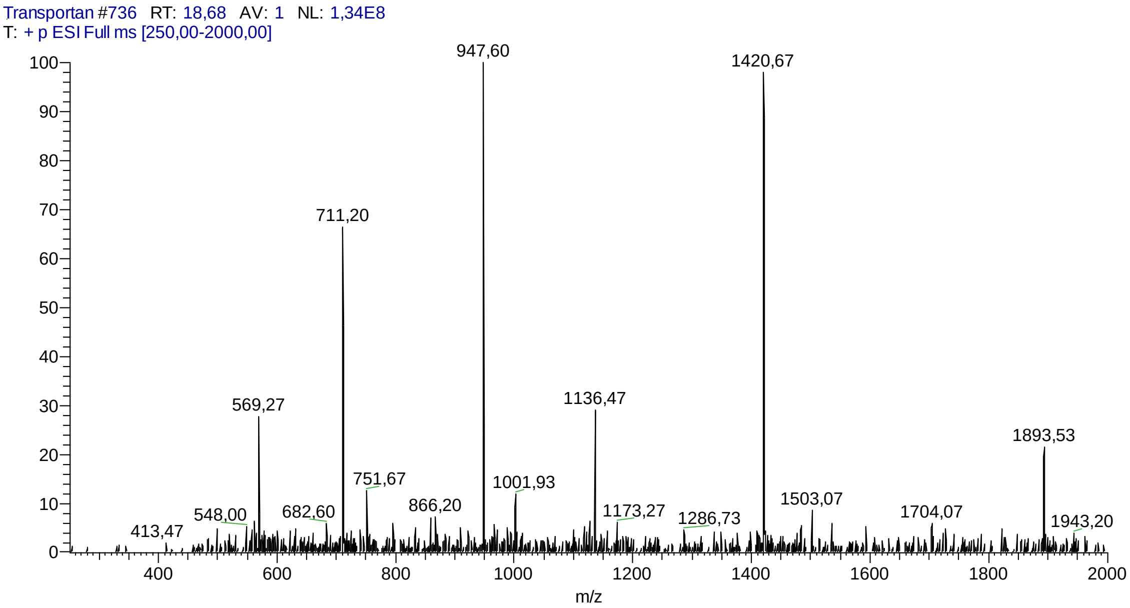

Figure 4.18 - Spectrum (ESI-IT MS, positive mode) obtained for crude Transportan.

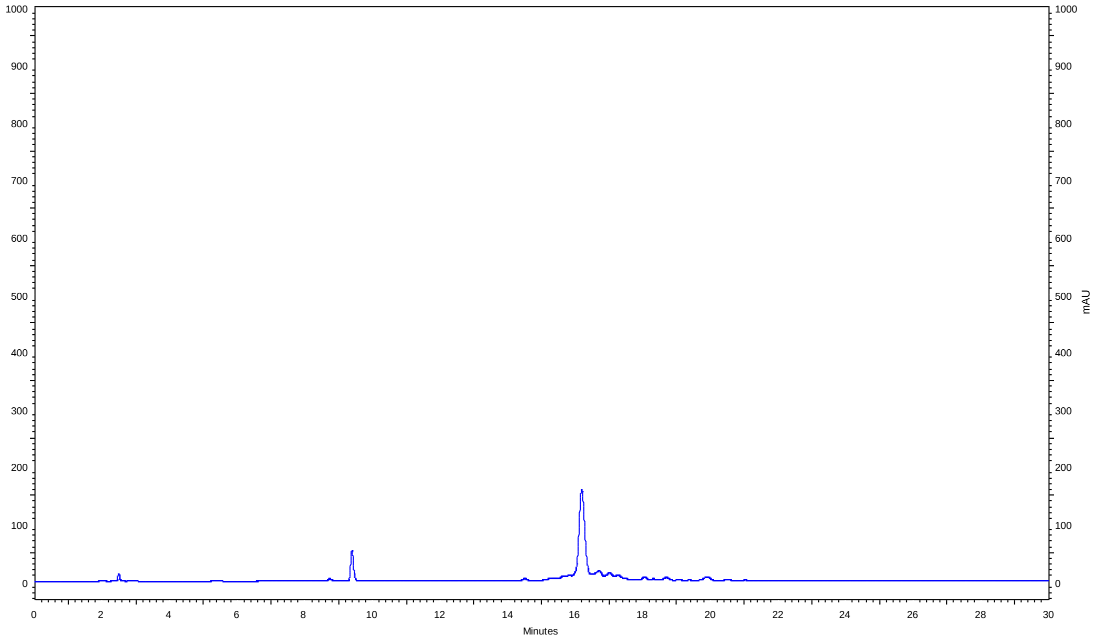

Figure 4.19 – Chromatogram obtained from the analysis of Transportan after purification, with a gradient elution of 0-100% ACN in water (0,05% TFA) in a RP-18E (5 μm), for 30 minutes and a flow of 1 ml/min, with detection at λ = 220 nm.

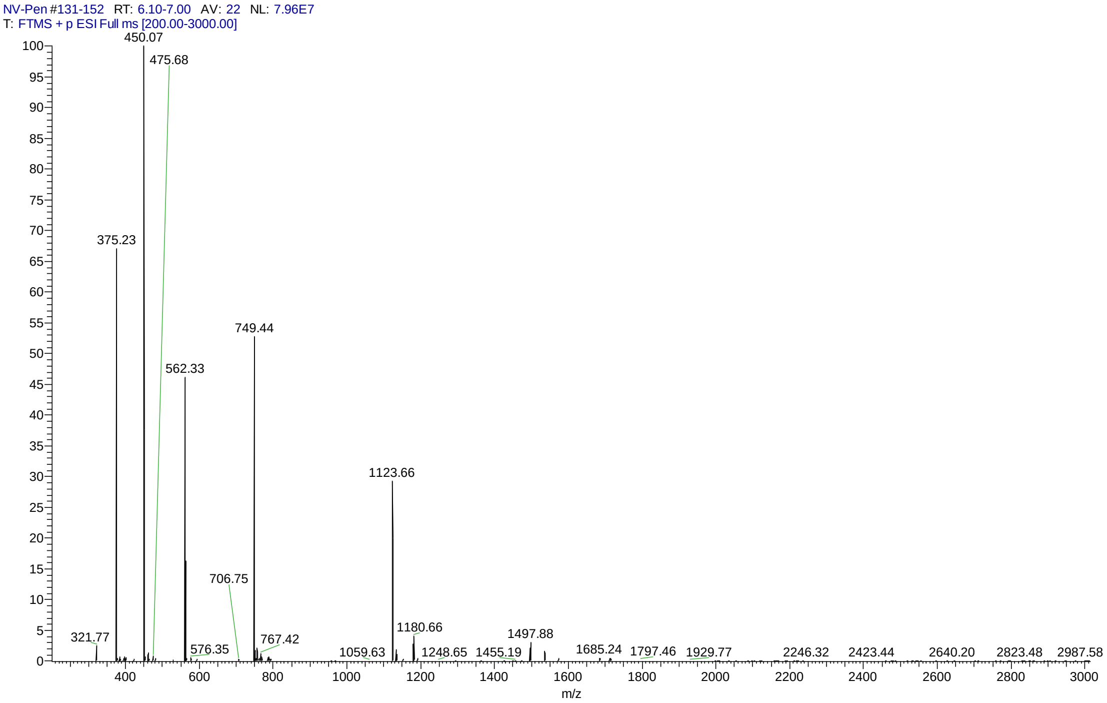

Figure 4.20 - Spectrum (ESI-IT MS, positive mode) obtained for crude Penetratin.

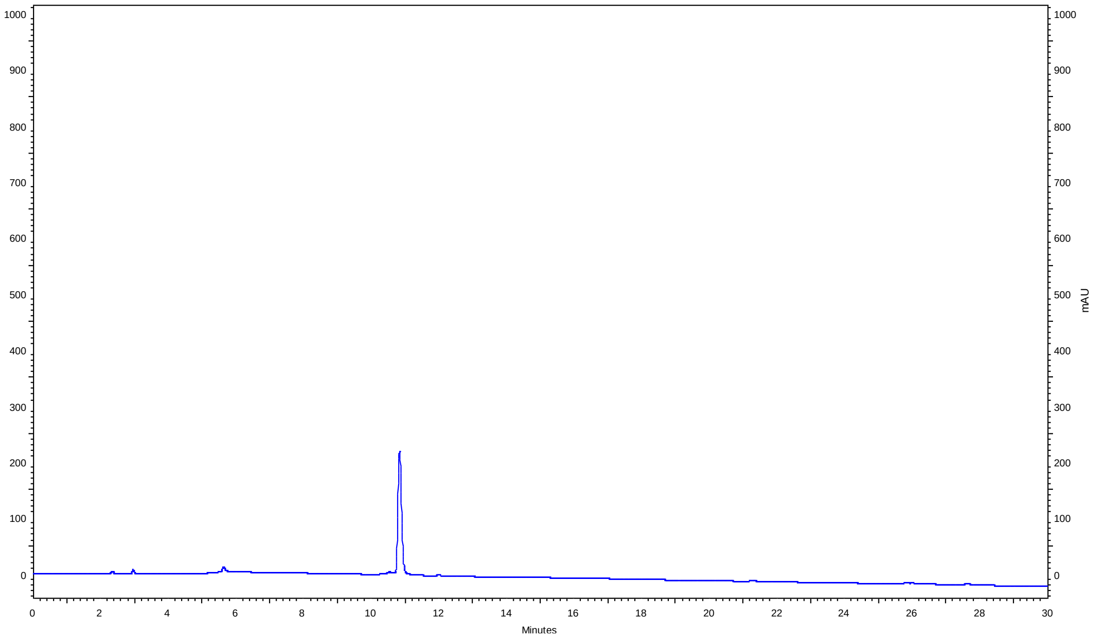

Figure 4.21 – Chromatogram obtained from the analysis of Penetratin after purification, with a gradient elution of 0-100% ACN in water (0,05% TFA) in a RP-18E (5 μm), for 30 minutes and a flow of 1 ml/min, with detection at λ = 220 nm.

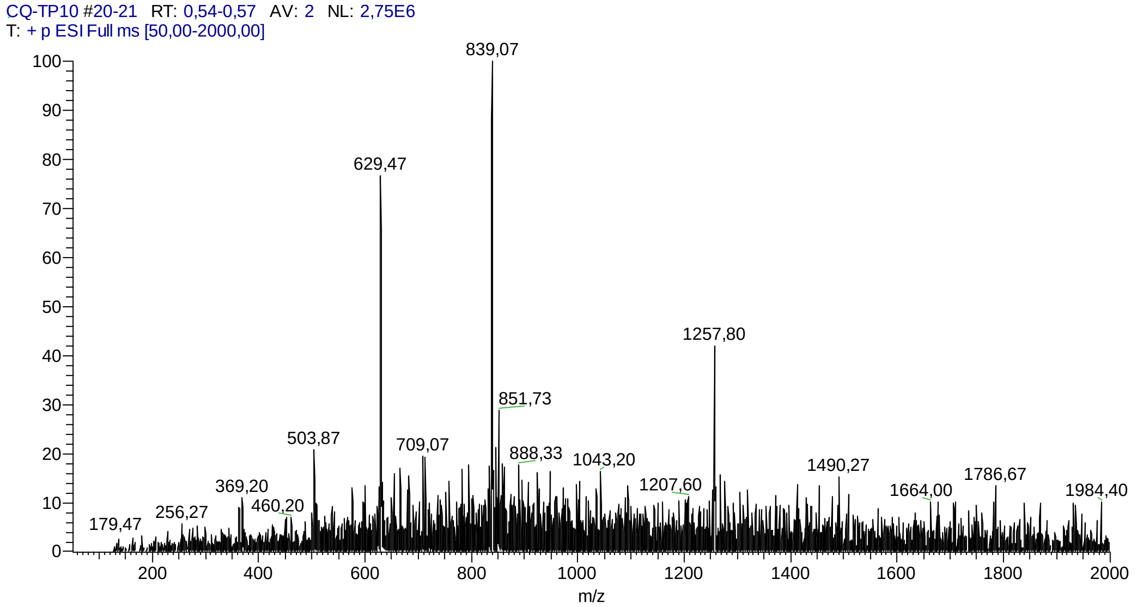

Figure 4.22 - Spectrum (ESI-IT MS, positive mode) obtained for crude CQn-C4-TP10.

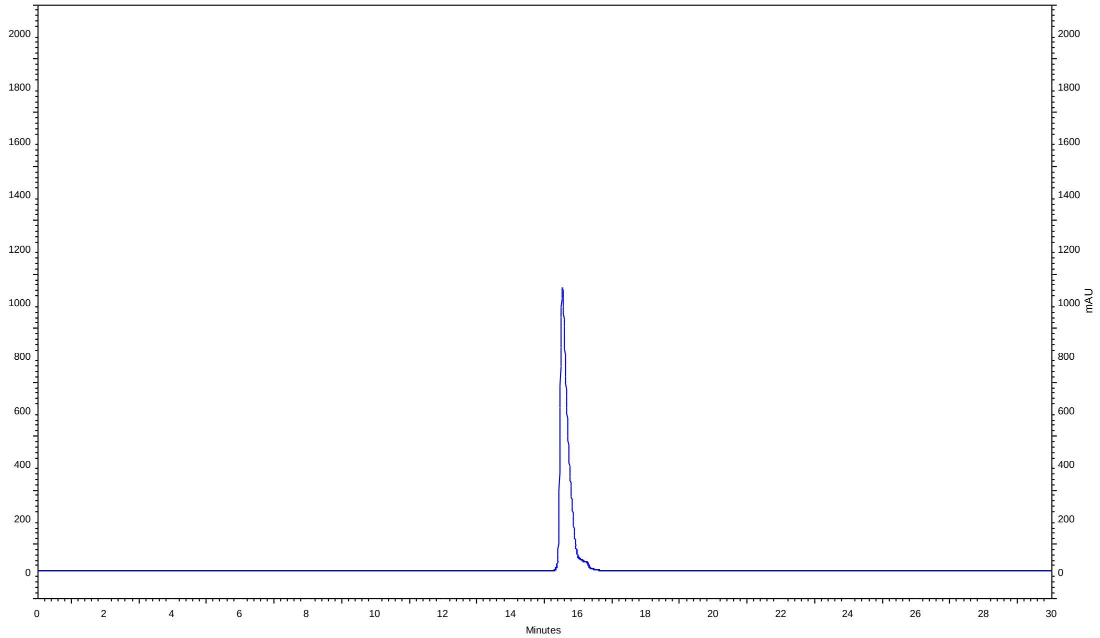

Figure 4.23 – Chromatogram obtained from the analysis of CQn-C4-TP10 after purification, with a gradient elution of 0-100% ACN in water (0,05% TFA) in a RP-18E (5 µm), for 30 minutes and a flow of 1 ml/min, with detection at λ = 220 nm.

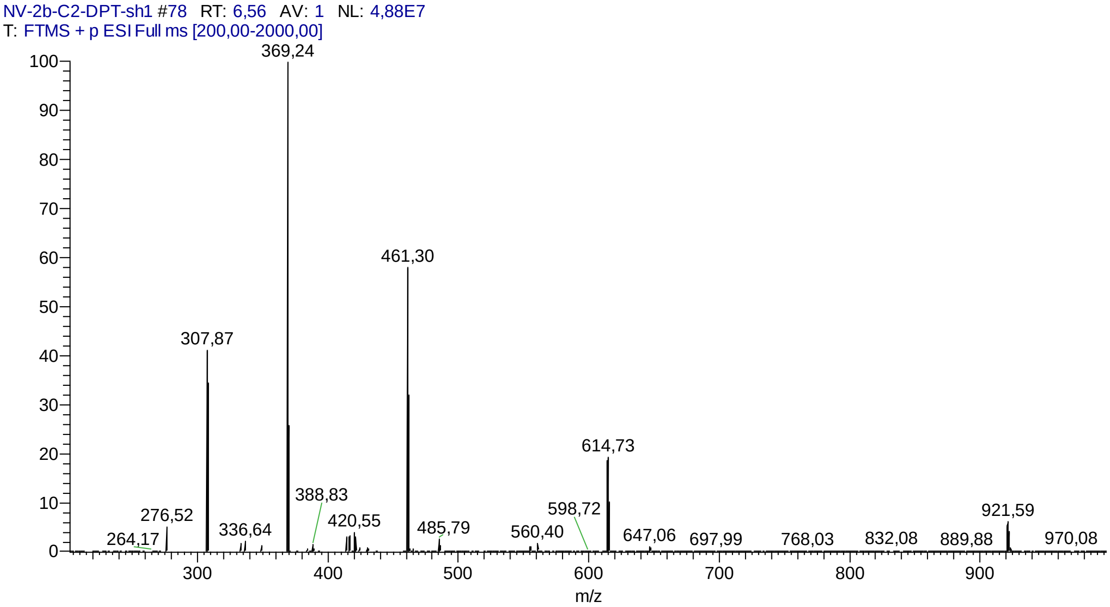

Figure 4.24 - Spectrum (ESI-IT MS, positive mode) obtained for crude CQn-C4-DPT-sh1.

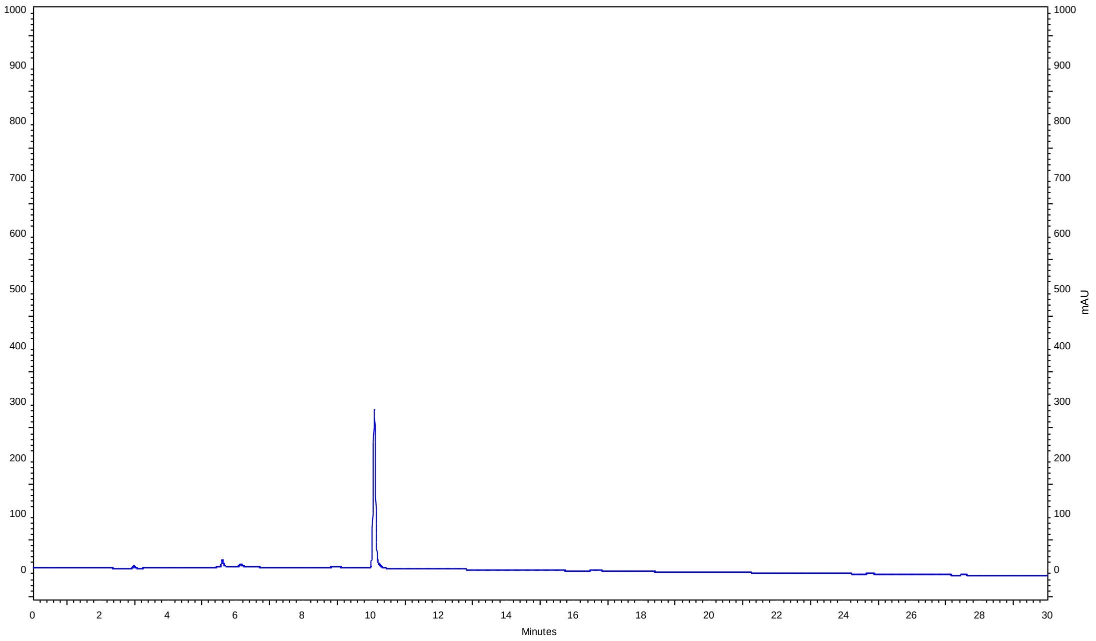

Figure 4.25 – Chromatogram obtained from the analysis of CQn-C4-DPT-sh1 after purification, with a gradient elution of 0-100% ACN in water (0,05% TFA) in a RP-18E (5 μm), for 30 minutes and a flow of 1 ml/min, with detection at λ = 220 nm.

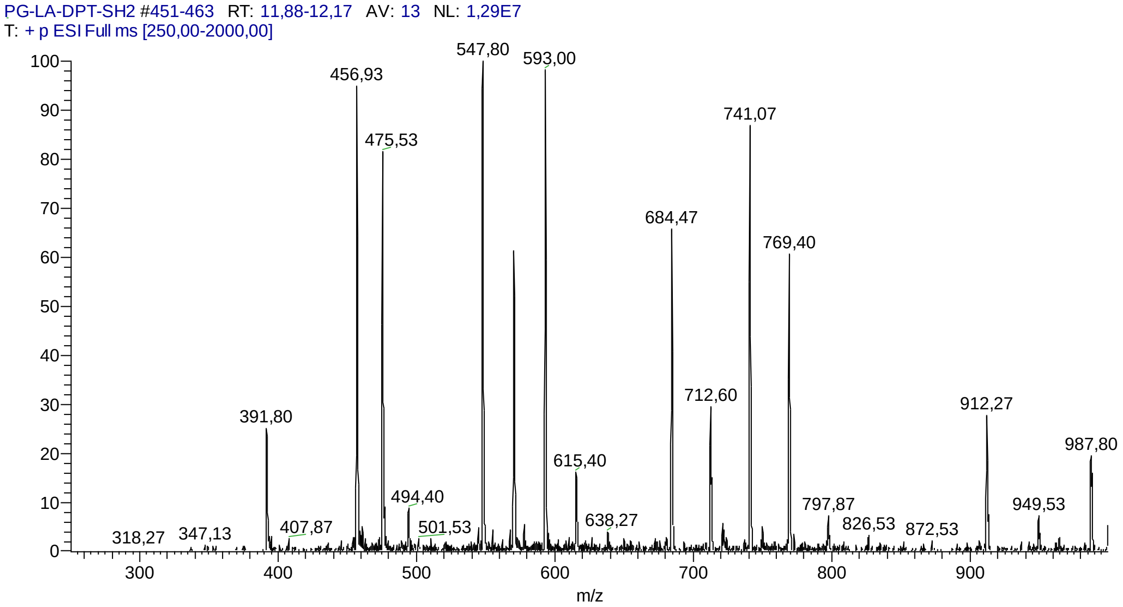

Figure 4.26 - Spectrum (ESI-IT MS, positive mode) obtained for crude CQn-C4-DPT-sh2.

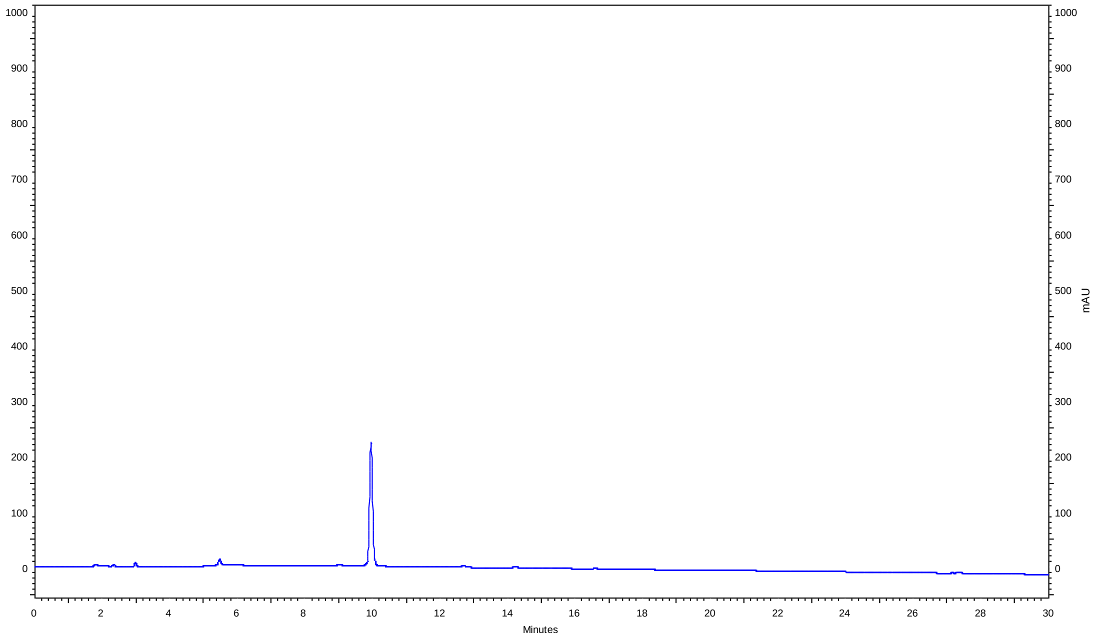

Figure 4.27 – Chromatogram obtained from the analysis of CQn-C4-DPT-sh2 after purification, with a gradient elution of 0-100% ACN in water (0,05% TFA) in a RP-18E (5 µm), for 30 minutes and a flow of 1 ml/min, with detection at λ = 220 nm.

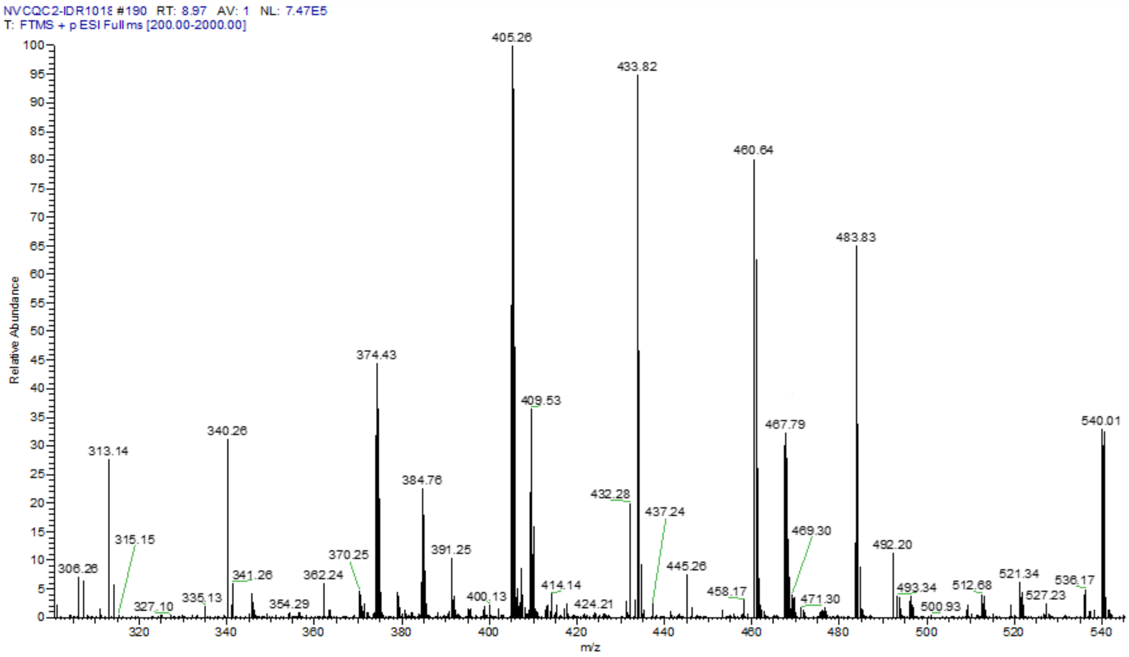

Figure 4.28 - Spectrum (ESI-IT MS, positive mode) obtained for crude CQn-C4-IDR-1018.

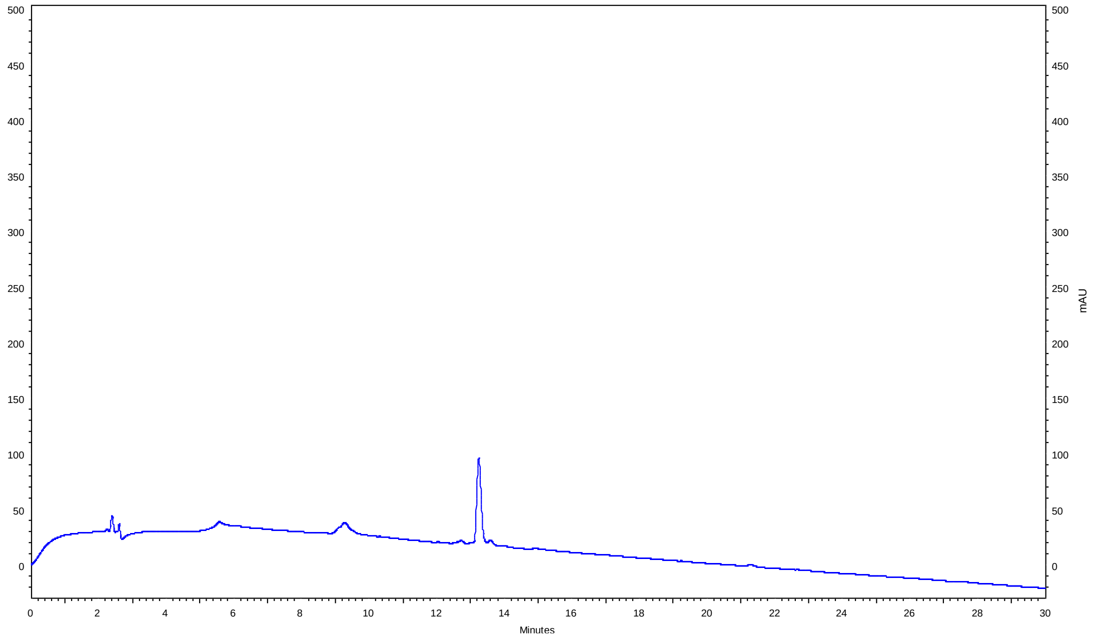

Figure 4.29 – Chromatogram obtained from the analysis of CQn-C4-IDR-1018 after purification, with a gradient elution of 0-100% ACN in water (0,05% TFA) in a RP-18E (5 µm), for 30 minutes and a flow of 1 ml/min, with detection at λ = 220 nm.

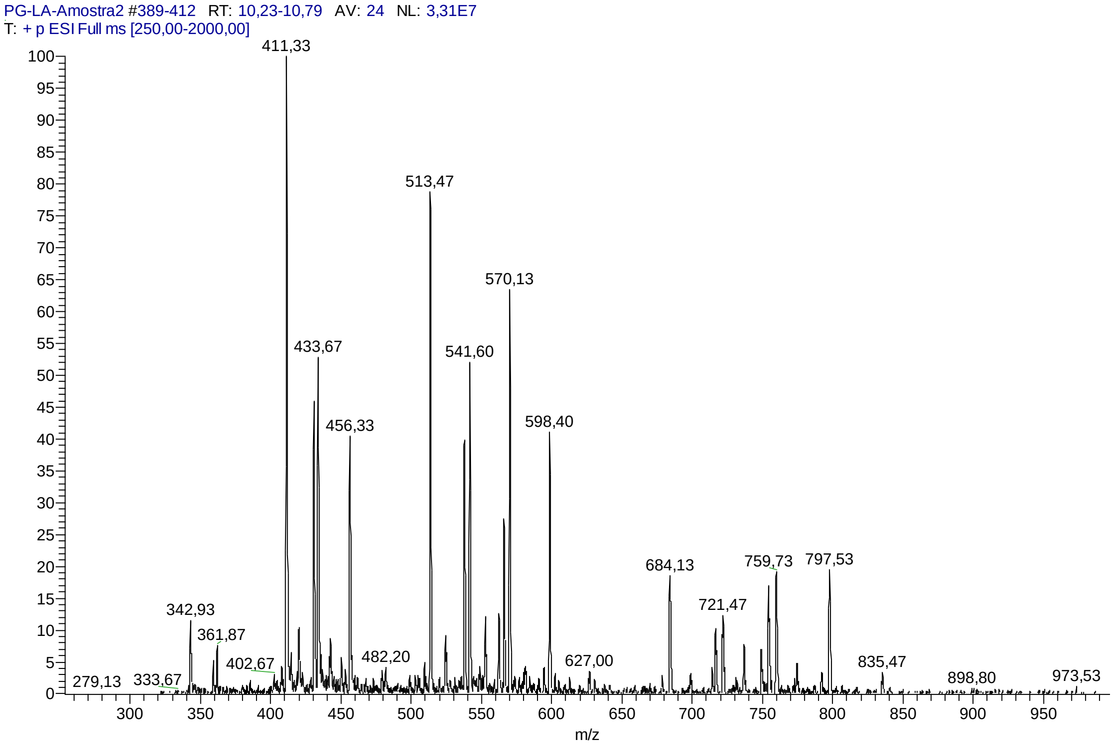

Figure 4.30 - Spectrum (ESI-IT MS, positive mode) obtained for crude CQn-C4-TAT.

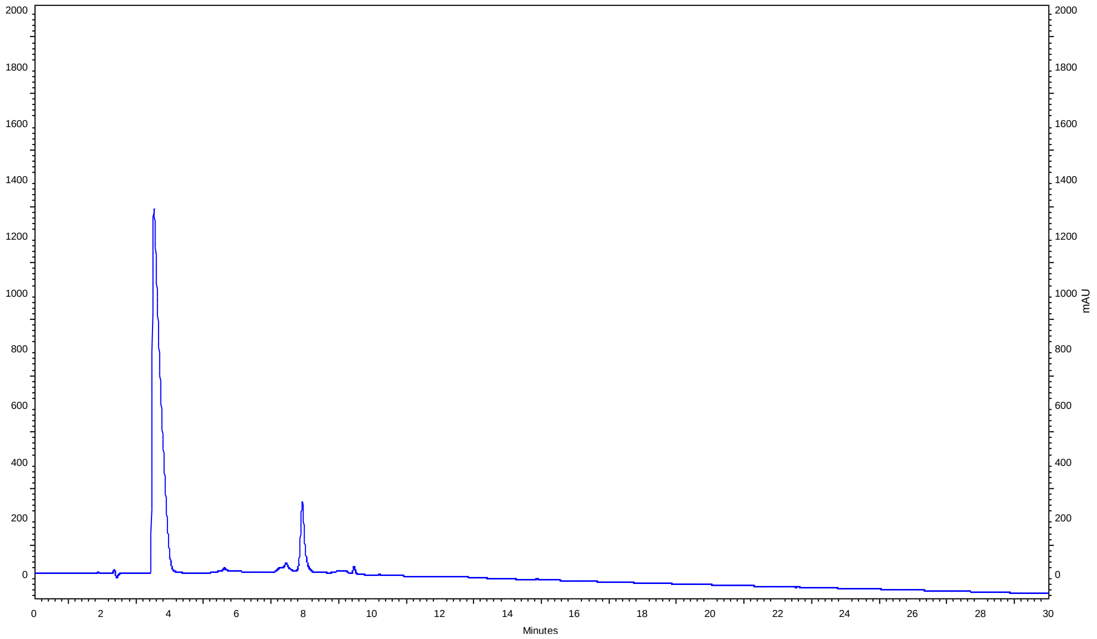

Figure 4.31 – Chromatogram obtained from the analysis of CQn-C4-TAT after purification, with a gradient elution of 0-100% ACN in water (0,05% TFA) in a RP-18E (5 µm), for 30 minutes and a flow of 1 ml/min, with detection at λ = 220 nm.

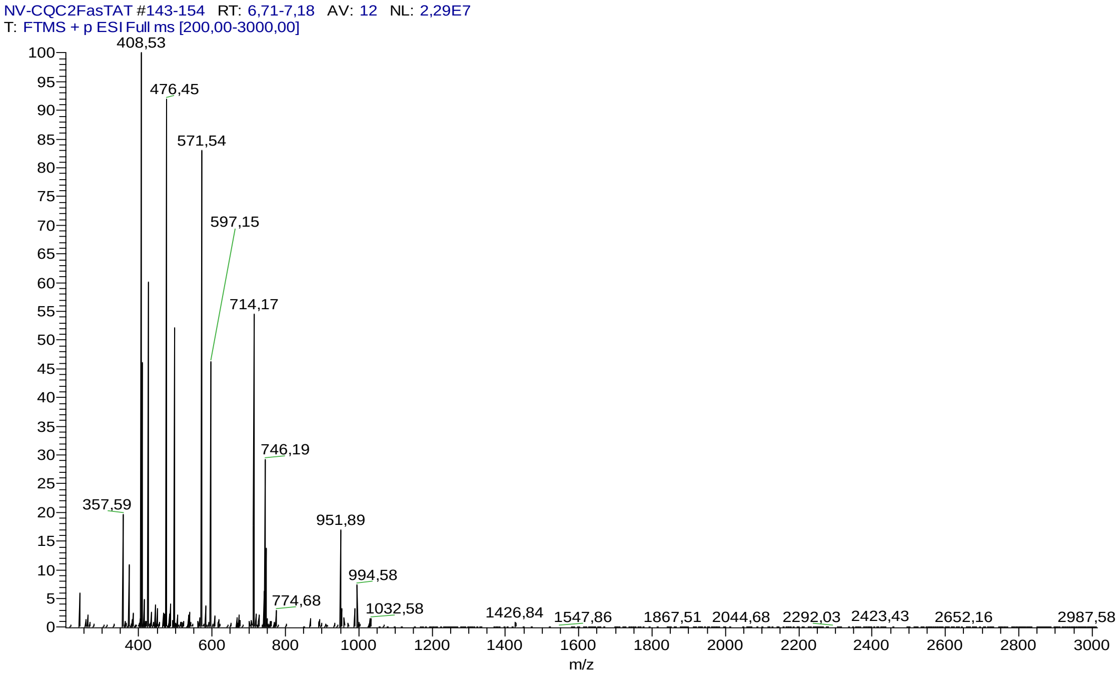

Figure 4.32 - Spectrum (ESI-IT MS, positive mode) obtained for crude CQn-C4-PasTAT.

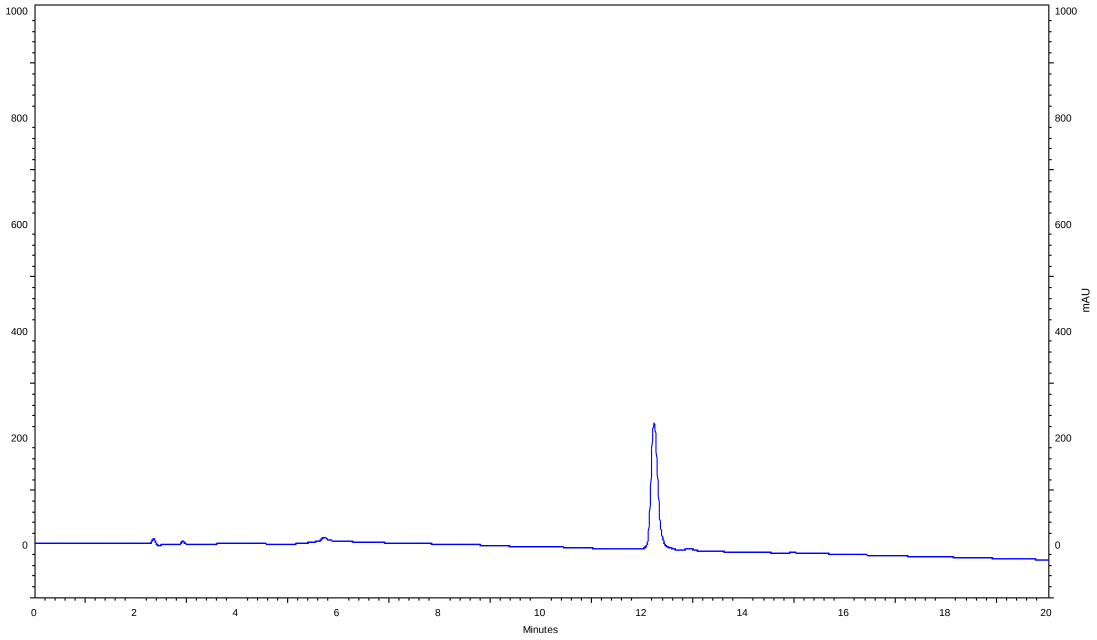

Figure 4.33 – Chromatogram obtained from the analysis of CQn-C4-PasTAT after purification, with a gradient elution of 0-66% ACN in water (0,05% TFA) in a RP-18E (5 μm), for 20 minutes and a flow of 1 ml/min, with detection at λ = 220 nm.

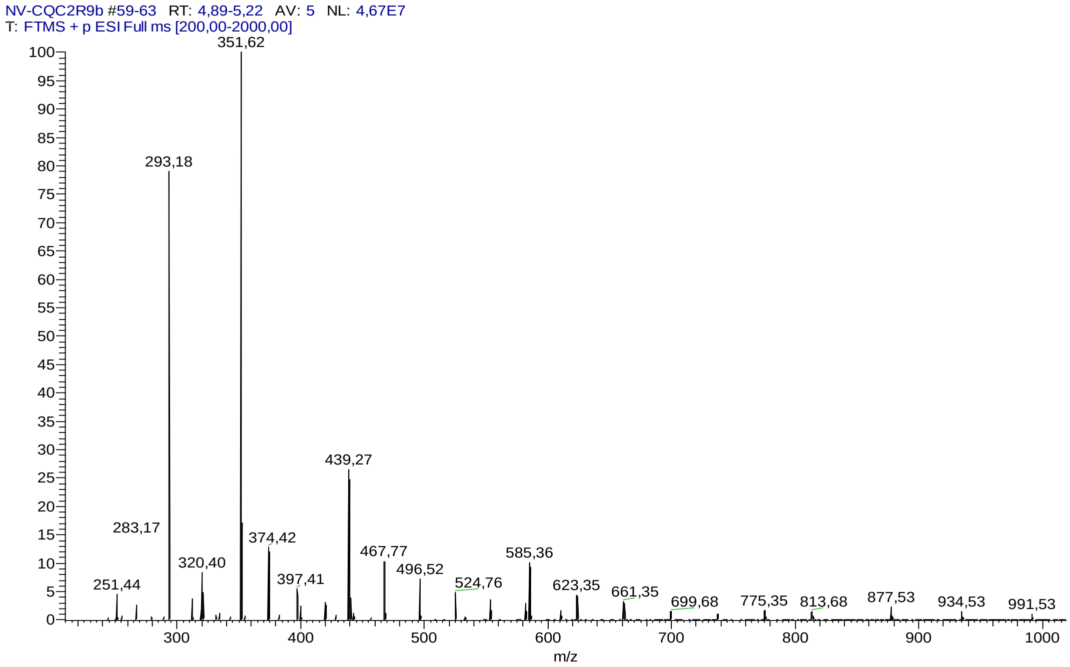

Figure 4.34 - Spectrum (ESI-IT MS, positive mode) obtained for crude CQn-C4-R9.

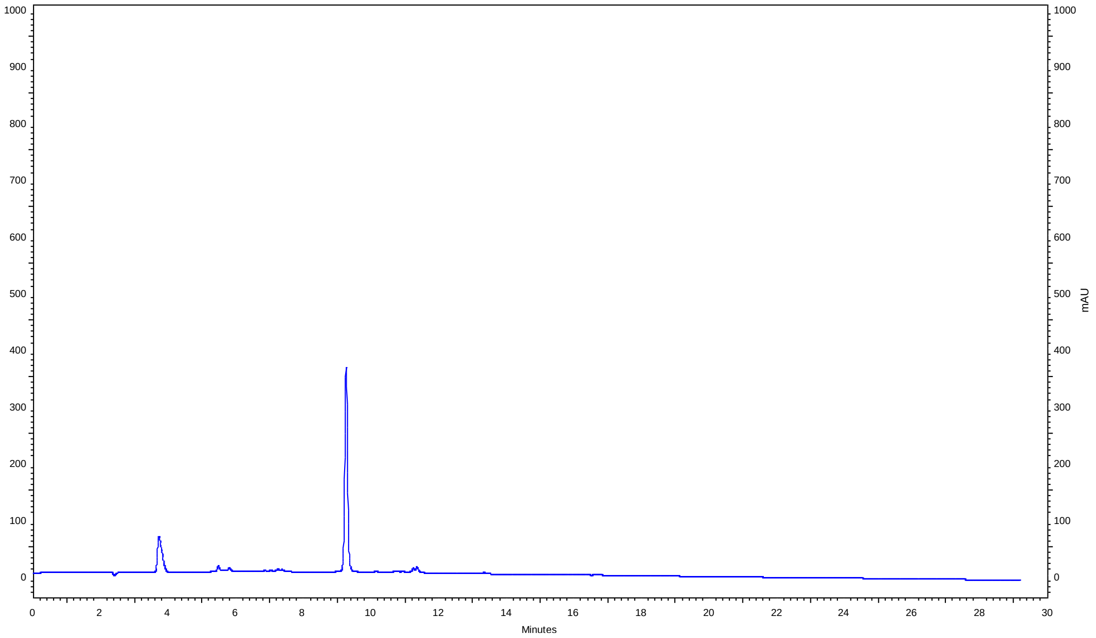

Figure 4.35 – Chromatogram obtained from the analysis of CQn-C4-R9 after purification, with a gradient elution of 0-100% ACN in water (0,05% TFA) in a RP-18E (5 µm), for 30 minutes and a flow of 1 ml/min, with detection at λ = 220 nm.

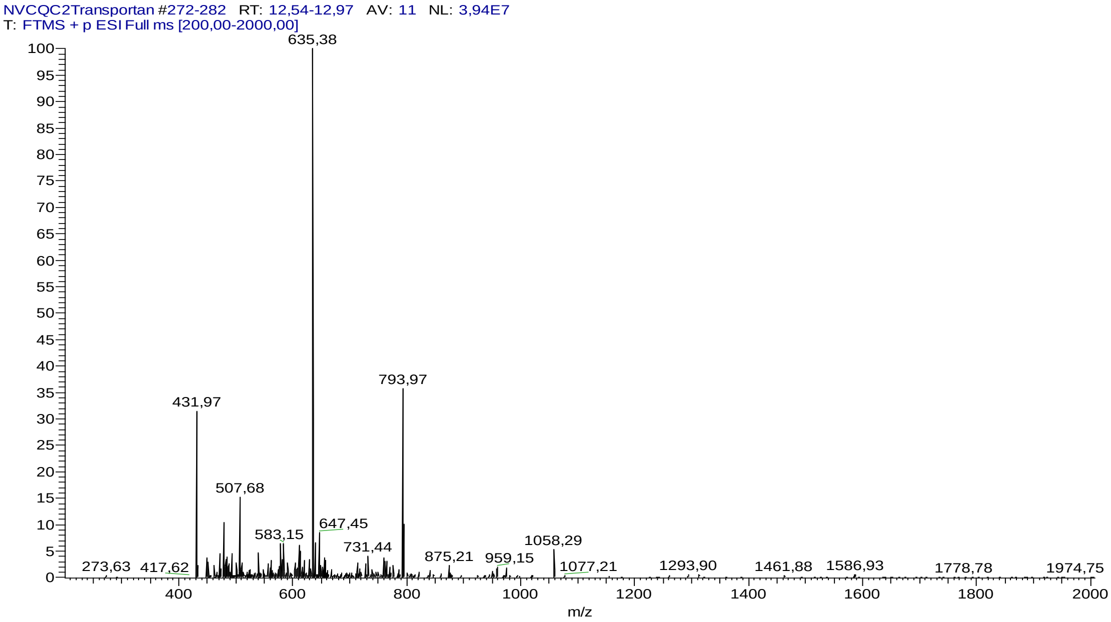

Figure 4.36 - Spectrum (ESI-IT MS, positive mode) obtained for crude CQn-C4-Transportan.

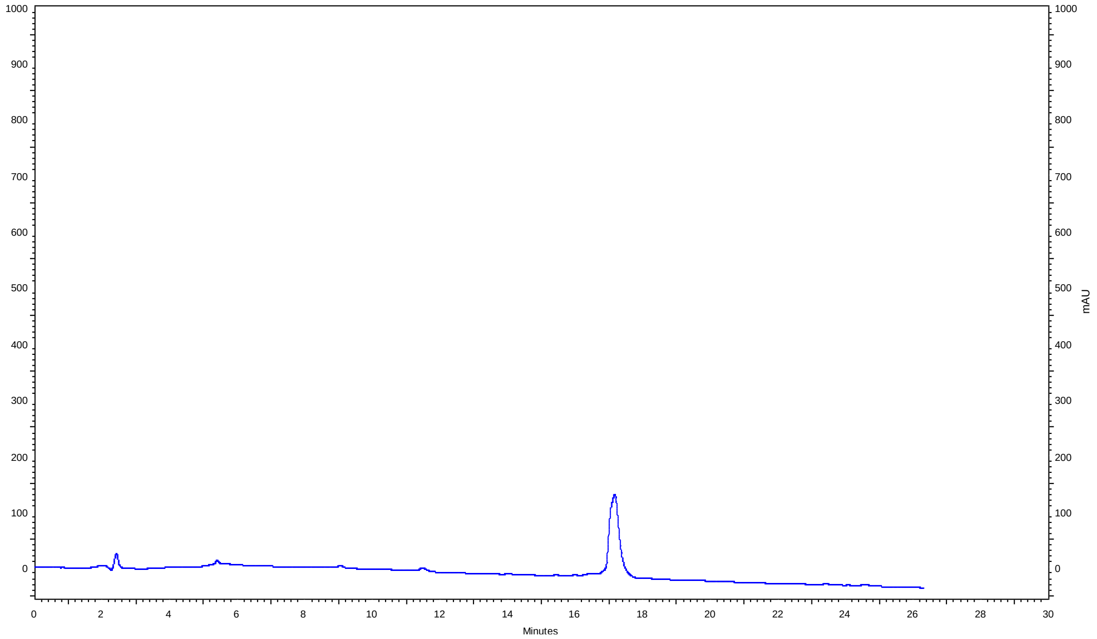

Figure 4.37 – Chromatogram obtained from the analysis of CQn-C4-Transportan after purification, with a gradient elution of 0-100% ACN in water (0,05% TFA) in a RP-18E (5 μm), for 30 minutes and a flow of 1 ml/min, with detection at λ = 220 nm.

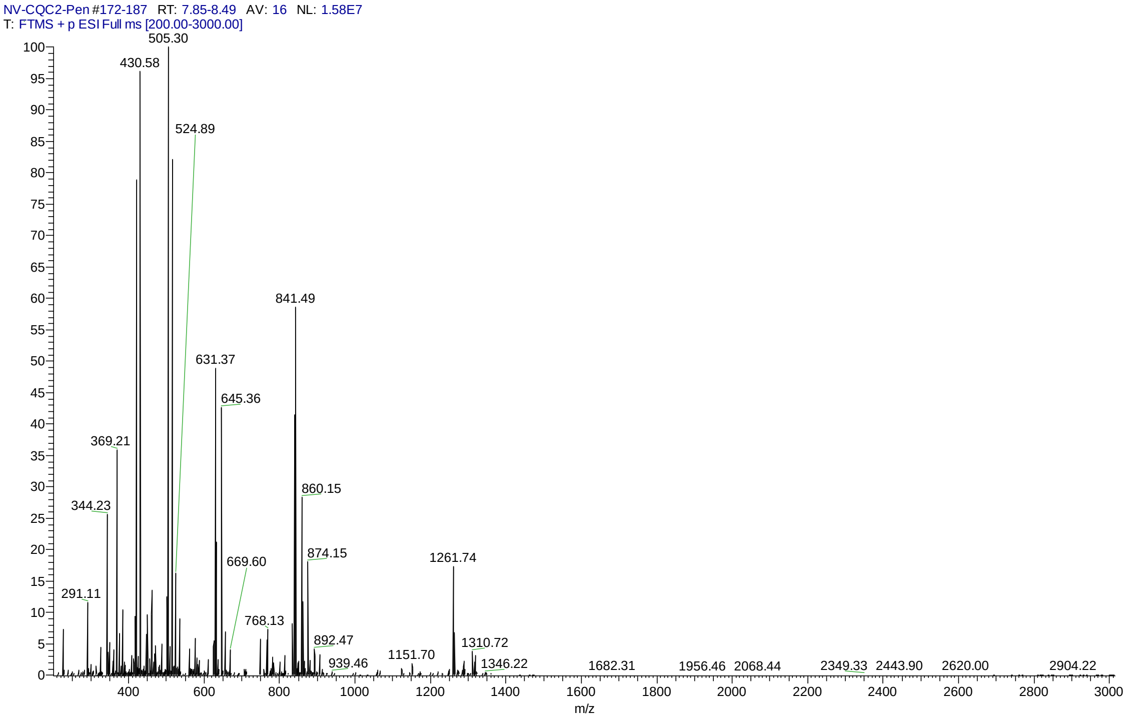

Figure 4.38 - Spectrum (ESI-IT MS, positive mode) obtained for crude CQn-C4-Penetratin.

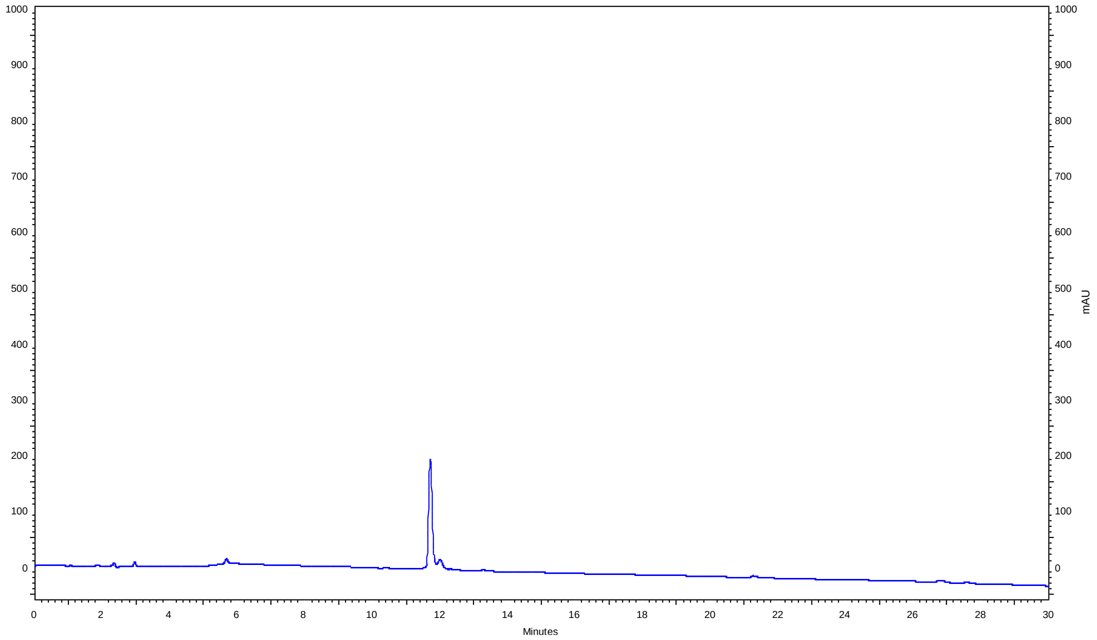

Figure 4.39 – Chromatogram obtained from the analysis of CQn-C4-Penetratin after purification, with a gradient elution of 0-100% ACN in water (0,05% TFA) in a RP-18E (5 µm), for 30 minutes and a flow of 1 ml/min, with detection at λ = 220 nm.

4.4.7. *In vitro* assays

The *in vitro* assays were done at the Prof. Philip J. Rosenthal's lab, by his team, in the University of California at San Francisco, USA. Briefly, synchronized ring-stage W2 strain *P. falciparum* were incubated with control compounds, for 48 hours, in RPMI 1640 medium containing 10 % human serum or 0.5 % Albumax serum substitute. Parasites were then fixed with 1% formaldehyde in phosphate-buffered saline (PBS), pH 7.4, for 48 h at room temperature and then labeled with YOYO-1 (1 nM; Molecular Probes) in 0.1% Triton X-100 in PBS. Parasitemias were determined from dot plots (forward scatter *versus* fluorescence) acquired on a FACSort flow cytometer using CellQuest software (Becton, Dickinson). For 50% inhibitory concentration (IC_{50}) determinations, dose-response studies were performed, with the values normalized to percent control activity, and IC_{50}'s were calculated using Prism 3.0 (GraphPad Software) with data fitted by nonlinear regression. Goodness of curve fit was documented by R^2 values of 0.95[4].

4.5. Bibliography

1. F. A. Carey and R. J. Sundberg, *Advanced Organic Chemistry*, Springer, New York, NY, USA, Fifth., 2007.
2. S. W. Goldstein, A. Bill, J. Dhuguru and O. Ghoneim, *J. Chem. Educ.*, 2017, **94**, 1388–1390.
3. B. Uff, in *Comprehensive Heterocyclic Chemistry*, eds. A. Boulton and A. McKillop, Pergamon Press, Oxford, 1984, pp. 315–364.
4. B. Pérez, C. Teixeira, J. Gut, P. Rosenthal, J. Gomes and P. Gomes, *ChemMedChem*, 2012, **7**, 1537–1540.
5. R. Morrison and R. Boyd, in *Organic Chemistry*, Prentice - Hall, Inc, 1992, pp. 851–896.
6. A. K. Ghose, V. N. Viswanadhan and J. J. Wendoloski, *J. Comb. Chem.*, 1999, **1**, 55–68.
7. B. S. Jursic and Z. Zdravkovski, *Synth. Commun.*, 1993, **23**, 2761–2770.
8. C. A. G. N. Montalbetti and V. Falque, *Tetrahedron*, 2005, **61**, 10827–10852.
9. www.nobelprize.org/prizes/chemistry/1984/summary/.
10. R. Merrifield, *J. Am. Chem. Soc.*, 1963, **85**, 2149–2154.
11. L. Carpino and G. Han, *J. Am. Chem. Soc.*, 1970, **92**, 5748–5749.
12. J. C. Sheehan and G. P. Hess, *J. Am. Chem. Soc.*
13. T. Kimmerlin and D. Seebach, *J. Pept. Res.*, 2005, **65**, 229–260.
14. W. Konig and R. Geiger, *Chemishe Berichte*, 1970, **103**, 788–798.
15. W. Konig and R. Geiger, *Chemiesche Berichte*, 1970, **103**, 2024–2033.
16. A. Williams and I. Ibrahim, *Chem. Rev.*, 1981, **81**, 589–636.
17. V. Dourtoglou, J.-C. Ziegler and B. Gross, *Tetrahedron Lett.*, 1978, **19**, 1269–1272.
18. V. Dourtoglou, B. Gross, V. Lambropoulou and C. Zioudrou, *Synthesis (Stuttg).*, 1984, **7**, 572–574.
19. M. H. Kim and D. V. Patel, *Tetrahedron Lett.*, 1994, **35**, 5603–5606.

20. T. I. Al-Warhi, H. M. A. Al-Hazimi and A. El-Faham, *J. Saudi Chem. Soc.*, 2012, **16**, 97–116.

21. B. Castro, J. R. Dormoy, G. Evin and C. Selve, *Tetrahedron Lett.*, 1975, **16**, 1219–1222.

22. E. Kaiser, R. Colescott, C. Bossinger and P. Cook, *Anal. Biochem.*, 1970, **34**, 595–598.

23. D. A. T. Pires, M. P. Bemquerer and C. J. Do Nascimento, *Int. J. Pept. Res. Ther.*, 2014, **20**, 53–69.

24. D. King, G. Fields and G. Fields, *Int. J. Pept. Protein Res.*, 1990, **36**, 255–266.

25. M. P. Draper, B. Bhatia, H. Assefa, L. Honeyman, L. K. Garrity-Ryan, A. K. Verma, J. Gut, K. Larson, J. Donatelli, A. Macone, K. Klausner, R. G. Leahy, A. Odinecs, K. Ohemeng, P. J. Rosenthal and M. L. Nelson, *Antimicrob. Agents Chemother.*, 2013, **57**, 3131–3136.

26. R. B. G. Arrighi, C. Ebikeme, Y. Jiang, L. Ranford-Cartwright, M. P. Barrett, Ü. Langel and I. Faye, *Antimicrob. Agents Chemother.*, 2008, **52**, 3414–3417.

27. U. Soomets, M. Lindgren, X. Gallet, M. Hällbrink, A. Elmquist, L. Balaspiri, M. Zorko, M. Pooga, R. Brasseur and Ü. Langel, *Biochim. Biophys. Acta - Biomembr.*, 2000, **1467**, 165–176.

28. J. Guergnon, F. Dessauge, V. Dominguez, J. Viallet, S. Bonnefoy, V. J. Yuste, O. Mercereau-Puijalon, X. Cayla, A. Rebollo, S. A. Susin, P. Bost and A. Garcia, *Mol. Pharmacol.*, 2006, **69**, 1115–24.

29. T. J. Egan, R. Hunter, C. H. Kaschula, H. M. Marques, A. Misplon and J. Walden, *J. Med. Chem.*, 2000, **43**, 283–291.

30. J. D. McChesney, *Bull. World Health Organ.*, 1981, **59**, 459–462.

31. S. J. Hocart, H. Liu, H. Deng, D. De, F. M. Krogstad and D. J. Krogstad, *Antimicrob. Agents Chemother.*, 2011, **55**, 2233–2244.

32. A. Gomes, M. Machado, L. Lobo, F. Nogueira, M. Prudêncio, C. Teixeira and P. Gomes, *ChemMedChem*, 2015, **10**, 1344–1349.

33. J. Matos, F. P. Da Cruz, É. Cabrita, J. Gut, F. Nogueira, V. E. Do Rosário, R. Moreira, P. J. Rosenthal, M. Prudêncio and P. Gomes, *Antimicrob. Agents Chemother.*, 2012, **56**, 1564–1570.

34. B. Pérez, C. Teixeira, I. S. Albuquerque, J. Gut, P. J. Rosenthal, M. Prudêncio and P. Gomes, *Medchemcomm*, 2012, **3**, 1170–1172.

35. B. Pérez, C. Teixeira, A. S. Gomes, I. S. Albuquerque, J. Gut, P. J. Rosenthal, M. Prudêncio and P. Gomes, *Bioorganic Med. Chem. Lett.*, 2013, **23**, 610–613.

5

Synthesis and *in vitro* evaluation of CQn-TP10 conjugates linked through different spacers

5.1. Overview

Considering the findings described in the previous chapter, a new set of CQn-CPP conjugates was planned, where the drug-peptide linker was varied, to investigate its impact on the conjugate's ability to inhibit parasite's growth. In fact, while the peptide carrier is an important component of CPP-drug conjugates, as it is the most important tool for intracellular delivery of the drug, it is easy to infer that the spacer that links the drug to the peptide might as well play an important role. Features like stability, length, lipophilicity or lability towards specific environments will probably affect the overall performance of the peptide-drug conjugate[1–3]. Moreover, the orientation of the drug relatively to the peptide, i.e., drug attachment to either the peptide's *N*- or *C*-terminus, might as well influence the activity of the final construct[4].

In connection with the above, and with the purpose of improving the activity of CQn-TP10 constructs, a series of novel conjugates (Figure 5.1) was synthesized (**5.2**), where CQn was linked to TP10 through different spacers, namely: (**5.2.1**) a larger flexible alkyl spacer, to increase lipophilicity and CQn's exposure (CQn-C10-TP10, **15**), (**5.2.2**) a rigid 1,2,3-triazole ring, which has been widely explored for the modification of antiplasmodial agents[5–8] (CQn-TR-TP10, **16**), and (**5.2.3**) a disulfide bond, providing a more labile (chemo- and bio-reducible) linkage between peptide and drug (CQn-S-S-TP10, **17**). Additionally, to evaluate the relevance of the position for CQn attachment to TP10 (at *N*-terminus *vs* at *C*-terminus), two other conjugates were synthesized, where CQn was conjugated to TP10's *C*-terminus region through (**5.2.4**) a succinyl spacer (TP10-C4-CQn, **18**) and (**5.2.5**) a disulfide bond (TP10-S-S-CQn, **19**).

The new series of synthetic CQn-CPP and CPP-CQn conjugates was next screened *in vitro* for their ability to inhibit the growth of intraerythrocytic *P. falciparum* parasites, and also for their hemolytic activity (**5.3**). These *in vitro* assays were performed by the author of this thesis, at the Institute of Hygiene and Tropical Medicine (IHMT).

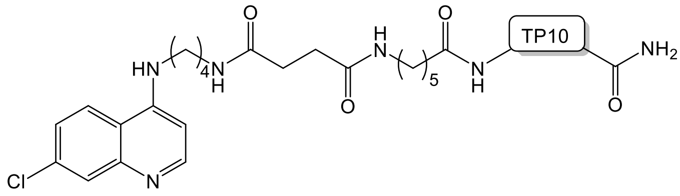
TP10
NH2
Cl
N

CQn-C10-TP10 (15)

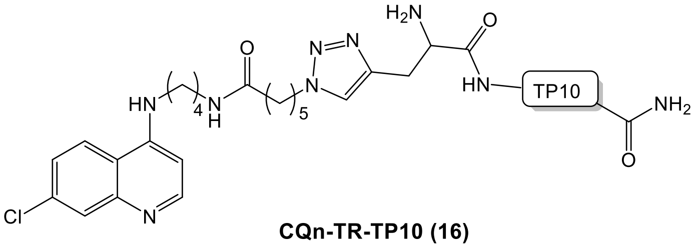
TP10
H2N
NH2
Cl
N

CQn-TR-TP10 (16)

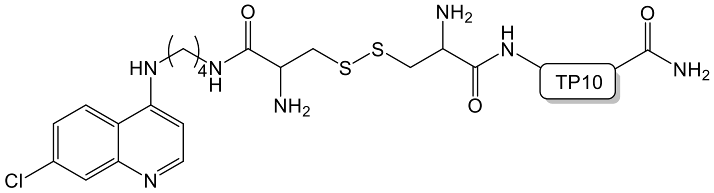
TP10
NH2
S
Cl
N

CQn-S-S-TP10 (17)

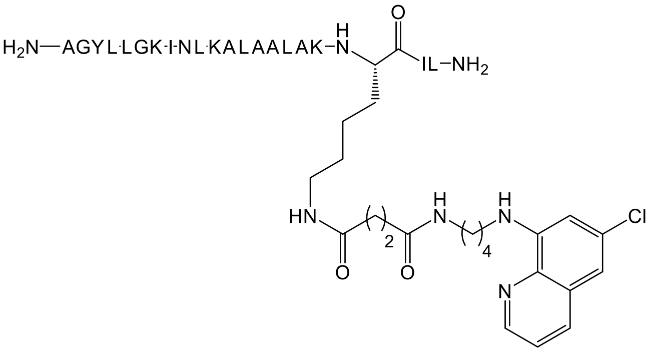
H2N—AGYL·LGK·I·NL·KALAALAK–N
IL–NH2
Cl
N

TP10-C4-CQn (18)

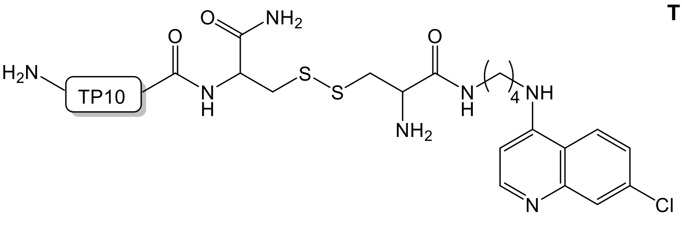
H2N
TP10
NH2
S
Cl
N

TP10-S-S-CQn (19)

Figure 5.1 – Structures of CQn-TP10 conjugates **15-19**.

5.2. Chemical synthesis

5.2.1. CQn-C10-TP10 (15)

The route applied to synthesize CQn-C10-TP10 (**15**) is depicted in Scheme 5.1. Briefly, both CQn-C4 (**5**) and TP10 were first synthesized, as described in Chapter 4 (*cf.* **4.2.1**, **4.2.2** and **4.2.3**). Once of the aa sequence of TP10 was assembled, 6-(*N*-Fmoc)aminohexanoic acid (**20**) was coupled to the *N*-terminus of TP10, *via* HBTU-mediated *in situ* coupling; after subsequent removal of the *N*-protecting group, to render 6-aminohexanoyl-TP10 (**21**) still anchored to the solid support, CQn-C4 (**5**) was coupled to the peptidyl-resin as described in Chapter 4 (*cf.* **4.2.4**). Acidolytic cleavage of the final peptidyl-resin, using the methods described in Chapter 4 (*cf.* **4.2.4**), delivered the crude target product, CQn-C10-TP10 (**15**).

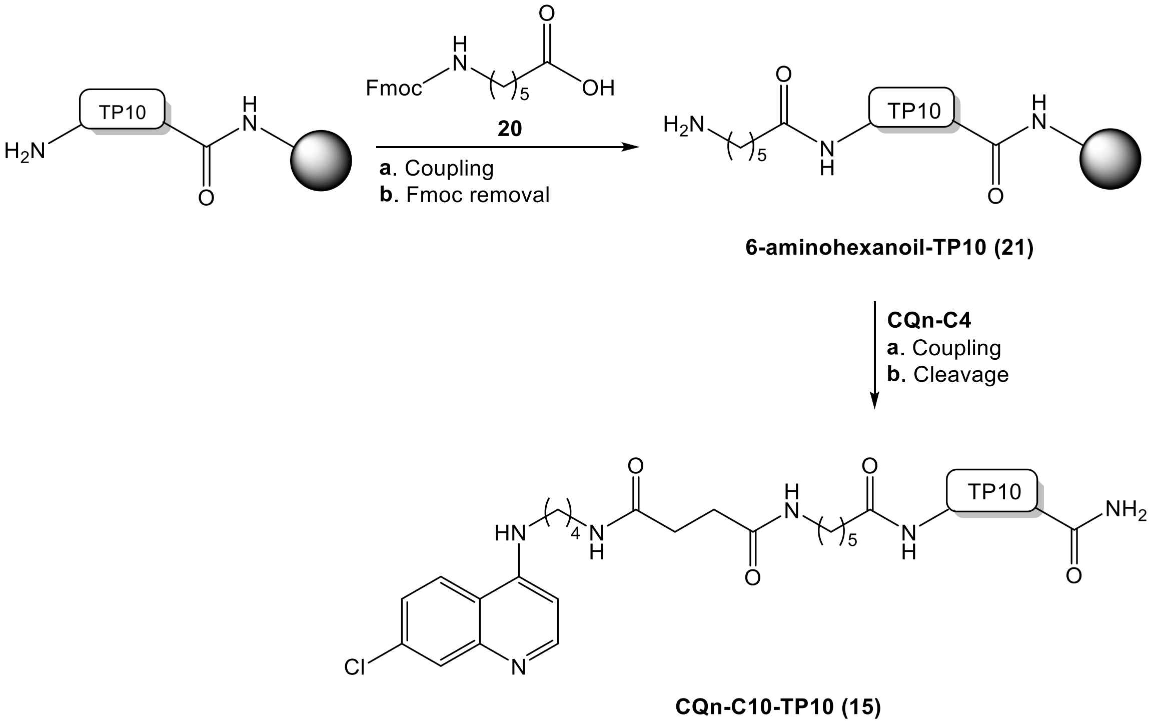
TP10
H2N
H N
O
Fmoc
H N
5
O
OH
20
a. Coupling
b. Fmoc removal
H2N
5
O
N H
TP10
H N
O
6-aminohexanoil-TP10 (21)
CQn-C4
a. Coupling
b. Cleavage
HN
4
N H
O
O
H N
5
O
N H
TP10
NH2
O
Cl
N
CQn-C10-TP10 (15)

Scheme 5.1 –Route employed for the synthesis of CQn-C10-TP10 (**15**).

After purification *via* preparative HPLC, using a gradient elution of 20-50% ACN in water (0.05% TFA) in 1 hour, following the procedures reported in Chapter 4, CQn-C10-TP10 (**15**) was isolated in 93% purity, as determined by HPLC (Figure 5.2).

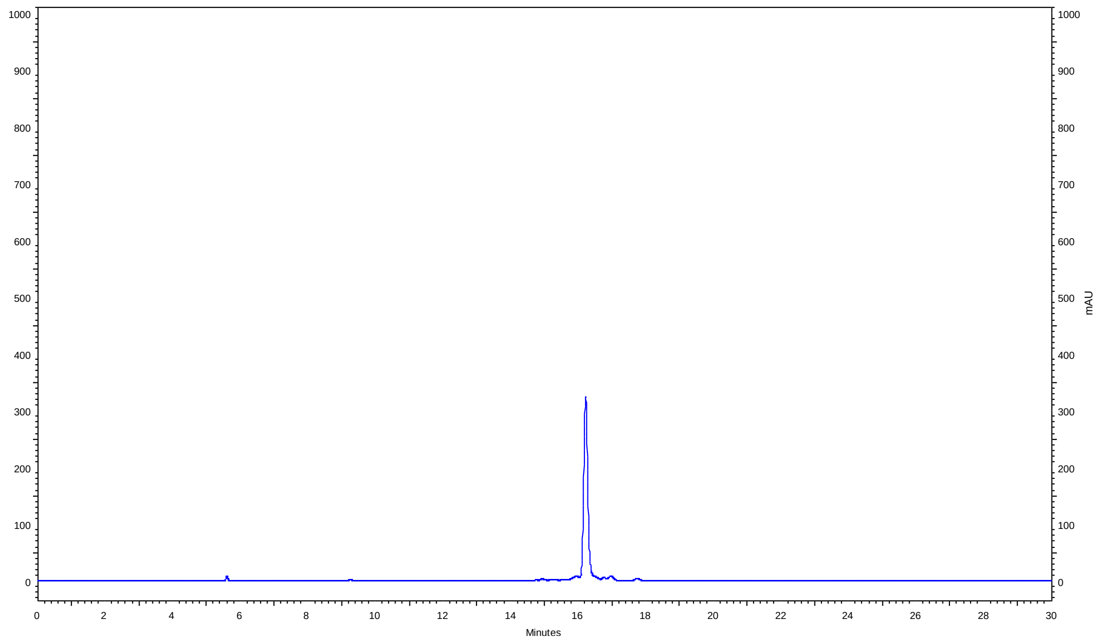

Figure 5.2 – Chromatogram obtained from the analysis of CQn-C10-TP10 (**15**) after purification, with a gradient elution of 0-100% ACN in water (0.05% TFA) in a RP-18E (5 μm), for 30 minutes and a flow of 1 ml/min, with detection at λ = 220 nm.

ESI-IT MS analysis of the isolated product was compatible with the structure of the target conjugate **15** (Figure 5.3): the spectrum presents several peaks, which derive from the detection of the protonated peptide ([P+nH$^+$]), whose exact mass is 2625.59 a.m.u. (Table 5.1).

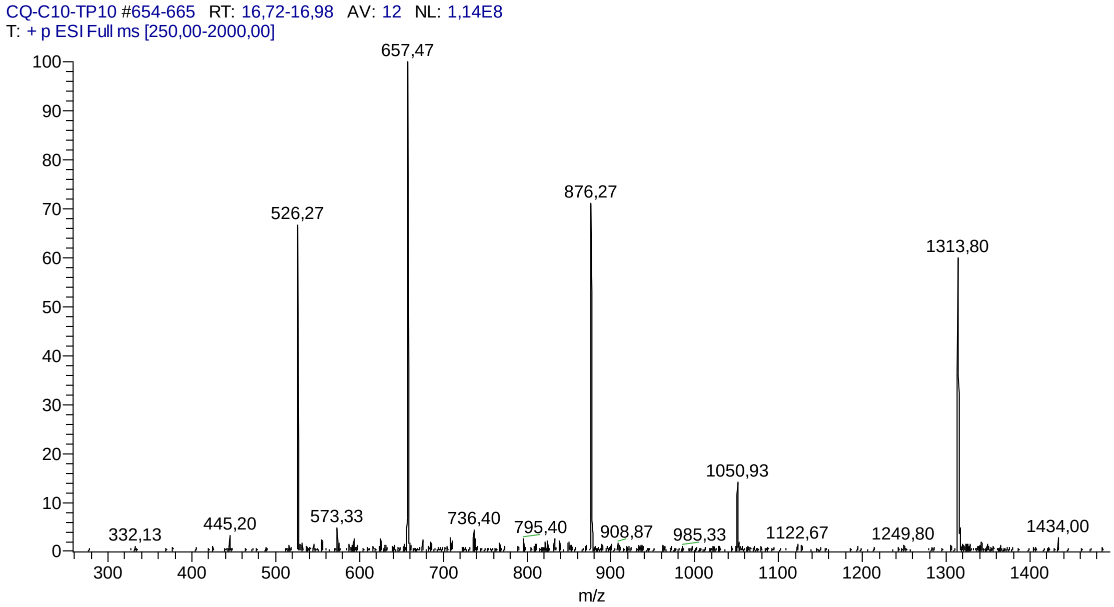

Figure 5.3 - Spectrum (ESI-IT MS, positive mode) obtained for crude CQn-C10-TP10 (**15**).

Table 5.1 – Adducts of CQn-C10-TP10 (P) with H$^+$, detected by ESI-IT MS.

Adduct	Expected $^m/_z$	Detected $^m/_z$
P + 2H$^+$	1313.80	1313.80
P + 3H$^+$	876.21	876.27
P + 4H$^+$	657.41	657.47
P + 5H$^+$	526.13	526.27

5.2.2. CQn-TR-TP10 (16)

5.2.2.1. Azide-alkyne coupling: a central piece of the synthetic route

The synthesis of CQn-TR-TP10 (**16**) was planned according to the route displayed in Scheme 5.2, shown below.

The synthetic route involves an 1,3-dipolar cycloaddition between azide **23** and alkyne **25**. Azide-alkyne cycloadditions (AAC) generate 1,2,3-triazoles (TR), whose biological relevance is well documented[5,7,9–12]. TR readily associate with diverse biological targets, through hydrogen bonding and dipole interactions, while being remarkably stable from both the chemical and metabolic viewpoints: they are resistant to acidic and basic hydrolysis, to reductive and oxidative conditions, and to metabolic degradation, due to an accentuated aromatic stabilization[10,11]. These characteristics, together with the reported antibacterial, antiviral, antitumor and antiprotozoal activity for TR, makes them quite interesting for therapeutic applications[5,7,9–12]. As such, AAC have gained prominence not only because of their remarkable chemoselectivity, but also because they produce TR.

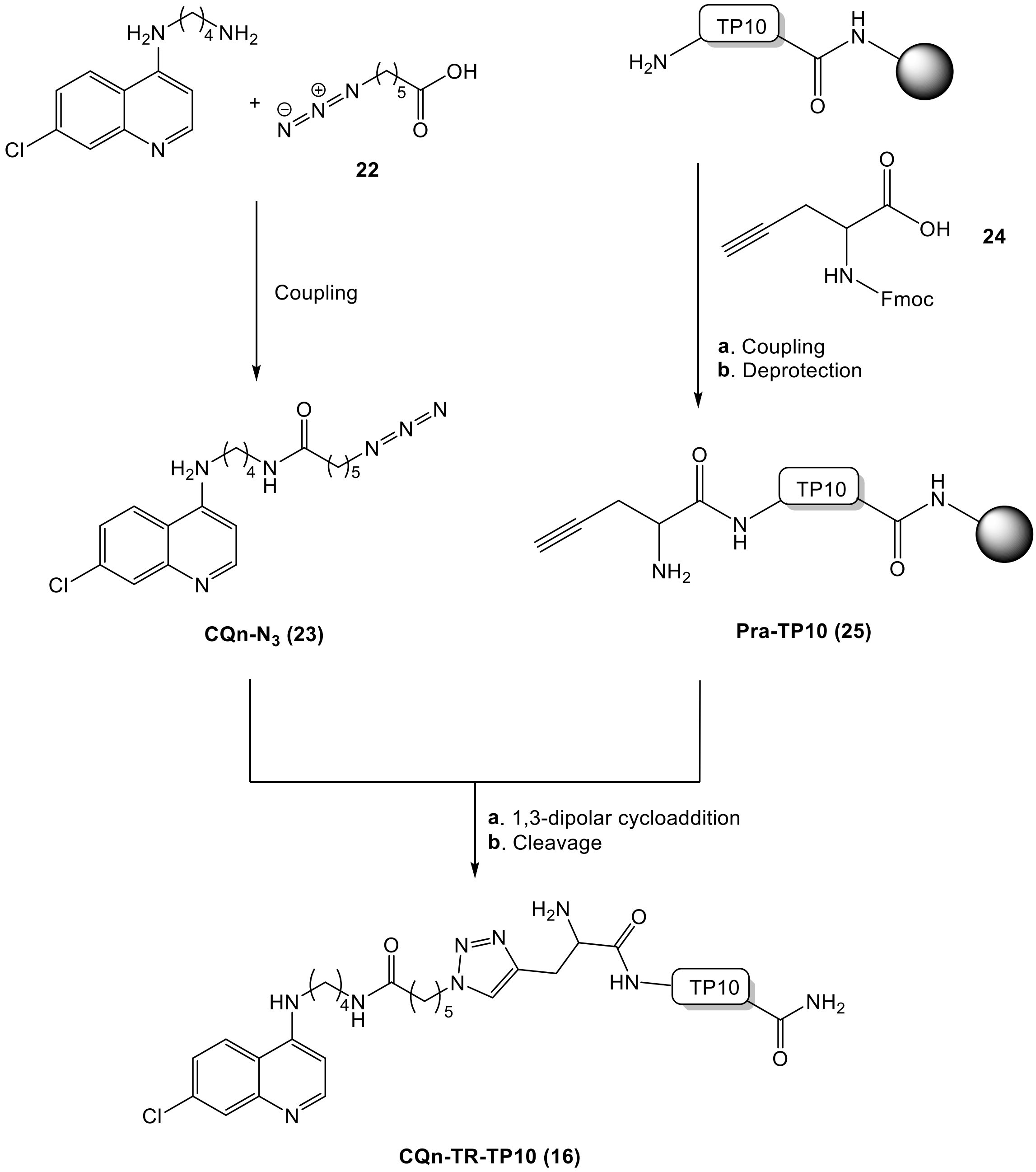
22
24
Coupling
a. Coupling
b. Deprotection
CQn-N3 (23)
Pra-TP10 (25)
a. 1,3-dipolar cycloaddition
b. Cleavage
CQn-TR-TP10 (16)
TP10
Fmoc

Scheme 5.2 – Route for the synthesis of CQn-TR-TP10 (**16**)

AAC are Huisgen's 1,3-dipolar cycloadditions of the type 3+2→5. These reactions require an 1,3-dipole (*e.g.* azides, nitriloxides or diazoalkanes) to react with a dipolarophile (*e.g.* alkenes, alkynes or carbonyls) *via* a concerted mechanism (Figure 5.4) to form a five-membered heterocycle[13]. Huisgen's 1,3-dipolar cycloadditions between an organic azide and an alkyne result in the formation of a disubstituted TR (Figure 5.5).

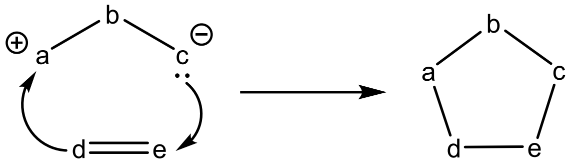

Figure 5.4 – Schematic view of a 1,3-dipolar cycloaddition of type 3+2→5. Adapted from [13]

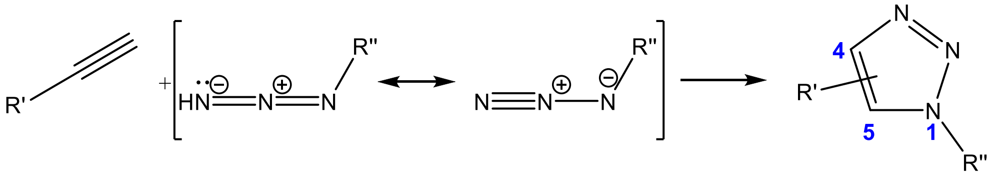

Figure 5.5 - Huisgen's 1,3-dipolar cycloaddition between an alkyne and an organic azide.

In the absence of a suitable catalyst, AAC have relevant drawbacks: they require high temperatures, extended reaction times and unavoidably lead to the formation of the two possible structural isomers, namely, 1,4- and 1,5-disubstituted TR. As such, these reactions were not very appealing until the beginning of the new millennium, when introduction of copper(I)-mediated catalysis revolutionized this reaction: rate and yield are significantly increased, even at room temperature, and, more importantly, the reaction becomes regioselective, exclusively yielding the 1,4-disubstituted TR[14,15]. While the uncatalyzed azide-alkyne 1,3-dipolar cycloaddition is a one-step process, copper-catalyzed AAC (CuAAC) is considered to be a step-wise process which involves copper(I) in the intermediate steps (Scheme 5.3). In the initial step, copper(I) coordinates with the alkyne (**26**) to form acetylide (**27**); then, azide (**28**) binds to copper (**29**) followed by the formation of a copper(III)metallacycle (**30**). This intermediate then undergoes ring contraction to originate a copper triazolyl derivative (**31**) which, upon proteolysis, renders the desired TR (**32**)[16].

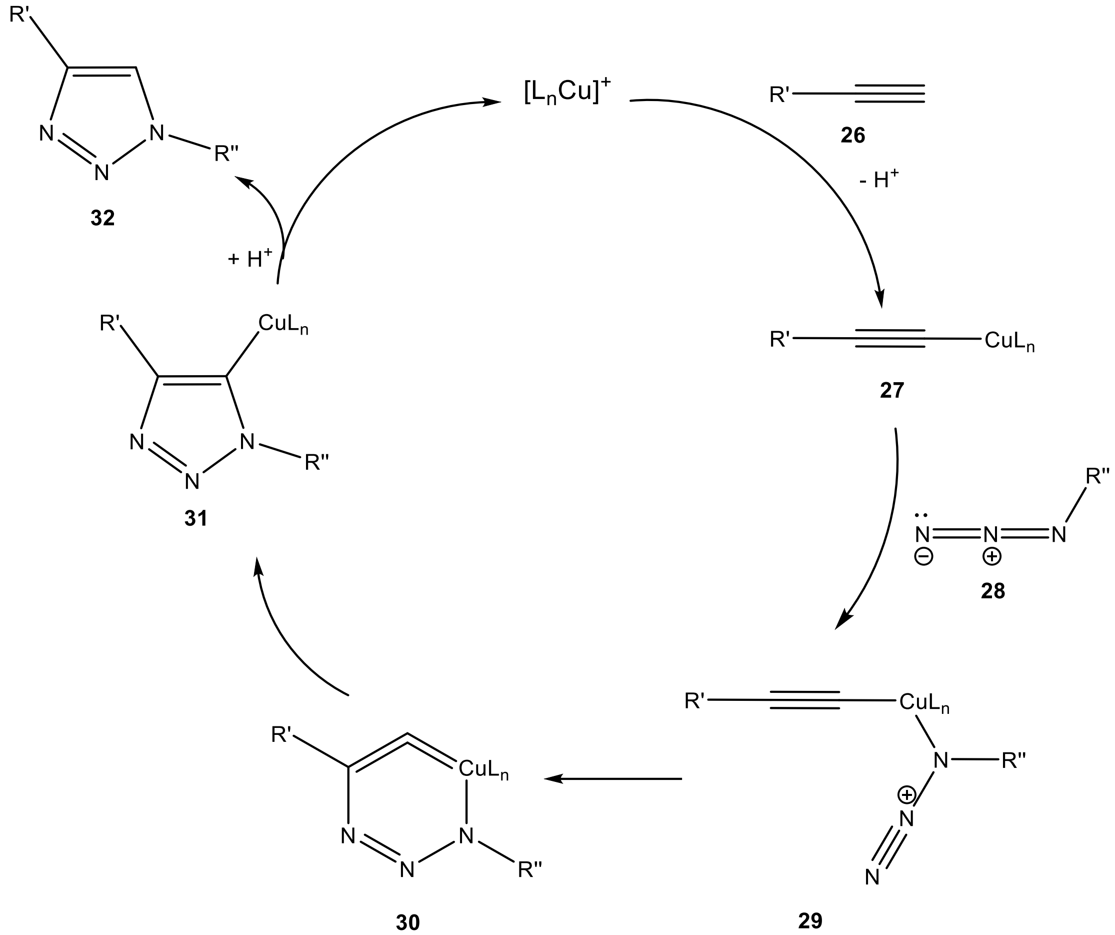

Scheme 5.3 - Proposed mechanism for copper-catalyzed azide-alkyne cycloadditions (CuAAC).

As depicted in Scheme 5.2, conjugation of CQn to TP10 *via* CuAAC required previous modification of both the drug and the peptide, in order to respectively incorporate an azide and an alkyne moiety in each of them. As such, synthetic intermediates **23** and **25** were first synthesized, as follows.

5.2.2.2. Synthesis of CQn-N₃ (23)

In order to prepare synthetic intermediate **23**, 6-azido hexanoic acid (**22**) was coupled to the primary amine group of CQn (**2**). To this end, **22** was first activated with HBTU in the presence of DIPEA, in DMF, at 0 °C for 30 minutes. Then, CQn (**2**) was added to the reaction medium, and the coupling allowed to proceed for 3 hours at 0 °C. Reaction progress was monitored by TLC, which showed that **2** had been totally consumed after 3 hours, with formation of multiple products. After the necessary purification steps - *via* liquid column chromatography, using silica gel as stationary phase and DCM/MeOH (5:1 v/v) as eluent, 4-{*N*-[*N*'-(6-azidohexanoyl)]aminobutyl}amino-7-chloroquinoline (CQn-N_3, **23**) was isolated in moderate yield (57%), and presented spectral data (ESI-IT MS) compatible with the expected structure (Figure 5.6). The spectrum presents a peak at $^m/_z$ = 389.73, which is compatible with the quasi-molecular ion (MH^+) of CQn-N_3, whose exact mass is 388.19 a.m.u..

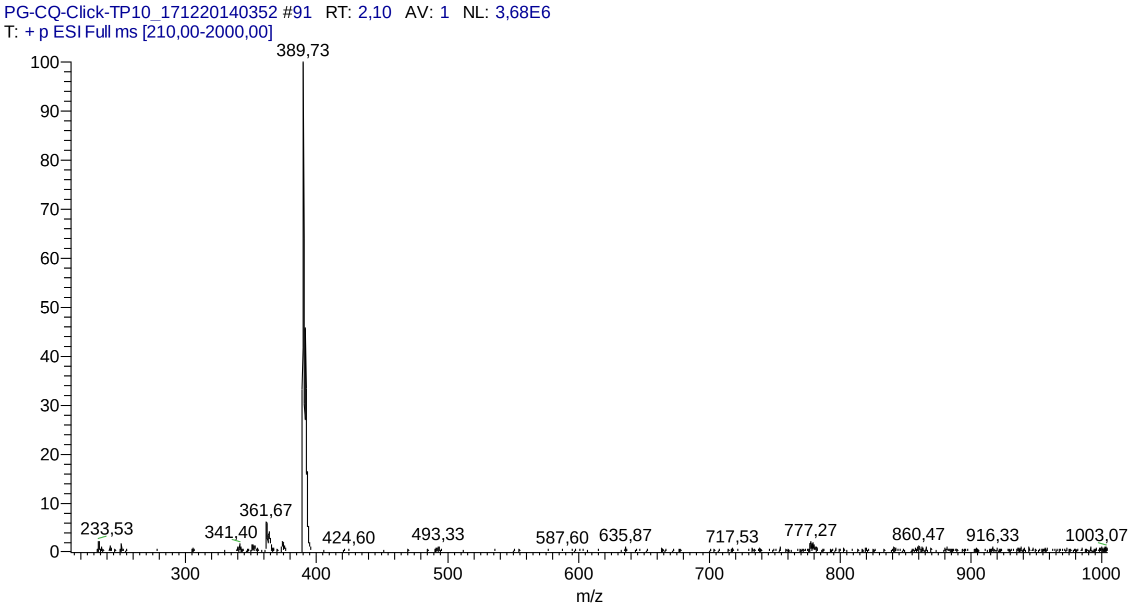

Figure 5.6 - Spectrum (ESI-IT MS, positive mode) obtained for CQn-N_3 (**23**).

Noteworthy, the reaction failed to deliver the target compound (**23**) when carried out at room temperature: only a small proportion of the reactants was converted into the desired product, and too many by-products were formed; this rendered the target product practically impossible to isolate, and consequently the reaction was extremely inefficient.

5.2.2.3. Synthesis of intermediate 42 and of target conjugate CQn-TR-TP10 (16)

TP10 was assembled by SPPS as before described, and its *N*-terminus further modified through coupling to the non-natural amino acid Fmoc-propargylglycine (Pra, **24**). Following Fmoc removal, the alkyne-modified peptide (**25**) was reacted on-resin with CQn-N_3 (**23**) in the presence of Cu(I) bromide, 2,6-lutidine, sodium ascorbate and DIPEA, to produce the CQn-TR-TP10 (**16**) conjugate *via* CuAAC[17]. Release of the target CQn-TR-TP10 (**16**) from the resin was achieved after acidolytic cleavage, following procedures already described (Chapter 4). The crude product was purified *via* preparative HPLC, with a gradient elution of 35-45% ACN in water (0.05% TFA). As shown in Figure 5.7, the product was isolated in 91% purity, as determined by HPLC.

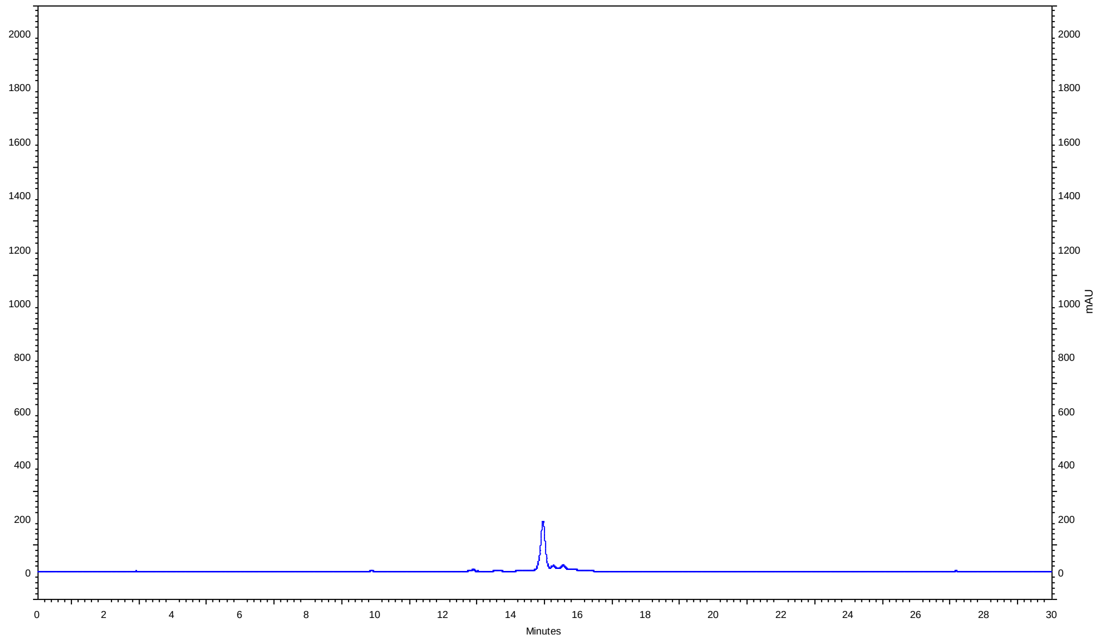

Figure 5.7 – Chromatogram obtained from the analysis of CQn-TR-TP10 (**16**) after purification, with a gradient elution of 0-100% ACN in water (0.05% TFA) in a RP-18E (5 µm), for 30 minutes and a flow of 1 ml/min, with detection at λ = 220 nm.

ESI-IT MS analysis of the isolated product was compatible with the structure of the target conjugate **16** (Figure 5.8). This spectrum presents several peaks, corresponding to the target product (with an exact mass of 2664.61 a.m.u.) with different levels of protonation (Table 5.2).

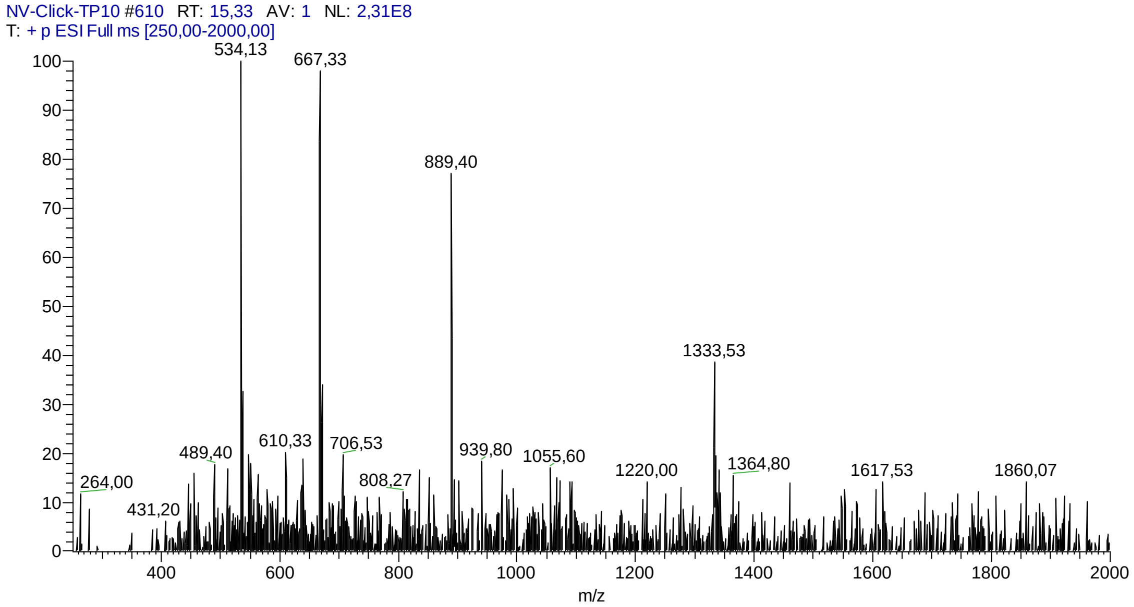

Figure 5.8 - Spectrum (ESI-IT MS, positive mode) obtained for crude CQn-TR-TP10 (**16**).

Table 5.2 – Adducts of the peptide CQn-TR-TP10 (P), detected by ESI-IT MS.

Adduct	Expected $^{m}/_{z}$	Detected $^{m}/_{z}$
P + 2H⁺	1333.32	1333.53
P + 3H⁺	889.21	889.40
P + 4H⁺	667.16	667.33
P + 5H⁺	533.93	534.13

5.2.3. CQn-S-S-TP10 (17)

Conjugate CQn-S-S-TP10 (**17**) was designed to offer a bio-reducible bond between the drug and the peptide, to eventually take advantage of the antioxidant machinery that malaria parasites utilize to resist oxidative stress inside host cells[18–21]. *Plasmodia* are quite susceptible to reactive oxygen (ROS) and nitrogen (RNS) species that rise inside *P*iRBC, due to both hemoglobin degradation and activation of the host immune system upon infection; hence, survival of intraerythrocytic parasites is highly dependent on an adequate redox balance[18–21]. Although *Plasmodium spp* parasites lack catalase and classical glutathione reductases, they utilize an intricate redox network largely based on enzymes of the thioredoxin superfamily[18], and cause drastic changes in the metabolism of reduced glutathione (GSH)[19], to ensure a convenient thiol status for their survival. As such, it was hypothesized that, once inside *P*iRBC, conjugate CQn-S-S-TP10 (**17**) might readily release the antimalarial moiety upon bio-reductive cleavage of the disulfide linker, eventually through, e.g., a thiol-disulfide exchange reaction (TDER) with intracellular GSH[22]. Interestingly, a TDER is also used in the route devised to synthesize conjugate **17** (Scheme 5.4), which highlights the important role of TDER in both Biology and Chemistry, as next explained.

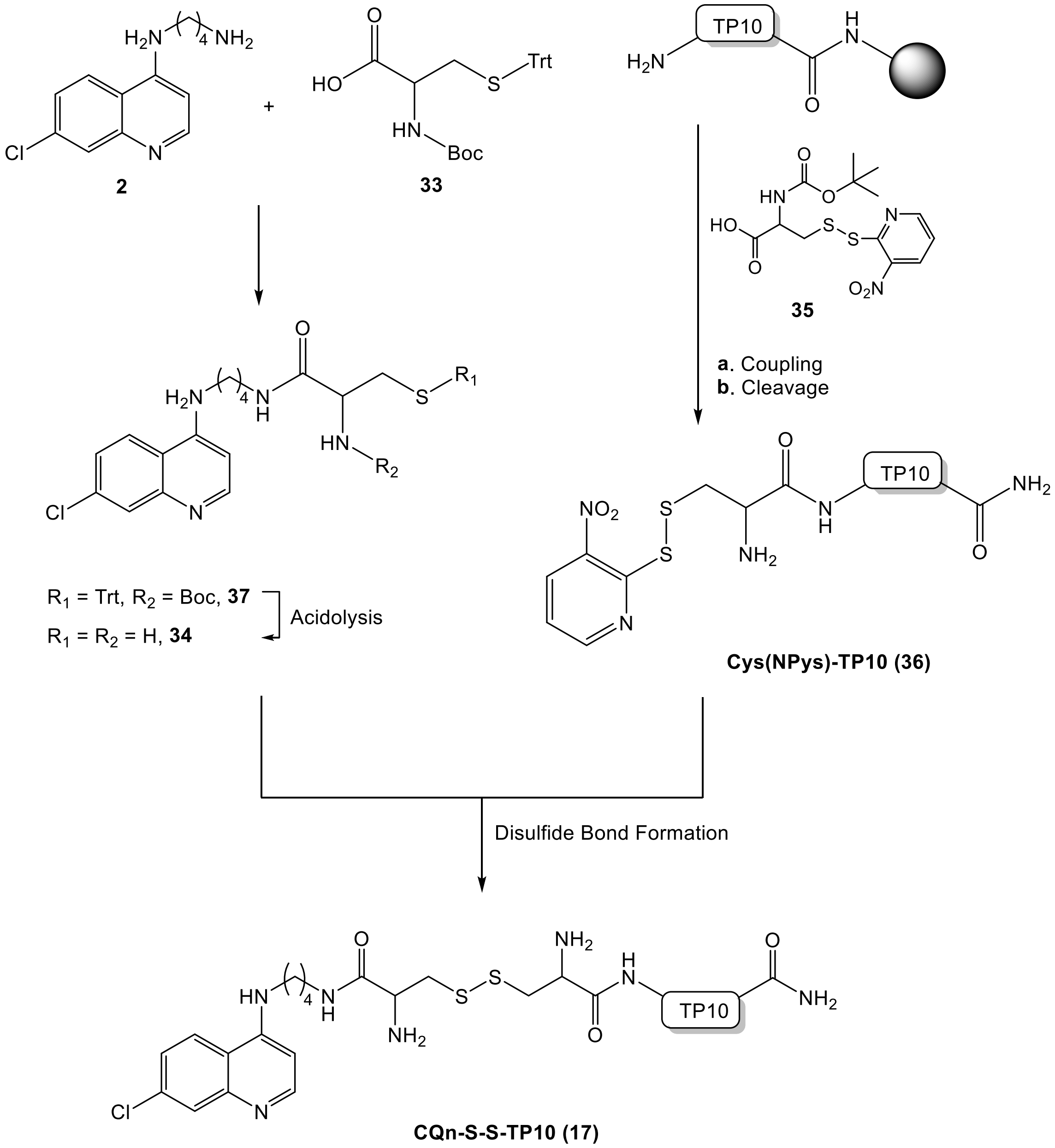
2
33
35
a. Coupling
b. Cleavage
R1 = Trt, R2 = Boc, 37
R1 = R2 = H, 34
Acidolysis
Cys(NPys)-TP10 (36)
Disulfide Bond Formation
CQn-S-S-TP10 (17)
TP10

Scheme 5.4 – Route for the synthesis of CQn-S-S-TP10 (**17**).

5.2.3.1. *Disulfide bonds and thiol-disulfide exchange reactions*

The conversion of thiols to disulfides plays a key role in biological systems. For example, disulfide bonds among peptides and proteins – established between cysteine residues present in their structures, are capable of imposing conformational constraints and increase the thermal and metabolic stability of those biomolecules[23]. Disulfides are also the major products of thiol oxidation, a process that has primary roles in defense mechanisms against oxidative stress and in redox regulation of cell signaling[22,24]. Although disulfide bonds are relatively stable, particularly in the extracellular medium, they may be easily reduced by GSH in the intracellular medium, including inside *P*iRBC, as mentioned above[25,26], which makes disulfides particularly interesting spacers between CPP and cargo.

The conversion of thiols into disulfides can occur *via* either direct substitution (TDER) or a series of redox reactions[22]. TDER involve the reaction of a thiol (RSH) with a disulfide (R'SSR'), whereby a new disulfide compound (RSSR') and a thiol (R'SH) derived from the original disulfide (Scheme 5.5) are produced. TDER follow an S_N2 nucleophilic substitution mechanism, which is consistent with a concerted reaction with a single transition state complex, where the nucleophile attacks the disulfide moiety of the second molecule[27].

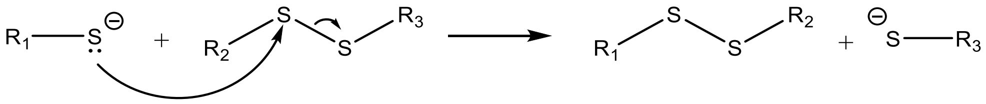

Scheme 5.5 –A thiol-disulfide exchange reaction (TDER).

As depicted in Scheme 5.4, formation of the target conjugate CQn-S-S-TP10 (**17**) involved a TDER between intermediates CQn-Cys (**34**) and Cys(Npys)TP10 (**36**), whose chemical synthesis was firstly addressed, as follows.

5.2.3.2. *Synthesis of CQn-Cys (34)*

Introduction of a thiol group in the antimalarial building block CQn was pursued upon coupling this drug to the protected cysteine derivative Boc-Cys(Trt)-OH (**33**), in the presence of appropriate coupling agents (HBTU and DIPEA as the auxiliary base), using DMF as solvent (Scheme 5.6). After purification through liquid column chromatography

– using silica gel as stationary phase and a mixture of DCM/MeOH (20:1 v/v) as eluent, the chromatographically homogeneous (TLC) protected intermediate (**37**) was obtained in a moderate yield (54%). ESI-IT MS analysis of the isolated product (Figure 5.9) was compatible with the structure of the target compound, **37**, whose exact mass is 694.27 a.m.u..

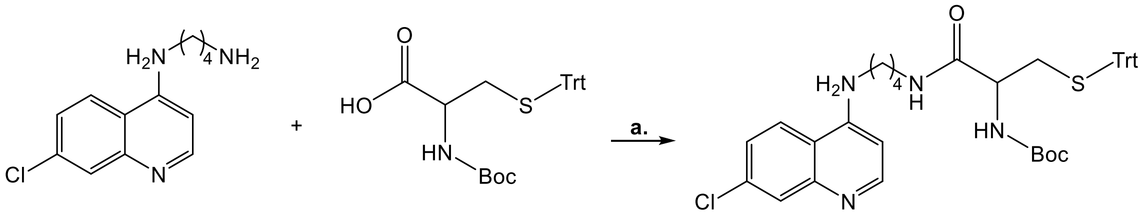

CQn (2) **Boc-Cys(Trt)-OH (33)** **Boc-Cys(Trt)-CQn (37)**

a. HBTU and DIPEA in DMF

Scheme 5.6 – Coupling of CQn to Boc-Cys(Trt)-OH.

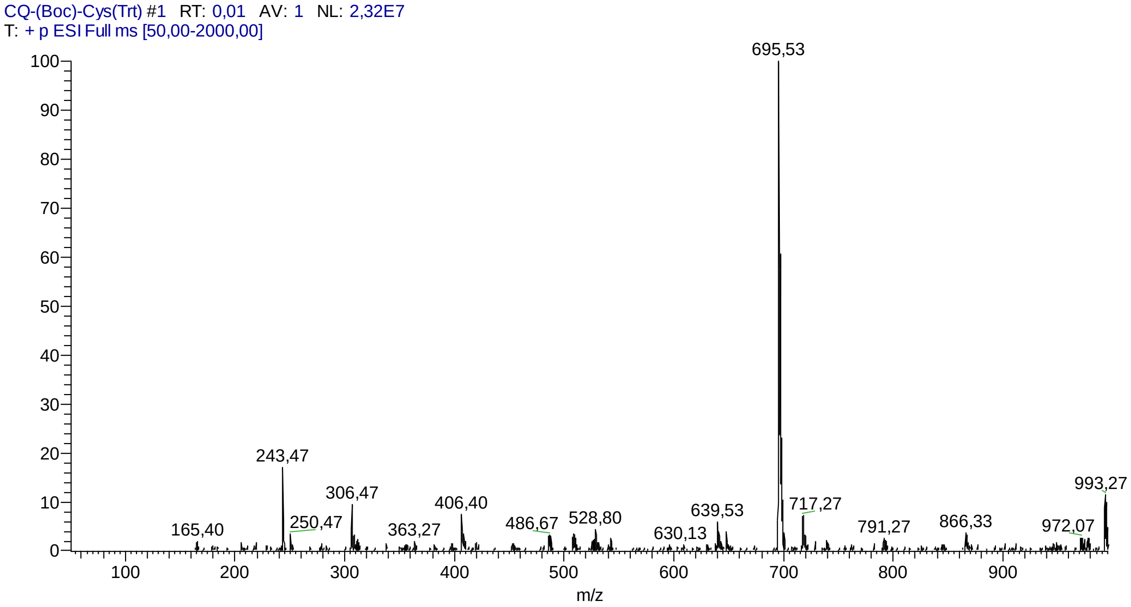

Figure 5.9 - Spectrum (ESI-IT MS, positive mode) obtained for **37**.

Removal of the amine and thiol protecting groups (Boc and Trt, respectively) from **37** was carried out by direct dissolution in a TFA-based cleavage cocktail (95% TFA, 2.5% TIS and 2.5% water; Scheme 5.7), and the acidolysis was run for 1 hour at room temperature. After convenient work-up of the reaction mixture, the target CQn-Cys intermediate (**34**) was obtained in high yield (75%), as a chromatographically homogeneous (TLC) yellow oil. The structure of this intermediate, whose exact mass is 352.11 a.m.u., was confirmed by ESI-IT MS. The obtained spectrum (Figure 5.10) shows a peek at $^{m}/_{z}$ = 353.47, which is compatible with the quasi-molecular ion (MH^+) of CQn-Cys.

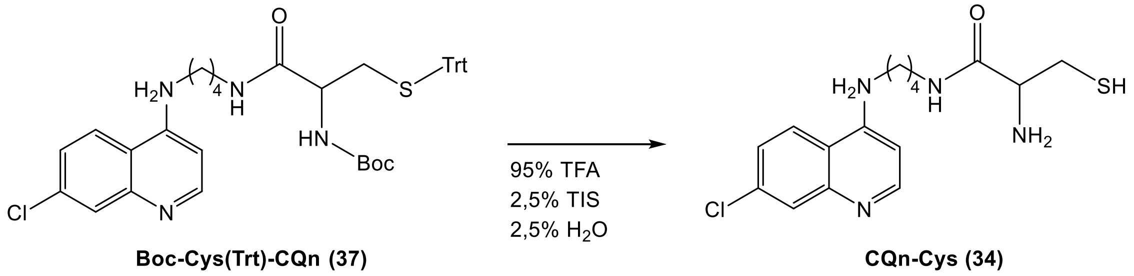

Scheme 5.7 – Acidolytic deprotection of Boc-Cys(Trt)-CQn (**37**) to produce CQn-Cys (**34**).

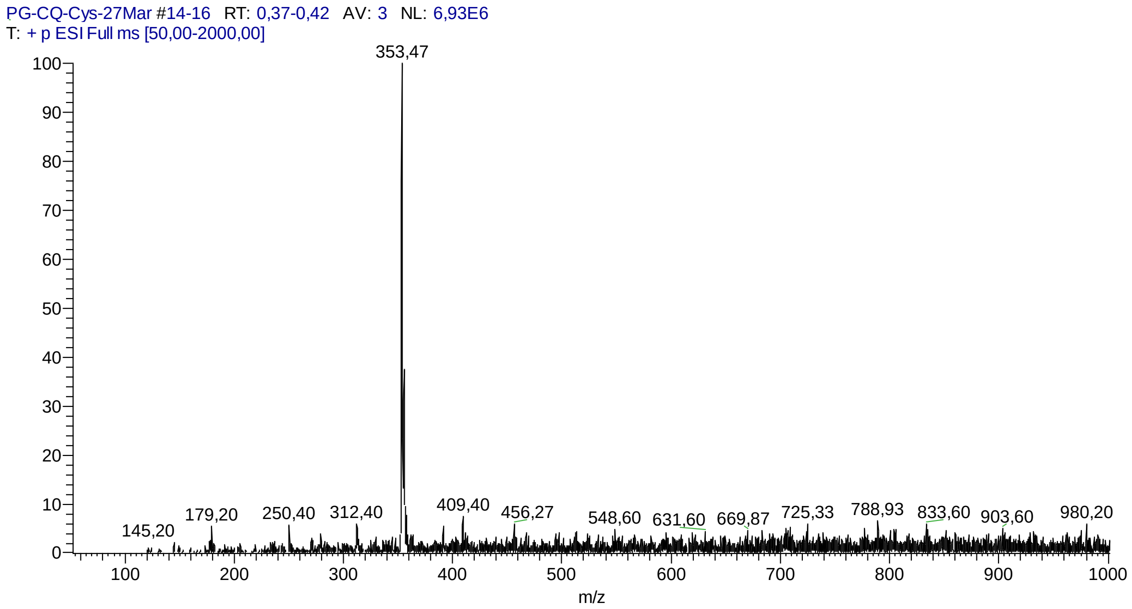

Figure 5.10 - Spectrum (ESI-IT MS, positive mode) obtained for **34**.

5.2.3.3. Synthesis of Cys(NPys)-TP10 (36)

The aa sequence of TP10 was assembled by SPPS as usual, and upon removal of the *N*-terminal Fmoc protecting group, an additional coupling with the protected Cys derivative Boc-Cys(NPys)-OH (**35**) was carried out, *via* standard coupling in the presence of HBTU and DIPEA, in DMF. Once the coupling was completed and the peptidyl-resin conveniently washed, standard acidolytic cleavage using 95% TFA, 2.5%

TIS and 2.5% water, followed by the usual work-up (*cf.* Chapter 4) produced the crude Cys(NPys)-TP10 peptide (**36**). This peptide was dissolved in na aqueous solution of acetic acid (10% v/v) and analysed by LC-DAD/ESI-IT MS (Figure 5.11), through which it was possible to confirm that the obtained peptide was effectively the desired Cys(NPys)-TP10 (**36**). In the spectrum, three major peeks are depicted, which correspond to different protonation states of the peptide, whose exact mass is 2438.39 a.m.u. (Table 5.3).

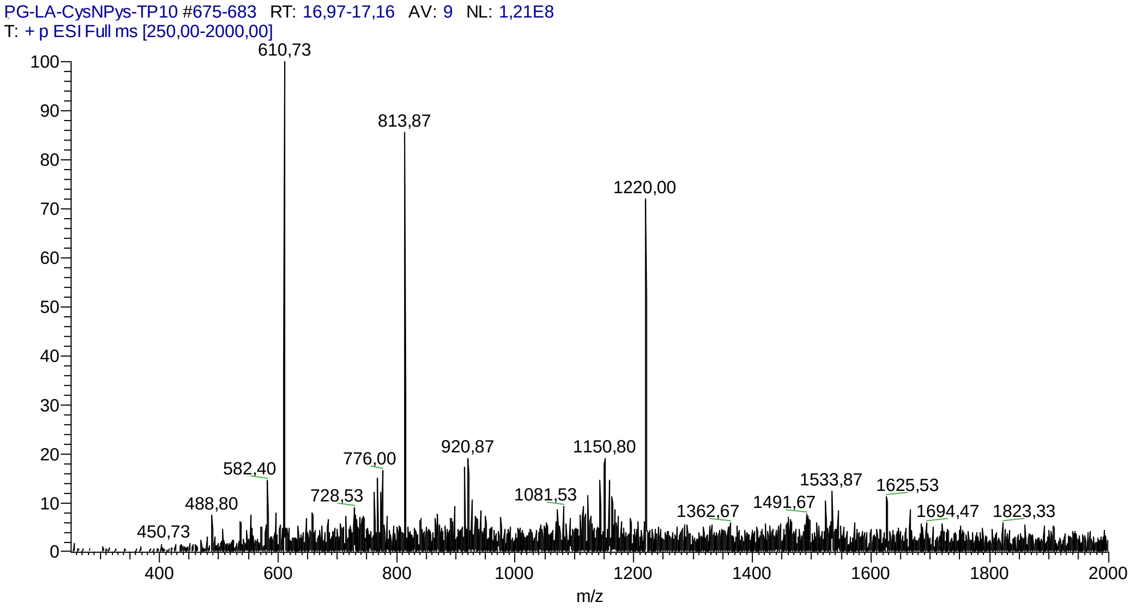

Figure 5.11 - Spectrum (ESI-IT MS, positive mode) obtained for crude Cys(NPys)-TP10 (**36**).

Table 5.3 – Adducts of the peptide Cys(NPys)-TP10 (P), detected by ESI-IT MS.

Adduct	Expected $^{m}/_{z}$	Detected $^{m}/_{z}$
P + 2H^{+}	1220.19	1220.00
P + 3H^{+}	813.80	813.87
P + 4H^{+}	610.59	610.73

Final peptide was dissolved distilled water, freeze-dried, and stored at -20 °C until further use.

5.2.3.4. Synthesis of the target CQn-S-S-TP10 conjugate (17) via a TDER

CQn-S-S-TP10 (**17**) was obtained *via* a TDER between CQn-Cys (**34**) and the activated Cys(NPys)-TP10 peptide (**36**), as depicted in Scheme 5.4. The 3-nitro-2-pyridylsulfenyl (NPys) is an acid-stable and nucleophile-labile protecting group that plays the double role of protecting amines, hydroxyls and thiols while activating them towards reaction with nucleophiles; hence, when linked to the side chain thiol of a Cys residue in a peptide, NPys is not removed upon acidolytic cleavage of the peptidyl-resin, and keeps the thiol activated to undergo nucleophilic substitution reactions like TDER [28,29]. As such, upon reaction of **34** with **36**, the nitrogen from the pyridine moiety in NPys establishes an hydrogen bond with the CQn-Cys thiol, producing a more nucleophilic *quasi*-thiolate that then attacks the disulfide moiety, leading to loss of 3-nitro-1*H*-pyridine-2-thione (**38**, Scheme 5.8)[30] with concomitant formation of the target CQn-S-S-TP10 conjugate (**17**).

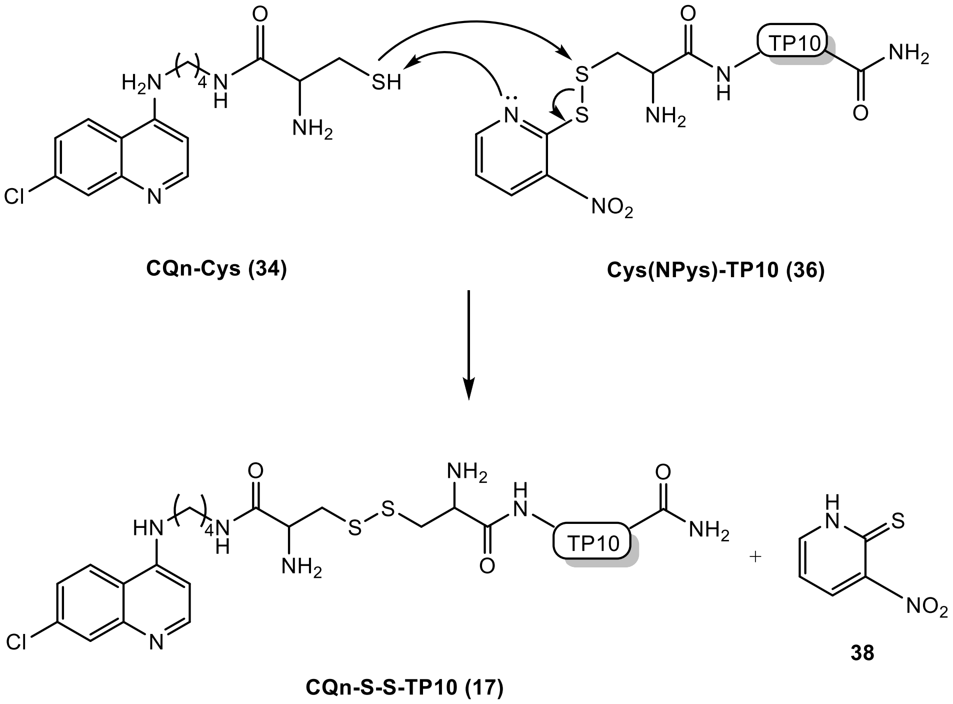

Scheme 5.8 – TDER between CQn-Cys (**34**) and Cys(NPys)-TP10 (**36**), yielding conjugate **17**.

The TDER between CQn-Cys (**34**) and Cys(NPys)-TP10 (**36**) was carried out by dissolving equimolar amounts of both intermediates in 1 *M* aqueous acetic acid, and allowing the reaction to proceed for 36 hours, at room temperature. Reaction progress was monitored by HPLC, and resulting conjugate was purified by preparative HPLC, as previously described for other CQn-CPP conjugates (*cf.* Chapter 4), using a gradient elution of 20-50% ACN in water (0.05% TFA) for 60 minutes. Conjugate CQn-S-S-TP10 (**17**) was isolated in 96% purity (Figure 5.12) and its structure confirmed by ESI-IT MS. Figure 5.13 represents the obtained spectrum, which shows two main peaks, corresponding to the protonated peptide ([P+nH$^+$]; Table 5.4), whose exact mass is 2634.51 a.m.u..

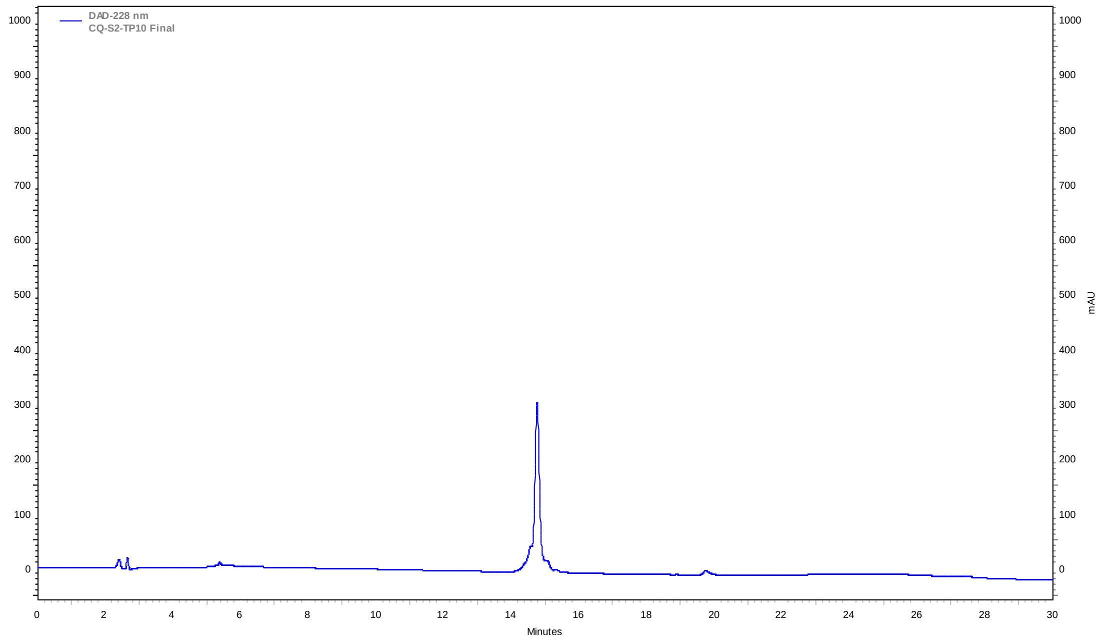

Figure 5.12 – Chromatogram obtained from the analysis of CQn-S-S-TP10 (**17**) after purification, with a gradient elution of 0-100% ACN in water (0.05% TFA) in a RP-18E (5 μm), for 30 minutes and a flow of 1 ml/min, with detection at λ = 220 nm.

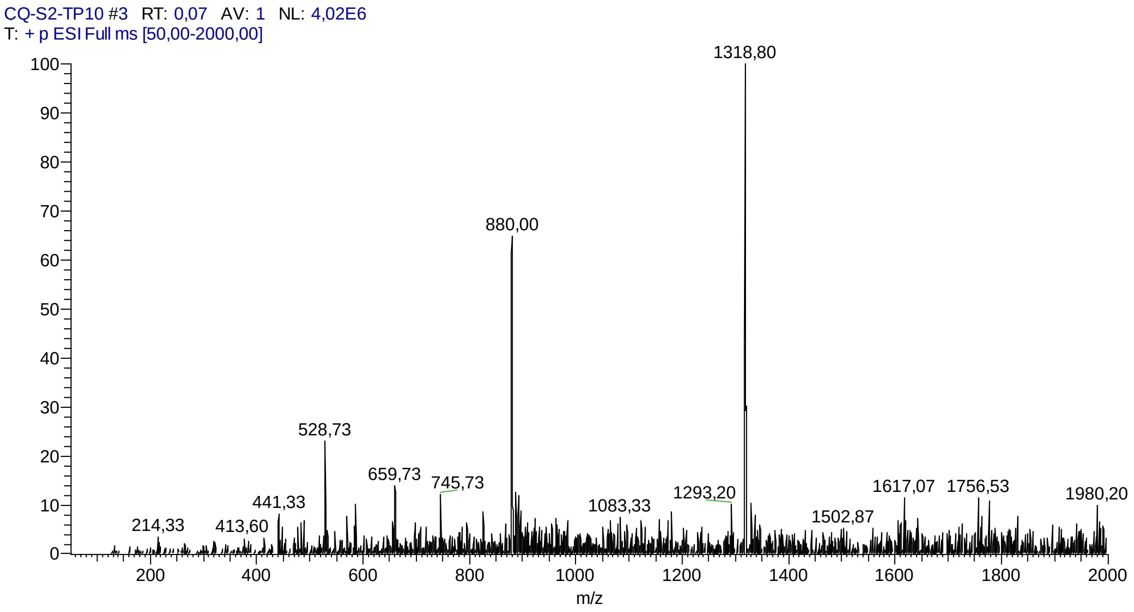

Figure 5.13 - Spectrum (ESI-IT MS, positive mode) obtained for crude CQn-S-S-TP10 (**17**).

Table 5.4 – Adducts of the peptide CQn-S-S-TP10 (P), detected by ESI-IT MS.

Adduct	Expected $^{m}/_{z}$	Detected $^{m}/_{z}$
P + 2H$^+$	1318.77	1318.80
P + 3H$^+$	879.51	880.00
P + 4H$^+$	659.88	659.73

5.2.4. TP10-C4-CQn (18)

For positioning of CQn to the *C*-terminus proximity of TP10, CQn-C4 (**5**) was coupled to the lysine present on the peptide's *C*-terminal region (AGYLLGKINLKALAALAK**K**IL). For this, TP10 was assembled by SPPS, as previously described, and the third residue introduced was Fmoc-Lys-(Mtt)-OH, coupled to the resin by standard methods, prior to elongation of the remaining *aa* of TP10's sequence (**39**, Scheme 5.9).

Once the full sequence was assembled, and before the *N*-terminal Fmoc protecting group was removed as usual, the acid-hyperlabile Mtt group that was protecting the side chain of the *C*-terminal Lys was selectively removed with a solution of 1% TFA in DCM. This produced the free ε-amine group of the additional *C*-terminal Lys, which was next coupled to CQn-C4 similarly to the previously described in Chapter 4 (*cf.* **4.2.5**). Once this coupling was complete, the *N*-terminal Fmoc was removed by the standard treatment with piperidine in DMF, and subsequent acidolytic cleavage of the peptidyl-resin delivered the crude target conjugate TP10-C4-CQn (**18**) (Scheme 5.9).

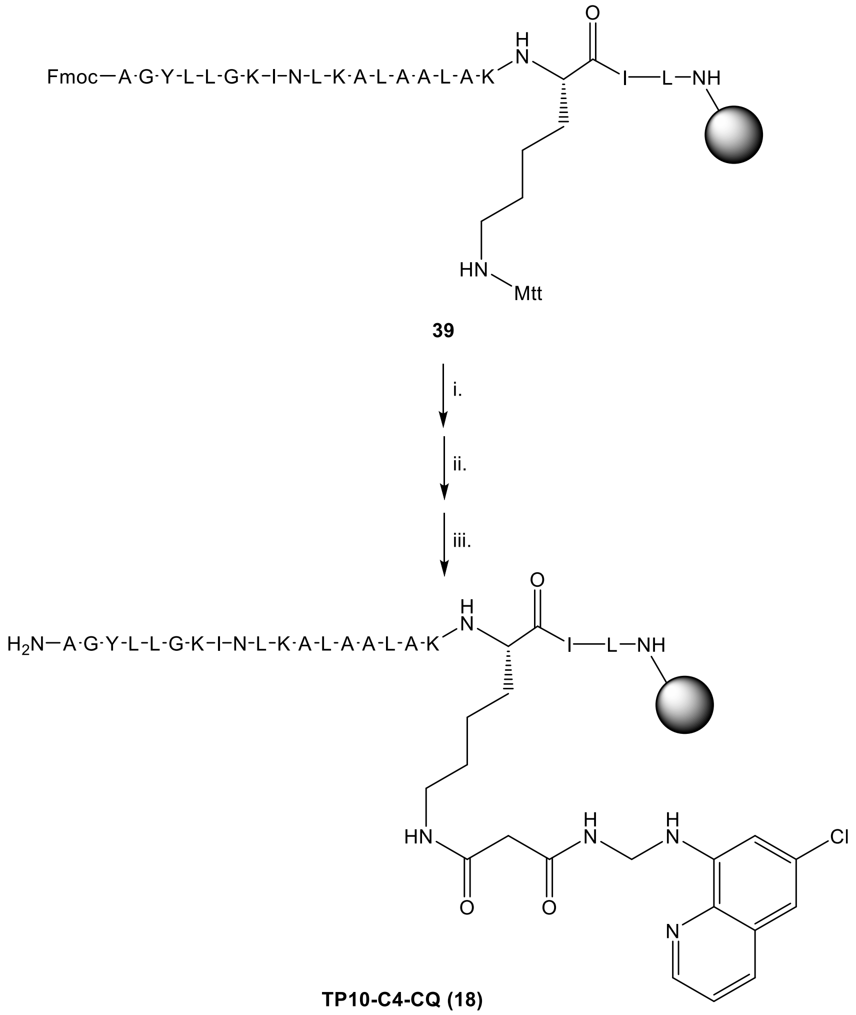
Fmoc—A·G·Y-L-L-G·K-I-N-L-K·A-L-A·A-L-A·K
H
N
O
I—L—NH
HN
Mtt
39
i.
ii.
iii.
H₂N—A·G·Y-L-L-G·K-I-N-L-K·A-L-A·A-L-A·K
HN
H
N
H
N
O
O
Cl
N
TP10-C4-CQ (18)

i. Mtt removal
ii. Coupling of CQn-C4
iii. Fmoc removal

Scheme 5.9 – Route devised for the synthesis of TP10-C4-CQn (**18**).

This conjugate was purified *via* preparative HPLC, as previously described (*cf.* Chapter 4), using a gradient elution of 30-50% ACN in water (0.05% TFA) for 60 minutes; this purification rendered the target conjugate **18** in 93% purity (Figure 5.14). ESI-IT MS analysis was carried out to confirm the achievement of the desired structure: the obtained spectrum (Figure 5.15) presents four main peaks, correspondent to the protonated peptide ([P+nH$^+$]; Table 5.5), whose exact mass is 2511.52 a.m.u..

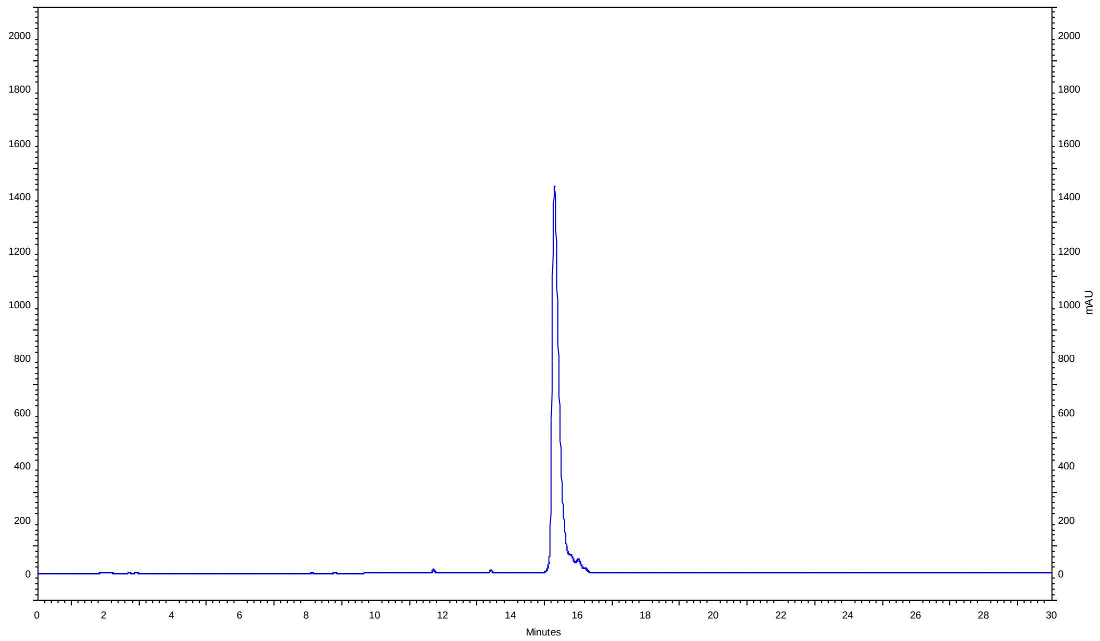

Figure 5.14 - Chromatogram obtained from the analysis of TP10-C4-CQn (**18**) after purification, with a gradient elution of 0-100% ACN in water (0.05% TFA) in a RP-18E (5 µm), for 30 minutes and a flow of 1 ml/min, with detection at λ = 220 nm.

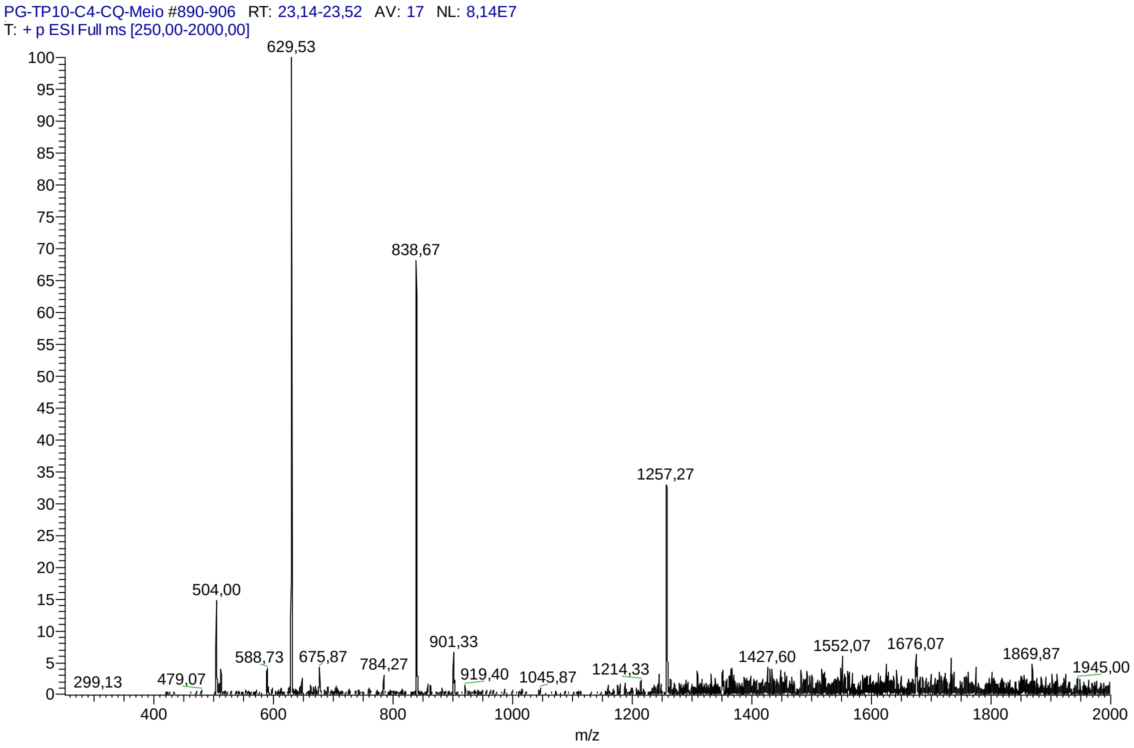

Figure 5.15 - Spectrum (ESI-IT MS, positive mode) obtained for crude TP10-C4-CQn (**18**).

Table 5.5 – Adducts of the peptide TP10-C4-CQn (P), detected by ESI-IT MS.

Adduct	Expected $^m/_z$	Detected $^m/_z$
P + 2H$^+$	1256.77	1257.27
P + 3H$^+$	838.18	838.67
P + 4H$^+$	628.89	629.53
P + 5H$^+$	503.31	504.00

5.2.5. TP10-S-S-CQn (19)

TP10-S-S-CQn was obtained *via* disulfide bond formation between the cleaved TP10-Cys (**40**) (peptide with an additional *C*-terminal Cys residue) and the “activated” CQn-Cys-TP (**41**), similarly to the synthesis described in **5.2.3** (Scheme 5.4). In this case, the thiol present in CQn-Cys (**34**) was activated by means of a reaction with dithiopyridine (**42**), prior to the formation of a disulfide bond with TP10-Cys (**40**), *via* a thiol-disulfide exchange (Scheme 5.10).

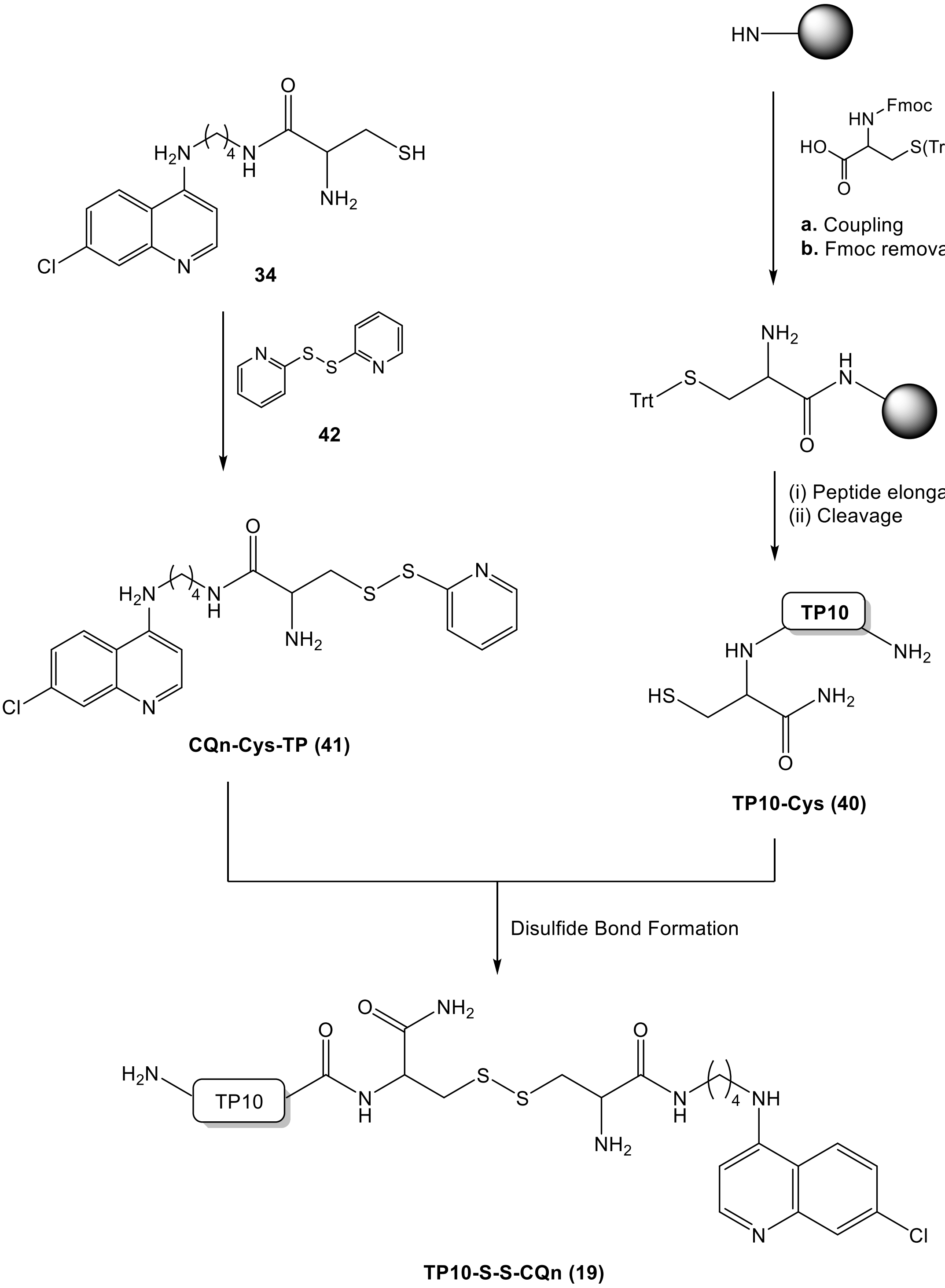
HN
HN
Fmoc
HO
S(Trt)
O
a. Coupling
b. Fmoc removal
34
42
NH2
H
N
Trt
S
O
(i) Peptide elongation
(ii) Cleavage
CQn-Cys-TP (41)
TP10
HN
NH2
HS
TP10-Cys (40)
Disulfide Bond Formation
H2N
TP10
TP10-S-S-CQn (19)

Scheme 5.10 – Synthetic route towards conjugate TP10-S-S-CQn (**19**).

5.2.5.1. Synthesis of CQn-Cys-TP (41)

CQn-Cys (**34**) was synthesized as above described (*cf.* **5.2.3.2**) and then reacted with 2,2'-dithiodipyridine (**42**) *via* a TDER (Scheme 5.11) in a solution of anhydrous methanol containing glacial acetic acid, to produce the activated intermediate CQn-Cys-TP (**41**). Isolation of **41** was carried out *via* liquid column chromatography, to render this compound as a chromatographically homogeneous (TLC) yellow oil in a good yield (60%). Its analysis by ESI-IT MS confirmed the achievement of the desired structure (Figure 5.16). The obtained spectrum reveals a main peak, correspondent to quasi-molecular ion (MH^+) of CQn-Cys-TP (**41**), whose exact mass is 461.11 a.m.u..

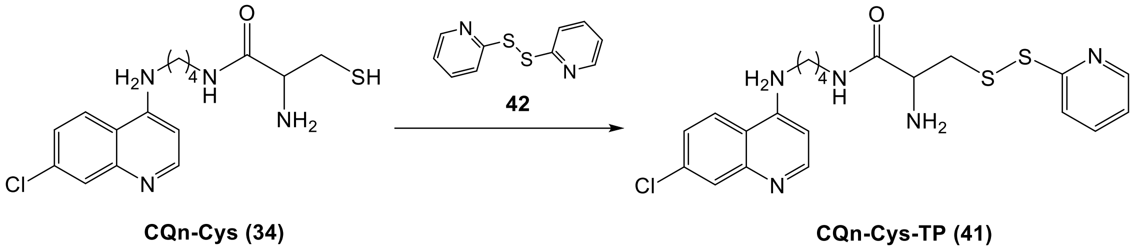

Scheme 5.11 – Activation of the thiol group present in CQn-Cys with 2,2'-dithiodipyridine.

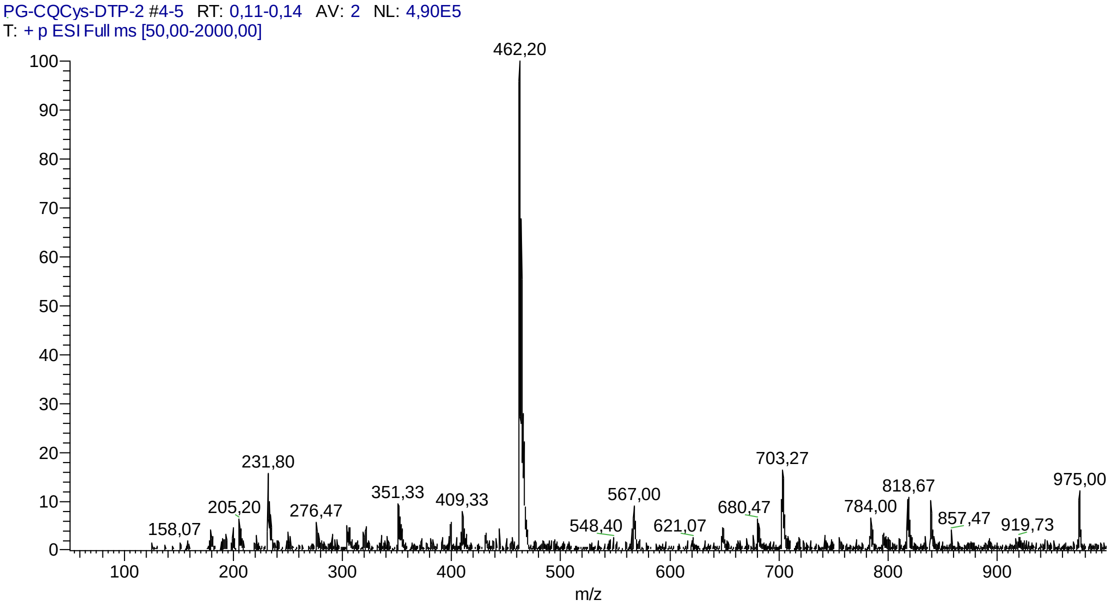

Figure 5.16 - Spectrum (ESI-IT MS, positive mode) obtained for CQn-Cys-TP (**41**).

5.2.5.2. Synthesis of TP10-Cys (40) and of target conjugate TP10-S-S-CQn (19)

TP10-Cys (**40**) was synthesized *via* standard SPPS procedures, cleaved by the usual acidolytic treatment with a TFA-based cocktail, and analyzed by HPLC - to determine its retention time, and LC-DAD/ESI-IT MS (Figure 5.17). The obtained spectrum depicts three main peaks, correspondent to different protonations of TP10-Cys (**40**) (Table 5.6), whose exact mass is 2283.42 a.m.u..

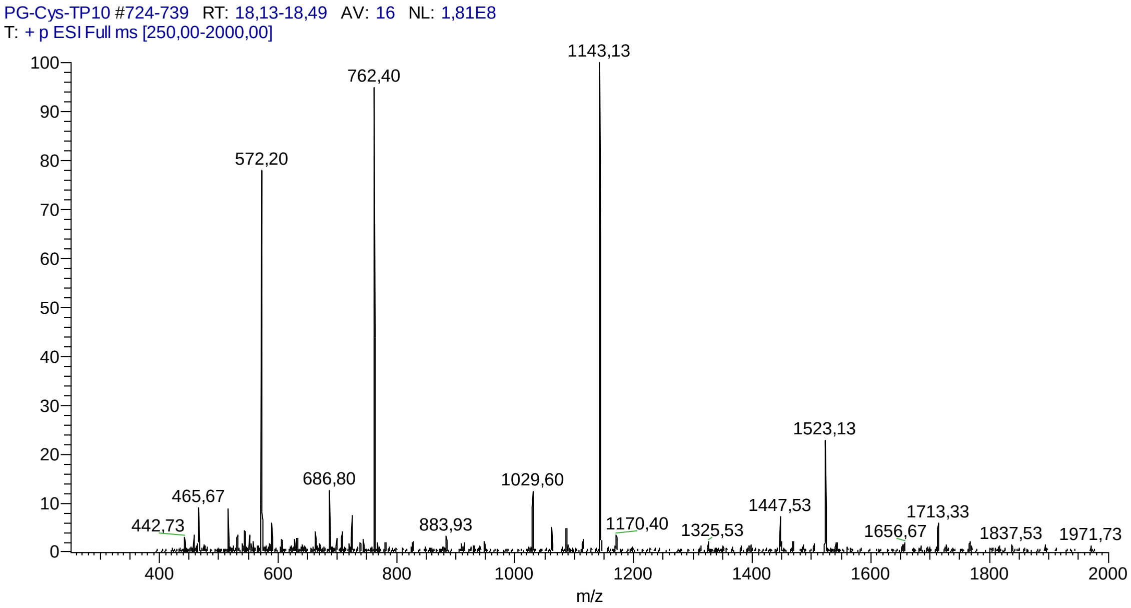

Figure 5.17 - Spectrum (ESI-IT MS, positive mode) obtained for TP10-Cys (**40**).

Table 5.6 – Adducts of the peptide TP10-Cys (P), detected by ESI-IT MS.

Adduct	**Expected $^{m}/_{z}$**	**Detected $^{m}/_{z}$**
P + 2H$^+$	1143.21	1143.13
P + 3H$^+$	762.78	762.40
P + 4H$^+$	572.11	572.20

Crude TP10-Cys (**40**) was then reacted with CQn-Cys-TP (**41**) *via* a TDER that occurred at room temperature for 48 hours, in a solution of acetic acid (1 *M*), to render TP10-S-S-CQn (**19**). Reaction was monitored by HPLC and, after 18 hours, when TP10-Cys was no longer detected, the mixture was directly submitted to purification by preparative HPLC. TP10-S-S-CQn (**19**) was obtained in 93% purity (Figure 5.18) and its structure confirmed by LC-DAD/ESI-IT MS. Figure 5.19 represents the obtained spectrum, which shows two main peaks, corresponding to the protonated peptide ([P+nH$^+$]; Table 5.7), whose exact mass is 2635.51 a.m.u..

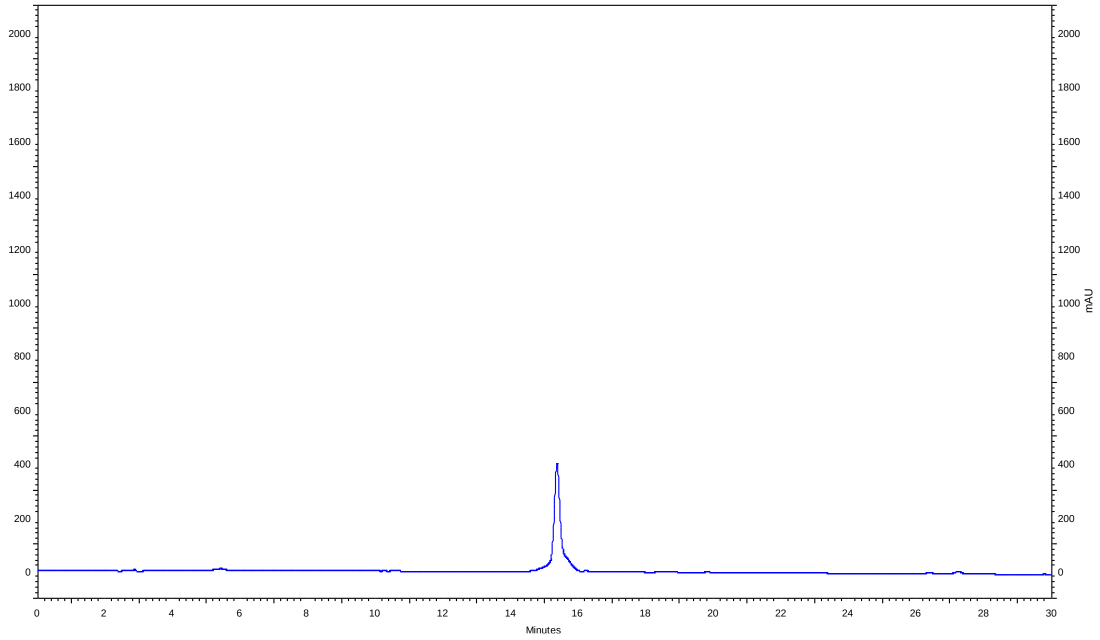

Figure 5.18 - Chromatogram obtained from the analysis of TP10-S-S-CQn (**19**) after purification, with a gradient elution of 0-100% ACN in water (0.05% TFA) in a RP-18E (5 µm), for 30 minutes and a flow of 1 ml/min, with detection at λ = 220 nm.

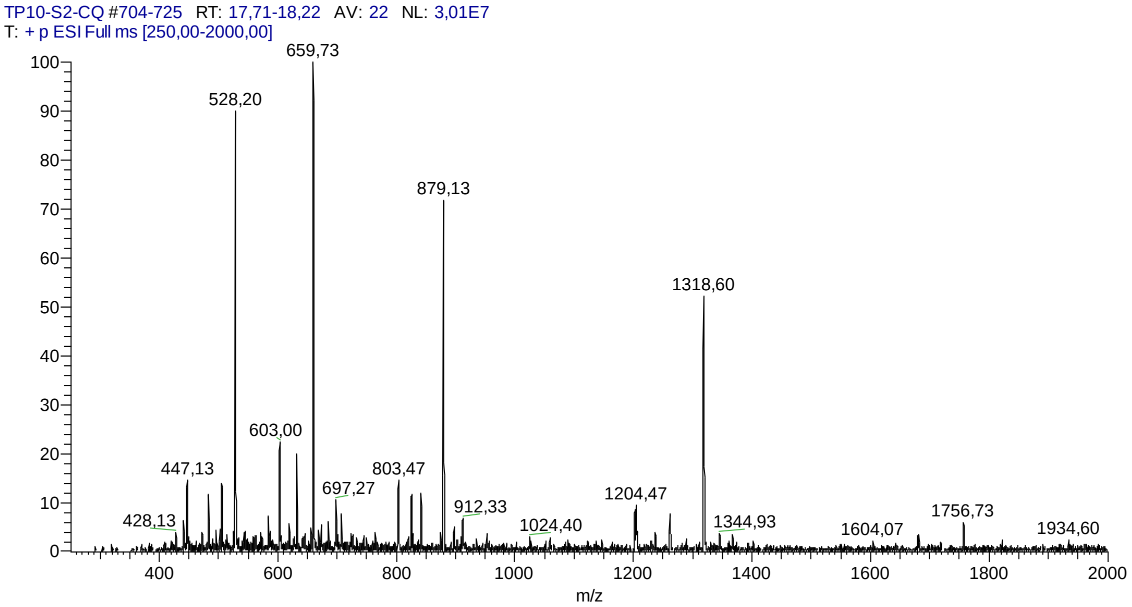

Figure 5.19 - Spectrum (ESI-IT MS, positive mode) obtained for TP10-S-S-CQn (**19**).

Table 5.7 – Adducts of the peptide TP10-S-S-CQn (P), detected by ESI-IT MS.

Adduct	Expected $^{m}/_{z}$	Detected $^{m}/_{z}$
P + 2H⁺	1318.26	1318.60
P + 3H⁺	879.17	879.13
P + 4H⁺	659.63	659.73
P + 5H⁺	527.91	528.20

5.3. *In vitro* assays

CQn-TP10 conjugates synthesized as described in 5.2 were evaluated *in vitro* against blood-stage forms of the CQ-sensitive 3D7 strain of *Pf*; the parent building blocks CQn and TP10, as well as the commercial chloroquine bisphosphate salt, were included in the assay, for comparison. Briefly, synchronized ring stage parasites were cultured with serially diluted test compounds for 48 h; after this period, parasitemia was estimated by whole-cell SYBR green I (SG)-based fluorescence assay[31]. IC_{50} values thus obtained are shown in Table 5.8.

While carrying out the growth inhibition assays, significant lysis of the erythrocytes was observed upon treatment with some conjugates, particularly at the higher concentrations tested. Hence, hemolysis assays were conducted using both hRBC and *P*iRBC cultures, to gain deeper insight into the hemolytic activity of the conjugates. These were incubated in cultures of either hRBC (3% hematocrit) or *P*iRBC (3% hematocrit with 1% parasitemia), at a final concentration of 10 µM, for 1 hour. Percentages of erythrocytes suffering lysis under these conditions are given in Table 5.8.

Table 5.8 - *In vitro* antiplasmodial (on blood stage *Pf* 3D7 parasites) and hemolytic (on both hRBC and *P*iRBC) activity of CQn-TP10 conjugates.

Compound	IC_{50} (nM)	% Hemolysis (at 10 µM)	
		hRBC	*P*iRBC
TP10	1930	3.7	3.4
CQn-C4-TP10	830	23	6.5
CQn-C10-TP10	817	38	19
CQn-S-S-TP10	1232	9	2
CQn-TR-TP10	1037	23	10
TP10-C4-CQn	[a]	50	41
TP10-S-S-CQn	2337	18	7.2
CQn	71	[c]	[c]
CQ-Diphosphate	21[b]	-	-

[a] a consistent IC_{50} value could not be determined; [b] taken from ref [32]; [c] no detectable hemolysis.

Noteworthy, in the screening of this second generation of CQn-CPP conjugates, we used a CQ-sensitive *Pf* strain, as comparison of the IC_{50} value now obtained for CQ-C4-TP10 with that previously determined for the same conjugate against the CQ-resistant W2 strain (*cf.* Chapter 4, Table 4.4) reflects how CQ-sensitivity affects activity of the conjugates. As such, it was possible to conclude that the conjugate's activity is clearly higher against the CQ-sensitive than the CQ-resistant strain, which overthrows the hypothesis that conjugation of CQn to a CPP might bypass resistance mechanisms in CQ-resistant *Pf*. Curiously, the intrinsic antiplasmodial activity of TP10 itself was also higher against the CQ-sensitive than against the CQ-resistant strain, which might suggest that both the antimalarial drug, the CPP and their conjugate share a common pathway to reach the parasite, and/or to be expelled from the site of action in resistant strains. In fact, on the one hand, it is widely known that CQ's basicity underpins its effective accumulation inside the parasite's acidic DV[33,34], and this basic character is also quite pronounced in the cationic CPP; on the other hand, it has been advocated that the *Pf*CRT involved in CQ expulsion from the FV in CQ-resistant strains is a polyspecific drug and nutrient exporter[35] eventually able to expel the CPP or the drug-CPP conjugate as well.

Regarding the effect of the linkage between peptide and drug on the *in vitro* antiplasmodial activity of conjugates where CQn is attached to the peptide's *N*-terminus, the first eye-catching observation is that stable (amide bonded) alkyl spacers provide the best outcome in terms of parasite growth inhibition; moreover, increasing the size of the alkyl chain does not greatly affect antiparasitic activity, although it does seem to potentiate hemolysis, eventually due to increased hidrophobicity. Replacing the alkyl by a triazole linker, equally stable, but more rigid and able to establish hydrogen bonds, was not beneficial for antiplasmodial action, and leads to an intermediate hemolytic activity as compared to the four- and the ten-carbon alkyl spacers. Finally, using the labile disulfide linker leads to the lowest activity. Notwithstanding, all these conjugates were more active than unconjugated TP10. In turn, comparison of CQn-S-S-TP10 with TP10-S-S-CQn conjugation of CQn to the *C*-terminus of TP10 significantly worsens antiplasmodial activity, as compared to both its *N*-terminus congener and with the unconjugated building blocks. This might be the result of a diminished penetration ability of TP10 when its *C*-terminus is blocked, although it has been suggested that anchoring the cargo the *C*-terminus of CPP is, in some cases, the best option[36–38]. Alternatively, conformational constraints posed by *C*-terminal immobilization of the drug might hinder its antimalarial action. Additionally, conjugates where the drug is linked to the peptide's *C*-terminus are more hemolytic than their respective *N*-terminally-linked congeners, which comes with dramatic consequences for TP10-C4-CQn, whose exacerbated hemolytic activity hampered the possibility to derive a consistent half-maximal growth inhibitory concentration for this conjugate.

Taken together, the above observations hint that the *in vitro* activity of the conjugates will hardly arise from intracellular release of the bioactive moiety, as it differs from those of both the unconjugated building blocks, and depends on specific spacer and peptide-drug relative orientation. Moreover, the fact that all conjugates are slightly to significantly more hemolytic than the unconjugated building blocks,[39] suggests that conjugation to the CPP potentiates disruption of erythrocyte membranes. Interestingly, as compared to the other conjugates, those where CQn was conjugated to TP10 *via* a disulfide bond were less hemolytic, eventually due to partial bioreductive cleavage of the linker, with concomitant release of the non-hemolytic building blocks.

Another interesting remark regarding hemolysis assays is the evidently higher hemolytic effect of the conjugates on hRBC than on *P*iRBC, which was intuitively unexpected, as parasitized erythrocytes would likely be more “damaged” than healthy ones. However, upon invasion by *Plasmodia* parasites, RBC undergo substantial changes, including in their membranes, to face the stress posed upon infection[40,41], which might explain our observations.

In face of the hypotheses raised in the course of the study reported in this chapter, further exploratory biophysical studies have been conducted to gain some insight into the ways the conjugates (i) interact with model membranes mimicking hRBC and *P*iRBC, as described in Chapter 6, and (ii) internalize healthy and parasitized erythrocytes, as reported in Chapter 7.

5.4. Experimental section

5.4.1. Materials, instrumentation and general methods

For the chemical synthesis, materials, instrumentation and general methods were previously described in Chapter 4 (*cf.* **4.4.1**).

5.4.2. Synthesis of CQn-C10-TP10 (32)

TP10 was synthesized *via* standard SPPS in accordance to the previously described in Chapter 4 (*cf* **4.4.4**), but its sequence further elongated upon coupling of an additional 6-aminohexanoyl (Ahx) residue at the peptide's *N*-terminus. To this end, Fmoc-Ahx-OH was coupled to the peptidyl-resin *via* HBTU-mediated *in situ* coupling, after which the standard procedure for Fmoc removal with 20% piperidine in DMF was employed. The resin was then properly washed and CQn-C4, previously prepared as described in Chapter 4 (cf. **4.4.2** and **4.4.3**), was pre-activated with PyBOP, in the presence of DIPEA, and coupled overnight to the peptide's terminal amine, as previously explained (*cf.* **4.4.5**). After convenient washing and drying of the peptidyl-resin, this was cleaved by a 2-hour acidolysis using 95% TFA, 2.5% TIS and 2.5% water, as described before in Chapter 4 (*cf.* **4.4.6**). The crude CQn-C10-TP10 was purified *via* preparative HPLC, using a gradient elution of 20-50% of ACN in water, in 1 hour. Final peptide, which was obtained with a purity of 94% and correct mass spectral data, was freeze-dried and stored at -20 ºC until further use.

Experimental data for CQn-C10-TP10 (**32**)

$^{m}/_{z}$ ($C_{127}H_{213}ClN_{30}O_{27}$, 2625.59 a.m.u.): 1313.80 ($[M+2H^{+}]^{2+}$); 876.21 ($[M+3H^{+}]^{3+}$); 657.41 ($[M+4H^{+}]^{4+}$); 526.13 ($[M+5H^{+}]^{5+}$).

Elution conditions: 0-100% ACN in water (0.05% TFA) in 30 minutes, at a flow rate of 1 mL/min.

R_t = 16.3 minutes

5.4.3. Synthesis of CQn-TR-TP10 (16)

6-azido hexanoic acid (1.2 eq) was activated with HBTU (1.2 eq), in the presence of DIPEA (2.4 eq), in DMF; the mixture was placed under stirring in an ice-water bath, for 30 minutes. Then, CQn (1.0 eq) was added, and the reaction was kept under stirring in the ice-water bath. Reaction progress was monitored by TLC and, after 3 hours, the mixture was diluted in ethyl acetate (20 mL) and washed with 5% aqueous Na_2CO_3 (3 × 15 mL). The organic layer was then dried with anhydrous Na_2SO_4 and, after filtration, ethyl acetate was evaporated under reduced pressure. The resulting mixture was then purified via liquid column chromatography using silica gel as stationary phase and DCM/MeOH (5:1 v/v) as eluent. ESI-IT MS analysis of the isolated compound resulted compatible with the structure of CQn-N_3, as shown below.

Experimental data for CQn-N_3 (**40**)

R_f (DCM/MeOH 5:1 (v/v)): 0.43

$^m/_z$ ($C_{19}H_{26}ClN_6O$; 389.19 a.m.u.): 389.73 ($[M+H^+]^+$)

TP10 was assembled by SPPS as before, and its sequence further elongated by coupling Fmoc-protected propargylglycine (Fmoc-Pra-OH) to the peptide's *N*-terminus, using the standard *in situ* coupling procedure. After removal of Fmoc using the usual piperidine-based method and proper resin washing, the peptidyl-resin was reacted with CQn-N_3 (**40***,* 1.2 eq) in the presence of copper(I) bromide (1.2 eq), 2,6-lutidine (10 eq), sodium ascorbate (3 eq), and DIPEA (10 eq), solubilized in a mixture of ACN and DMF (1:2 v/v)[17]. The reaction medium was stirred overnight at room temperature, after which the resin was thoroughly washed with DCM (3×), MeOH (3×), ACN (3×) and DMF (3×). A 2-hours acidolysis using 95% TFA, 2.5% TIS and 2.5% water, carried out as described before, delivered the crude peptide that was purified *via* preparative HPLC, using a gradient elution of 35-45% of ACN in water, in 1 hour. Final peptide, which was obtained with a purity of 94% and correct mass spectral data, was freeze-dried and stored at -20 ^oC until further use.

Experimental data for CQn-TR-TP10 (**16**)

$^{m}/_{z}$ ($C_{128}H_{214}ClN_{33}O_{26}$, 2664.61 a.m.u.): 1333.53 ($[M+2H^{+}]^{2+}$); 889.40 ($[M+3H^{+}]^{3+}$); 667.33 ($[M+4H^{+}]^{4+}$); 534.13 ($[M+5H^{+}]^{5+}$).

Elution conditions: 0-100% ACN in water (0.05% TFA) in 30 minutes, at a flow rate of 1 mL/min.

R_t = 14.9 minutes

5.4.4. Synthesis of CQn-S-S-TP10 (17)

Boc-Cys(Trt)-OH (**33**, 1.2 eq) was activated with HBTU (1.2 eq) in the presence of DIPEA (2.4 eq). These reactants were dissolved in DMF, and the mixture was put in an ice-water bath, for 30 minutes. After this time, CQn (1.0 eq) was added to the reaction, which was left in the ice-water bath for 3 more hours. After this time the mixture was diluted in ethyl acetate (20 mL) and extracted with an aqueous solution of 5% Na_2CO_3 (15 mL, x3). The organic phase was then dried with anhydrous Na_2SO_4 and, after filtration, ethyl acetate was evaporated under reduced pressure. The resulting mixture was then purified via silica gel column chromatography, using DCM/MeOH (20:1) as eluent, to obtain CQn-Boc-Cys(Trt) (**37**) in high purity. Isolated CQn-Boc-Cys(Trt) was characterized by ESI-IT MS; the obtained spectrum was compatible with the structure of **37**, as shown below.

Experimental data for CQn-Boc-Cys(Trt) (**37**)

R_f (DCM/MeOH 20:1 (v/v)): 0.45

$^{m}/_{z}$ ($C_{40}H_{43}ClN_4O_3S$; 694.27 a.m.u.): 695.53 ($[M+H^{+}]^{+}$).

Removal of cysteine's protecting groups (Boc and Trt) was carried out *via* acidolysis with a mixture of TFA (95%), TIS (2.5%) and H_2O (2.5%). For this, CQn-Boc-Cys(Trt) (**37**) was dissolved in the previously described acidolytic mixture and the reaction was placed in an ice-water bath. After 1 hour, the reaction mixture was distributed by 15 mL Falcons (1 mL/tube) and the volume of each tube was completed with cold TBME, to precipitate CQn-Cys (**34**). The tubes were then centrifuged and the addition of dried diethyl ether followed by centrifuging was repeated three more times, after which the tubes were placed in a desiccator. The supernatant solution was discarded and characterization of CQn-Cys (**34**) was carried out by ESI-IT MS, which confirmed the achievement of the desired structure.

Experimental data for CQn-Cys (**34**)

R_f (DCM/MeOH 20:1 (v/v)): 0.09

$^m/_z$ ($C_{16}H_{21}ClN_4OS$; 352.11 a.m.u.): 353.47 ($[M+H^+]^+$).

TP10 was assembled by SPPS as described in **4.4.4**, and Boc-Cys(NPys)-OH (**35**, 5.0 eq) was coupled to TP10's *N*-terminal (1.0 eq), using HBTU (5.0 eq) and DIPEA (10 eq) for the activation of the protected aa; the peptidyl-resin was then cleaved by a 2-hours acidolysis using 95% TFA, 2.5% TIS and 2.5% water (*cf* **4.4.6**), to render free Cys(NPys)-TP10 (**36**).

Experimental data for Cys(NPys)-TP10 (**36**)

$^m/_z$ ($C_{112}H_{191}N_{29}O_{27}S_2$, 2438.39 a.m.u.): 1220.00 ($[M+2H^+]^{2+}$); 813.87 ($[M+3H^+]^{3+}$); 610.73 ($[M+4H^+]^{4+}$).

Elution conditions: 0-100% ACN in water (0.05% TFA) in 30 minutes, at a flow rate of 1 mL/min.

R_t = 16.0 minutes

Thiol-disulfide exchange between Cys(NPys)-TP10 (**36**, 1.0 eq) and CQn-Cys (**34**, 1.2 eq) was carried out in an aqueous solution of acetic acid (1 *M*), for 36 hours, at room temperature. This reaction was monitored by HPLC, using a gradient elution of 0-100% ACN in water (0.05% TFA) for 30 minutes, and by LC-DAD/ESI-IT MS. After this time, CQn-S-S-TP10 (**17**) was purified by preparative HPLC, with a gradient elution of 30-45% ACN in water (0.05% TFA) for 1 hour. Fractions of pure conjugate were freeze-dried and stored at -20 ºC until further use.

Experimental data for CQn-S-S-TP10 (**17**)

$^{m}/_{z}$ ($C_{107}H_{188}N_{27}O_{25}S$, 2634.51 a.m.u.): 1318.80 ($[M+2H^{+}]^{2+}$); 880.00 ($[M+3H^{+}]^{3+}$); 528.73 ($[M+4H^{+}]^{4+}$).

Elution conditions: 0-100% ACN in water (0.05% TFA) in 30 minutes, at a flow rate of 1 mL/min.

R_t = 15.8 minutes

5.4.5. Synthesis of TP10-C4-CQn (18)

TP10 (AGYLLGKINLKALAALAKKIL) was assembled by SPPS as previously described and Fmoc-Lys(Mtt)-OH (represented in blue, in the aa sequence) was coupled to isoleucine's α-amino group using standard coupling conditions. After this coupling and following Fmoc removal, the aa sequence was elongated through repetitive coupling/deprotection cycles. After complete coupling of the last aa, Fmoc-Ala-OH, and prior to its deprotection, Lysine's side chain PG (Mtt) was selectively removed with a solution of 1% TFA in DCM. Mtt removal leads to the formation of a yellow solution; thus, the addition of 1% TFA in DCM was repeated until this phenomenon was no longer observable.

After Mtt removal, CQn-C4 (*cf* **4.4.2** and **4.4.3**) was coupled to the generated free α-amine group of the *C*-terminal Lys, after activation with PyBOP (5.0 eq) and DIPEA (10 eq), in DMF. This reaction was kept overnight, after which the resin was filtered and washed with DCM (3x) and DMF (3x).

Crude TP10-C4-CQn was obtained upon cleavage of the peptidyl resin with a solution of TFA (95%), TIS (2.5%) and water (2.5%), as previously described (*cf* **4.4.6**), and was analyzed by LC/MS/DAD and purified by preparative HPLC, using a gradient elution of 20-50% ACN in water (0.05% TFA), in 1 hour. Fractions of pure conjugate were freeze-dried and stored at -20 ºC until further use.

Experimental data for TP10-C4-CQn (**18**)

$^{m}/_{z}$ ($C_{121}H_{203}ClN_{30}O_{25}$, 2511.52 a.m.u.): 1257.27 ($[M+2H^{+}]^{2+}$); 838.67 ($[M+3H^{+}]^{3+}$); 629.53 ($[M+4H^{+}]^{4+}$); 504.00 ($[M+5H^{+}]^{5+}$).

Elution conditions: 0-100% ACN in water (0.05% TFA) in 30 minutes, at a flow rate of 1 mL/min.

R_t = 15.5 minutes

5.4.6. Synthesis of TP10-S-S-CQn (19)

Synthesis of TP10-Cys (**40**, AGYLLGKINLKALAALAKKILC) was carried out *via* SPPS, as previously described and cleaved *via* acidolysis (*cf* **4.4.6**).

Experimental data for TP10-Cys (**40**)

$^{m}/_{z}$ ($C_{107}H_{189}N_{27}O_{25}S$, 2284.41 a.m.u.): 1143.13 ($[M+2H^{+}]^{2+}$); 762.40 ($[M+3H^{+}]^{3+}$); 572.20 ($[M+4H^{+}]^{4+}$).

Elution conditions: 0-100% ACN in water (0.05% TFA) in 30 minutes, at a flow rate of 1 mL/min.

R_t = 15.5 minutes

CQn-Cys (**34**) was synthesized in accordance to previously described procedures (*cf* **5.4.4**). For thiol activation, CQn-Cys (1.0 eq) and 2,2'-dithiodipyridine (**42**, 2.0 eq) were dissolved in anhydrous methanol (4 mL) containing glacial acetic acid (0.3 eq). The mixture was stirred at room temperature for 18 h and the solvent was removed under reduced pressure to obtain the crude product. The crude product was purified by flash chromatography using at first a mixture of DCM/MeOH (10:1) and then, after removal of thiopyridine, a more polar mixture of DCM/MeOH (1:1), to render CQn-Cys-TP (**41**) in high purity.

Experimental data for CQn-Cys-TP (**41**)

R_f (DCM/MeOH 10:1 (v/v)): 0.35

$^m/_z$ ($C_{16}H_{21}ClN_4OS$; 461.11 a.m.u.): 462.20 ($[M+H^+]^+$).

Thiol-disulfide exchange between TP10-Cys (**40**, 1.0 eq) and "activated" CQn-Cys-TP (**41**, 1.2 eq) was carried out in a solution of acetic acid (1 *M*), for 48 hours, at room temperature. This reaction was monitored by HPLC, with a gradient elution of 1-100% ACN in water (0.05% TFA), and by LC-DAD/ESI-IT MS. TP10-S-S-CQn (**19**) was finally purified by preparative HPLC, with the elution of 30-40% of ACN in water (0.05% TFA) for 1 hour. Fractions of pure conjugate were freeze-dried and stored at -20 °C until further use.

Experimental data for TP10-S-S-CQn (**19**)

$^m/_z$ ($C_{107}H_{188}N_{27}O_{25}S$, 2634.51 a.m.u.): 1318.60 ($[M+2H^+]^{2+}$); 879.13 ($[M+3H^+]^{3+}$); 659.73 ($[M+4H^+]^{4+}$); 528.20 ($[M+5H^+]^{5+}$).

Elution conditions: 0-100% ACN in water (0.05% TFA) in 30 minutes, at a flow rate of 1 mL/min.

R_t = 15.4 minutes

5.4.7. Growth Inhibition Assays

Pf 3D7 (chloroquine sensitive strain) was cultured in human 0+ erythrocytes by standard procedures under a low oxygen atmosphere (5% CO_2), in a culture medium containing 0.5% AlbuMAX I (Invitrogen) and 5 g/mL hypoxanthine. Hematocrit (% of RBC in the culture medium) was maintained at 3%, while parasitemia (% of *P*iRBC in RBC population) was kept below 5%, by dilution (when required) with washed hRBC[42–44]. Prior to the assays, cultures were synchronized in ring-stage by double sorbitol treatment[45].

To determine the IC_{50} of the test compounds, *P*iRBC (3% hematocrit, 1% parasitemia) were incubated in a micro titre plate for 48 hours in the presence of two-fold serial dilutions of TP10 and its derivatives (10000 - 10 nM) and three-fold serial dilutions of CQ (commercial bisphosphate) and synthetic CQn (8000 - 0.1 nM). For control, culture without test compounds was also added to the microtitre plate. After incubation (48h), 100 µL of a solution of SG (0.001% v/v in PBS) was added to each well and plates incubated for another 60 minutes under standard culture conditions. Plates were then centrifuged at 2500 rpm for 2 min, supernatant was discarded, and cells re-suspended in 100 µL of PBS. Fluorescence was collected in a fluorimeter plate reader with excitation 485 nm and emission 535 nm[31].

Fluorescence values were normalized (to take into account the normal growth of the parasite) and then plotted against log (C). IC_{50} were determined using a GraphPad Prism 6.

5.4.8. Hemolysis assays

*P*iRBC and hRBC were plated in a in micro titre plates and cultured for 1 hour in the presence of four-fold serial dilutions of CQn, TP10 and their conjugates (10000 – 40 nM). For positive and negative controls, 1% triton X-100 and PBS were added, respectively. After this period, plates were centrifuged and supernatants transferred to another plate. Supernatant absorbance at 450 nm was assessed in a plate reader and values were treated using the following equation:

$$\% \text{ Hemolysis} = \frac{\text{Abs (compound) - Abs } (C^-)}{\text{Abs } (C^+) \text{ - Abs } (C^-)}$$

5.5. Bibliography

1. J. Kumai, K. Hozumi, Y. Yamada, F. Katagiri, Y. Kikkawa and M. Nomizu, *Biopolymers*, 2016, **106**, 512–520.
2. L. Mbatha, S. Chakravorty, C. B. de Koning, W. A. L. van Otterlo, P. Arbuthnot, M. Ariatti and M. Singh, *Curr. Drug Deliv.*, 2016, **13**, 935–945.
3. Y. Wang, A. G. Cheetham, G. Angacian, H. Su, L. Xie and H. Cui, *Adv. Drug Deliv. Rev.*, 2017, **110–111**, 112–126.
4. A. Ashkenazi and Y. Shai, *Biophys. Struct. Mech.*, 2011, **40**, 349–357.
5. N. Yadav, D. Agarwal, S. Kumar, A. K. Dixit, R. D. Gupta and S. K. Awasthi, *Eur. J. Med. Chem.*, 2018, **145**, 735–745.
6. P. Singh, S. Sachdeva, R. Raj, V. Kumar, M. P. Mahajan, S. Nasser, L. Vivas, J. Gut, P. J. Rosenthal, T.-S. Feng and K. Chibale, *Bioorg. Med. Chem. Lett.*, 2011, **21**, 4561–4563.
7. N. Boechat, M. D. L. G. Ferreira, L. C. S. Pinheiro, A. M. L. Jesus, M. M. M. Leite, C. C. S. Júnior, A. C. C. Aguiar, I. M. De Andrade and A. U. Krettli, *Chem. Biol. Drug Des.*, 2014, **84**, 325–332.
8. S. A. Bakunov, S. M. Bakunova, T. Wenzler, M. Ghebru, K. A. Werbovetz, R. Brun and R. R. Tidwell, *J. Med. Chem.*, 2010, **53**, 254–272.
9. N. Ma, Y. Wang, B. X. Zhao, W. C. Ye and S. Jiang, *Drug Des. Devel. Ther.*, 2015, **9**, 1585–1599.
10. H. C. Kolb and K. B. Sharpless, *Drug Discov. Today*, 2003, **8**, 1128–1137.
11. G. C. Tron, T. Pirali, R. A. Billington, P. L. Canonico, G. Sorba and A. A. Genazzani, *Med. Res. Rev.*, 2008, **28**, 278–308.
12. D. Dheer, V. Singh and R. Shankar, *Bioorg. Chem.*, 2017, **71**, 30–54.
13. R. Huisgen, *Angew. Chemie - Int. Ed.*, 1963, **2**, 535–632.
14. V. V. Rostovtsev, L. G. Green, V. V. Fokin and K. B. Sharpless, *Angew. Chemie - Int. Ed.*, 2002, **41**, 2596–2599.
15. C. W. Tornøe, S. J. Sanderson, J. C. Mottram, G. H. Coombs and M. Meldal, *J. Comb. Chem.*, 2004, **6**, 312–324.

16. M. S. Singh, S. Chowdhury and S. Koley, *Tetrahedron*, 2016, **72**, 5257–5282.
17. R. A. Turner, A. G. Oliver and R. S. Lokey, *Org. Lett.*, 2007, **9**, 5011–5014.
18. E. Jortzik and K. Becker, *Int. J. Med. Microbiol.*, 2012, **302**, 187–194.
19. K. Luersen, R. D. Walter and S. Muller, *Biochem. J*, 2000, **346**, 545–552.
20. M. Goyal, A. Alam and U. Bandyopadhyay, *Curr. Med. Chem.*, 2012, **19**, 1475–1503.
21. S. Kehr, N. Sturm, S. Rahlfs, J. M. Przyborski and K. Becker, *PLoS Pathog.*, 2010, **6**, e1001242.
22. P. Nagy, *Antioxid. Redox Signal.*, 2013, **18**, 1623–1641.
23. T. M. Postma and F. Albericio, *European J. Org. Chem.*, 2014, **2014**, 3519–3530.
24. T. Bechtel and E. Weerapana, *Proteomics*, 2017, **17**, 1600391.
25. S. Meierjohann, R. D. Walter and S. Müller, *Biochem. J.*, 2002, **368**, 761–768.
26. F. Meng, W. E. Hennink and Z. Zhong, *Biomaterials*, 2009, **30**, 2180–2198.
27. G. M. Whitesides and R. Singh, in *The chemistry of sulphur-containing functional groups*, eds. S. Patai and Z. Rappoport, John Wiley & Sons Ltd, 1993, pp. 633–658.
28. R. Matsueda and R. Walter, *Int. J. Pept. Protein Res.*, 1980, **16**, 392–401.
29. F. Albericio, D. Andreu, E. Giralt, C. Navalpotro, E. Pedroso, B. Ponsati and M. Ruiz-Gayo, *Int. J. Pept. Protein Res.*, 1989, **34**, 124–128.
30. J. W. Drijfhout, E. W. Perdijk, W. J. Weijer and W. Bloemhoff, *Int. J. Pept. Protein Res.*, 1988, **32**, 161–166.
31. F. Nogueira, M. Machado, F. Murtinheira and E. Lobo, *Ann Clin Med Microbio*, 2016, **2**, 5–8.
32. A. Gomes, M. Machado, L. Lobo, F. Nogueira, M. Prudêncio, C. Teixeira and P. Gomes, *ChemMedChem*, 2015, **10**, 1344–1349.
33. A. F. G. Slater, *Pharmacol. Ther.*, 1993, **57**, 203–2355.
34. R. Thomé, S. C. P. Lopes, F. T. M. Costa and L. Verinaud, *Immunol. Lett.*, 2013, **153**, 50–57.

35. N. Juge, S. Moriyama, T. Miyaji, M. Kawakami, H. Iwai and T. Fukui, *Proc. Natl. Acad. Sci.*, 2015, **112**, 3356–3361.

36. H. D. Herce and A. E. Garcia, *Proc. Natl. Acad. Sci. United State Am.*, 2007, **104**, 20805–20810.

37. P. Zhang, A. G. Cheetham, L. L. Lock and H. Cui, *Bioconjug. Chem.*, 2013, **24**, 604–613.

38. A. D. Frankel and C. O. Pabo, *Cell*, 1988, **55**, 1189–1193.

39. G. Guidotti, L. Brambilla and D. Rossi, *Trends Pharmacol. Sci.*, 2017, **38**, 406–424.

40. L. Tilley, M. W. A. Dixon and K. Kirk, *Int. J. Biochem. Cell Biol.*, 2011, **43**, 839–842.

41. B. M. Cooke, N. Mohandas and R. L. Cooper, *Adv. Parasitol.*, 2001, **50**, 1–86.

42. W. Trager and J. B. Jensen, 1976, **193**, 673–675.

43. A. Radfar, D. Méndez, C. Moneriz, M. Linares, P. Marín-García, A. Puyet, A. Diez and J. M. Bautista, *Nat. Protoc.*, 2009, **4**, 1899–1915.

44. F. Nogueira, A. Diez, A. Radfar, S. Pérez-Benavente, V. E. d. Rosario, A. Puyet and J. M. Bautista, *Acta Trop.*, 2010, **114**, 109–115.

45. C. Lambros and J. P. Vanderberg, *J. Parasitol.*, 1979, **65**, 418–420.

6

Study of the interactions between CQn-TP10 conjugates and lipid model membranes

6.1. Overview

Following the results from the *in vitro* assays reported in the previous chapter, several questions emerged: are CQn-TP10 conjugates able to efficiently permeate *P*iRBC? Do they permeate hRBC? How different are their interactions with hRBC *versus* *P*iRBC membranes? In order to shed some light on these questions, we carried out a study focused on the interactions of CQn-TP10 conjugates - as well as their parent building blocks, with lipid model membranes (liposomes), simulating both healthy and parasitized RBC. To this end, a toolbox of biophysical techniques, encompassing dynamic light scattering (DLS), UV-Vis derivative spectrophotometry, and surface plasmon resonance (SPR) was used, to provide an integrated view of biophysical modifications on model membranes, when exposed to the test compounds. A short introduction is provided in regard to on how lipid domains in *P*iRBC differ from those in hRBC, how such differences can be mimicked by model membranes, and how the aforementioned biophysical techniques can be used to study conjugate-membrane interactions (**6.2**), prior to discussion of results obtained (**6.3**).

6.2. Concise presentation of relevant phenomena and techniques

6.2.1. Modifications on the lipid domain of host RBC's upon *Plasmodium* invasion

After the erythrocyte invasion step, the parasite is isolated from the erythrocyte cytoplasm by the parasitophorous vacuole (PV) membrane and undergoes a sequential development through ring forms, trophozoites, schizonts, and finally differentiation into 10-20 merozoites[1].

Erythrocyte remodeling begins immediately after invasion by the *Plasmodium* parasite, by expression and exportation of many hundreds of proteins in order to assemble a molecular machinery in the host cell, which allows for protein trafficking, harvesting of nutrients and mechanisms to evade host immune responses[2,3]. This implies distinct morphological and biochemical changes in the host cell membrane[4]. These modifications include a marked increase in the fluidity of the erythrocyte membrane[5], whose lipid fatty acid composition is altered[6], as well as increased permeability through new membrane pores[3,7–9]. Other significant alterations include phospholipid composition and transbilayer distribution[4,8].

Erythrocytes infected with late-stage schizonts contain up to five times more phospholipids that uninfected erythrocytes[1,10]. The lipid domain of hRBC is composed of nearly equal parts of lipid and protein, with the majority of lipids consisting of cholesterol and phospholipids. While cholesterol is equally distributed between the two halves or leaflets of the lipid bilayer, the other lipids are asymmetrically distributed: whereas glycolipids, phosphatidylcholine (PC), and sphingomyelin (SM) are located in the outer leaflet, phosphatidylinositol (PI), phosphatidylethanolamine (PE), and phosphatidylserine (PS) occur in the inner leaflet, facing the cytoplasm[11]. The development of *Plasmodium* inside RBC results in a partial loss of the normal asymmetry of the membrane's phospholipids, with increased amounts of PE and PS and a decreased amount of PC in the exoplasmic (outer) leaflet of infected cells. These alterations are gradual and depend upon the stage of parasite development: cells infected with early stages show a partial redistribution of PE and PC but not PS, while cells infected with late stages present an additional redistribution of PS[4,8,12,13]. Additionally, parasite growth is accompanied by a depletion in SM content (~ 47%) and cholesterol/phospholipid ratio (~ 55%), accompanied by the aforementioned increase in membrane fluidity[5].

6.2.2. Membrane model systems

Cell membranes function as active barriers, isolating the interior of a cell from its surroundings[14]. Moreover, they play an important role on cell-to-cell communication, between-cell and within-cell control of micro-environments, and metabolism[15]. These membranes consist in a self-assembled, intricate mixture of lipids, proteins and other macromolecules (e.g. sugars), unique for each cell type and tissue[16,17].

There is a wide variety of lipids in biological membranes, which can be divided into sterols (e.g. cholesterol), sphingolipids and phospholipids, the latter occupying a major proportion in cell membranes[14]. Phospholipids, by having a polar head group and a non-polar region (hydrophobic alkyl chains), are amphiphilic molecules able to self-assemble into bilayer sheets with a thickness of approximately 5 nm: whereas the hydrophobic tails are densely packed and therefore shielded from the aqueous environment, the hydrophilic parts interact with the aqueous environment. Thus, the bilayer acts as an efficient barrier for water-soluble compounds, such as amino acids, nucleic acids, carbohydrates, proteins and ions, preventing their uncontrolled entrance and exit from the cell, which is kept under control by specific transporters[17].

The structural intricacy of cell membranes and their highly dynamic nature regarding lipid-lipid and lipid-protein interactions make biophysical interactions with drugs and drug delivery systems very difficult to investigate[18]. Therefore, simplified artificial membrane systems, which mimic the natural bilayer lipid membrane, have been developed. This implies a substantial simplification on the structure of biological membranes to be mimicked: for example, the lipid asymmetry found in native biological membranes is difficult to reproduce and proteins are difficult to incorporate in these models. Although this may seem a disadvantage, it actually allows for the study of an individual component and its isolated role on the behavior of the original membrane[19]. Moreover, these models allow for experiments under conditions which might not be supported by cells.

There are several model systems available to carry out biophysical experiments[19]. Plasma membrane vesicles, derived from blebs of native cellular membranes[20], have been advocated as to better mimic the lipid composition of the parent cell, while also containing membrane proteins which diffuse into the detached area during bleb formation[19]. However, the most common membrane model systems are lipid vesicles (or liposomes), supported lipid bilayers and monolayers[20]. These artificial membrane models allow for the manipulation of lipid content, pH and temperature, in order to mimic the composition, curvature, electrostatic potential or permeability properties of the biological membranes[21]. Liposomes are the most popular for studying membrane phase behavior and membrane processes such as fusion, molecular recognition, cell adhesion and membrane trafficking[22]. Based on their size and number of bilayers, liposomes can be classified into multilamellar vesicles (MLV; where several concentric phospholipid bilayers generate an onion-like structure), ranging from 0.5-10 µM and unilamellar vesicles, which can be obtained from multilamellar vesicles[22,23] (Figure 6.1). Unilamellar vesicles may be divided into large (> 0.1 µm) or small (≤ 0.1 µm) unilamellar vesicles (LUV and SUV, respectively)[24].

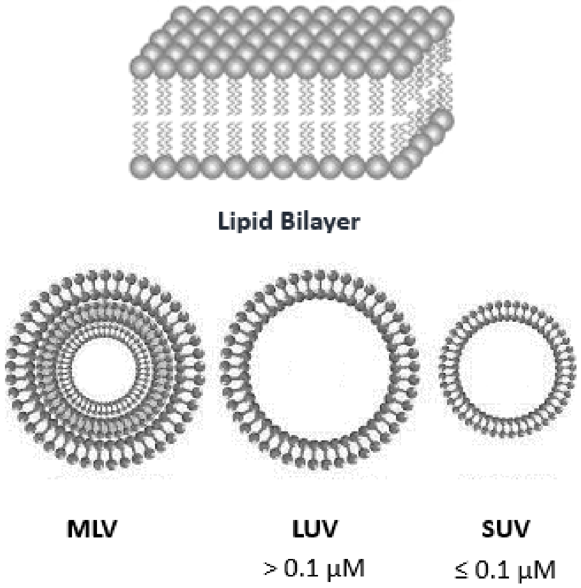

Figure 6.1 – Schematic representation of different types of lipid vesicles (liposomes).

6.2.3. Dynamic light scattering in the study of drug-liposome interactions

The average size and polydispersity (size distribution) of liposomes are important parameters for liposome characterization[25], as they are indicative of liposomes' stability, as such may provide a qualitative assessment of the interactions between a test compound (e.g., a drug, or drug conjugate) and model membranes.

DLS is the gold standard technique for determination of size and polydispersity of liposomes, derived from time-dependent fluctuations of light scattered from particles experiencing Brownian motion, which results from collisions between suspended particles and solvent molecules[26]. Another relevant parameter that can be derived by DLS is the main phase transition temperature (T_m), which is the temperature at which the lipid vesicle undergoes the transition between the gel and fluid phases (Figure 6.2)[22]. Indeed, temperature has an important effect on the structure of liposomes membranes: below their specific T_m, the individual phospholipids are closely packed and form a rigid ordered gel phase; as the temperature approaches the $\mathrm{T_m}$, this tight packing starts to loosen up, resulting in more empty space between the phospholipids. The structure of the membrane becomes looser until a final disordered fluid crystalline phase is established[27]. Interaction of molecules (e.g., drugs, peptides, or their conjugates) with membrane phospholipids may change membrane fluidity and cooperativity, which affects T_m. Overall, use of DLS to quantitate the aforementioned parameters (liposome size, polydispersity, T_m) may provide valuable informations about the nature of such interactions.

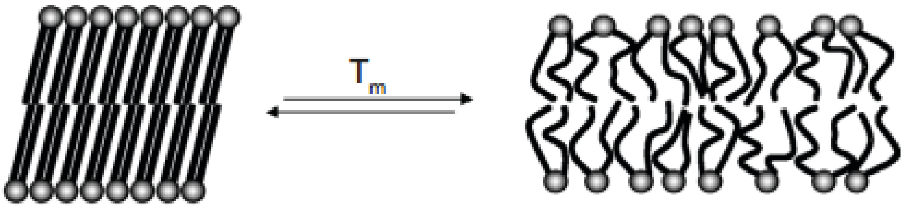

Gel, solid-ordered phase

Fluid, liquid-disordered phase

Figure 6.2 – Gel (below T_m) and fluid (above T_m) phases of lipid bilayers. Adapted from [22].

T_m and cooperativity (*i.e.* the number of lipophilic chains that change simultaneously) are biophysical parameters which may be determined by exploiting the count rate (average number of photons detected per second) in DLS, as changes in the measured scattering intensity reflect alterations in the optical properties of the material due to temperature variations (transition from gel to fluid phase)[28]. Data as the normalized mean count rate versus temperature are collected and fitted using Equation 1, [29]

$$r_s = r_{s1} + p_1 T + \frac{r_{s2} - r_{s1} + p_2 T - p_1 T}{1 + 10^{B\left(\frac{1}{T} - \frac{1}{Tm}\right)}} \qquad \textbf{(Equation 1)}$$

where r_s is the average count rate, T is the temperature (in Celsius degrees, °C), p_1 and p_2 correspond to the slopes of the straight lines at the beginning and the end of the plot, and r_{s1} and r_{s2} are the respective count rate intercepting values at the y axis. From the experimental data, it is possible to calculate the cooperativity (B) and the midpoint of the phase transition, which corresponds to T_m. Additionally, T_m may be calculated from the slope and the inflection point of the data-fitted sigmoid curves of count rate *vs.* T (Figure 6.3).[28,29]

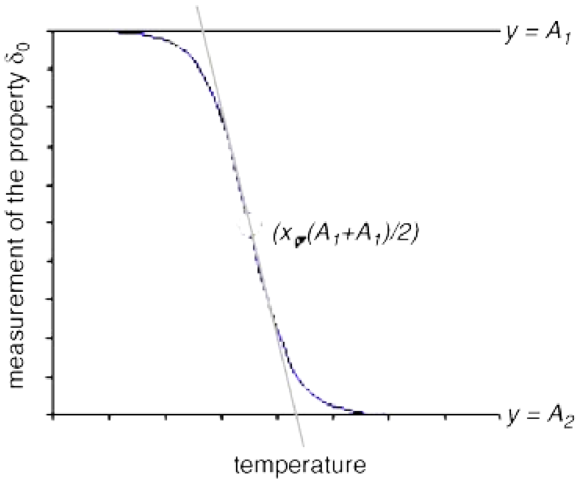

Figure 6.3 – Variation of a physical property (e.g. count rate) as a function of *T*. Adapted from [28].

6.2.4. UV-Vis derivative spectrophotometry to quantify partition into membranes

Partition between aqueous media and lipid membranes is of paramount importance for the biological action of many biomolecules and drugs[30]. As such, determination of membrane partition coefficients (*Kp*) provides an indication of the extent to which a given drug interacts with lipid membranes and/or penetrates into cells. This is of great interest for predicting the pharmacokinetics of a drug, i.e., its absorption, distribution, metabolism and excretion, as well as in assessing its toxic and/or therapeutic effects[31,32].

Kp of a given compound (e.g, drug) may be determined *via* UV-Vis derivative spectrophotometry, in the presence of increasing concentrations of liposomes[33]. This technique is based on a change of an absorption parameter, such as molar absorptivity (ε) or maximum absorption wavelength (λ_{max}) of the compound when it permeates from the aqueous to the nonpolar medium[31]. In this case, the absorbance of each sample is measured at a wide range of wavelength values in the UV-Vis range (200 - 500 nm); the mathematical treatment of absorbance data collected is then performed using a developed routine application for Microsoft Excel®, designated as *Kp* calculator[31], which (i) subtracts each reference spectrum from the correspondent sample spectrum, to obtain corrected absorption spectra (Figure 6.4); (ii) determines the second and third-derivative spectra in order to both eliminate the spectral interferences due to light scattered by the lipid vesicles and enhance the ability to detect minor spectral features by improving band resolution (Figures 6.5 and 6.6, respectively); and (iii) calculates *Kp* values by plotting the second- or third-derivative spectra values at wavelengths with better signal-to-noise ratio *versus* the lipid concentrations[34].

Kp, is the molar partition coefficient expressed as M^{-1}, [31,33] and is generally calculated by fitting Equation 2 to the experimental data (D_T *vs.* [L]).

$$D_T = D_w + \frac{(D_l - D_w)\, K_p\,[L]}{1 + K_p\,[L]} \qquad \textbf{(Equation 2)}$$

In Equation 2, *D* is the second or third derivative intensity (*D* = (d^nAbs)/($d^n\lambda$)). Subscript T stands for the derivative intensity of the drug in a sample solution with a certain concentration of lipid [L]. Subscripts *w* and *l* stand for the value of the derivative intensity in aqueous phase and the value that would be obtained if all the partitioning molecules were in the lipid phase, respectively.

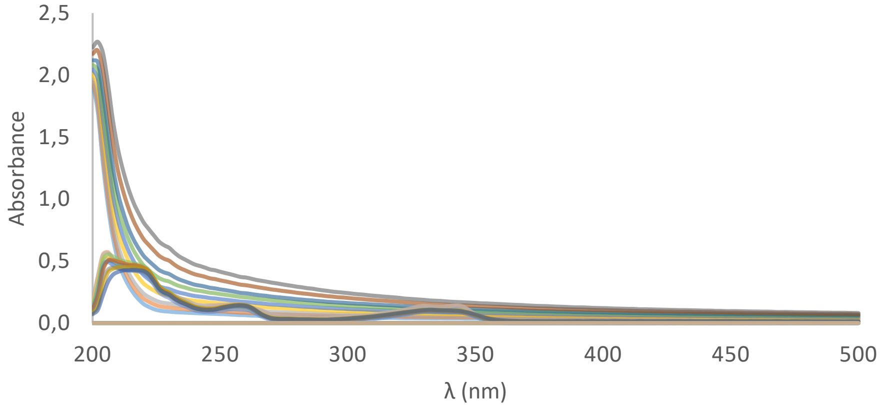

Figure 6.4 – Example of corrected absorbance spectra of a compound incubated, at a fixed concentration, with increasing concentrations of lipid vesicles.

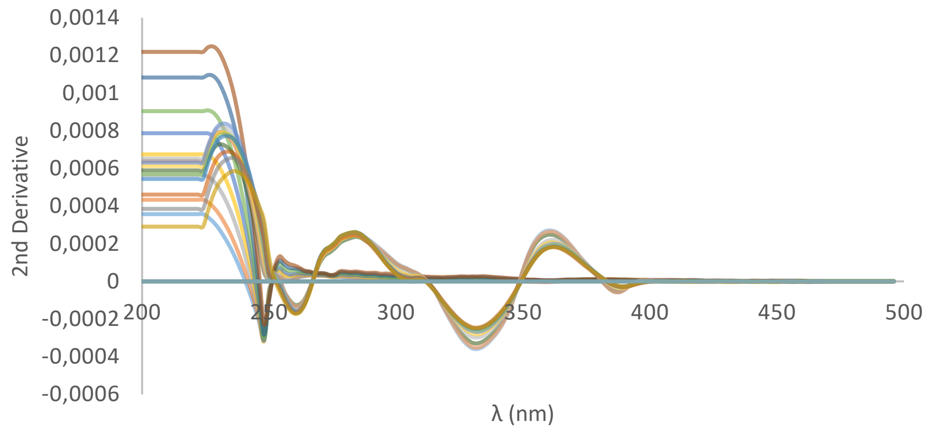

Figure 6.5 – Second derivative spectra of the data presented above (Figure 6.4).

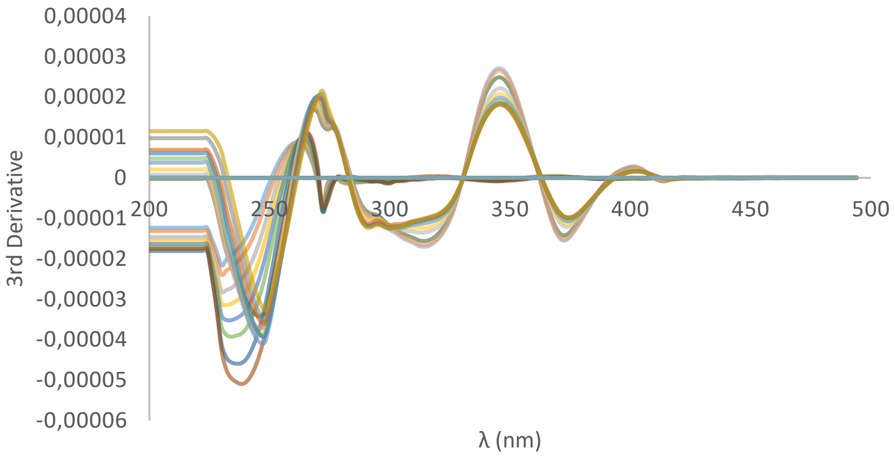

Figure 6.6 – Third derivative spectra of the data presented above (Figure 6.4).

6.2.5. Surface plasmon resonance

Use of optical biosensors is another important approach to study molecular interactions, including those involving lipid bilayers. Biosensors that employ the surface plasmon resonance phenomenon are particularly interesting, as they provide a label-free method to monitor molecular interactions in real time[35]. SPR biosensors are used to characterize bimolecular interactions that occur at the surface of a so-called “sensor chip” – usually, a glass slide coated with a very thin layer of gold conveniently functionalized to retain one of the components (denominated “ligand”) of the interaction that is going to be measured. The other component (“analyte”) is the solute of a liquid phase (usually, aqueous buffer) that is put into contact with the sensor-ship, either in a stop- or, more often, in a continuous-flow mode *via* a microfluidic system[35].

When polarized laser light is directed through a medium with high refractive index (often a prism) to the thin layer of gold that lies at the interface with a medium of low refractive index at a critical angle of incidence, surface plasmons are generated at the surface of the gold layer. This absorbs light, hence is detected as a decrease in the intensity of reflected light. The critical angle depends on the refractive index of the medium in contact with the metal within a few hundred nanometers of the metal surface, which changes when molecules bind to this surface[36]. As such, upon interaction between the surface-bound ligand and the added analyte, the refractive index at the surface of the sensor chip changes and this is viewed as an increase in signal in real time. In other words, if the dielectric constant of the liquid phase remains unchanged, the SPR signal is sensitive to changes in mass concentration at the gold surface of the sensor chip; this signal is expressed in resonance units (RU), where 1 RU = 1 pg/mm^2. [30,35,37] During the experiment, a sensorgram is generated, where the SPR signal is depicted in function of the time (Figure 6.7).

The most widely distributed and well known SPR biosensors are those from Biacore (https://www.biacore.com/lifesciences/index.html). To study the interactions between a given analyte and lipid vesicles by means of a Biacore SPR biosensor, one should make use of L1 sensor chips, where lipophilic groups covalently attached to the carboxymethylated dextran coating of the gold chip enable direct non-covalent immobilization of liposomes while maintaining the structure of the lipid bilayer (Figure 6.8). Hence, the liposome-binding analyte is used dissolved in running buffer. Regeneration of this type of surface removes not only the analyte, but the liposomes as well; thus, after regeneration, liposomes have to be once again immobilized onto the surface of the L1 sensor chip.

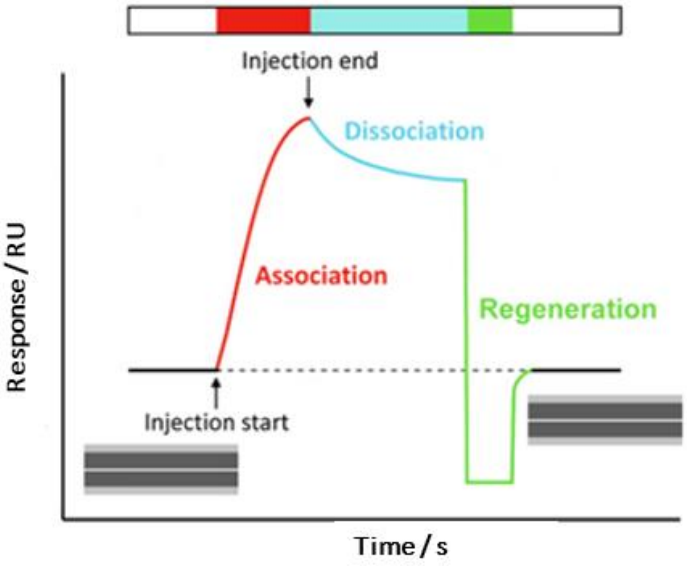

Figure 6.7 – A typical SPR sensorgram. The sensor chip is equilibrated with running buffer prior to injection; the analyte solution is then injected across the chip at a fixed concentration for the desired association period (in red), which stimulates a response increase owing to analyte binding to the surface-immobilized ligand; the sensor chip is then washed with running buffer and a decrease in response is observed as a result of dissociation of the bimolecular complex (in green); finally, the ligand surface is conveniently regenerated for a new analysis cycle. Adapted from [35].

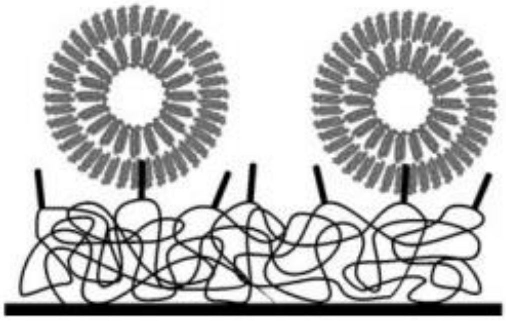

Figure 6.8 – Schematic view of liposomes immobilized onto the surface of an L1 sensor chip.

While the visual comparative inspection of binding curves (sensorgrams) obtained offers sufficient grounds on which to draw unambiguous conclusions regarding qualitative aspects of the bimolecular interaction, quantitative determination of binding constants can be derived from the kinetics (association and dissociation rates) by numerical integration analysis of the sensorgrams, conveniently done by the Biacore BIAevaluation software[36].

6.3. Results and discussion

To gain some insight into the phenomena underlying the behavior of the CQn-TP10 conjugates towards healthy *vs* parasitized RBC, two conjugates were selected, namely, CQn-C4-TP10, CQn-S-S-TP10, based on their different antimalarial and hemolytic activities, and parent building blocks TP10 and CQn were included as well, for comparison.

For the of the biophysical interactions between peptide-drug conjugates and lipid model membranes, liposomes composed by zwitterionic 1,2-dimyristoyl-sn-glycero-3-phosphocholine (DMPC) were selected as simplistic mimics of hRBC membranes. This model is typically used to simulate the neutral outer leaflet of eukaryotic cells, which are mainly composed of PC headgroups[38]. On the other hand, 1,2-dimyristoyl-sn-glycero-3-phosphorylglycerol (DMPG) vesicles served as simplistic models for *P*iRBC, as they represent the increased amount of negatively charged phospholipids present in the outer leaflet of *Plasmodium*-infected erythrocytes[39–41].

6.3.1. Influence of CQn-TP10 conjugates on lipid model membranes

DMPC and DMPG vesicles (100 nm) were prepared (pH = 7.4) and incubated for 30 minutes, at 37 °C, with increasing concentrations of CQn (0.5, 10 and 20 µM), CQn-C4-TP10, CQn-S-S-TP10, and TP10 (0.5, 1, 2 and 5 µM). Vesicles' hydrodynamic diameter and polydispersion were then assessed by DLS, with results as depicted in Figure 6.9. Analyzing the graphic, it is possible to gather a few informations. First of all, CQn does not promote any changes in DMPG and DMPC vesicles – neither in their size nor in the polydispersion of the sample; moreover, increasing concentrations of TP10 promoted an increase in the size of both DMPG and DMPC liposomes, while polydispersion remains relatively low. On the other hand, both CQn-TP10 conjugates exhibited a different behavior towards the two different models: whereas increasing concentrations of both CQn-TP10 conjugates did not promote any significant alterations in DMPG liposomes, increasing concentrations of these constructs triggered a visible increase in DMPC vesicles, accompanied by a large increase in polydispersion, which may ultimately be responsible for the observed changes in the hydrodynamic diameter:

this increase in polydispersion suggests the formation of vesicles' aggregates and is indicative of the toxicity of these conjugates.

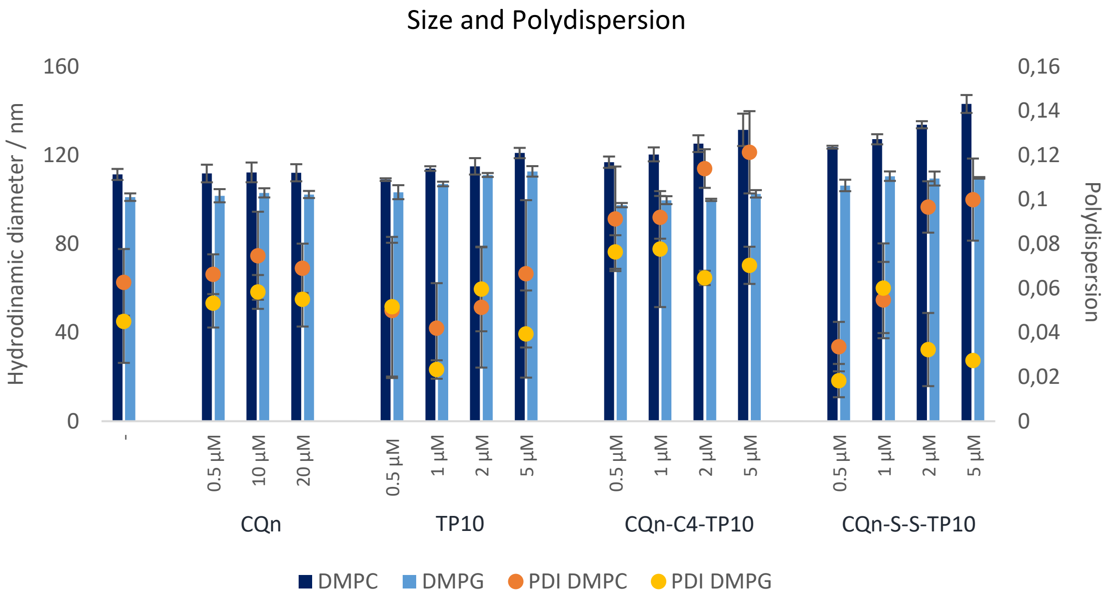

Figure 6.9 – Hydrodynamic diameter of the lipid vesicles after incubation with increasing concentrations of the compounds (bars) and polydispersion of the liposomes sample (dots).

Additionally, we evaluated the influence of our compounds on the packing of the membrane's phospholipids. For this, DMPC and DMPG vesicles were incubated with CQn (20 µM), TP10, and CQn-TP10 conjugates (5 µM) for 30 minutes, at 37 °C and their T_m and cooperativity were determined by DLS, with temperatures of each experiment increasing from 13 to 33 °C. Values obtained are depicted in Figure 6.10, and allow to conclude that neither compound seems to significantly affect T_m of DMPC liposomes. However, decreased cooperativity is observed when these vesicles interact with CQn-C4-TP10, which suggests that this particular conjugate interacts with the cooperative region involving the first carbons of the alkyl chains, preventing some lipid molecules from participating in the melting transition[42,43]. On the other hand, the T_m of DMPG vesicles was largely affected by all the compounds, which suggests that these are interacting with the polar region of the bilayer, responsible for the packing of the phospholipids. This was not surprising, as the positively charged (at pH 7.4) test compounds would necessarily interact more strongly with the headgroups of negatively charged phospholipids. While TP10 and CQn-C4-TP10 did not alter the cooperativity of the main phase transition, suggesting they are interacting with the more superficial area of the lipids, the opposite was observed for CQn-S-S-TP10 and CQn: the induced changes in the cooperativity of DMPG vesicles suggest that these compounds interact with the alkyl chains close to the headgroups (C1-C9)[43]. Interestingly, these compounds have a smaller impact on the size and polydispersion of DMPG vesicles, which is suggestive of their lower toxicity towards *P*iRBC.

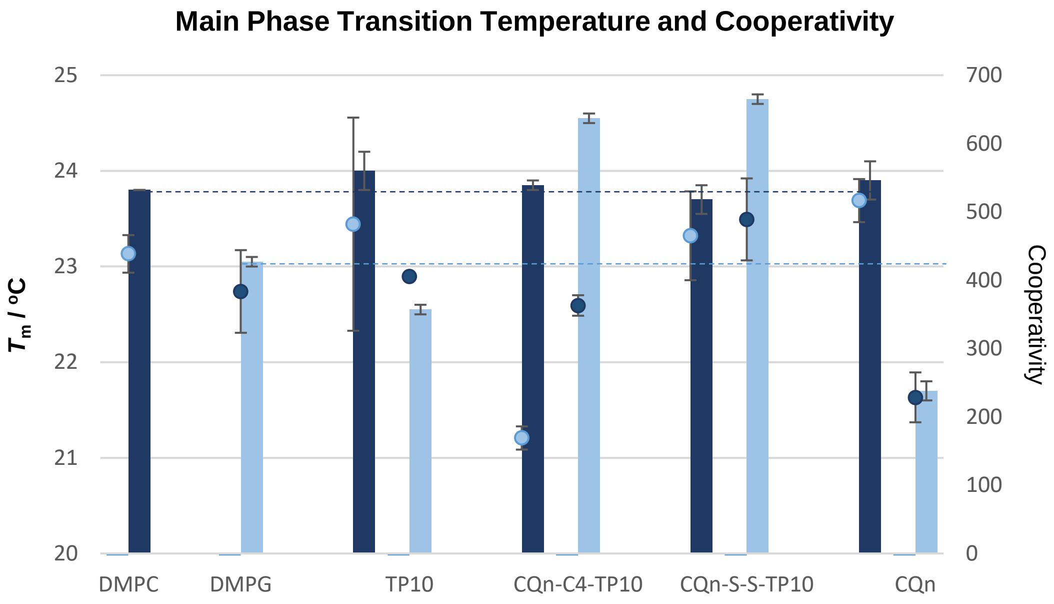

Figure 6.10 – Main phase transition temperature (*T*m; bars) and cooperativity (B; dots) for DMPC and DMPG alone and in the presence of CQn (20 µM), TP10, CQ-C4-TP10 and CQ-S-S-TP10 (5 µM).

6.3.2. Compounds partition between aqueous medium and lipid membranes

The partition coefficients between an aqueous medium and lipid vesicles was measured for the aforementioned conjugates and their parent building blocks. To this end, test compounds (at a fixed concentration) were firstly incubated for 30 minutes, at 37 °C, with increasing concentrations of DMPC or DMPG vesicles, after which the absorption spectra were recorded (200-500 nm, at 2 nm intervals). Since the maximum absorbance of TP10 alone ($\lambda_{max} \simeq 220$ nm) overlaps with the dispersion of the liposomes (*cf.* Figure 6.4), the inclusion of TP10 in this study implicated the synthesis of a derivative of this peptide, which included in its sequence an additional *C*-terminal tryptophan residue (λ_{max} = 280 nm)[44]. The partition coefficients (K_p), expressed in terms of log *D* (distribution coefficient), were determined by fitting the data obtained to Equation 2, and values obtained are shown in Table 6.1. Comparing these values with each other, and taking into account the experimental error, it is possible to infer that neither of the compounds seems to have a preferential partition for the different lipid models.

Table 6.1- Partition coefficients (Log *D*) of the compounds in DMPC and DMPG vesicles, at 37 ºC.

Compound	**Log *D***	
	DMPC	DMPG
CQn	3.7 ± 0.7	3.4 ± 0.6
TP10-W	3.5 ± 0.3	4.2 ± 0.9
CQn-C4-TP10	4.4 ± 0.5	4.5 ± 0.7
CQn-S-S-TP10	4.2 ± 0.8	4.1 ± 0.6

6.3.3. Binding affinity between TP10 and its conjugates and model membranes

In face of the apparently similar lipid partition behavior of both conjugates and their parent building blocks, as determined by UV-Vis derivative spectrometry prompted us to carry out additional experiments by SPR. Moreover, SPR studies allowed use of TP10 instead of its tryptophan-modified derivative. CQn was not included in the SPR study, as its low molecular weight hampers the obtainment of a detectable response upon interaction with the lipid model membranes.

POPC and POPG LUV (100 nm) were prepared and immobilized onto the surface of a Biacore L1 sensor chip and peptide solutions (at increasing concentrations, ranging from 1 to 64 µM) were injected over the liposomes. Response units were converted into mass of peptide or lipid assuming 1 RU = 1 pg/mm^2 (Figure 6.11). Additionally, the amount of peptide bound to the lipid bilayer was calculated at a reporting point at the end of the association phase (t= 180 s), normalized to the amount of lipid deposited onto the chip surface, and represented as a peptide-to-lipid ratio (P/L; mol/mol) (Figure 6.12).

Inspection of Figures 6.11 and 6.12 reveals that TP10 and its tested conjugates clearly showed a preference for POPG bilayers, as expected. Moreover, CQn-C4-TP10 and CQn-S-S-TP10 were found to bind more strongly to neutral POPC membranes than TP10 alone, which suggests that CQn might have an important role in establishing interactions with the zwitterionic membranes. Interestingly, we also observed that at higher concentrations (*e.g.,* 24 µM), CQn-C4-TP10 was able to disrupt the lipid bilayer in the POPC, but not in the DMPG matrix (Figure 6.13). This observation was consistent for the remaining samples, *i.e.* CQn-S-S-TP10 and the parent peptide: for CQn-S-S-TP10, we had to increase its concentration up to 32 µM to observe membrane damage in POPC models, while for TP10, only a slight fraction of the lipid bilayer was disrupted at the higher concentration assayed (64 µM; Figure 6.14). These findings correlate with the studies conducted to evaluate the biophysical modifications of the lipid membrane promoted by these peptides, which showed that they promote the formation of aggregates of DMPC vesicles (**6.3.1**). They are also consistent with the observed hemolytic activity (Chapter 5), where CQn-C4-TP10 was found significantly more hemolytic towards hRBC than TP10 and CQn-S-S-TP10.

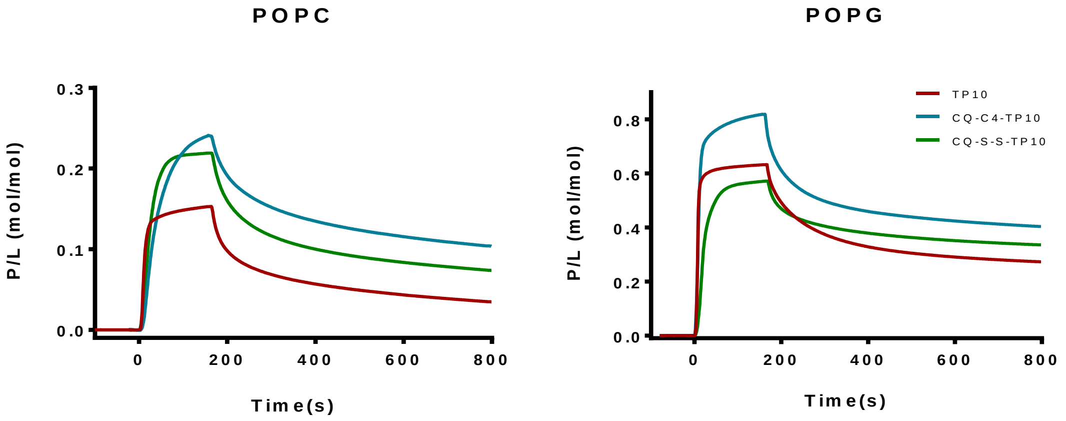

Figure 6.11 - SPR sensorgrams obtained upon injection of 18 µM TP10 (dotted lines) and its CQn conjugates over POPC or POPG bilayers deposited onto a L1 chip surface. Analytes were injected for 180 s and dissociation monitored for 600 s. Peptide-to-lipid ratio (P/L; mol/mol) was calculated by converting SPR response units (*i.e.*, RU) into mass (1RU=1 pg·mm^{-2} of lipid or protein) and into moles (see text).

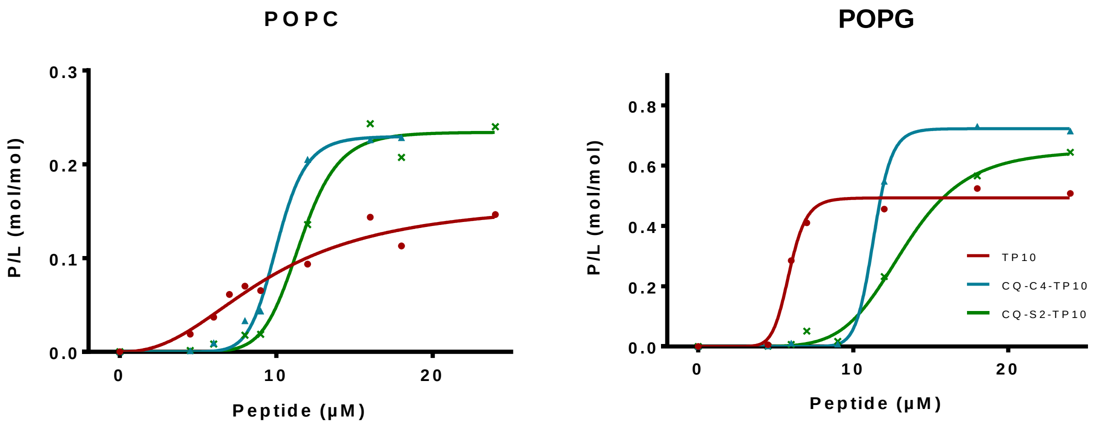

Figure 6.12 - Concentration-response curves determined by calculating P/L at the end of peptide injection (*i.e.,* end of the association phase; t=180 s) for each peptide concentration injected over each lipid bilayer (left); fitted curves using a nonlinear regression equation, dose-response binding with Hill slope (right).

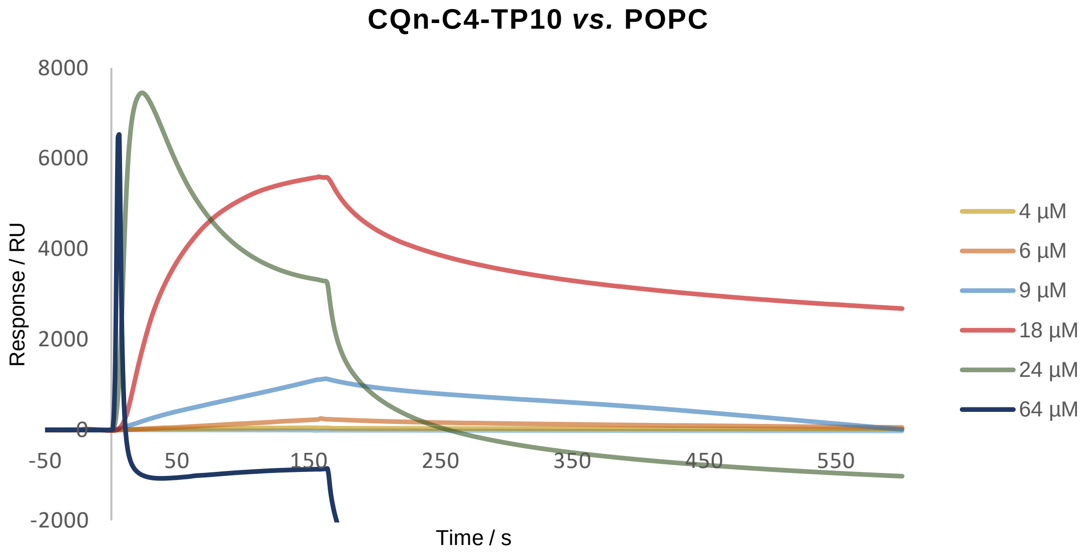

Figure 6.13 – Sensorgram obtained upon interaction of increasing concentrations of CQn-C4-TP10 with POPC membranes. At 24 and 64 µM, it is possible to observe that this conjugate acts like a “detergent”, disrupting membranes and removing them from the sensor chip (negative RU).

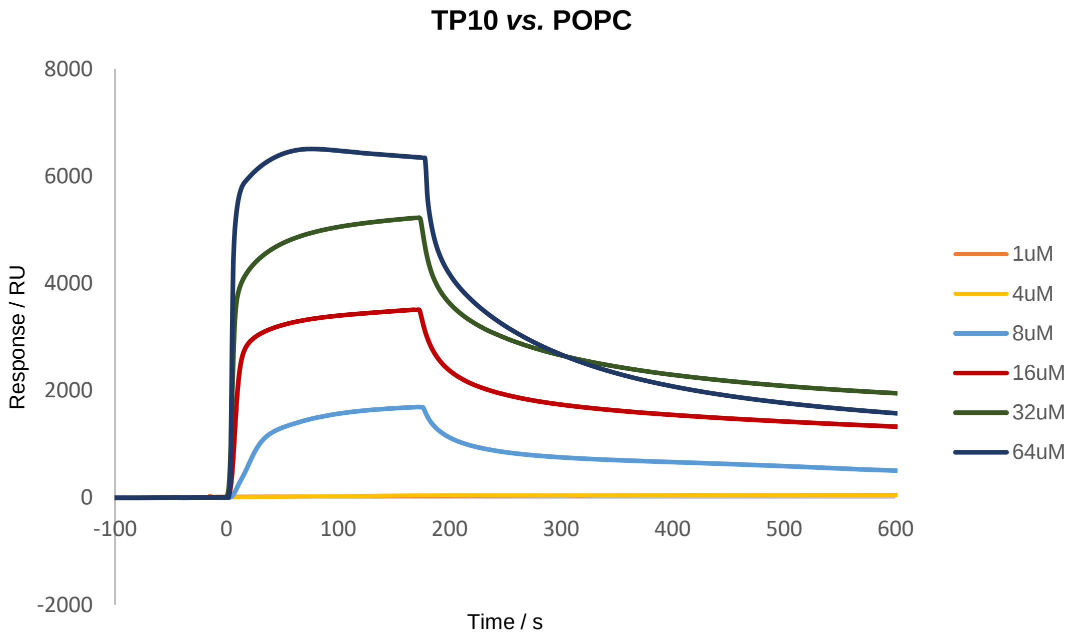

Figure 6.14 – Sensorgram obtained upon interaction of increasing concentrations of TP10 with POPC membranes. At 64 µM, slight membrane disruption is observed as a decrease in RU during the association phase (< 170 s).

Taken together, results from the above studies on the interactions between TP10, and its CQn conjugates, and lipid model membranes suggest those compounds to be highly disruptive to DMPC vesicles (especially, CQn-C4-TP10), despite having a higher binding affinity towards DMPG liposomes. SPR studies further show that conjugates present a higher affinity than parent peptide towards both model membranes, i. e., not having a marked preference for negatively-charged (DMPG) over zwitterionic (DMPC) membranes. At a first glance, these are somewhat puzzling findings, as one would expect that the cationic nature of both TP10 and its conjugates would make them have a much more pronounced and eventually disruptive (antimicrobial peptide-like) interaction with DMPG as compared to DMPC membranes. As such, both the lack of a marked preference for one membrane type, and the significant damage that the conjugates cause to DMPC vesicles suggest that CQn is responsible for the high hemolytic effects observed in vitro (*cf.* Chapter 4) for CQn-TP10 conjugates on both *P*iRBC and, especially, hRBC; these effects may eventually rise from hydrophobic interactions between the quinoline moiety and hydrophobic tails in the core of the erythrocyte membrane lipid bilayer. Still, membrane models used in this study are too simplistic, for a number of reasons. First, lipid composition of membranes from both hRBC and *P*iRBC is significantly more intricate than that of DMPC or DMPG vesicles;

also, RBC membranes undergo substantial alterations, not only upon invasion by the parasites, but also throughout their intracellular development[8,10,45,2]. These alterations are in part responsible for an increased fluidity and permeability of *P*iRBC as compared to hRBC[2,8,46], which were not taken into account in this study. Additionally, the surface of both hRBC and *P*iRBC is actually negatively charged[47], due to the presence of several non-lipidic components; for example, it has been reported that glycophorins (proteins rich in sialic acid) expressed in the erythrocyte membrane surface are altered by an enzyme-like material released by the parasite upon invasion, to prevent further invasion by other parasites[10,48]. This results in a decreased content in negatively charged sialic acid at the outer leaflet of the membrane, hence possibly reducing the number of "hot spots" on which cationic CPP and their conjugates might bind through electrostatic interactions. In addition, positively charged knob-like protuberances (partly composed by histidine-rich proteins) emerge on the erythrocyte surface upon parasite entry[49], which might contribute to the same effect.

Overall, results herein reported support previous findings from *in vitro* assays, in the sense that they correlate with the observed (i) strong hemolytic effects of CQn-TP10 conjugates on both *P*iRBC and, especially, hRBC, and (ii) lack of a potent and selective antimalarial action. However, model membranes used in this exploratory study have limitations, which prompted us to engage into studies using cells, as described in Chapter 7.

6.4. Experimental procedures

6.4.1. Preparation of the vesicles

Lipids (DMPC, DMPG, POPC and POPG) were dissolved in chloroform/methanol (9:1 v/v), dried under a stream of nitrogen and left under reduced pressure overnight to remove all traces of the organic solvent, yielding a dried lipid film. Phosphate buffer (0.05 M KH_2PO_4; 0.04 M NaOH; 0.1 M NaCl; pH = 7.4) was then added in order to obtain a final lipid concentration of 1200 µM, followed by vortexing at 37.0 ± 0.1◦C (well above the main phase transition temperature, T_m, of the lipids) for 30 min, to generate a suspension of MLV. Unilamellar vesicles were prepared by extrusion of the MLV suspension, through polycarbonate filters with a pore diameter of 600 nm (x10), 200 nm (x10) and finally, 100 nm (for DMPC and DMPG) or 50 nm (for POPC and POPG), using a LIPEX Extruder, Northern Lipids Inc. (Burnaby, Canada). The size of the LUV obtained was confirmed through dynamic light scattering (DLS) analysis in a Brookhaven Instrument (Holtsville, NY).

6.4.2. Determination of vesicles size

DMPC or DMPG vesicles (500 µM) were incubated with increasing concentrations of CQn (0,5, 10 and 20 µM), TP10, CQn-S-S-TP10 and CQn-C4-TP10 (0,5, 1, 2 and 5 µM) in phosphate buffer, for 30 minutes, at 37^{o}C. Size of the vesicles was determined through DLS analysis.

6.4.3. Determination of phase transition temperature and cooperativity

The effect of CQn (20 µM), TP10, CQn-S-S-TP10 and CQn-C4-TP10 (5 µM) on the biophysical parameters (T_m and cooperativity) of DMPC and DMPG LUVs (500 µM) were determined by DLS, as described by Michel et al.[28] The count rate was obtained using a BI-MAS DLS instrument (Brookhaven Instruments, USA), equipped with a controlled temperature cell holder. The samples were heated from 15.0 ± 0.1 ^{o}C to 35.0 ± 0.1 ^{o}C with intervals of 1.0 ± 0.1 ^{o}C and with an equilibration period of 2 min. At each temperature, 6 runs of 2 min were performed. Data were analyzed as previously reported (*cf.* 6.2.4).

6.4.4. Determination of *K*p by UV-Vis Derivative Spectrophotometry

Partition coefficients (K_p) of CQn, CQn-S-S-TP10, CQn-C4-TP10 and TP10-W between DMPC and DMPG vesicles, and aqueous phosphate buffer were determined by UV-Vis derivative spectrophotometry, as described by Magalhães *et al.*[31]. Briefly, CQ (75 µM) or CQ-TP10 conjugates (5 µM) in phosphate buffer were added to vesicles' suspensions with increasing concentrations of lipids (from 0 to 1000 µM) in a microplate, and incubated in the dark for 30 min and 37 °C, with gentle stirring. The corresponding reference solutions were identically prepared in the absence of test compound. The absorption spectra (220−500 nm range) of samples and reference solutions were recorded at 37°C, in a multidetection microplate reader (Synergy HT; Bio-Tek Instruments) and the mathematical treatment of the obtained data was performed using a K_p Calculator developed by Magalhães *et al.*[31].

6.4.5. Surface Plasmon Resonance

Peptide-membrane interactions were studied by SPR at 25 ^{o}C, using a Biacore sensor chip L1 in a Biacore 3000 instrument (GE Healthcare, Uppsala, Sweden), with HBS-N buffer (0.01 M HEPES, pH 7.4, 0.15 M NaCl) as running buffer. POPC and POPG

SUV with 50 nm of diameter were prepared with HBS-N, through a similar procedure to that described above (*cf.* **6.4.1**) and deposited onto the L1 chip at a flow rate of 2 µL/min for 40 minutes, reaching a steady-state plateau that confirmed chip surface coverage with deposited lipid bilayers. Several dillutions of TP10 and CQn-TP10 conjugates were prepared in HBS-N buffer and injected over the lipid bilayer (flow rate of 5 µL/min, 180 s). Peptide-lipid dissociation was followed for 600 s[38]. Treatment of the obtained data was performed as previously described (**6.3.3**).

Regeneration of the sensor chip's surface was achieved upon the injection of an aqueous solution of CHAPS (20 m*M*; flow rate of 5 µL/min, 60 s; two times), followed by the injection of aqueous solutions of HCl 100 m*M*, NaOH 10 m*M* with 20% MeOH (v/v) and NaOH 10 m*M* (30 µL; flow rate of 50 µL/min). Finally, CHAPS was once again injected (20 m*M*; flow rate of 5 µL/min, 60 s), prior to lipid deposition.

6.5. Bibliography

1. P. Grellier, D. Rigomier, V. Clavey, J. C. Fruchart and J. Schrevel, *J. Cell Biol.*, 1991, **112**, 267–277.
2. J. A. Boddey and A. F. Cowman, *Annu. Rev. Microbiol.*, 2013, **67**, 243–269.
3. H. Ginsburg, S. Kutner, M. Krugliak and Z. I. Cabantchik, *Mol. Biochem. Parasitol.*, 1985, **14**, 313–322.
4. R. S. Schwartz, J. A. Olson, C. Raventos-Suarez, M. Yee, R. H. Health, B. Lubin and R. L. Nigel, *Blood*, 1987, **69**, 401–407.
5. P. A. Maguire and I. W. Sherman, *Mol. Biochem. Parasitol.*, 1990, **38**, 105–112.
6. I. Sherman, *Microbiol. Rev.*, 1979, **43**, 453–495.
7. L. L. Hsiao, R. J. Howard, M. Aikawa and T. F. Taraschi, *Biochem. J.*, 1991, **274**, 121–132.
8. T. F. Taraschi, A. Parashar, M. Hooks and H. Rubin, *Science*, 1986, **232**, 102–104.
9. K. Kirk and A. M. Lehane, *Biochem. J.*, 2014, **457**, 1–18.
10. L. Li Hsiao, R. J. Howard, M. Aikawa and T. F. Taraschi, *Biochem. J*, 1991, **274**, 121132.
11. J. E. Smith, *Vet. Pathol.*, 1987, **24**, 471–476.
12. G. G. Holz, *Bull. World Health Organ.*, 1977, **55**, 237–248.
13. S. Eda and I. W. Sherman, *Cell. Physiol. Biochem.*, 2002, **12**, 373–384.
14. S. J. Singer and G. L. Nicolson, *Science*, 1972, **175**, 720–731.
15. C. G. Siontorou, G.-P. Nikoleli, D. P. Nikolelis and S. K. Karapetis, *Membranes (Basel).*, 2017, **7**, 38.
16. G. van Meer, D. R. Voelker and G. W. Feigenson, *Nat. Rev. Mol. Cell. Biol.*, 2008, **9**, 112–124.
17. H. R. Marsden, I. Tomatsu and A. Kros, *Chem. Soc. Rev.*, 2011, **40**, 1572–1585.
18. C. Peetla, A. Stine and V. Labhasetwar, *Mol. Pharmacol.*, 2009, **6**, 1264–1276.
19. Y. H. M. Chan and S. G. Boxer, *Curr. Opin. Chem. Biol.*, 2007, **11**, 1–7.

20. E. Sezgin and P. Schwille, *Mol. Membr. Biol.*, 2012, **29**, 144–154.

21. M. T. Le, J. K. Litzenberger and Elmar J. Prenner, in *Advances in Biomimetics*, ed. M. Cavrak, InTech, 2011, pp. 253–276.

22. M. Eeman and M. Deleu, *Biotechnol. Agron. Soc. Env.*, 2010, **14**, 719–736.

23. A. Akbarzadeh, R. Rezaei-Sadabady, S. Davaran, S. W. Joo, N. Zarghami, Y. Hanifehpour, M. Samiei, M. Kouhi and K. Nejati-Koshki, *Nanoscale Res. Lett.*, 2013, **8**, 1–8.

24. A. Sharma and U. S. Sharma, *Int. J. Pharm.*, 1997, **154**, 123–140.

25. M. Kanásová and K. Nesměrák, *Monatshefte fur Chemie*, 2017, **148**, 1581–1593.

26. A. Laouini, C. Jaafar-Maalej, I. Limayem-Blouza, S. Sfar, C. Charcosset and H. Fessi, *J. Colloid Sci. Biotechnol.*, 2012, **1**, 147–168.

27. W. Chen, F. Duša, J. Witos, S.-K. Ruokonen and S. K. Wiedmer, *Sci. Rep.*, 2018, **8**, 14815.

28. N. Michel, A. S. Fabiano, A. Polidori, R. Jack and B. Pucci, *Chem. Phys. Lipids*, 2006, **139**, 11–19.

29. M. Pinheiro, M. Arêde, J. M. Caio, C. Moiteiro, M. Lúcio and S. Reis, *Eur. J. Pharm. Biopharm.*, 2013, **85**, 597–603.

30. T. N. Figueira, J. M. Freire, C. Cunha-Santos, M. Heras, J. Gonçalves, A. Moscona, M. Porotto, A. Salomé Veiga and M. A. R. B. Castanho, *Sci. Rep.*, 2017, **7**, 1–10.

31. L. M. Magalhães, C. Nunes, M. Lúcio, M. A. Segundo, S. Reis and J. L. F. C. Lima, *Nat. Protoc.*, 2010, **5**, 1823–1830.

32. L. Di and E. H. Kerns, *Curr. Opin. Chem. Biol.*, 2003, **7**, 402–408.

33. B. De Castro, P. Gameiro, J. L. F. C. Lima, C. Matos and S. Reis, *Lipids*, 2001, **36**, 89–96.

34. A. R. Neves, C. Nunes and S. Reis, *J. Phys. Chem. B*, 2015, **119**, 11664–11672.

35. V. Hodnik and G. Anderluh, in *Lipid-Protein Interactions*, ed. J. H. Kleinschmidt, Humana Press, New York, NY, 2013.

36. M. Besenicar, P. Macek, J. H. Lakey and G. Anderluh, *Chem. Phys. Lipids*, 2006, **141**, 169–178.

37. R. V. Stahelin, G. Cevc, J. H. Kleinschmidt, T. N. Figueira, J. M. Freire, C. Cunha-

Santos, M. Heras, J. Gonçalves, A. Moscona, M. Porotto, A. Salomé Veiga and M. A. R. B. Castanho, *Eur. J. Pharm. Biopharm.*, 2013, **24**, 1–10.

38. E. Deplazes, S. T. Henriques, J. J. Smith, G. F. King, D. J. Craik, A. E. Mark and C. I. Schroeder, *Biochim. Biophys. Acta - Biomembr.*, 2016, **1858**, 872–882.
39. R. Ferraz, M. Pinheiro, A. Gomes, C. Teixeira, C. Prudêncio, S. Reis and P. Gomes, *Bioorganic Med. Chem. Lett.*, 2017, **27**, 4190–4193.
40. I. Porcar, A. Codoner, C. M. Gomez, C. Abad and A. Campos, *J. Pharm. Sci.*, 2003, **92**, 45–57.
41. T. E. Goto and L. Caseli, *J. Colloid Interface Sci.*, 2014, **431**, 24–30.
42. O. Cañadas and C. Casals, in *Lipid-Protein Interactions*, ed. Jörg H. Kleinschmidt, Humana Press, New York, NY, USA, 2013.
43. C. Nunes, G. Brezesinski, C. Pereira-Leite, J. L. F. C. Lima, S. Reis and M. Lúcio, *Langmuir*, 2011, **27**, 10847–10858.
44. W. G. Lesniak, A. Jyoti, M. K. Mishra, N. R. R. Louissaint, D. C. Chugani, S. Kannan and R. M. Kannana, *Anal. Biochem.*, 2013, **443**, 222–231.
45. V. L. Hale, J. M. Watermeyer, F. Hackett, G. Vizcay-barrena, C. Van Ooij and J. A. Thomas, *Proc. Natl. Acad. Sci.*, 2017, **114**, 3439–3444.
46. P. A. Maguire and I. W. Sherman, *Mol. Biochem. Parasitol.*, 1990, **38**, 105–112.
47. M. Akaki, E. Nagayasu, Y. Nakano and M. Aikawa, *Parasitol Res*, 2002, **88**, 16–20.
48. M. T. Makler, *Biochem. Biophys. Res. Commun.*, 1987, **143**, 461–466.
49. L. Florens, M. P. Washburn, J. D. Raine, R. M. Anthony, M. Grainger, J. D. Haynes, J. K. Moch, N. Muster, J. B. Sacci, D. L. Tabb, A. A. Witney, D. Wolters, Y. Wu, M. J. Gardner, A. A. Holder, R. E. Sinden, J. R. Yates and D. J. Carucci, *Nature*, 2002, **419**, 520–526.

7

Insights into conjugates and parent peptide interactions with both healthy and parasitized human erythrocytes

7.1. Overview

Findings reported in Chapter 6 suggest that CQn-TP10 conjugates, despite displaying a preferential affinity towards negatively charged DMPG model membranes, as expected form their cationic nature, are more disruptive to DMPC vesicles, which agrees with their higher hemolytic activity towards healthy than parasitized RBC (cf. Chapter 5). Still, model membranes used are too simplistic, as they only reflect the altered distribution of zwitterionic *vs.* negatively charged phospholipids of RBC membranes upon *Plasmodium* invasion, while there are numerous other factors at play. As such, the interactions of selected CQn-C4-CPP conjugates and their respective parent CPP with both *P*iRBC and hRBC was further explored. To this end, fluorescently-labelled conjugates and parent peptides were synthetized (**7.2**) and their internalization monitored through fluorescence microscopy and fluorescence-assisted cell sorting (FACS) analysis (**7.3**), as herein reported.

7.2. Synthesis of fluorescently-labelled peptides and their conjugates

In order to gain deeper insight into the differential modes of interaction, with hRBC and *P*iRBC, of distinct CQn-C4-CPP conjugates, the most active (CQn-C4-TP10) and an inactive (CQn-C4-TAT) conjugates, were selected for cell internalization studies. The parent TP10 peptide was included in the study, for reference. Since fluorescence-based techniques were to be used for the interaction studies to be undertaken (*cf*. **7.3**), peptides and conjugates labelled with carboxyfluorscein (CF, **62**) were first synthesized. To this end, an additional Fmoc-Lys(Mtt)-OH residue (**63**, Scheme 7.1) was introduced at the *C*-terminal end of the peptides, i.e., peptides TAT-Lys(Mtt) – RKKRRQRRRPPQK(Mtt), and TP10-Lys(Mtt) – AGYLLGKINLKALAALAKKILK(Mtt), were assembled by standard SPPS procedures as those described in Chapter 4.

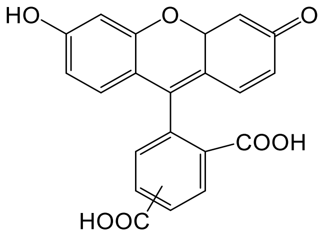

62

Figure 7.1 – Chemical structure of 5(6)-carboxyfluorescein

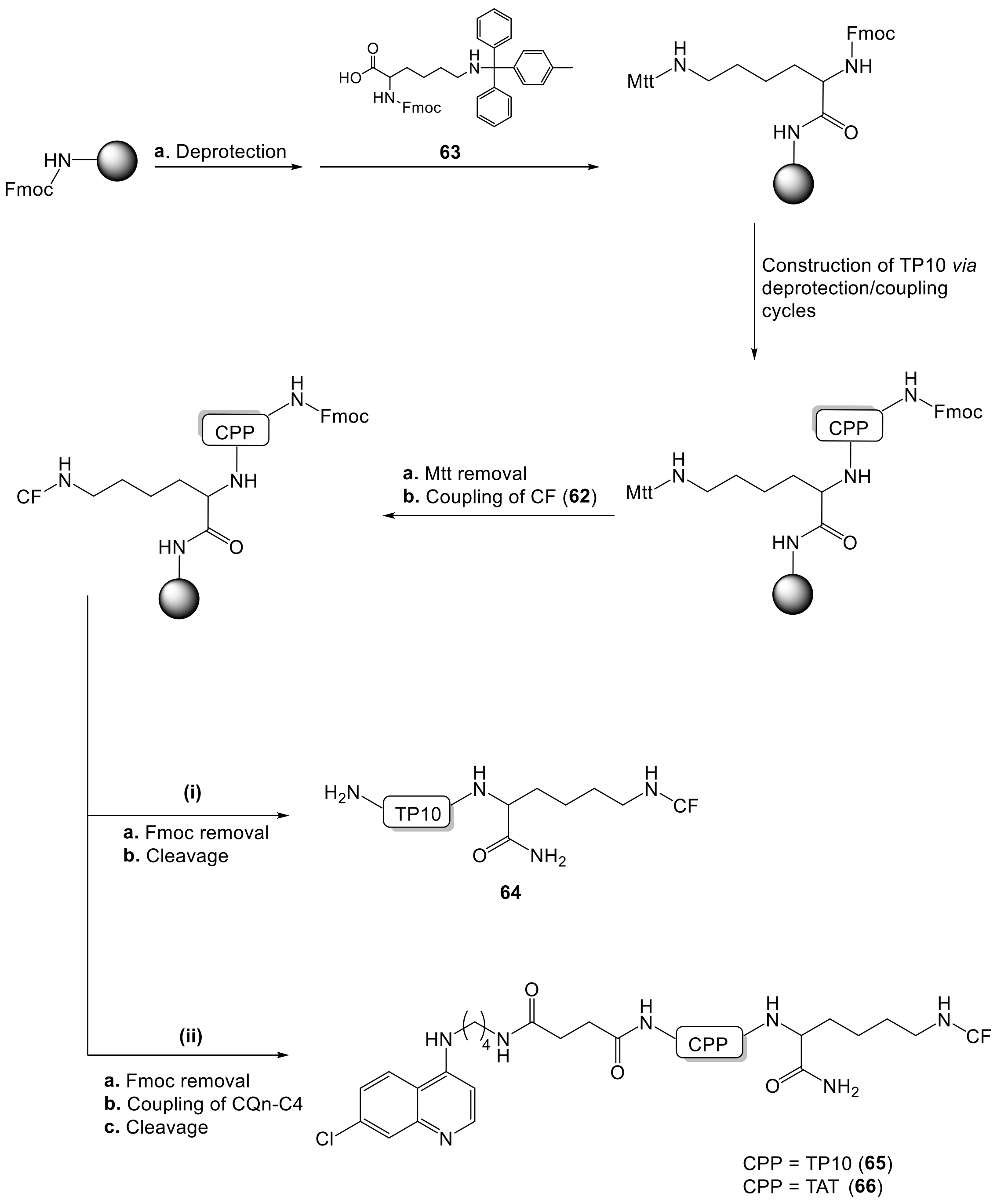
HN
Fmoc
a. Deprotection
HO
O
HN
Fmoc
H
N
63
Mtt
H
N
Fmoc
NH
HN
O
Construction of TP10 via deprotection/coupling cycles
H
N
Fmoc
CPP
Mtt
H
N
NH
HN
O
a. Mtt removal
b. Coupling of CF (62)
H
N
Fmoc
CPP
CF
H
N
NH
HN
O
(i)
a. Fmoc removal
b. Cleavage
H2N
TP10
H
N
H
N
CF
O
NH2
64
(ii)
a. Fmoc removal
b. Coupling of CQn-C4
c. Cleavage
HN
4
N
H
O
O
H
N
CPP
H
N
H
N
CF
O
NH2
Cl
N
CPP = TP10 (65)
CPP = TAT (66)

Scheme 7.1 – Synthetic route towards fluorescently labelled CPP (**64**) and conjugates **65** and **66**.

After assembling the AA sequence *via* standard SPPS protocols, and prior to the removal of the *N*-terminal Fmoc, the side chain protecting group of the *C*-terminal lysine, Mtt, was removed with a solution of 1% TFA in DCM; this released the side-chain amine to which CF was then coupled in the presence of PyBOP and DIPEA. Then, *N*-terminal Fmoc was removed, and the TP10-Lys(CF) peptidyl-resin was split into two halves, each of which was treated according to procedures (i) and (ii), below. TAT-Lys(CF) peptidyl-resin was only subject to procedure (ii).

(i) standard acidolytic cleavage (*cf.* **4.4.6**), to render the fluorescently labelled parent peptide, TP10-Lys(CF) (**64**);

(ii) coupling of pre-synthesized CQn-C4 (*cf.* **4.4.3**) to the CPP's *N*-terminal residue, followed by acidolytic cleavage, to deliver the CQn-C4-CPP-Lys(CF) conjugates (**65** for TP10, and **66** for TAT).

Once isolated, all crude products were analyzed and purified, according to methods and procedures previously described in Chapter 4 (*cf.* **4.4.1**).

Table 7.1 - Synthesized fluorescently labelled peptides and respective analytical data, obtained by HPLC (purity and retention time – R_t) and LC-DAD/ESI-IT MS (detected m/z).

CPP	Molecular Weight	Purity / %	R_t / minutes	Detected $^{m}/_{z}$
TP10-Lys(CF)	2666.56	93	16.0	1334.93 ($[M+2H]^{2+}$); 890.60 ($[M+3H]^{3+}$); 668.47 ($[M+4H]^{4+}$); 535.00 ($[M+5H]^{5+}$)
CQn-C4-CPP-Lys(CF)	2997.67	98	16.4	1500.00 ($[M+2H]^{2+}$);1000.8 ($[M+3H]^{3+}$); 751.00 ($[M+4H]^{4+}$); 601.13 ($[M+5H]^{5+}$)
CQn-C4-Tat-Lys(CF)	2534.32	83	15.7	844.73 ($[M+3H]^{3+}$); 633.80 ($[M+4H]^{4+}$); 507.40 ($[M+5H]^{5+}$); 423.00 ($[M+6H]^{6+}$)

* Value determined by HPLC, with a gradient elution of 1-100% ACN in water (0.05% TFA), for 30 minutes, at a flow rate of 1 mL/min.

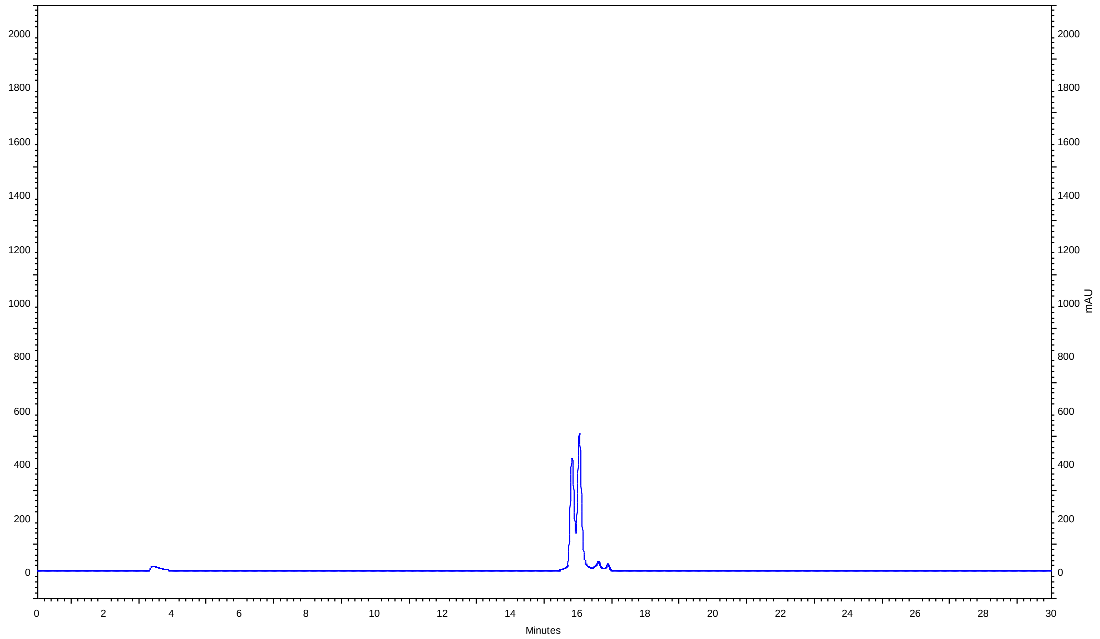

Figure 7.2 – Chromatogram obtained from the analysis of TP10-Lys(CF) (**64**) after purification, with a gradient elution of 0-100% ACN in water (0,05% TFA) in a RP-18E (5 µm), for 30 minutes and a flow of 1 ml/min, with detection at λ = 220 nm.

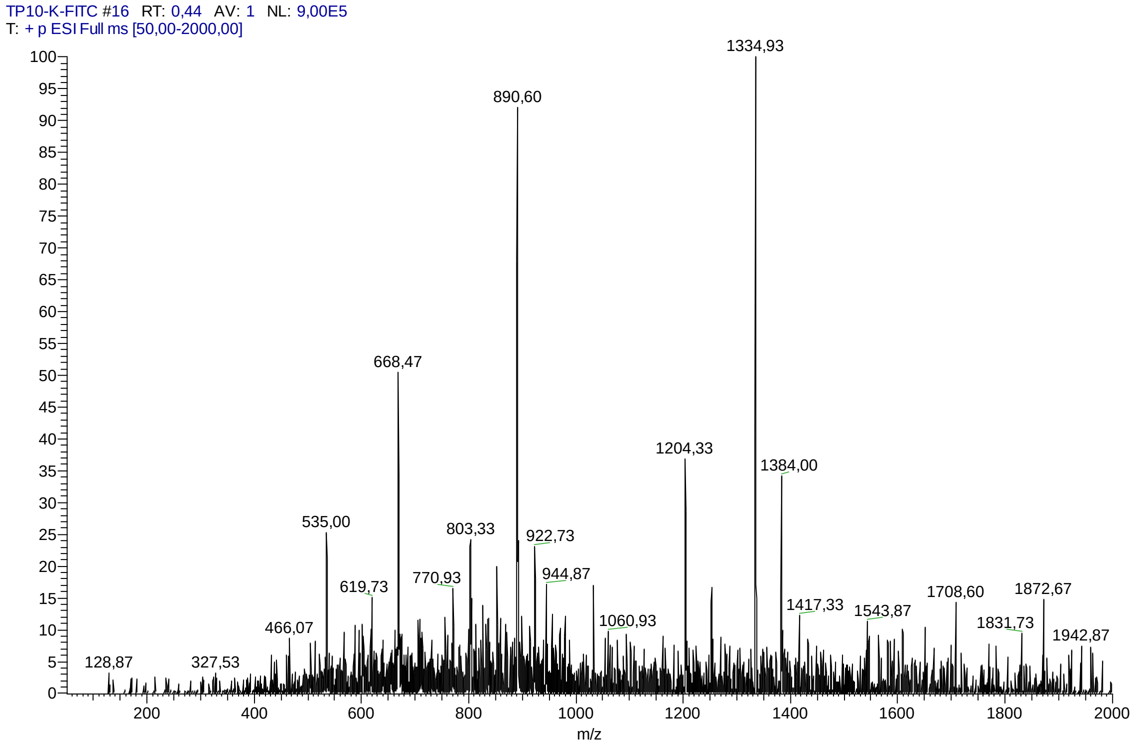

Figure 7.3 - Spectrum (ESI-IT MS, positive mode) obtained for crude TP10-Lys(CF) (**64**).

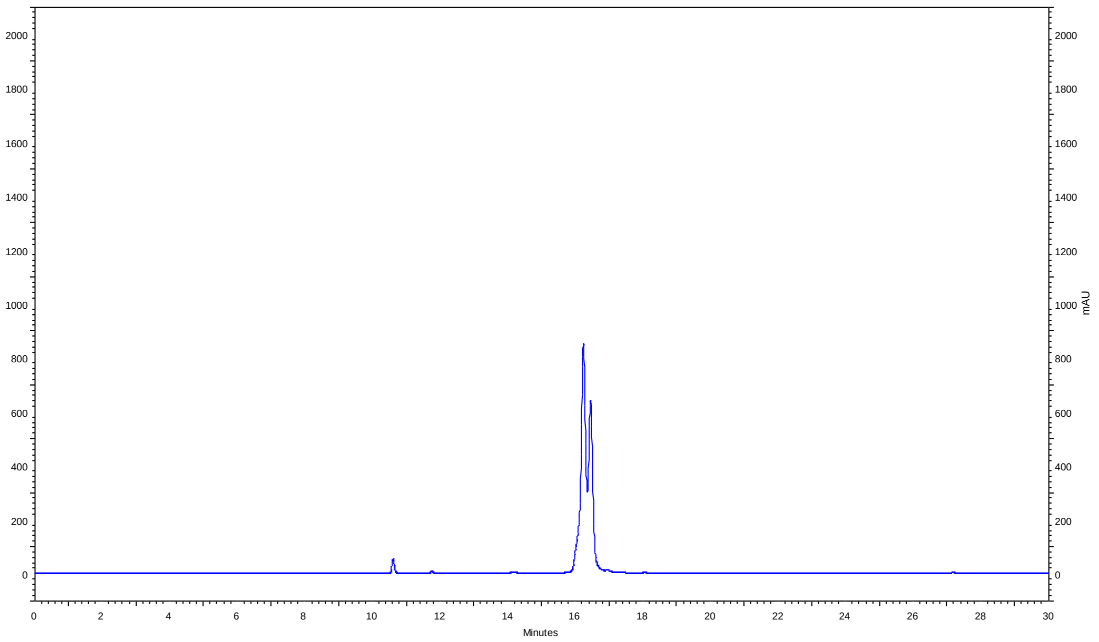

Figure 7.4 – Chromatogram obtained from the analysis of CQn-C4-TP10-Lys(CF) (**65**) after purification, with a gradient elution of 0-100% ACN in water (0,05% TFA) in a RP-18E (5 μm), for 30 minutes and a flow of 1 ml/min, with detection at λ = 220 nm.

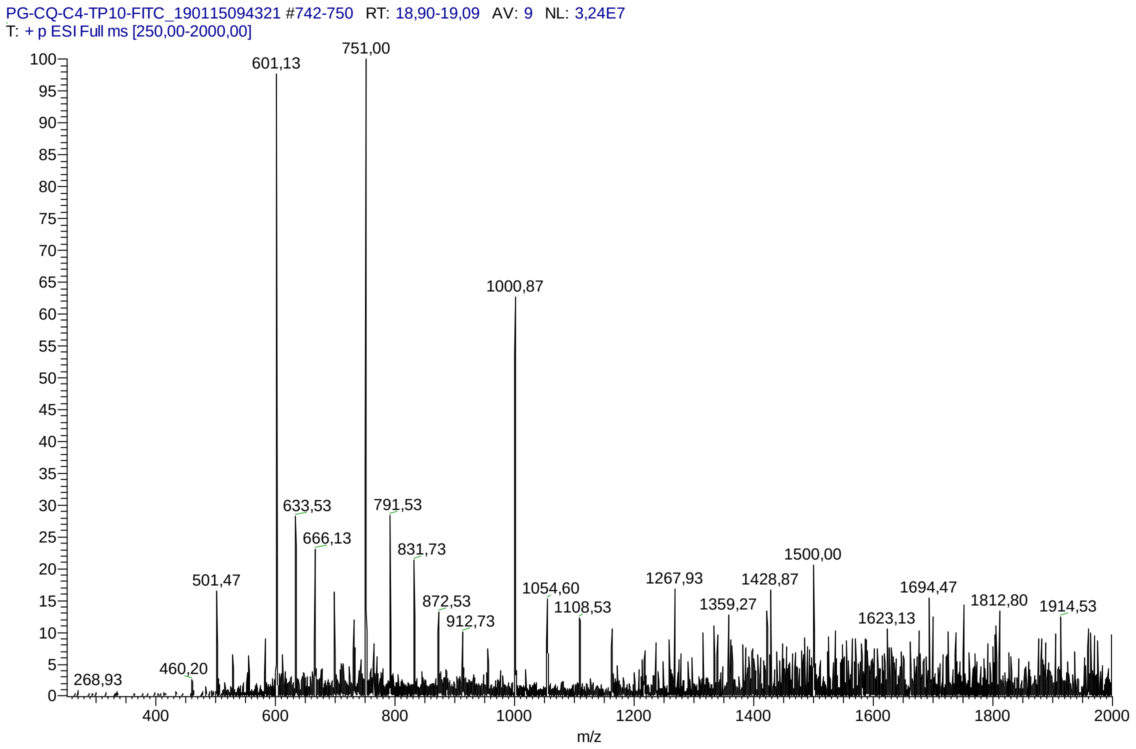

Figure 7.5 - Spectrum (ESI-IT MS, positive mode) obtained for crude CQn-C4-TP10-Lys(CF) (**65**).

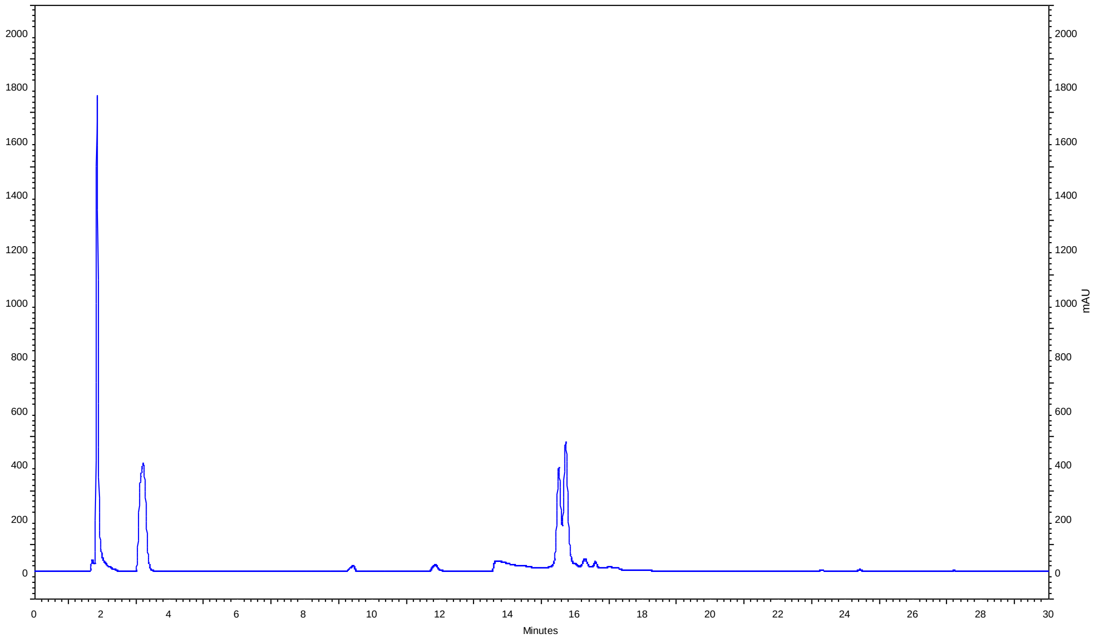

Figure 7.6 – Chromatogram obtained from the analysis of CQn-C4-TAT-Lys(CF) (**66**) after purification, with a gradient elution of 0-100% ACN in water (0,05% TFA) in a RP-18E (5 µm), for 30 minutes and a flow of 1 ml/min, with detection at λ = 220 nm.

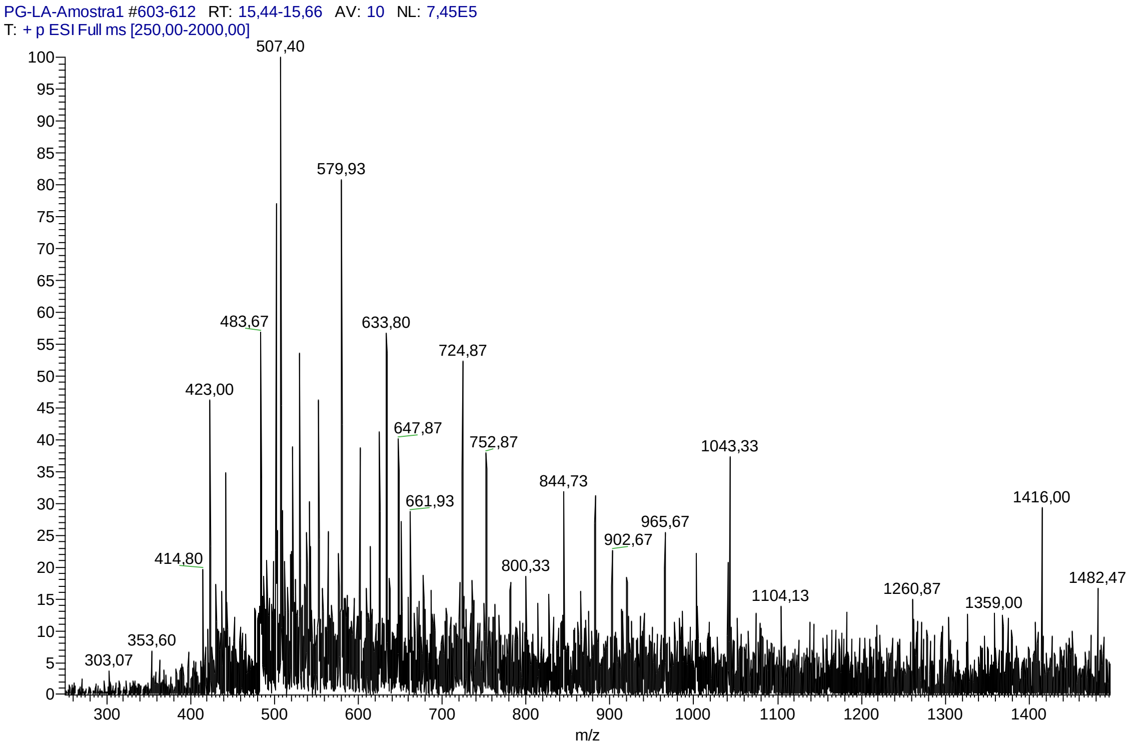

Figure 7.7 - Spectrum (ESI-IT MS, positive mode) obtained for crude CQn-C4-TAT-Lys(CF) (**66**).

7.3. Fluorescence-based studies

7.3.1. Fluorescence microscopy

Fluorescence microscopy is, nowadays, a technique of major relevance for the study of cell physiology; this technique, allied with the wide variety of fluorescent markers specific for, *e.g.*, proteins, lipids, ions or DNA, has been delivering key information towards the understanding of cell biology[1,2]. As such, fluorescence microscopy was the tool of choice to visualize the interactions between the fluorescently labelled CQn-CPP conjugates and both healthy and parasitized human RBC.

Conjugate and parent peptide interactions with hRBC and *P*iRBC were assessed by incubating asynchronous cultures of human RBC at 3% parasitemia (*i.e.,* containing 3% *P*iRBC and 77% hRBC) with the test compounds, after which the nuclei of intraerythrocytic parasites were stained with DNA-binding Hoechst 33342[3]. This staining allows not only to visualize the parasites' nuclei, but also to distinguish between hRBC (naturally enucleated) and *P*iRBC. Cells suspensions were then observed in a fluorescence microscope, equipped with a fluorescence mirror unit cassette for UV/blue/green excitation, and detection of the corresponding blue/green/red emission ranges.

Observations made (Figures 7.8 to 7.13) show that fluorescently labelled TP10 and its CQn-C4-TP10 conjugate behave similarly: they both show preferential interaction with erythrocytes, parasitized or not, that show significant membrane damage, namely, much thinner membranes (the so-called "ghost" erythrocytes).

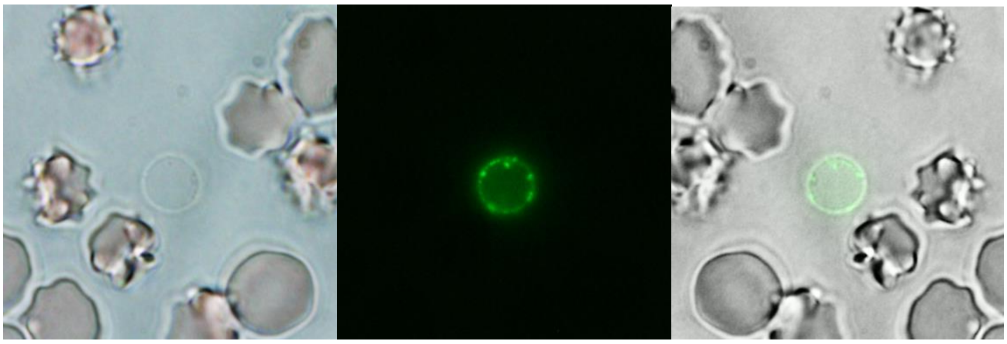

Figure 7.8 – Interaction of fluorescently labelled TP10 (**64**) with human RBC at 3% parasitemia. TP10 is seen accumulating at the membrane of an erythrocyte that, despite not being parasitized, shows a very thin, almost invisible membrane ("ghost" erythrocyte).

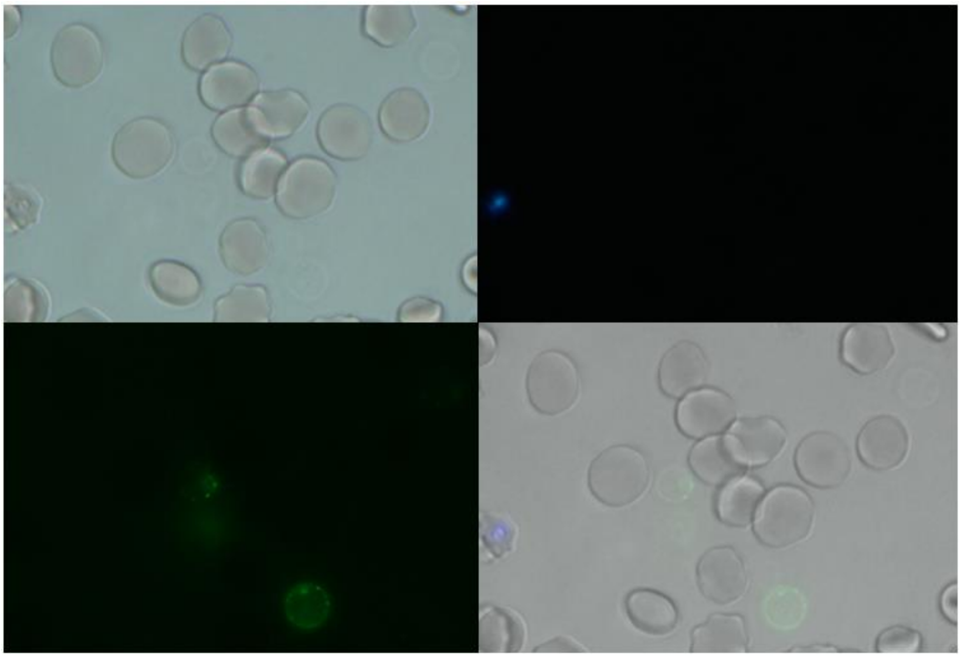

Figure 7.9 – Interaction of fluorescently labelled CQn-C4-TP10 (**65**) with human RBC at 3% parasitemia. **65** is seen accumulating at the membrane of two “ghost” erythrocytes.

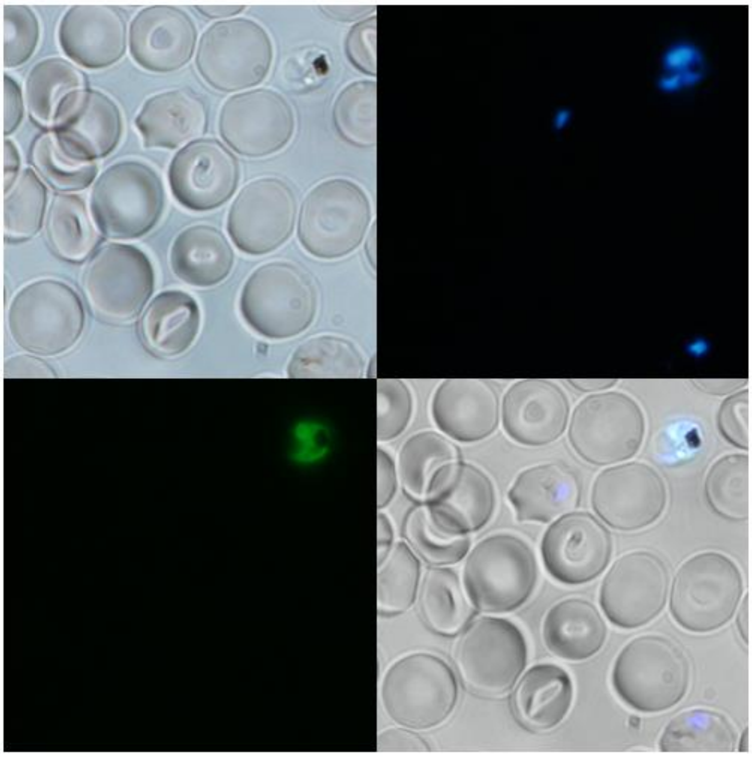

Figure 7.10 – Interaction of fluorescently labelled TP10 (**64**) with human RBC at 3% parasitemia. TP10 (green fluorescence) is seen interacting with a late stage *P*iRBC (blue staining), which presents a very thin membrane, while ring-stage *P*iRBC – with apparently healthy membranes, were not internalized by this peptide.

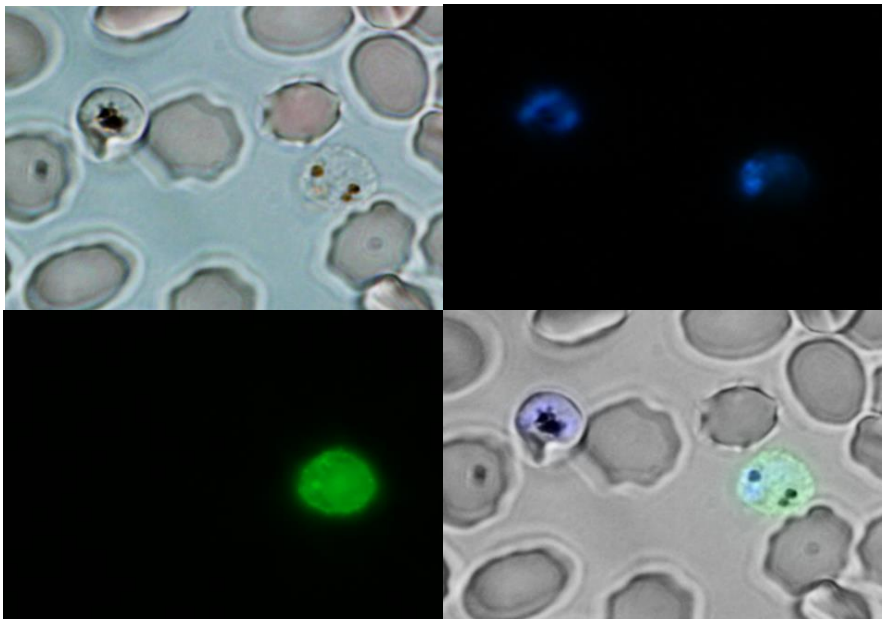

Figure 7.11 – Interaction of fluorescently labelled CQn-C4-TP10 (**65**) with human RBC at 3% parasitemia. Internalization is only visualized (green fluorescence) for one of the two observable *P*iRBC (blue staining), which is – once again – the one that shows a much thinner membrane.

The uneven distribution of TP10 and its conjugate within the cell culture, i.e., their observed preferential interaction with erythrocytes (infected or not) having thinned membranes raises the following question: is interaction only possible when the membrane is already damaged (erythrocyte ghosts), or is the damage a consequence of the interaction? Taking into account the non-negligible hemolytic activity of these compounds (*c.f.* Chapter 5), the latter option seems to be more plausible. Still, even if that is the case, it remains unclear why not all cells are equally affected by the peptide and its conjugate. Eventually, asynchronies in the development of cultured intraerythrocytic parasites may underlie this differentiation; this hypothesis is supported by the fact that none of the compounds was observed inside early trophozoite (ring) stage *P*iRBC, only in hRBC or *P*iRBC at later stages of parasite development. This suggests that, as soon as it internalizes the RBC, the parasite immediately induces modifications in the membrane that turn it more impermeable to both the CPP and its drug conjugate; later, as the merozoite stage and subsequent egress are approached, increased permeability of both the parasitophorous vacuole and the erythrocyte membrane may facilitate internalization and subsequent antimalarial action[4]. Indeed, it was possible to observe that both TP10 and its conjugate are able to strongly interact with free parasites (released after egress, Figures 7.12 and 7.13), apparently in close vicinity to the parasitic DNA.

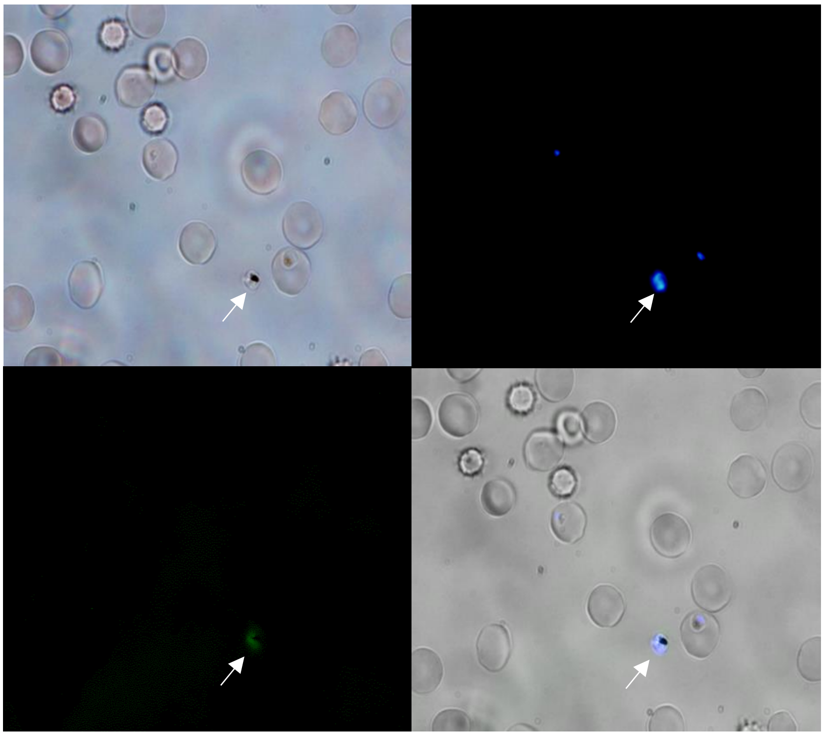

Figure 7.12 - Co-localization of a merozoite outside the host cell (blue staining), and fluorescently labelled TP10 (green fluorescence), showing the ability to bind to free parasites.

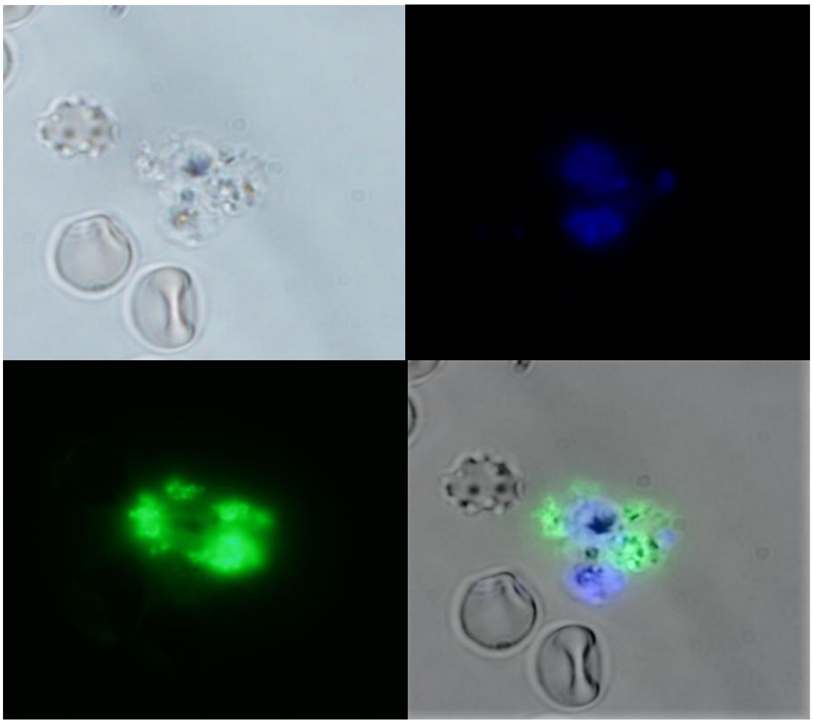

Figure 7.13 – Superimposition of green fluorescence from CQn-C4-TP10 (green) with blue fluorescence due to Hoechst-stained DNA from free parasites (burst schizont).

The overall analysis of the obtained images suggests that both TP10 and its conjugate CQn-C4-TP10 are able to interact with both hRBC and *P*iRBC (except early ring-stage *P*iRBC), possibly causing membrane damage. This agrees with findings reported in previous chapters, namely, (i) conjugate's hemolytic activity *in vitro* against both healthy and parasitized erythrocytes (*c.f.*, Chapter 5), and (ii) strong perturbations on both DMPC and DMPG model membranes, caused by CQn-C4-TP10 (*c.f.*, Chapter 6).

Relevantly, both the CPP and its conjugate are able interact with free *Plasmodium* (released upon egress, *i.e.*, burst of schizonts), and bind to parasitic DNA, which might be indicative of their mechanism of antimalarial action. Nonetheless, it seems that such action cannot be efficiently exerted at the early stages of blood infection, possibly because the altered membranes of early stage *P*iRBC are more resistant to peptide internalization.

7.3.2. Fluorescence-assisted cell sorting analysis (FACS)

Flow cytometry (FC) is a sophisticated technique, which is able to assess multiple physical characteristics of a single cell, such as size, granularity and fluorescence, among many other parameters; these measurements are simultaneous, and occur as the cell flows in suspension through a measuring device. FC may be applied to the study of cells, microorganisms, nuclei, or chromosome preparations in a fluid stream passing through a light source, hence enabling detailed analysis of complex populations, in a short period of time[5]. Fluorescent-assisted cell sorters (FACS) are flow cytometers which have the ability to sort fluorescent-labelled cells from a mixed cell population, based on the specific fluorescent characteristics of each cell[6,7].

While fluorescence microscopy offered a visual assessment of the interactions between fluorescently labelled TP10 and its CQn-C4-TP10 conjugate and healthy and parasitized RBC, giving a few hints on the antimalarial behavior of these compounds, it did not provide quantitative data. To fill this gap, a FACS analysis was carried out, using the same test compounds, and asynchronous cultures of human RBC at 4% parasitemia (i.e., containing 4% *P*iRBC and 76% hRBC). As before (*c.f.* **7.3.1**), after an incubation period, nuclei in *P*iRBC were stained with Hoescht 33342. Cells suspensions incubated with the CF-labelled compounds were analyzed by FACS (Figure 7.14 and 7.15, respectively). Additionally, the fluorescently labelled CQn-C4-TAT conjugate **65** was included in this study, in order to discern whether lack of antimalarial activity by this conjugate is due to its inability to interact with *P*iRBC (Figure 7.16).

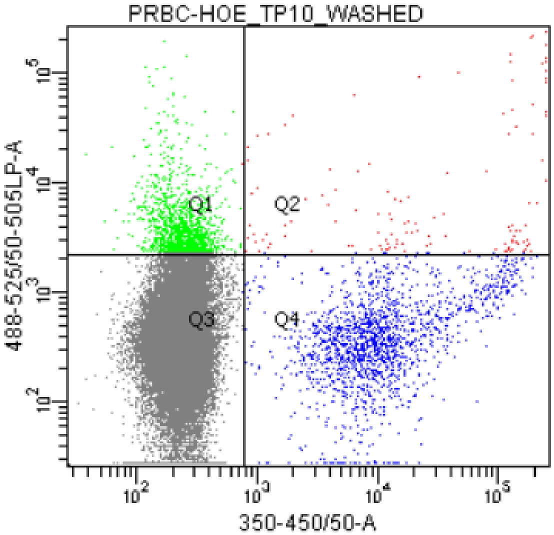

Figure 7.14 – FACS analysis of the interaction of peptide TP10 with hRBC and *P*iRBC. Upper quadrants (Q1 and Q2) refer to peptide-bound cells (CF fluorescence) and right-hand quadrants (Q2 and Q4) refer to *P*iRBC (Hoechst fluorescence). Q3 includes hRBC which were not internalized by fluorescently-labelled peptide.

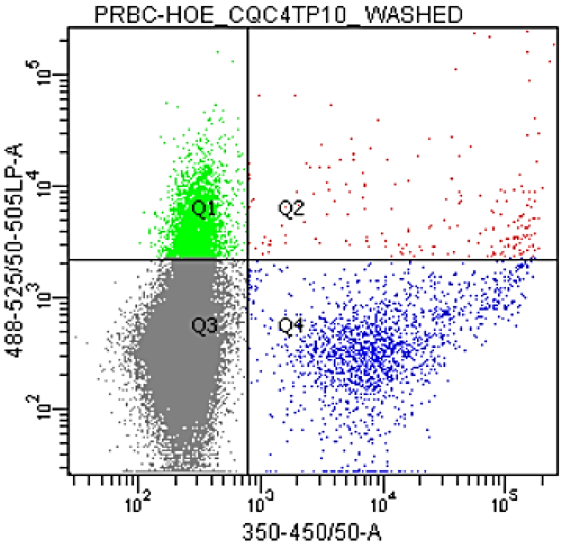

Figure 7.15 - FACS analysis of the interaction of conjugate **64** with hRBC and *P*iRBC. Upper quadrants (Q1 and Q2) refer to peptide-bound cells (CF fluorescence) and right-hand quadrants (Q2 and Q4) refer to *P*iRBC (Hoechst fluorescence). Q3 includes hRBC which were not internalized by fluorescently-labelled conjugate.

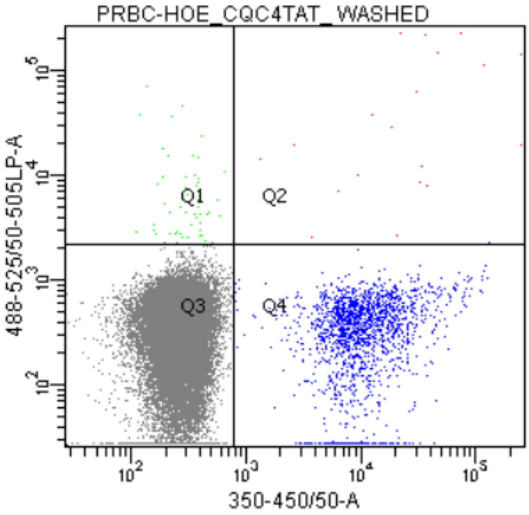

Figure 7.16 - FACS analysis of the interaction of inactive conjugate **65** with hRBC and *P*iRBC. Upper quadrants (Q1 and Q2) refer to peptide-bound cells (CF fluorescence) and right-hand quadrants (Q2 and Q4) refer to *P*iRBC (Hoechst fluorescence). Q3 includes hRBC which were not internalized by fluorescently-labelled conjugate.

Taken together, results from FACS analysis show that:

- binding of CQn-TP10 conjugate (**65**) to RBC (hRBC + *P*iRBC) is significantly higher than that of the parent peptide, TP10 (**64**);
- binding of conjugate **65** to *P*iRBC does not substantially differ from that of the parent peptide **64**;
- conjugate **66** does not appreciably bind to RBC.

From the above, it seems that the antimalarial action of both TP10 and, particularly, of its CQn conjugate **65**, is primarily driven by erythrocyte membrane destabilization leading to hemolysis, an effect that is significantly enhanced in the conjugate, but which does not significantly differentiate hRBC from *P*iRBC. Gathering these observations with results from Chapter 6, it seems clear that substantial differences in the interaction of TP10 with RBC cell membranes are induced upon conjugation to CQn. Still, CQn alone cannot account for the hemolytic and antimalarial properties of conjugate **65**, or else conjugate **64** would have displayed a similar behavior; instead, **65** was unable to internalize erythrocytes or disrupt their membranes, which is clearly correlated with its lack of antimalarial activity. Overall, it seems that TP10 and, more expressively, its CQn conjugate could owe their antimalarial effects to an antimicrobial peptide-like action, rather than to cell penetrating properties, *i.e.*, acting through disrupting erythrocytes and then binding to released parasites, eventually targeting their DNA.

7.4. Experimental procedures

7.4.1. Synthesis of TP10-K-CF

TP10-Lys (AGYLLGKINLKALAALAKKILK) was synthetized *via* SPPS, as described in Chapter 4. After resin preparation and deprotection, Fmoc-Lys(Mtt)-OH (5.0 eq) was coupled to the resin (1.0 eq), upon activation with HBTU (5.0 eq) and DIPEA (10.0 eq) in DMF. After this coupling and following Fmoc removal, the AA sequence was elongated through repetitive coupling/deprotection cycles. After complete coupling of the last AA - Fmoc-Ala-OH, and prior to its deprotection, Lysine's side chain PG (Mtt) was selectively removed with a solution of 1% TFA in DCM. This Deprotection generated a free ε-amine group of the additional *C*-terminal Lys, to which CF was coupled, upon activation with PyBOP (5.0 eq) and DIPEA (10.0 eq), in DMF. This reaction was kept for 2 hours, after which the resin was filtered and washed with DCM (3x) and DMF (3x), to render Fmoc-TP10-K-CF.

Crude TP10-Lys(CF) was obtained upon Fmoc removal of TP10's *N*-terminus and cleavage of the peptidyl resin with a solution of TFA (95%), TIS (2,5%) and water (2,5)%, as previously described (*cf* **4.4.6**), and was analyzed by LC-DAD/ESI-IT MS and purified by preparative HPLC, using a gradient elution of 20-50% ACN in water (0,05% TFA), in 1 hour. Fractions of pure peptide were freeze-dried.

Experimental data for TP10-Lys(CF) (**64**)

$^{m}/_{z}$ ($C_{131}H_{207}N_{29}O_{30}$, 2666.56 a.m.u.): 1334.93 ($[M+2H^+]^{2+}$); 890.60 ($[M+3H^+]^{3+}$); 668.47 ($[M+4H^+]^{4+}$); 535.00 ($[M+5H^+]^{5+}$)

Elution conditions: 0-100% ACN in water (0.05% TFA) in 30 minutes, at a flow rate of 1 mL/min.

R_t = 16.0 minutes

7.4.2. Synthesis of CQn-C4-CPP-K-CF

Fmoc-CPP-Lys(CF) was synthetized as previously reported (*cf.* **7.4.1**), with CPP being either TAT (RKKRRQRRRPPQ) or TP10 (AGYLLGKINLKALAALAKKIL). After coupling of CF, peptide's *N*-terminus was deprotected with a solution of 20% piperidine in DMF and CQn-C4 (**5**) (*cf* **4.4.2** and **4.4.3**) was coupled to the generated primary amine, upon activation with PyBOP (5.0 eq) and DIPEA (10.0 eq), in DMF. This reaction was kept overnight, after which the resin was filtered and thoroughly washed with DCM (3x) and DMF (3x).

Crude CQn-C4-CPP-Lys(CF) were obtained after cleavage of the peptidyl resins with a solution of TFA (95%), TIS (2,5%) and water (2,5)% (*cf* **4.4.6**); the peptides were finally analyzed by LC-DAD/ESI-IT MS and purified by preparative HPLC, using a gradient elution of 20-50% ACN in water (0,05% TFA), in 1 hour. Fractions of pure conjugates were freeze-dried.

Experimental data for CQn-C4-TP10-Lys(CF) (**65**)

$^{m}/_{z}$ ($C_{148}H_{225}ClN_{32}O_{32}$, 2997.67 a.m.u.): 1500.00 ($[M+2H^{+}]^{2+}$); 1000.8 ($[M+3H^{+}]^{3+}$); 751.00 ($[M+4H^{+}]^{4+}$); 601.13 ($[M+5H^{+}]^{5+}$).

Elution conditions: 0-100% ACN in water (0.05% TFA) in 30 minutes, at a flow rate of 1 mL/min.

R_t = 16.4 minutes

Experimental data for CQn-C4-TP10-Lys(CF) (**66**)

$^{m}/_{z}$ ($C_{114}H_{172}ClN_{41}O_{24}$, 2534.32 a.m.u.): 844.73 ($[M+3H^{+}]^{3+}$); 633.80 ($[M+4H^{+}]^{4+}$); 507.40 ($[M+5H^{+}]^{5+}$); 423.00 ($[M+6H^{+}]^{6+}$).

Elution conditions: 0-100% ACN in water (0.05% TFA) in 30 minutes.

TR = 15.7 minutes

7.4.3. Fluorescence microscopy

RBC suspensions (3% Htc, 3% Parasitemia) were incubated for 1 hour with CF-labelled TP10 and CQn-C4-TP10 (to a final concentration of 8 µM), at 37ºC. After incubation, cells were washed twice with culture medium and finally resuspended in a solution of 2 µg/mL of Hoescht 33342 in culture medium, in order to stain *P*iRBC nuclei. Cells were then diluted to 0.1 % Htc in RPMI and finally deposited onto a Lab-TekTM chambered coverglass slide. Microscopic analysis was performed with an Olympus IX51 inverted system microscope, equipped with an IX2-SFR X-Y stage, a U-TVIX-2 camera and a fluorescence mirror unit cassette for UV/blue/green excitation and detection of the corresponding blue/green/red emission ranges.

7.4.4. FACS analysis

FACS analysis was used to determine the targeting efficiency of TP10 and CQ-C4-CPP conjugates towards an unsynchronized *P. falciparum* 3D7 culture. To this end, parasitemia was adjusted to approximately 3% and the culture was incubated for 1 hour at 37°C in the presence of CF-labelled TP10 and CQn-C4-TP10 (8 µM). After incubation, these suspensions were washed twice with RPMI complete medium and finally resuspended in a solution of 2 µg/mL of Hoescht 33342 in RPMI, in order to stain *P*iRBC nuclei. Samples were finally diluted in PBS to a final concentration of 1 to 10 × 10^6 cells/mL, prior to analysis in a BD LSRFortessa cell analyzer (Becton, Dickinson and Company, New Jersey, USA). Forward- and side-scatter areas (FSC-A, SSC-A) in a linear scale were used to gate the RBC population and *P*iRBC stained with Hoescht 33342 were detected by excitation through a 350 nm laser and emission collection with a 450/50 nm bandpass filter in a logarithmic scale. RBC targeted by CF-labelled test compounds were detected by excitation through a 488 nm laser and emission collection with a 525/50 nm bandpass filter in a logarithmic scale.

7.5. Bibliography

1. M. J. Sanderson, I. Smith, I. Parker and M. D. Bootman, *Cold Spring Harb. Protoc.*, 2014, **10**, doi:10.1101/pdb.top0717951043.
2. B. N. Giepmans, S. R. Adams, E. M. H. and T. R. Y., *Science*, 2006, **312**, 217–224.
3. R. M. Franklin, R. Brun and A. Grieder, *Z Parasitenkd*, 1986, **72**, 201–212.
4. V. L. Hale, J. M. Watermeyer, F. Hackett, G. Vizcay-barrena, C. Van Ooij and J. A. Thomas, *Proc. Natl. Acad. Sci.*, 2017, **114**, 3439–3444.
5. A. Adan, G. Alizada, Y. Kiraz, Y. Baran and A. Nalbant, *Crit. Rev. Biotechnol.*, 2017, **37**, 163–176.
6. M. J. Wilkerson, *Vet. Clin. North Am. Small Anim. Pract.*, 2012, **42**, 53–71.
7. M. G. Macey, *Flow Cytometry: Principles and Applications*, Humana Press, 1st edn., 2007.

8

Application of the cell penetrating peptide conjugation strategy to the liver-stage antimalarial drug primaquine

8.1. Overview

In order to investigate how would conjugation to CPP affect the antimalarial performance of drugs whose action is exerted on exoerythrocytic stages of infection, (**8.2.1**) PQ was conjugated to the *N*-terminus of selected CPP *via* a butanedioyl (C4) spacer, whose choice was based on our previous findings for CQn-CPP conjugates (*cf.* Chapter 4); to this end, the synthetic route depicted in Scheme 8.1 was applied, which required (**8.2.1.1**) previous synthesis of intermediate PQ-C4 (**67**, Scheme 8.1), and its subsequent (**8.2.1.2**) coupling on-resin to the selected CPP. Additionally, in order to compare the effect of attaching the drug to the CPP's *C*-terminus instead of the *N*-terminus, the (**8.2.2**) chemical synthesis of TP10-S-S-PQ conjugate was also carried out following the route depicted in Scheme 8.2, which required the previous synthesis of both (i) PQ-Cys (**8.2.2.1**), and (ii) TP10-Cys (**49**, *cf.* section **5.2.5.2**), for their subsequent conjugation *via* a disulfide bridge (**8.2.2.2**). Finally, (**8.3**) the antimalarial activity of all PQ-CPP constructs thus prepared was evaluated *in vitro* against liver-stage parasites of the *P. berghei* species, causative of rodent malaria. Results obtained are herein presented and discussed.

8.2. Chemical Synthesis

8.2.1. PQ-C4-CPP conjugates

The route devised for the chemical synthesis of the target PQ-C4-CPP conjugates is shown in Scheme 8.1, below.

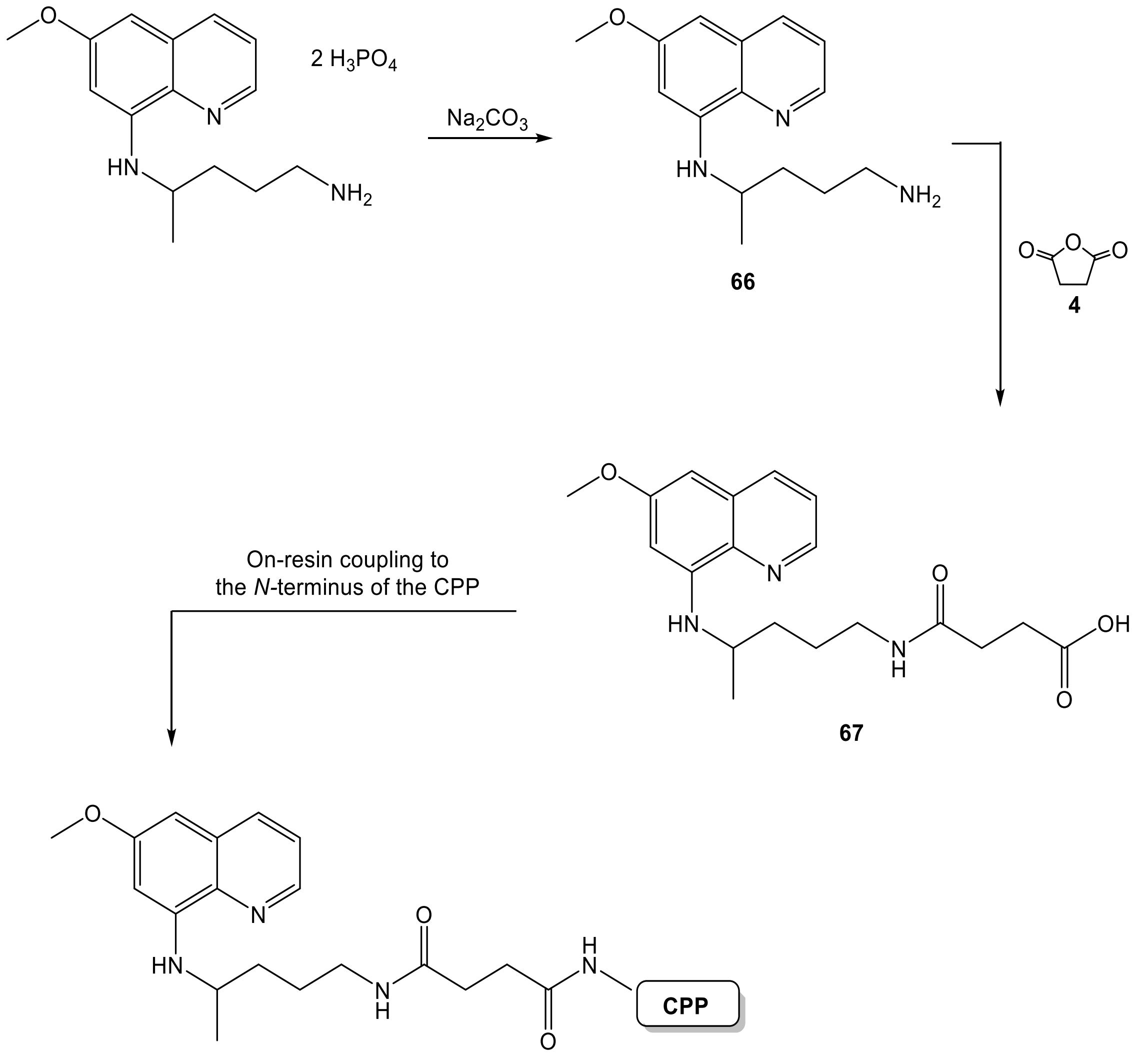
2 H_3PO_4
Na_2CO_3
66
4
67
On-resin coupling to the *N*-terminus of the CPP
CPP

Scheme 8.1 – Route employed for the chemical synthesis of PQ-C4-CPP conjugates.

8.2.1.1. *Synthesis of* N^4*-(6-methoxyquinolin-8-yl)pentane-1,4-diamine* (*PQ-C4)*

For the synthesis of the target PQ-CPP conjugates, intermediate PQ-C4 (**67**) had to be prepared beforehand. To this end, the commercially available bisphosphate salt of PQ was first neutralized with aqueous sodium carbonate, to afford the antimalarial drug in the free base (amine) form (**66**) in nearly quantitative yields (~95%). PQ (**66**) was next reacted with succinic anhydride (**4**) to produce the desired intermediate PQ-C4 (**67**), by methods similar to those previously applied for the synthesis of CQn-C4 (**5**, *cf.* Scheme 4.1 and section **4.2.4**). The addition-elimination (condensation) reaction evolved swiftly at room temperature, with an apparently clean formation of only the target product, as monitored by TLC. The crude product was submitted to liquid chromatography on a silica gel column, to ensure removal of any traces of succinic anhydride that would interfere with the following reactional step. PQ-C4 (**67**) was isolated in high yield (~ 85%), presenting correct spectral data, as follows. Figure 4.1 depicts the obtained mass spectrum (ESI-IT MS), which presents a peak at m/z = 360.93, which is compatible with the quasi-molecular ion (MH+) of PQ-C4, whose exact mass is 359.18 atomic mass units (a.m.u.).

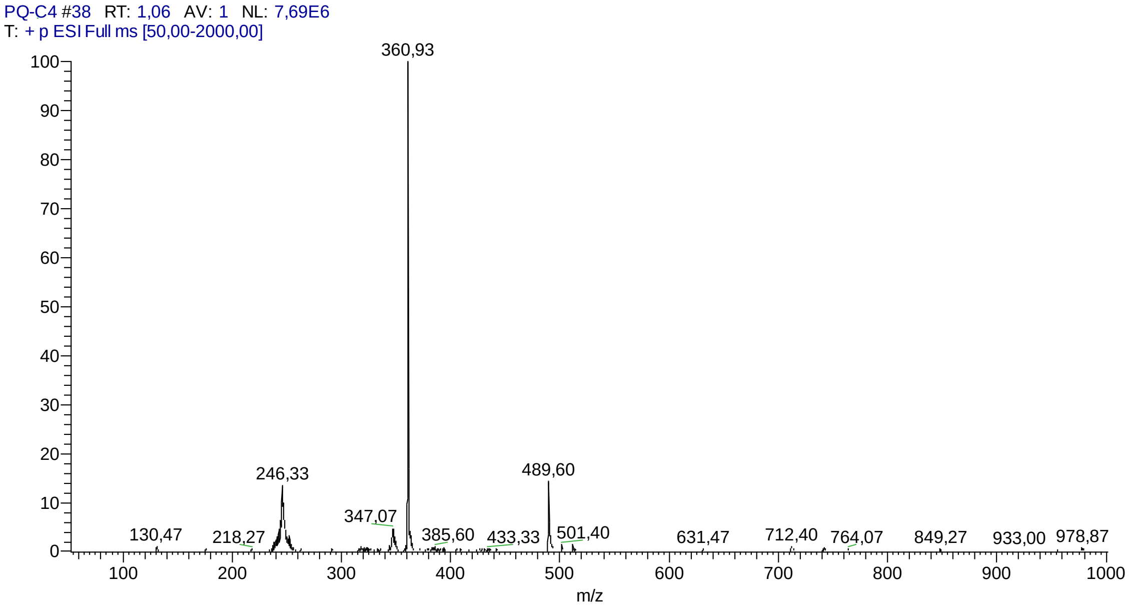

Figure 8.1 – ESI-IT MS spectrum (positive mode) of PQ-C4 (**67**).

8.2.1.2. Synthesis of the PQ-C4-CPP conjugates

For the synthesis of the PQ-C4-CPP conjugates, selected CPP shown in Table 8.1 were first synthesized by standard SPPS methods, as those described in Chapter 4 and 5. Compared to the set of CPP previously used for conjugation to CQn (*cf.* Chapter 4), this is a smaller one, as we opted to (i) keep only the minimal possible set still able to introduce size and net charge variations, to see how these might affect conjugates' activity, and (ii) exclude peptides whose previous choice had been based on their reported ability to specifically internalize *P*iRBC (DPT-sh1 and DPT-sh1), as this is not relevant for targeting exoerythrocytic forms of malaria parasites.

Once the CPP sequences were completed and the *N*$^{\square}$-protecting group (Fmoc) of the *N*-terminal amino acid removed, peptidyl-resins were split in two halves, one of which was stored for later cleavage to render the unmodified parent CPP, and the other was coupled to PQ-C4 (**67**), in the presence of PyBOP and DIPEA, as given in the Experimental Section.

Table 8.1 – CPP selected for conjugation to PQ.

CPP	Amino Acid Sequence	Molecular Weight	Net charge
TP10	AGYLLGKINLKALAALAKKIL	2181.40	+5
IDR-1018	VRLIVAVRIWRR	1535.99	+5
Tat	GRKKRRQRRRPPQ	1718.05	+9
PasTat	FFLIPKGGRKKRRQRRRPPQ	2520.53	+10
Transportan	GWTLNSAGYLLGKINLKALAALAKKIL	2839.71	+5

All peptidyl-resins obtained (*i.e.*, CPP-resins as well as PQ-C4-CPP resins) were next cleaved by a two-hour acidolysis with TFA-based cleavage cocktails, as described before (*cf.* Chapter 4). Briefly, for constructs with up to two Arg residues, a TFA/TIS/water (95:2.5:2.5 v/v/v) cocktail was used, whereas for those with more than two arginines, a TFA/thioanisole/ethane-1,2-dithiol/anisole (90:5:3:2 v/v/v/v) cocktail was preferred. Crude products were then submitted to purification and analysis as previously described in Chapter 4 and 5, with their structures and purity confirmed as adequate. Spectral and chromatographic traces of the synthetized CPP are depicted in Chapter 4; data collected on PQ-C4-CPP conjugates is summarized in Table 8.2 and detailed in the Experimental Section.

Table 8.2 – Synthesized PQ-C4-CPP and respective analytical data, obtained by HPLC (purity and retention time – R$_t$) and LC-DAD/ESI-IT MS (detected m/z).

CPP	Molecular Weight	Purity / %	R_t / minutes *	Detected $^m/_z$
PQ-C4-TP10	2522.27	99	17.0	1262.13 ($[M+2H^+]]^{2+}$); 841.87 ($[M+3H^+]^{3+}$); 631.60 ($[M+4H^+]^{4+}$);
PQ-C4-IDR-1018	1877.16	98	15.1	939.60 ($[M+2H^+]^{2+}$); 626.74 ($[M+3H^+]^{3+}$); 470.30 ($[M+4H^+]^{4+}$); 376.44 ($[M+5H^+]^{5+}$);
PQ-C4-Tat	2058.24	95	10.1	2059.27 ($[M+H^+]^+$)
PQ-C4-PasTat	2860.72	99	14.1	716.44 ($[M+4H^+]^{4+}$); 573.35 ($[M+5H^+]^{5+}$); 476.31 ($[M+6H^+]^{6+}$); 409.82 ($[M+7H^+]^{7+}$)
PQ-C4-Transportan	3180.88	99	18.4	1061.31 ($[M+3H^+]^{3+}$); 796.48 ($[M+4H^+]^{4+}$); 637.39 ($[M+5H^+]^{5+}$)

* Value determined by HPLC, with a gradient elution of 1-100% ACN in water (0.05% TFA), for 30 minutes, at a flow rate of 1 mL/min.

8.2.2. TP10-S-S-PQ conjugate

The route established for the chemical synthesis of TP10-S-S-PQ (**68**) is depicted on Scheme 8.2, displayed below.

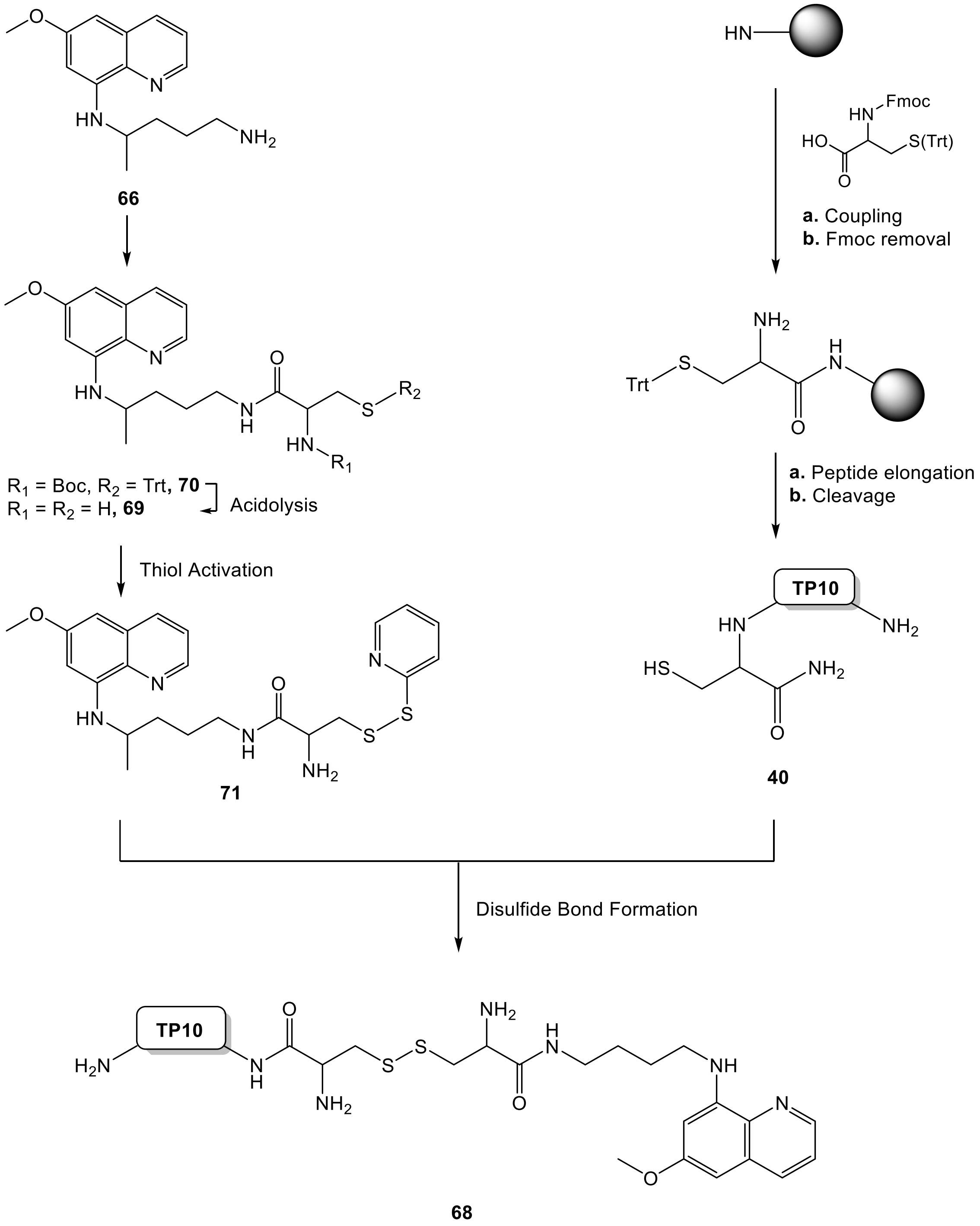
66
R$_1$ = Boc, R$_2$ = Trt, 70
R$_1$ = R$_2$ = H, 69
Acidolysis
Thiol Activation
71
HN-Fmoc
HO
S(Trt)
a. Coupling
b. Fmoc removal
Trt
a. Peptide elongation
b. Cleavage
TP10
40
Disulfide Bond Formation
68

Scheme 8.2 – route employed for the chemical synthesis of TP10-S-S-PQ (**68**).

The target conjugate was synthetized following a strategy identical to that employed for the synthesis of TP10-S-S-CQn (*cf.* **5.3.5**). Briefly, PQ (**66**) was coupled to Boc-Cys(Trt)-OH (**33**, *cf.* **5.2.3.2**), followed by removal of the *N*□-protecting group, to generate PQ-Cys (**69**). The thiol present in **69** was then activated by means of a reaction with dithiopyridine (**42**), prior to the formation of a disulfide bond with TP10-Cys (**40**), *via* a thiol-disulfide exchange (*cf.* **5.2.5**).

8.2.2.1. Synthesis of PQ-Cys (69)

For the introduction of a thiol group in PQ's core (**66**), this drug was coupled to the protected cysteine derivative Boc-Cys(Trt)-OH (**33**), in the presence of suitable coupling agents (HBTU and DIPEA as the auxiliary base), using DMF as solvent. After purification through liquid column chromatography – using silica gel as stationary phase and a mixture of DCM/MeOH (15:1 v/v) as eluent, the chromatographically homogeneous (TLC) protected intermediate (**70**) was obtained in a moderate yield (57%). ESI-IT MS analysis of the isolated product (Figure 8.2) was compatible with the structure of the target compound, **70**, whose exact mass is 704.34 a.m.u..

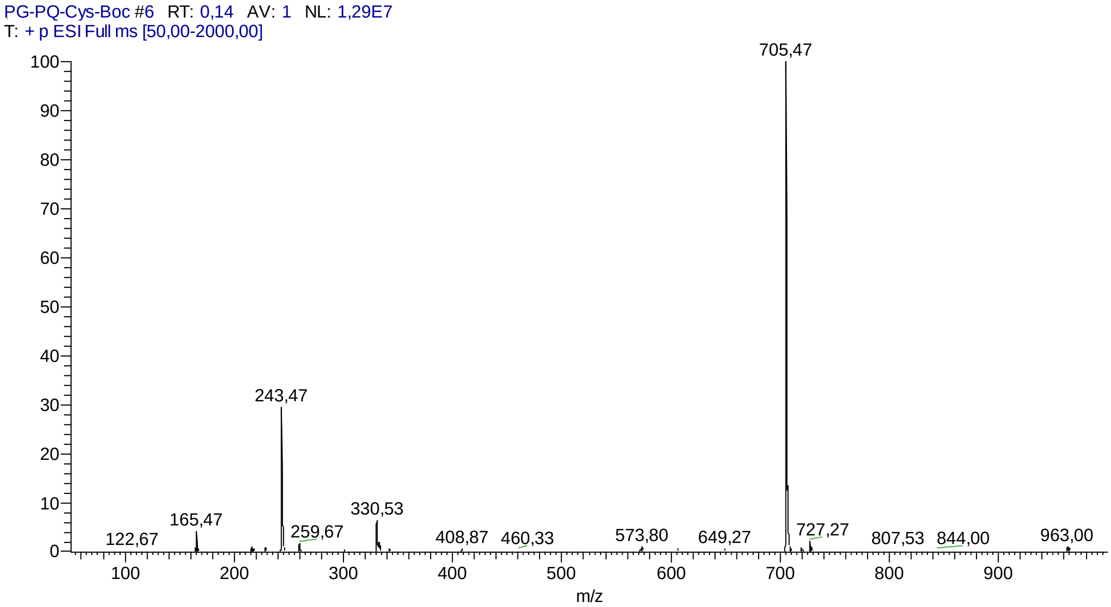

Figure 8.2 – ESI-IT MS spectrum (positive mode) of **70**.

Removal of the amine and thiol protecting groups (Boc and Trt, respectively) from **69** was carried out by direct dissolution in a TFA-based cleavage cocktail (95% TFA, 2.5% TIS and 2.5% water), and the acidolysis was run for 1 hour in an ice-water bath. After convenient work-up of the reaction mixture, the target PQ-Cys intermediate (**69**) was obtained in high yield (79%), as a chromatographically homogeneous (TLC) yellow oil. The structure of this intermediate, whose exact mass is 362.18 a.m.u., was confirmed by ESI-IT MS. The spectrum obtained for crude PQ-Cys (Figure 8.3) shows a peek at $^m/_z$ = 363.13, which is compatible with the quasi-molecular ion (MH^+) of this molecule.

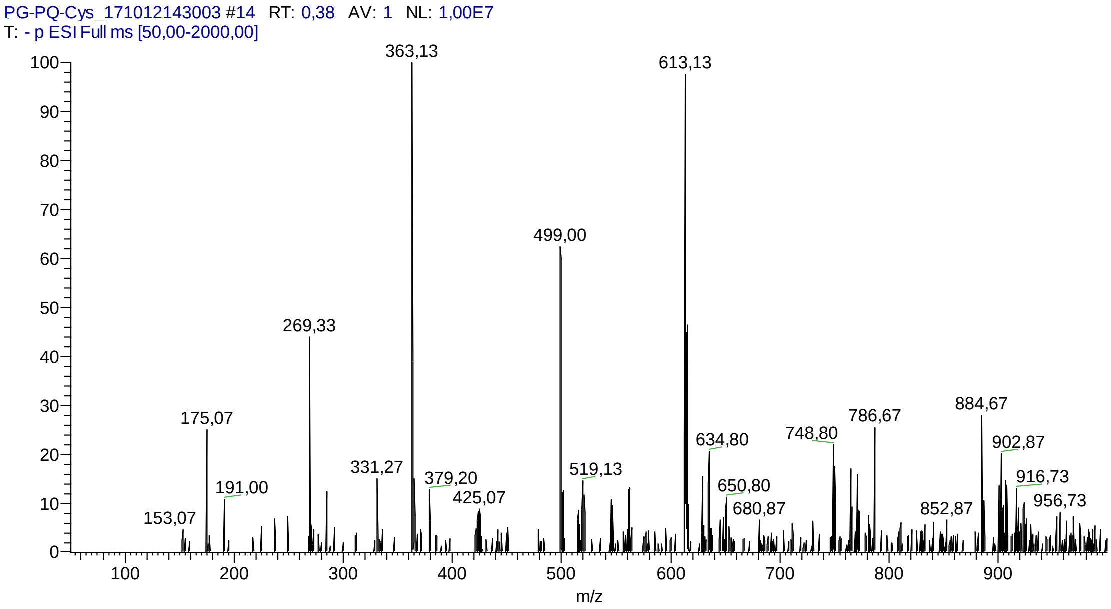

Figure 8.3 – ESI-IT MS spectrum (positive mode) of PQ-Cys (**69**).

8.2.2.2. Synthesis of PQ-Cys(TP) (71)

Activation of the thiol group of PQ-Cys (**69**) was achieved by following the procedure employed for the activation of CQn-Cys (**34**, *cf* **5.2.5.1**). PQ-Cys (**69**) was reacted with 2,2'-dithiodipyridine (**42**) *via* a TDER in a solution of anhydrous methanol containing glacial acetic acid, to produce the activated intermediate PQ-Cys-TP (**71**). Isolation of **71** was carried out *via* liquid column chromatography, to render this compound as a chromatographically homogeneous (TLC) yellow oil in a good yield (64%). Its analysis by ESI-IT MS confirmed the achievement of the desired structure (Figure 2.4). The obtained spectrum reveals a main peak, correspondent to quasi-molecular ion (MH^+) of PQ-Cys-TP (**71**), whose exact mass is 471.18 a.m.u..

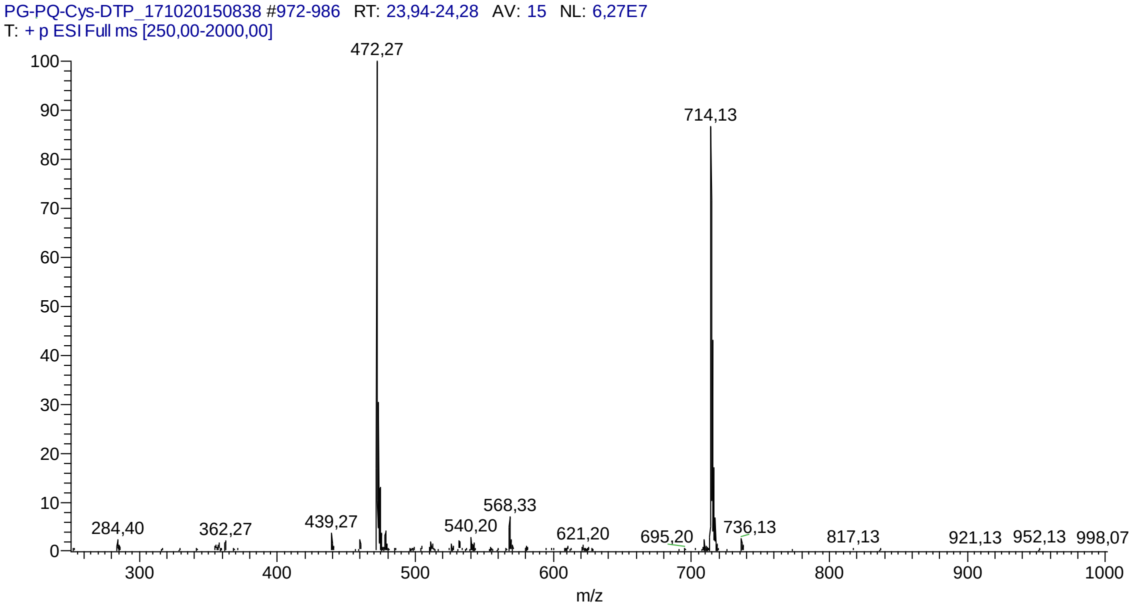

Figure 8.4 – ESI-IT MS spectrum (positive mode) of PQ-Cys(TP) (**71**).

8.2.2.3. Synthesis of the target TP10-S-S-PQ conjugate (68) via a TDER

For the synthesis of TP10-S-S-PQ, TP10-Cys (**40**) was first assembled *via* SPPS, cleaved, purified, and analyzed as explained before (*cf.* **5.2.5.2.**). The pure peptide was then mixed with PQ-Cys(TP) (**71**) in a solution of acetic acid (1 *M*) and the TDER allowed to proceed for 48 hours at room temperature. Reaction progress was monitored by HPLC and the target TP10-S-S-PQ conjugate (**70**) finally isolated in 93% purity upon purification by preparative HPLC, as previously described for its CQn analogue, TP10-S-S-CQn (**19**, *cf.* **5.2.5.2**). Chromatographic and spectral traces for the target conjugate are shown below. Figure 8.6 shows the obtained mass spectrum for TP10-S-S-PQ, which presents four main peaks, correspondent to different protonation states of TP10-S-S-PQ (Table 8.3).

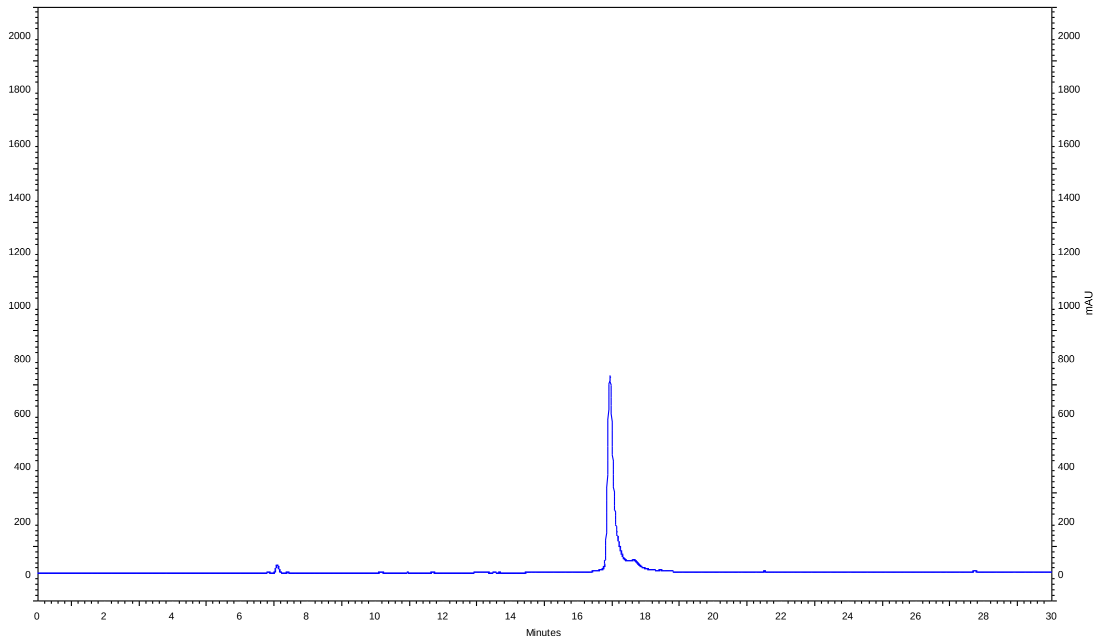

Figure 8.5 - Chromatogram obtained from the analysis of TP10-S-S-PQ (**68**) after purification, with a gradient elution of 0-100% ACN in water (0.05% TFA) in a RP-18E (5 µm), for 30 minutes and a flow of 1 ml/min, with detection at λ = 220 nm.

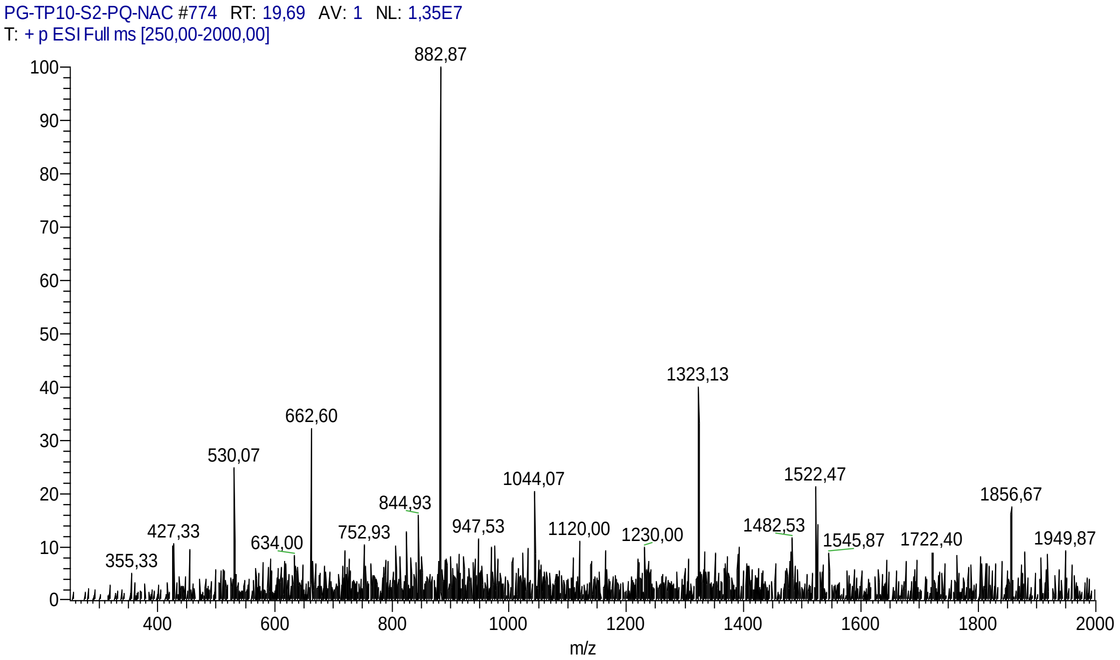

Figure 8.6 – ESI-IT MS spectrum (positive mode) of TP10-S-S-PQ (**68**).

Table 8.3 – Adducts of the peptide TP10-S-S-PQ (P), detected by ESI-IT MS.

Adduct	**Expected $^{m}/_{z}$**	**Detected $^{m}/_{z}$**
P + 2H$^+$	1323.30	1323.13
P + 3H$^+$	882.53	882.87
P + 4H$^+$	662.15	662.60
P + 5H$^+$	529.92	530.07

8.3. *In vitro* assays

All PQ-CPP conjugates prepared and their respective parent peptides were screened for their ability to inhibit *in vitro* hepatic infection by rodent *P. berghei* parasites at 1, 5 and 10 µM. Parasite load was assessed by luminescence measurements in lysates of human hepatocellular carcinoma cells (Huh-7) infected 48 h earlier with sporozoites of a firefly luciferase-expressing *P. berghei* parasite line[1], using PQ as the reference drug. These assays were carried out in the Miguel Prudêncio Lab, at IMM Lisboa - Instituto de Medicina Molecular João Lobo Antunes.

Results obtained (Figure 8.7) show that all the test compounds, with the exception of TP10-S-S-PQ, were non-cytotoxic, as they did not affect confluency of Huh-7 cells at any of the concentrations employed. Interestingly, this correlates with the higher hemolytic activity observed for CQn-TP10 conjugates where the drug was coupled to the peptide's *C*-terminus (*cf.* **5.3**), which suggests that, as a rule, *C*-terminal attachment of antimalarial aminoquinolines to TP10 leads to increased toxicity to host cells, irrespectively of specific cell type or aminoquinoline used.

Generally, unconjugated CPP ranged from inactive (IDR-1018, Transportan) or poorly active (TAT, PasTAT), to moderately active (TP10) against liver-stage *P. berghei* parasites; still, TP10 activity was slightly less active than the parent drug, PQ. Relevantly, PQ conjugation to either TP10 or Transportan resulted in significantly improved activity, even when compared to reference PQ. Once again, these findings correlate with those made for CQn-C4-CPP conjugates (*cf.* Chapter 4), where the only conjugates with discernible antimalarial activity were those where the CPP used was either TP10 or Transportan. Hence, it appears that, at least for CPP-aminoquinoline conjugates, the specific amino acid sequence of the peptide, rather than its cell penetrating properties, is relevant for the display of antimalarial activity. This agrees with the observation that CPP size or net charge do not seem key factors for antimalarial activity, since (i) PQ-C4-TP10 and PQ-C4-Transportan showed similar activities, despite their different size; (ii) PQ-C4-IDR1018 was inactive, despite having the same net charge as TP10, and (iii)

TAT and PasTAT, as well as their corresponding PQ conjugates, did not dramatically differ from each other, despite their quite different molecular weights.

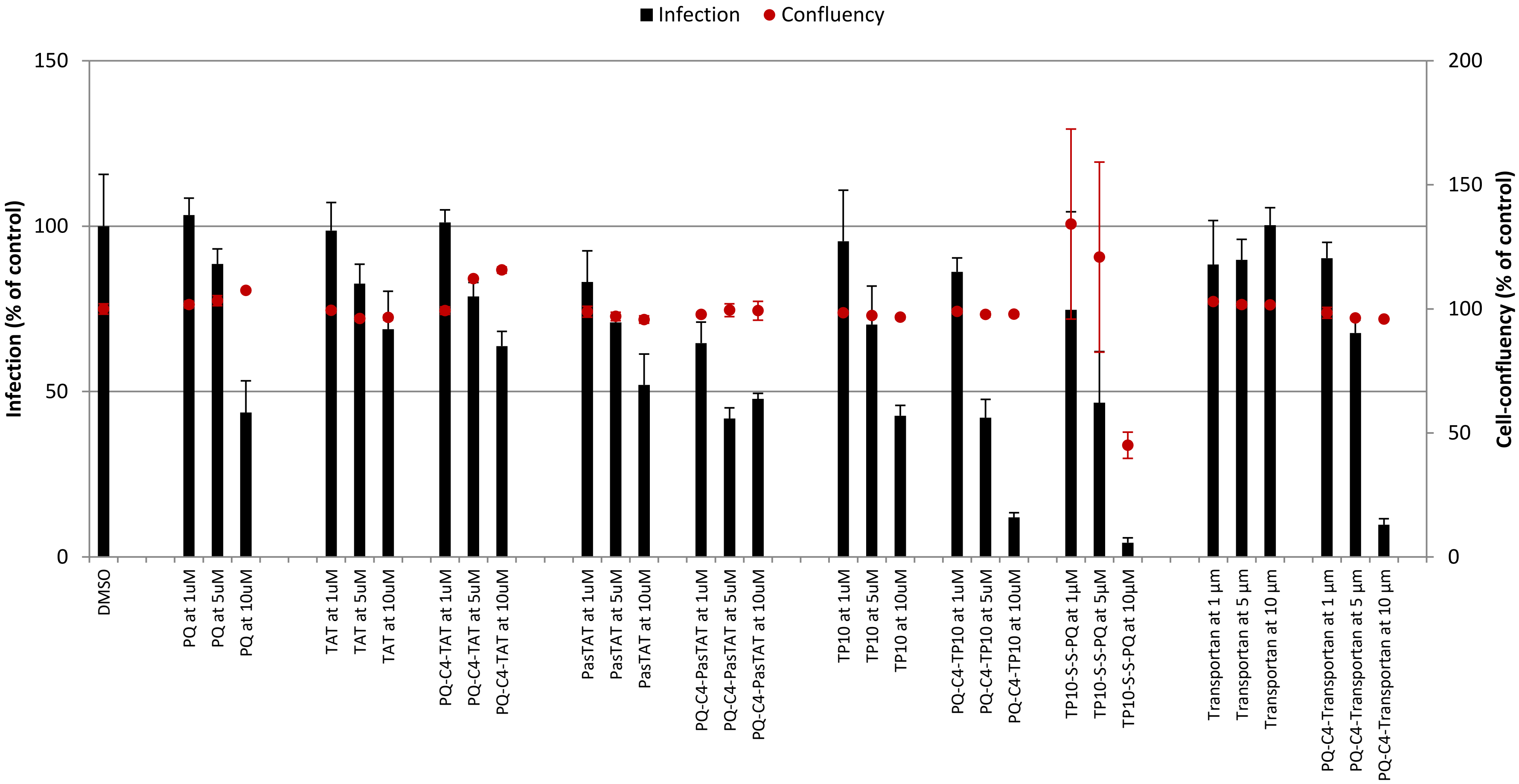

Figure 8.7 - *In vitro* screening of the activity of the selected CPP and their respective PQ-C4-CPP conjugates against liver-stage *P. berghei* parasites, according to a previously reported method[1]. Infection burden (bars) and host cell confluency (dots) are expressed as % of control. The compounds were assayed at 1, 5 and 10 µM, and PQ was included as the reference parent drug, for comparison.

8.4. Experimental Section

8.4.1. Materials, instrumentation and general methods

For the chemical synthesis, materials, instrumentation and general methods were previously described in Chapter 4 (*cf.* **4.4.1**).

8.4.2. Extraction of Primaquine

Primaquine bisphosphate was dissolved in an aqueous solution of $NaHCO_3$ (25 mL). The mixture was stirred for 10 minutes, after which it was washed with 45 mL of DCM (3 x 15 mL). The organic phase was then dried with anhydrous Na_2SO_4 and, after filtration, DCM was evaporated under reduced pressure. The resulting yellow oil was chromatographically homogeneous, which was confirmed by ESI-IT MS.

8.4.3. Derivatization of PQ with succinic anhydride

1.2 eq of PQ (**66**) and 1.0 eq of succinic anhydride (**4**) were dissolved in minimum amount of DMF, in the presence of DIPEA (1.2 eq) and the mixture was left stirring for 2 hours, at room temperature. In order to isolate the desired products, the mixture was diluted in DCM/Methanol (MeOH; 3:1) and purified *via* silica gel column chromatography, using the previous mixture of DMC and MeOH as eluent. PQ-C4 (**67**) rendered a yellow oil, which was characterized by ESI-IT MS.

Experimental data for PQ-C4 (**67**)

R_f (DCM/MeOH 5:1 (v/v)): 0.68

$^m/_z$ ($C_{15}H_{21}N_3O$, 359.18 a.m.u.):.360.93 ($[M+H^+]^+$).

8.4.4. Peptides' synthesis

Experimental procedures employed for the synthesis of peptides has already been described (*cf.* **4.4.4**).

8.4.5. Modification of peptides’ *N*-terminus with PQ-C4

After completion of the peptide chain – up until the deprotection of the last amino acid, the resin was divided in two parts - either for direct cleavage, leading to the free peptide, of for *N*-terminal modification with PQ-C4, to render PQ-C4-CPP conjugates.

For the synthesis of PQ-C4-CPP conjugates, a solution of 5.0 eq of PQ-C4, 5.0 eq of PyBOP and 10.0 eq of DIPEA in DMF was added to the peptidyl-resin and the mixture was left stirring overnight. The resin was then filtered and washed with DMF (3 mL, 3 x 1’) and DCM (3 mL, 3 x 1’). Upon a negative result of the Kaiser test, the final CPP and PQ-C4-CPP were cleaved.

8.4.6. Peptides and PQ-C4-CPP conjugates’ cleavage

Cleavage cocktails were prepared (either 95% TFA, 2.5% TIS and 2.5% H_2O or 90% TFA, 5% thioanisole, 3% 1,2-etanedithiol and 2% anisole). Dried peptidyl-resin was placed in a 45 mL falcon tube and cocktail cleavage was added (in a proportion of 1 mL to 100 mg of resin); the mixture was left in continuous stirring for 2 hours. After this time, the resin was filtered under reduced pressure, using a D4 porous plate funnel and the filtrated solution –containing the soluble peptide, was distributed through 15 mL falcon tubes (2 mL per tube). Each tube was then filled with dried diethyl ether, in order to precipitate the peptide and, after a few minutes in the freezer, the mixture was centrifuged and the supernatant decanted to a flask with a stopper. This addition of dried diethyl ether followed by centrifuging was repeated three more times, after which the tubes were placed in an desiccator. The supernatant solution was discarded

After drying, the peptide was dissolved in an aqueous solution of acetic acid (10%) and analyzed by HPLC and LC/MS/DAD. Peptides and AM-CPP conjugates were purified through preparative HPLC and, after purification, fractions containing the isolated product were combined, frozen and, finally, lyophilized. Spectral data related to the synthetized CPP is presented in Chapter 4.

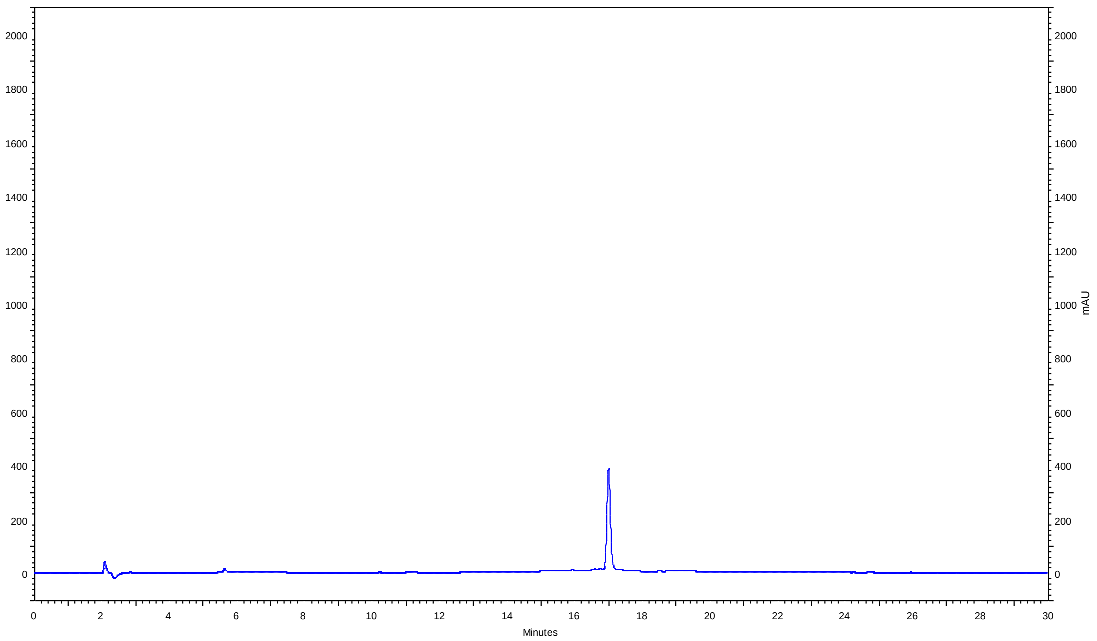

Figure 8.8 – Chromatogram obtained from the analysis of PQ-C4-TP10 after purification, with a gradient elution of 0-100% ACN in water (0,05% TFA) in a RP-18E (5 µm), for 30 minutes and a flow of 1 ml/min, with detection at λ = 220 nm.

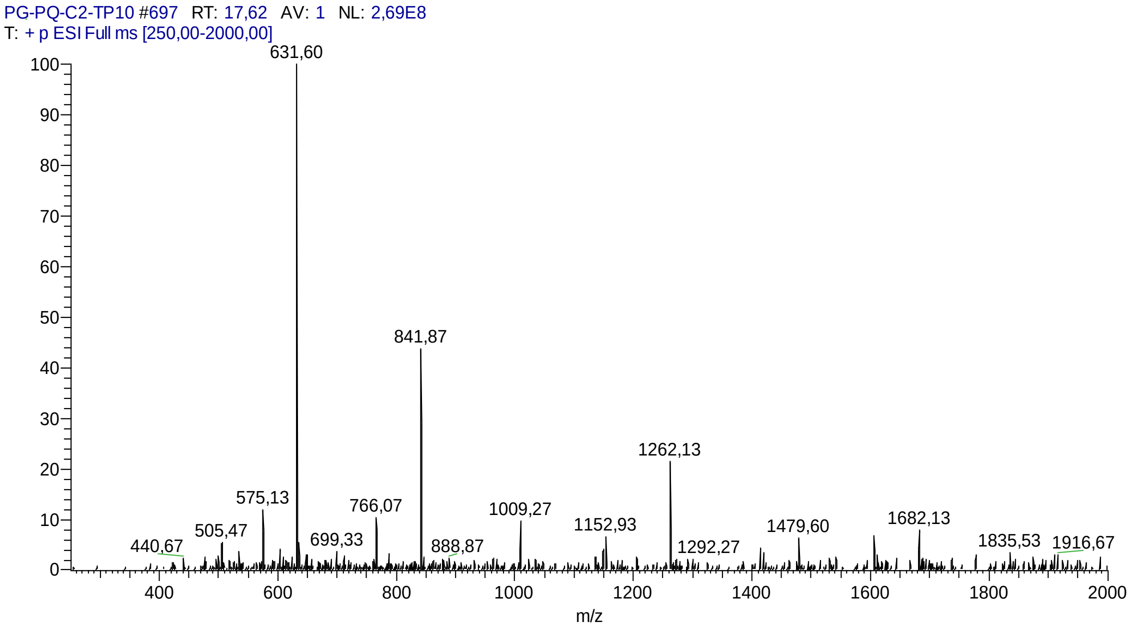

Figure 8.9 – ESI-IT MS spectrum (positive mode) of PQ-C4-TP10.

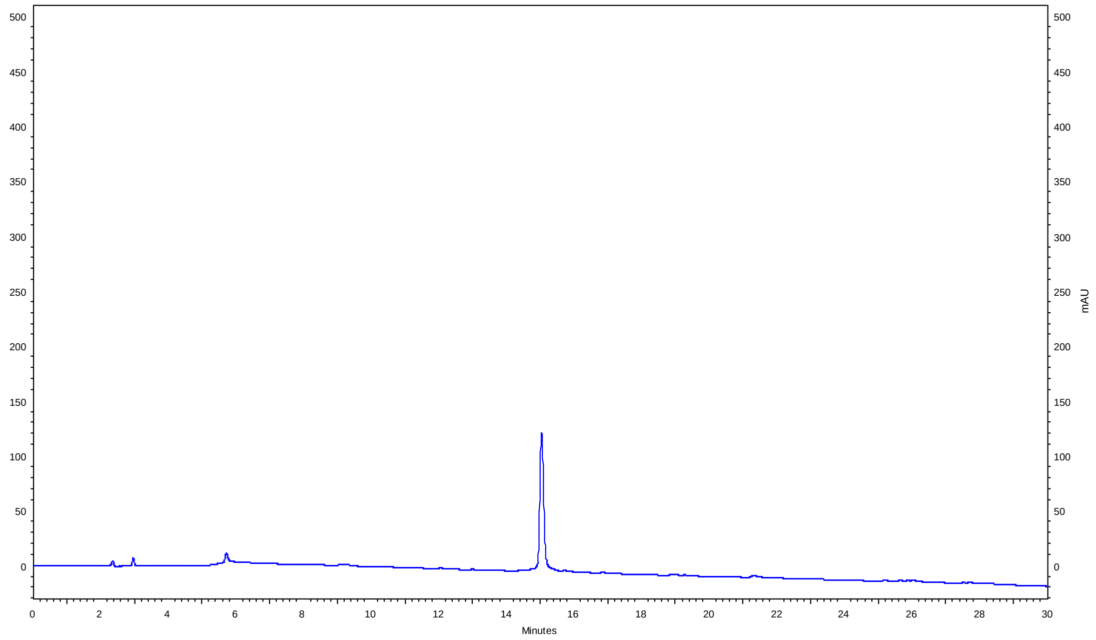

Figure 8.10 – Chromatogram obtained from the analysis of PQ-C4-IDR-1018 after purification, with a gradient elution of 0-100% ACN in water (0,05% TFA) in a RP-18E (5 µm), for 30 minutes and a flow of 1 ml/min, with detection at λ = 220 nm.

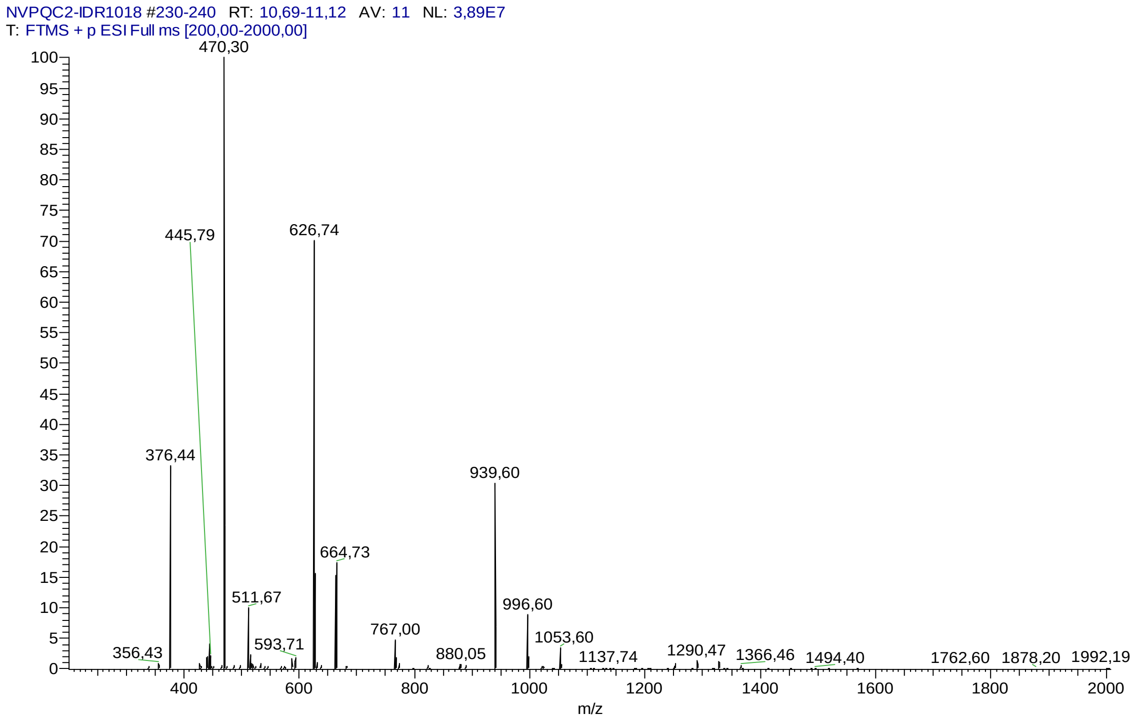

Figure 8.11 – ESI-IT MS spectrum (positive mode) of PQ-C4-IDR-1018.

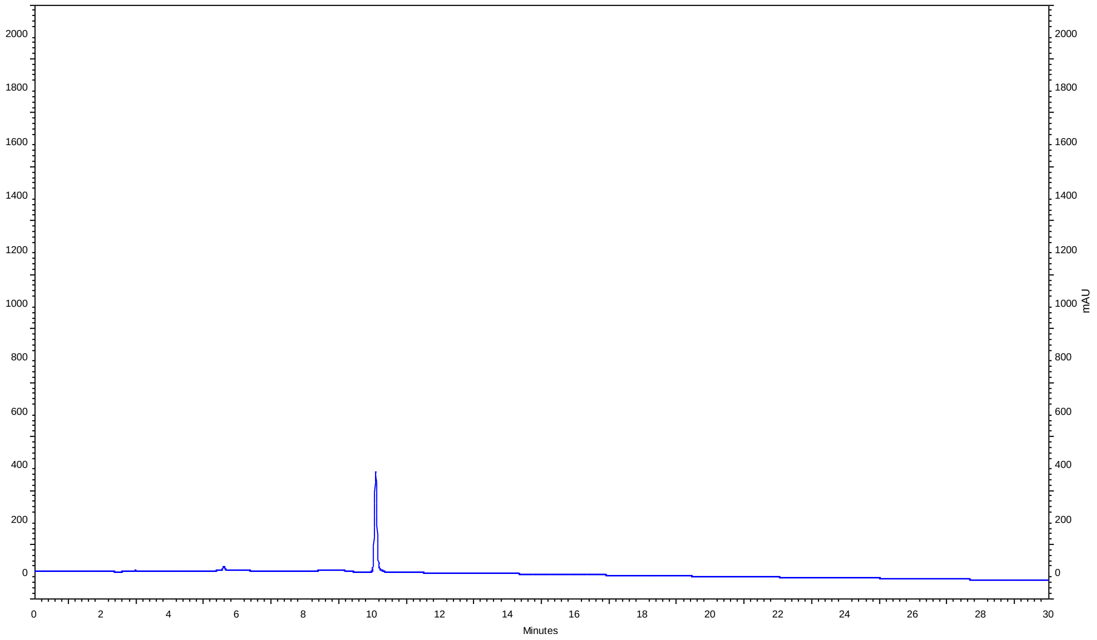

Figure 8.12 – Chromatogram obtained from the analysis of PQ-C4-TAT after purification, with a gradient elution of 0-100% ACN in water (0,05% TFA) in a RP-18E (5 µm), for 30 minutes and a flow of 1 ml/min, with detection at λ = 220 nm.

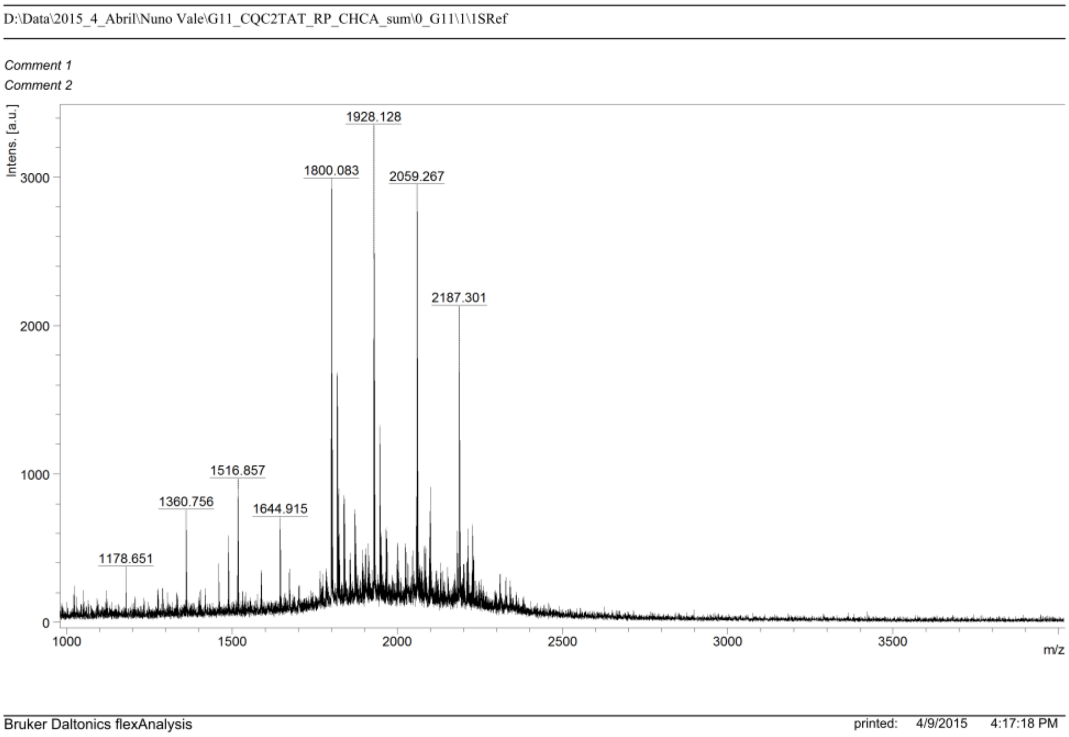
D:\Data\2015_4_Abril\Nuno Vale\G11_CQC2TAT_RP_CHCA_sum\0_G11\1\1SRef

Comment 1
Comment 2

Bruker Daltonics flexAnalysis printed: 4/9/2015 4:17:18 PM

Figure 8.13 – ESI-IT MS spectrum (positive mode) of PQ-C4-TAT.

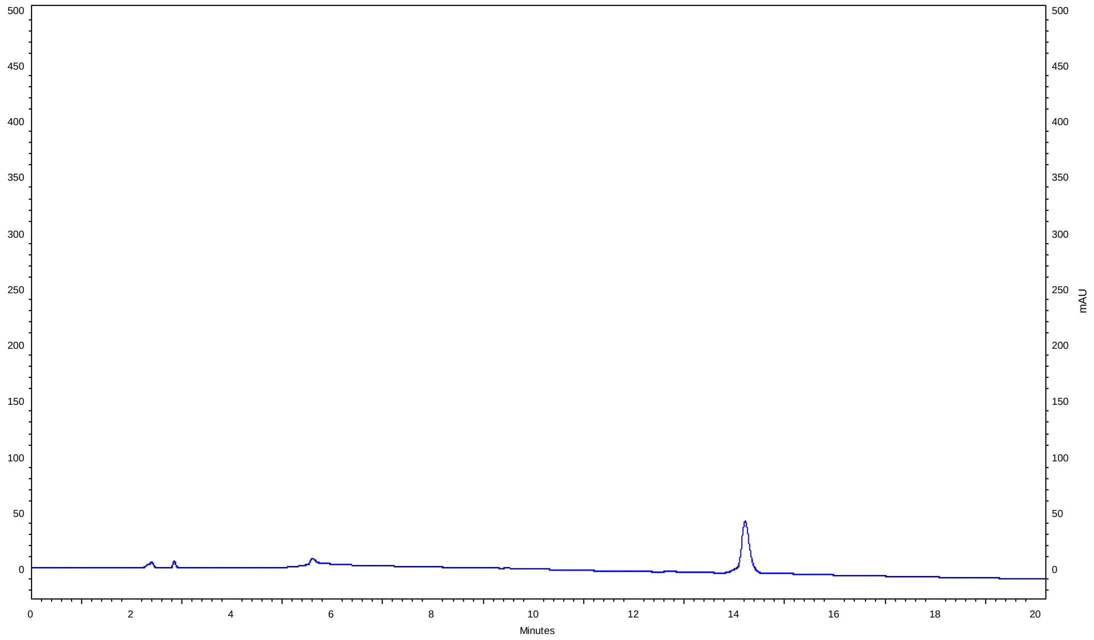

Figure 8.14 – Chromatogram obtained from the analysis of PQ-C4-PasTAT after purification, with a gradient elution of 0-66% ACN in water (0,05% TFA) in a RP-18E (5 μm), for 20 minutes and a flow of 1 ml/min, with detection at λ = 220 nm.

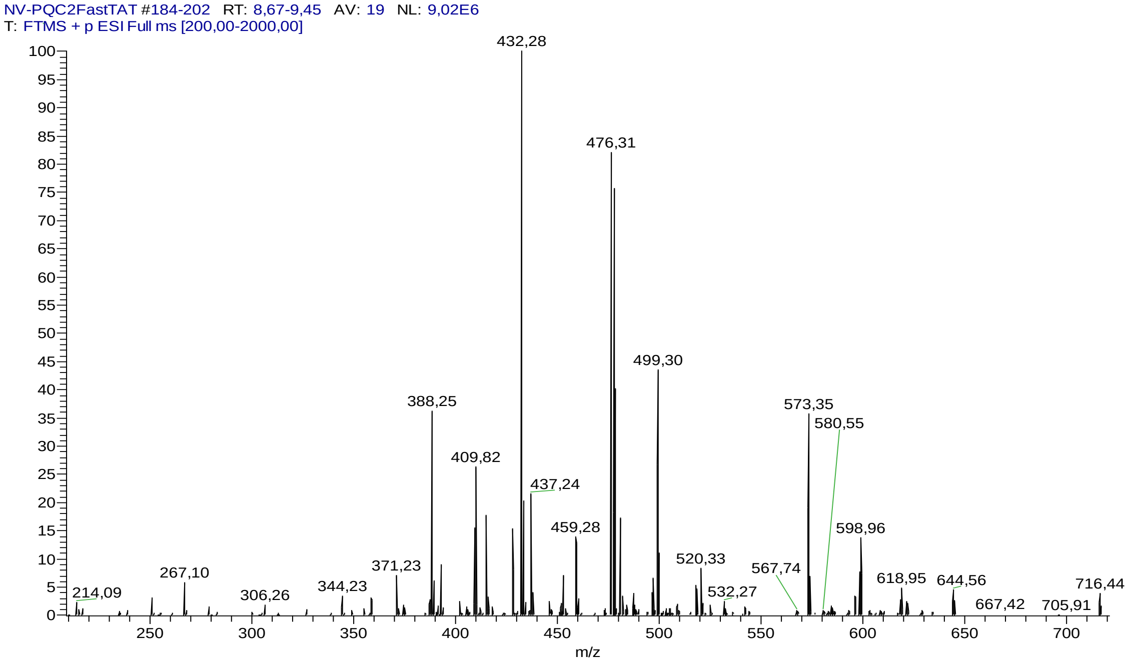

Figure 8.15 – ESI-IT MS spectrum (positive mode) of PQ-C4-PasTAT.

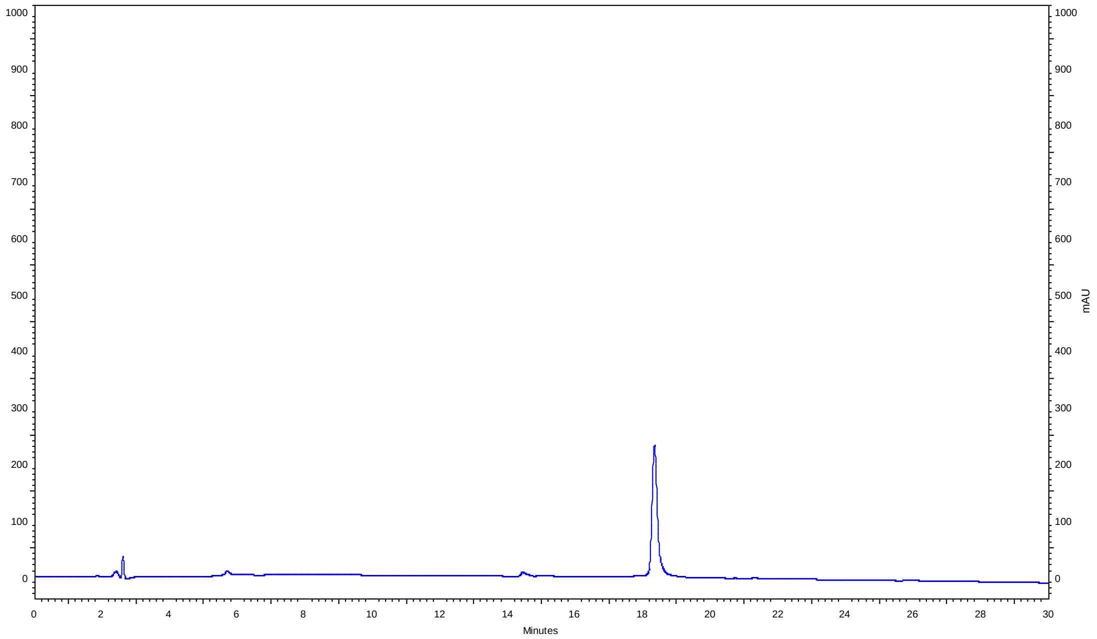

Figure 8.16 – Chromatogram obtained from the analysis of PQ-C4-Transportan after purification, with a gradient elution of 0-66% ACN in water (0,05% TFA) in a RP-18E (5 μm), for 20 minutes and a flow of 1 ml/min, with detection at λ = 220 nm.

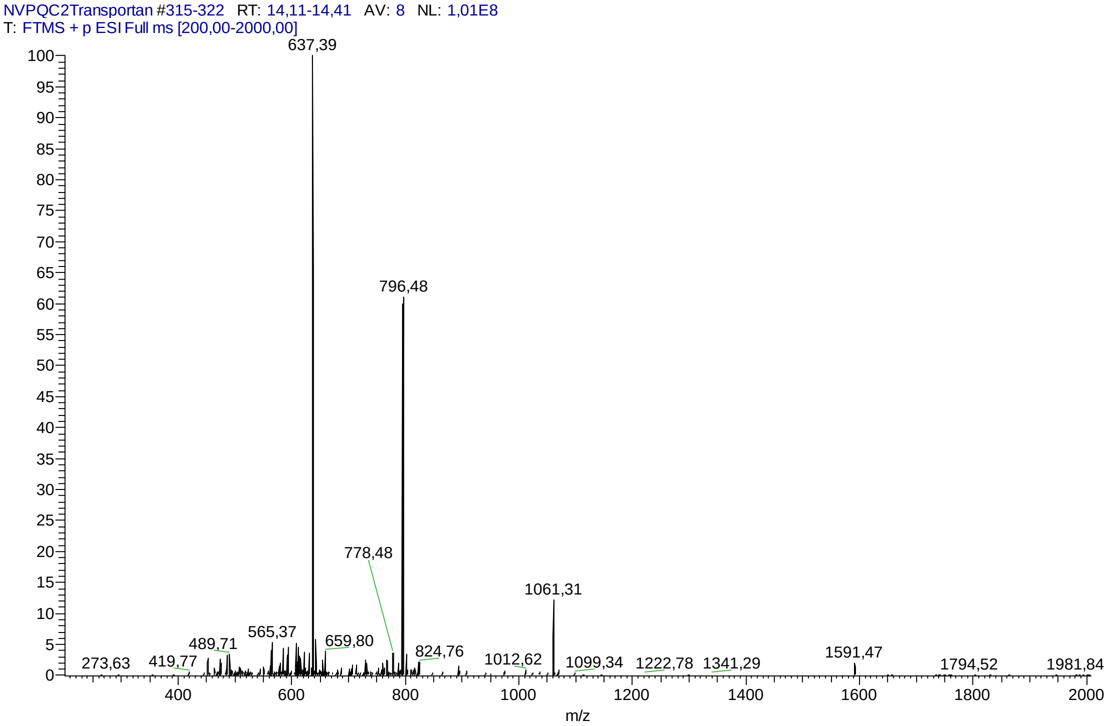

Figure 8.17 – ESI-IT MS spectrum (positive mode) of PQ-C4-Transportan.

8.4.7. Synthesis of TP10-S-S-PQ

Boc-Cys(Trt)-OH (1.2 eq) was activated with HBTU (1.2 eq) in the presence of DIPEA (2.4 eq). These reactants were dissolved in DMF, and the mixture was put in an ice-water bath, for 30 minutes. After this time, PQ (1.0 eq) was added to the reaction, which was left in the ice-water bath for 3 more hours. After this time the mixture was diluted in ethyl acetate (20 mL) and extracted with an aqueous solution of 5% Na_2CO_3 (15 mL, x3). The organic phase was then dried with anhydrous Na_2SO_4 and, after filtration, ethyl acetate was evaporated under reduced pressure. The resulting mixture was then purified via silica gel column chromatography, using DCM/MeOH (15:1) as eluent, to obtain PQ-Boc-Cys(Trt) (**70**) in high purity. Isolated PQ-Boc-Cys(Trt) was characterized by ESI-IT MS.

Experimental data for PQ-Boc-Cys(Trt) (**70**)

R_f (DCM/MeOH 15:1 (v/v)): 0.47

$^m/_z$ ($C_{42}H_{48}N_4O_4S$; 704.34 a.m.u.): 705.47 ($[M+H^+]^+$).

Then, in order to remove cysteine's PG – Boc and Trt, PQ-Boc-Cys(Trt) was dissolved in TFA-based cleavage cocktail (95% TFA, 2.5% TIS and 2.5% water) and the mixture was placed in an ice-water bath for 1 hour. After this time, the reaction mixture was distributed by 15 mL Falcons (1 mL/tube) and the volume of each tube was completed with cold diethyl ether, to precipitate PQ-Cys. The tubes were then centrifuged and the addition of dried diethyl ether followed by centrifuging was repeated three more times, after which the tubes were placed in a desiccator. The supernatant solutions were discarded. Final PQ-Cys was characterized by ESI-IT MS.

Experimental data for PQ-Cys (**69**)

R_f (DCM/MeOH 15:1 (v/v)): 0.05

$^m/_z$ ($C_{18}H_{26}N_4O_2S$; 362.18 a.m.u.): 363.13 ($[M+H^+]^+$).

For thiol activation, PQ-Cys (**69**, 1.0 eq) and 2,2'-dithiodipyridine (**42**, 2.0 eq) were dissolved in anhydrous methanol (4 mL) containing glacial acetic acid (0.3 eq). The mixture was stirred at room temperature for 18 h and the solvent was removed under reduced pressure to obtain the crude product. The crude product was purified by flash chromatography using at first a mixture of DCM/MeOH (10:1) and then, after removal of thiopyridine, a more polar mixture of DCM/MeOH (1:1), to render PQ-Cys-TP (**71**) in high purity.

Experimental data for PQ-Cys-TP (**71**)

R_f (DCM/MeOH 10:1 (v/v)): 0.36

$^{m}/_{z}$ ($C_{23}H_{29}N_5O_2S_2$; 471.18 a.m.u.): 472.27 ($[M+H^+]^+$).

TP10-C (AGYLLGKINLKALAALAKKILC) was synthetized *via* SPPS and immediately cleaved (*cf.* **4.4.4** and **4.4.6**).

Thiol-disulfide exchange between TP10-Cys (1.0 eq) and "activated" PQ-Cys(TP) (1.2 eq) was carried out in a solution of acetic acid (1M), for 48 hours, at room temperature. This reaction was monitored by HPLC, with a gradient elution of 1-100% ACN in water (0.05% TFA), and by LC/MS/DAD. TP10-S-S-PQ was finally purified by preparative HPLC, with the elution of 20-40 for 1 hour. Fractions of pure conjugate were freeze-dried and stored at -20 ^{o}C until further use.

Experimental data for TP10-S-S-PQ (**68**)

$^{m}/_{z}$ ($C_{125}H_{213}N_{31}O_{27}S_2$, 2644.57 a.m.u.): 1323.13 ($[M+2H^+]^{2+}$); 882.87 ($[M+3H^+]^{3+}$); 662.60 ($[M+4H^+]^{4+}$); 530.07 ($[M+5H^+]^{5+}$).

Elution conditions: 0-100% ACN in water (0.05% TFA) in 30 minutes, at a flow rate of 1 mL/min.

R_t = 16.9 minutes

8.4.8. *In vitro* assays

Huh-7 cells, a human hepatoma cell line, were cultured in 1640 RPMI medium supplemented with 10% fetal calf serum, 1% non-essential amino acids, 1% penicillin/streptomycin, 1% glutamine and 10 mM HEPES, pH 7, and maintained at 37 °C with 5% CO_2. Inhibition of liver stage infection was determined by measuring the luminescence intensity in Huh-7 cells infected with a firefly luciferase-expressing *P. berghei* line, *Pb*GFP-Luc_{con}.[1] Briefly, cells (12×10^3 /well) were seeded in 96-well plates the day before drug treatment and infection. Tested compounds were prepared in the following way: 10 mM stock solutions were obtained by dissolving accurately weighed S16 compounds in MeOH and dilutions subsequently made with medium to the desired concentration. Medium was replaced by fresh medium containing the appropriate concentration of each compound 1 hour prior infection. Sporozoites (10000 spz/well), freshly obtained through disruption of salivary glands of infected female *Anopheles stephensi* mosquitos, were added to the wells 1 hour after compound addition. Sporozoite addition was followed by centrifugation at 1700g for 5 min. At 24 hours post-infection, medium was once more replaced by fresh medium containing the appropriate concentration of each compound. Inhibition of parasite development in the liver was measured 48 hours after infection. The effect of the compounds on the viability of Huh-7 cells was assessed by the AlamarBlue assay (Invitrogen, UK), using the manufacturer's protocol. Nonlinear regression analysis was used to fit the normalized results of the dose-response curves, and IC_{50} values were determined using the SigmaPlot software[2].

8.5. Bibliography

1. I. H. J. Ploemen, M. Prudêncio, B. G. Douradinha, J. Ramesar, J. Fonager, G. J. Van Gemert, A. J. F. Luty, C. C. Hermsen, R. W. Sauerwein, F. G. Baptista, M. M. Mota, A. P. Waters, I. Que, C. W. G. M. Lowik, S. M. Khan, C. J. Janse and B. M. D. Franke-Fayard, *PLoS One*, 2009, **4**, 1–12.
2. T. Rodrigues, F. P. da Cruz, M. J. Lafuente-Monasterio, D. Gonçalves, A. S. Ressurreição, A. R. Sitoe, M. R. Bronze, J. Gut, G. Schneider, M. M. Mota, P. J. Rosenthal, M. Prudêncio, F.-J. Gamo, F. Lopes and R. Moreira†, *J. Med. Chem.*, 2013, **56**, 4811–4815.

9

Final remarks and future perspectives

The working hypothesis of this PhD Thesis was that it might be possible to improve the performance of antimalarial drugs, upon conjugation to cell penetrating peptides, given their widely reported advantages as carriers and intracellular targeting moieties for a variety of cargos. To this end, two classical aminoquinolines, from the portfolio of clinically available antimalarials, were chosen: chloroquine, a 4-aminoquinoline predominantly active against intraerythrocytic forms of malaria parasites, and primaquine, an 8-aminoquinoline well-known for its potent action against exoerythrocytic parasites, particularly, liver-stage forms and gametocytes. Besides the anticipated intracellular targeting effect of conjugating these two aminoquinolines to cell penetrating peptides, this approach might also contribute to overcome problems such as the widespread parasite resistance to chloroquine, as well as the hemotoxicity and low oral bioavailability of primaquine.

As blood-stage infections are responsible for the prostrating symptoms and life-threatening complications of malaria, the major effort was put on chloroquine conjugates. However, as reported in Chapter 4, conjugation of cell-penetrating peptides to the chloroquinoline moiety (CQn) resulted in loss of antimalarial activity in most cases, except when the cell penetrating peptide used was TP10. In this case, antimalarial activity of the conjugate was superior to that of the peptide alone, but still could not match that of free chloroquine. Hence, as described in Chapter 5, different linkers between this peptide and CQn were tested, in order to investigate how these might affect antimalarial performance. Still, the butanedioyl (C4) spacer originally used was the one yielding the most active conjugate, CQn-C4-TP10. Interestingly, the order in which building blocks were bound together was found to be relevant, as antimalarial activity was lost when the drug was alternatively coupled to the peptide *C*-terminus, producing TP10-C4-CQn. Another relevant observation was that, while TP10 is not significantly hemolytic *in vitro* at the concentrations assayed, its conjugation to CQn increases hemolysis, to extents that depend on the specific spacer used. An exception was observed for conjugation *via* disulfide bonds, which may be due to conjugate degradation caused by disulfide bond breakage in the cell culture medium.

To further understand the somewhat unexpected behavior of the CQn-CPP conjugates, four compounds were selected (TP10, CQn, CQn-C4-TP10 and CQn-S-S-TP10) and their interactions with model membranes were evaluated, as presented in Chapter 6. Results showed that CQn-TP10 conjugates promote the disruption of DMPC vesicles – used as mimics of healthy erythrocyte membranes, an effect that was more pronounced for CQn-C4-TP10 than for CQn-S-S-TP10, hence correlating with their respective hemolytic activities. Notwithstanding, the conjugates displayed higher binding affinity to DMPG vesicles – used as mimics of parasitized erythrocytes, which agrees with the expected stronger electrostatic interactions between the positively charged conjugates and the negatively charged membrane. As such, it seems that, while the overall cationic nature of the constructs confers them the expected ability to strongly interact with negatively charged lipid bilayers, conjugation to CQn – a hydrophobic heteroaromatic moiety, elicits severe perturbations on zwitterionic liposome mimics of hRBC, which may explain the observed hemolytic effects.

It is noteworthy that the membrane models used in the above study present several limitations, as the composition (both lipidic and non-lipidic) of membranes from both healthy and parasitized erythrocytes is significantly more intricate, and undergoes substantial alterations, not only upon invasion, but also throughout intracellular parasite development. In fact, there is a wide panoply of factors that cannot be taken into account when simulating cell membranes. As such, when possible, using whole cells and adequate tools to study their interactions with test compounds, is the best option. Fluorescence-based techniques, microscopy and FACS, were used to respectively visualize and quantitate interactions between selected CPP and CQn-CPP conjugates, and both healthy and parasitized erythrocytes. As reported in Chapter 7, this study provided confirmation that TP10 and its most active conjugate, CQn-C4-TP10, are both able to bind indistinguishably to hRBC and *P*iRBC, and that peptide/conjugate-bound cells show a much thinned membrane as compared to unbound ones. Additionally, FACS analysis allowed us to measure a higher internalization level for CQn-C4-TP10 in hRBC, which justifies the higher hemolysis perceived in the course of *in vitro* assays. Furthermore, it was possible to observe that, once having gained access to the parasites, the conjugate does strongly interact with them, supporting the antimalarial activity previously observed.

A last effort to establish whether or not the CPP conjugation approach might be of interest to rescue classical antimalarial drugs, an exoerythrocytic stage of infection was considered. Hence, CPP were conjugated to primaquine (PQ), and conjugates thus obtained were screened *in vitro* for their ability to inhibit liver-stage development of *P. berghei* parasites, as described in Chapter 8. Interestingly, as previously observed for CQn conjugates against blood-stage *Plasmodia*, only PQ conjugates where the CPP used was TP10 or the related peptide Transportan, were reasonably active *in vitro* against liver-stage parasites. Another similarity between PQ and CQn conjugates resides in the fact that drug conjugation to the peptide's *N*- rather than *C*-terminus leads to better results. Still, PQ-CPP conjugates seem more promising than their CQn counterparts, as they were generally non-toxic to hepatocytes, the host cells for liver-stage parasites. Moreover, PQ-C4-TP10 was more active than both the parent peptide and the parent drug. As such, we believe these conjugates deserve further investigation in the near future, eventually through exploration of other CPP and PQ-CPP linkers, and additional biophysical and biochemical assays, including cell internalization studies, and stability/metabolic conversion assessment in relevant physiologic media (e.g., human serum, liver homogenates, etc.). Furthermore, since PQ also exerts gametocytocidal activity, being able to block human-to-mosquito transmission and subsequent spread of the disease, it is important to determine whether PQ-CPP conjugates are able to impair gametocytogenesis, and also oocyst formation in the mosquito.

Altogether, findings made throughout this work demonstrate that, at least in what concerns antimalarial aminoquinolines, conjugation to any given CPP does not work as a universal tool for improvement of intracellular targeting and therapeutic activity. Our data shows that the specific amino acid sequence of the CPP, rather than its size or net charge, is crucial for the display of activity against both blood- and liver-stage parasites. Therefore, a general CPP structure-activity relationship cannot be drawn with the data gathered thus far, which makes it difficult to design the next generation of CPP for this particular application. Also, it is clear that the peculiarities of both intraerythrocytic parasites and their host cells, lead to unexpected and undesired effects in the case of blood-stage infection, where a general lack of selectivity, i.e., low activity-to-cytotoxicity ratio, was observed. Primaquine conjugates tested on liver-stage infection did not present this limitation, and showed an activity improvement over their parent building blocks; hence, these seem worthy of further research and development in a near future.